The Measurement and Analysis of Flux Variations in Seyfert Galaxy Nuclei

A thesis by

Hartmut Winkler

presented in fulfillment of the requirements
for the Degree of Doctor of Philosophy
in the Department of Astronomy
at the University of Cape Town

August 1990

To Timothy,

a seven month old budding scientist.

The Measurement and Analysis of Flux Variations in Seyfert Galaxies *by Hartmut Winkler, Department of Astronomy, University of Cape Town*

Abstract

Seyfert galaxies have compact nuclei with luminosities only surpassed by quasars, to which they are believed to be related. The most common interpretation of these objects is that their central power source is a black hole with matter accreting towards it. An understanding of these powerful energy sources would vastly increase our knowledge of high energy physics and cosmology.

One unexplained characteristic of Seyfert nuclei is that their luminosities are often variable. Some questions relating to this fact are:
What is the nature of the variability?
How much obscuration is there from matter in the line of sight?
What is the shape of the flux continuum?
What is the relationship between the variability and other properties of the galaxy and nucleus?
This thesis seeks to answer some of these questions, as they critically affect any model put forward to explain the Seyfert phenomenon.

29 southern Seyfert galaxies were chosen for observation. Flux measurements through five colour filters in the 0.3 to 1 μm range were made regularly in the period September 1986 to October 1989 with a single channel photometer and a CCD camera. These were analysed in conjunction with similar data collected by other investigators.

Flux changes of 10% or more were observed in most objects. Fluxes through individual colour filters varied proportionally to each other, indicating that the shape of the continuum at these wavelengths remains constant. The flux distribution derived in this manner is shown to be similar for all objects examined. A procedure potentially superior to existing methods is developed to estimate the extinction of Seyfert nuclei from the flux distribution.

Spectroscopic observations in the 0.34-0.72 μm range were made for most objects. From these spectra the gas densities and temperatures, degrees of activity and spectral line intensities and widths were derived. Possible spectral variations were investigated.

No definite periodic changes in the light curves could be found. However the possibility of regular variations is not completely excluded. The relative amplitude and rate of flux variations are shown to be independent of the luminosity and other nuclear properties.

Acknowledgements

It is impossible to give a complete list of all the people that have helped to contribute to the success of this thesis. All of the staff of the University of Cape Town astronomy department and the South African Astronomical Observatory been of assistance in some small way or another. A few people however deserve a special mention.

The director of the SAAO, Michael Feast, is thanked for allowing me to make extensive use of the institute's telescopes and other facilities.

The intensive photometric monitoring campaign of southern Seyfert galaxies that led to the publication of this thesis would not have been possible on that scale without the active participation of Ian Glass, who was also a major motivating force behind this project, Jonathan Spencer-Jones and Francois van Wyk. David Buckley and John Egan also contributed some individual measurements.

Ian Glass allowed me to use some of his yet unpublished infrared photometry. This information was crucial for the derivation of many of the flux distributions.

The spectra from the March 1985 observing run were recorded by Tony Fairall, with Freddie Marang assisting. They vastly improved the quality of some of the integrated spectra shown in this work.

Ian Glass made available to me the CCD observations that he made during February 1986. They proved very useful for the determination of the intensity profiles of a number of objects.

Dave Kilkenny is thanked for the permission to use his unpublished photometric data of several of the galaxies investigated. These data proved to be particularly important as almost no other photometric studies were made during the 1982-1984 period of the Seyfert galaxies studied in this work.

Some of the polarimetric measurements quoted in this thesis were unpublished results passed on to me by Paul Barrett.

Tony Fairall introduced me to the use of the spectrograph. He allowed me to utilise some of his telescope time and helped during the recording of a lot of the earlier spectra. Much of the credit for the spectroscopic results must also go to Francois van Wyk for his superb telescope guiding skills and his otherwise able night assisting.

John Menzies taught me to use the CCD camera and also helped me with smaller queries on numerous other occasions.

Rona Banfield and Isobel Bassett deserve a great word of thanks for offering to take on the laborious task of reducing some of the CCD data.

Joyce Westerhuys diligently reduced the vast number of photometric observations in a most efficient manner.

Angela Jones, Don Kurtz and Darragh O'Donoghue patiently sorted out many of my computing problems.

The progress that I made in this thesis is partly due to discussions that I have had with Toni Fairall, Ian Glass and Kaz Sekiguchi. These three also commented on some of the earlier drafts of this thesis.

The work that led to this thesis, while usually enjoyable and rewarding, also needed to be fuelled by moral support from many friends, particularly during those last few months. A special word of thanks goes to my housemates, Jane and Mike, who put up with my recluse existence during the final stages of this work.

Finally, a big word of thanks must go to my supervisor, Tony Fairall, who strongly encouraged my registration as a Ph.D. student and proposed the theme of this project. He was always most pleasant and helped me out with many problems of a scientific and bureaucratic nature.

Content

Abstract .....

Acknowledgement .....

1. Introduction 1

.1. Definition of a Seyfert galaxy 1

.2. Models proposed to explain the Seyfert phenomenon 4

.3. Aim and method of the thesis 5

.4. Preview of the thesis 7

2. Review of theory used in this thesis 9

.1. Thermal and non-thermal continuum emission 9

.2. Gaseous nebulae and emission lines 10

.1. Collisions between atoms and free electrons 11

.2. Photoionisation and recombination 13

.3. Photometry of galaxies 14

.1. Measurement of galaxy intensity profiles 14

.2. Redshift corrections 16

.3. Extinction 17

3. The sample 21

.1. Selection criteria 21

.2. Introduction of the candidates chosen for observation 22

4. The CCD imaging 26

.1. The instrument 26

.2. Imaging and photometry 27

.3. Reductions 31

5. UBVRI aperture photometry 37

.1. The instrument 37

.2. The observations 38

.3. The reductions 39

6. Spectroscopy 74

.1. The RETICON spectrograph 74

.2. Observations 75

.3. Spectroscopic reductions 78

7. General properties of Seyfert galaxies 89
.1. Flux distribution 89
.1. Ultraviolet 89
.2. Optical 90
.3. Near-infrared 99
.4. Far infrared 101
.5. X-ray 102
.6. Radio and sub-millimeter 104
.7. The nuclear continuum 105
.2. Spectroscopic properties.....112
.1. Iron lines 115
.2. Emission line ratios 115
.3. Line widths 116
.4. Line profile and intensity variations 116
.3. Morphology and polarisation 121
.4. Calculation of the nuclear extinction 123
.5. Variability 128
.1. Comparison between variability and other properties ...129
.2. Search for periodic variability 130

8. Discussions and models 136
.1. The flux distribution 136
.2. Variations 138
.3. The extinction of the nucleus 139

9. Notes on individual objects 142
.1. through to .29.
(each sub-chapter dedicated to one of the objects in the sample)

10. Conclusions 149

Appendix. Photometry and spectroscopy by other observers 152

References 171

1. Introduction

In 1943 Carl Seyfert published a paper in which he described the emission line spectra of six galaxies. Emission lines had by then already been detected in various galaxies, but these six objects had spectra which were at the time considered to be peculiar, as they had extremely broad hydrogen emission lines and forbidden lines with widths greater than had been found in other emission line nebulae. The nuclei of these galaxies had a starlike appearance. The presence of high excitation emission lines was also noted, as well as the fact that these galaxies were all luminous spirals. Seyfert was the first to recognise that these formed a new class of objects, one that was to be named after him.

Seyfert galaxies received little attention until the 1960's, when, after the discovery of quasars, active galactic nuclei (AGN's) became the subject of intensive study, as it was soon realised that Seyfert galaxies might be low luminosity quasars. Just as in quasars, the flux distribution in Seyfert galaxies could not be fitted by a thermal blackbody model. It was therefore proposed that their nuclei might contain black holes and could therefore be giant laboratories with some of the most exciting high energy physics happening in them.

Most of the pre-1985 developements in Seyfert galaxy research have been reviewed by Weedman (1977) and Osterbrock (1984).

1.1. Definition of a Seyfert Galaxy

Initially a Seyfert galaxy was defined as a galaxy with a starlike nucleus and a spectrum with broad emission lines. People soon realised that other properties were usually associated with them.

Seyfert galaxies are nearly always spirals. They have been detected at all frequencies from the radio to X-ray spectral regions. The dominant component of the flux distribution has the form of a power-law, i.e., $F(\nu) \propto \nu^{-\alpha}$ (Oke and Sargent, 1968). In addition to the power law component the flux distribution of Seyfert nuclei contains emission lines and thermal (blackbody) components (e.g., Edelson and Malkan, 1986). The emission lines are divisible into two sets, the broad and the narrow lines. The broad lines, which are usually hydrogen and helium lines, have widths of the order of 10000 km s^{-1} and are found in the more luminous nuclei. The narrow lines have widths of

~500 km s^{-1} and appear in all sub-types of Seyfert galaxies. Typically, the intensity of the [O III] 5007 Å line is greater than 5 times the intensity of the narrow Hβ line, and [N II] 6584 Å is comparable in strength to Hα(narrow). An [O III] 5007 A to Hβ(narrow) ratio of 3 or higher is often used as a criterion to define Seyfert activity (Baldwin et al, 1981).

Fitch et al (1967) found brightness changes in NGC 4151 and since then the luminosities of many Seyfert nuclei have been discovered to be variable (e.g. Penfold, 1979). The nature of the variability is largely irregular, although periodic changes have been suggested for a number of objects (e.g., Bisch et al, 1987).

Weedman (1970) introduced the Seyfert galaxy classification system that is now in use, in which Seyferts are graded into two types depending on whether the width of the hydrogen emission lines is greater than the width of the forbidden lines. A more detailed classification system that has also gained acceptance has been proposed by Osterbrock (1981). There galaxies are classified by their spectra and various sub-types are defined as follows.
Seyfert 1:- A Seyfert galaxy with very broad Balmer emission lines.
Seyfert 1.5:- A Seyfert where a narrow component is visible superimposed on the broad lines.
Seyfert 1.8:- A Seyfert where a broad component in Hβ is only just detectable.
Seyfert 1.9:- A Seyfert where a broad component is visible in Hα but not in Hβ.
Seyfert 2:- A Seyfert where no broad component is detectable.

This classification is often dependent on the quality of the spectrum available. Very high signal-to-noise spectra often show very weak broad or narrow components of the Balmer lines that are undetectable in lower quality spectra.

Seyfert galaxies are only one of the many types of objects that are often collectively described as active galactic nuclei (AGNs). The classification of AGNs has been reviewed by Lawrence (1987). In the next few paragraphs short descriptions of other types of active galaxies are presented. Sometimes galaxies falling in these categories are misclassified as Seyferts.

Quasars: The spectra of quasars are similar to those of type 1 Seyferts, but their nuclear luminosities are much greater, typically by a factor of over 100. However, the dividing line between Seyferts and quasars is not clearly defined. The different nomenclature has largely resulted from the fact that

the first quasars discovered were strong radio sources that were not then known to be of extra-galactic origin. Veron-Cetty and Veron (1989) arbitrarily differentiate between quasars and Seyferts by using a cut-off nuclear luminosity corresponding to $M_V = -23$ (with $H = 50$ km s^{-1} Mpc^{-1}). Other than in luminosity no obvious differences exist between the two sets of objects. There have however been suggestions that quasars are intrinsically more polarised than Seyferts.

BL Lacerta Objects: These objects distinguish themselves from other AGN's by having strong continua with very weak emission lines. They are rapidly variable and show strong polarisation. A popular model that could explain their characteristics pictures them as Seyfert-like nuclei with a relativistic jet spreading in the direction of the observer, amplifying the continuum in relation to the spectral lines (see Lawrence, 1987).

Radio Galaxies: These are galaxies with radio luminosities much larger than in normal (and Seyfert) galaxies, but their optical spectra are similar to Seyfert spectra. They are often ellipticals. Strong radio emitting galaxies seem to be on average more reddened than Seyferts, have broader lines and weaker Fe II lines. On the whole there is no reason to assume that they are not simply radio-loud Seyfert galaxies (Lawrence, 1987).

LINERs (Low Ionisation Nuclear Emission-line Regions): As the name implies, these objects do not possess strong high excitation lines such as the [O III] 4959, 5007 A doublet, but have prominent low excitation lines such as [O I] 6300 A. The mechanism for the formation of the emission lines was at first thought to be shock heating (Heckman, 1980). Since then a model where the photoionisation is caused by a power law source has been favoured, but the nuclear luminosities of LINER's are far lower than Seyferts (Halpern and Filippenko, 1984).

Starburst galaxies (also known as H II galaxies or narrow emission line galaxies): The emission line spectra of such galaxies resemble those of galactic H II regions. The spectral lines are more narrow than in Seyferts, [N II] 6584 Å is usually much weaker than Hα, and the intensity ratio of Hβ to [O III] 5007 Å is generally greater than 1/3. In these objects the excitation mechanism is thought to be photoionisation by the ultra-violet photons from hot stars (Balzano, 1983). The activity need not be confined to a small nuclear region like in other AGNs.

Since the early days many hundreds of Seyfert galaxies have been discovered. Many have been extensively studied. However the physics behind these objects and the mechanism that gives rise to the characteristic Seyfert line spectra and flux distributions is still not understood.

1.2. Models proposed to explain the Seyfert Phenomenon

Any model put forward to describe the physical processes happening in the nucleus of a Seyfert galaxy will have to account for the following observational evidence:

- the high luminosity
- the power law continuum ($f(\nu) \propto \nu^{-\alpha}$) with α about 1
- the relatively low luminosity in the radio wavelength region
- the ultra-violet and infrared luminosity excess above the power law continuum
- the large widths of the broad lines
- the presence of highly ionised atoms
- the presence of unusually strong iron emission line bands
- the continuum and spectral line variability
- the differences in activity class.

The picture that enjoys the widest support is one where the source of energy is a very massive body with matter falling onto it, as in this process enough energy can be released to account for the high luminosity (see, e.g., Wandel and Mushotzky, 1986). This central body may be a black hole. A strong magnetic field near this body would induce fast moving electrons to emit radiation through the synchrotron process and a power law continuum could result from this. Synchrotron radiation becomes self-absorbed at low frequencies, which could be a reason why the radio luminosity observed in Seyferts is so low. The infalling matter may also be forming an accretion disk, and thermal radiation from this will result in an ultra-violet excess. Atoms in the gas surrounding the nucleus are believed to be ionised by the power law continuum and the thermal radiation from the accretion disk. This would account for the emission line spectra observed, especially as the power law flux, which may extend to X-ray wavelengths, can explain the presence of emission lines originating from multiply ionised, high excitation ions. Photoionisation models (e.g., Kwan and Krolik, 1981, Wills et al, 1985, Collin-Souffrin et al, 1986), although reasonably successful in predicting the relative strength of the emission lines, do however underestimate the Fe II band strength. Outside the accretion

disk one can expect fast-moving, dense gas, which may be interpreted as the source of the broad lines. Further out, where the gas is less dense and moving slower, the narrow lines are expected to be formed. If the opacity of the high density region is large, the broad lines would not be visible. This might be the cause of the difference between type 1 and type 2 Seyferts. This obscuration is probably due to dust, which is believed to play a significant role in Seyfert galaxies and would be expected to be responsible for the infrared excess (Carleton et al, 1987).

On the whole, the model described above is not in serious disagreement with the observational evidence. It does however tell us very little about the source of the high energy, the central massive body. Understanding the nature of such an extreme object would offer an important test the laws of physics under extreme conditions and might lead to the discovery of unknown phenomena. To address this question one needs some stronger constraints on the physical characteristics of these objects. One such characteristic about which little is known is the behaviour of the luminosity as a function of time. An aim of this thesis will be to study that behaviour.

Most models proposed to explain the nuclei of Seyfert galaxies are variants of that described above. However some completely different pictures have not been ruled out yet. For example, Terlevich (1989) proposes that the nuclear regions of Seyferts are undergoing massive starbursts. These stars will later form supernovae. Supernovae have broad emission lines (e.g. SN 1987A) and these could mimick the broad lines observed in Seyferts.

1.3. Aim and Method of the Thesis

It has been said earlier that Seyfert nuclei offer the opportunity to study the laws of physics under extremely high energy conditions. Although most investigators accept that the observed characteristics of Seyfert nuclei are directly related to the presence of a massive body such as a black hole, very little can be said about this body. This is because observers have not been able to place sufficiently tight constraints to the physical parameters of the central source.

One such parameter about which relatively little is known is the nature of the variability. A better understanding of the mechanisms describing the Seyfert phenomenon could be gained from variability studies, as these could be used to

answer the following open questions:

- Are there any periodic changes in the luminosity? If such could be identified it would present theoreticians with a real challenge to determine its causes. Periodic variations could be the result of rotation of the black hole, or might be related to even more exotic phenomena.
- How do flux changes at different wavelengths compare? If the variations are unequal at different frequencies this would imply that several components are varying independently of each other.
- How is the nature of the variability related to the other properties of Seyferts? Any correlation between variability and other characteristics of a Seyfert galaxy would impose constraints on any model proposed to descibe these objects.
- Somewhat unexpectedly, the present work has revealed that as a result of the flux variability it is possible to gain information about the shape of the flux distribution and about the obscuration in the line of sight to these objects. This finding will be described later.

Observations of flux changes are often difficult and need to be made over a long span of time. As a result information on variability in Seyfert nuclei is limited. A series of flux measurements spread over a suitably long time interval could be used to determine whether the variations are of a periodic nature. Repeated measurements of the brightness at a range of wavelengths would enable one to monitor any colour changes. If possible it would also be of interest to compare the continuum flux changes to spectral line changes.

The luminosity variations need to be interpreted in relation to the other properties of the galaxy. The flux distribution at all wavelengths and the spectral lines are important sources of information on the physical conditions inside the nucleus. Properties of the galaxy such as morphology and surface brightness may be connected to the activity in their nuclei.

It was decided that the aim of this thesis should be to study the luminosity variations in Seyfert galaxies. In order to do so a large number of Seyferts had to be monitored for variability. A sample of 29 objects was selected. For these UBVRI aperture and CCD photometry was carried out over a period of three years. It was attempted to get a set of observations each month. For practical reasons (only seasonal coverage possible, no allocation of observing time, bad weather) such frequent observations were not possible. The CCD images were also to be used to study the morphological properties of the galaxy.

Spectroscopic observations were made of most of the galaxies in order to investigate the emission line spectra. If spectra were recorded at different epochs these were to be inspected for variability.

The literature was searched for references to the galaxies of the sample. This included the collecting of information about the galaxies investigated from outside the optical wavelength regime. Aperture photometry data from earlier epochs were of particular interest as it was hoped to study the flux variation over a time period longer than the three years allocated for this thesis.

From the data and other available information conclusions could be reached about the variability of the Seyfert nucleus and its implications. The results are presented in this thesis.

1.4. Preview of the Thesis

Chapter 2 gives the theoretical background to some of the methods that will be used later in this work. Firstly, types of continuum flux radiation usually associated with Seyfert nuclei will be described. Then, as much of our understanding of Seyferts is based on the interpretation of the emission line spectra, a review of the physics of gaseous nebulae and emission line formation in particular is presented. Finally, some empirical results of consequence for photometric studies of galaxies are discussed.

Chapter 3 gives details about the selection of the sample of galaxies for observation. The galaxies that were chosen are introduced and shortly described.

The next three chapters discuss the equipment, observations and data reductions. The results of the observational work are also shown. One chapter is dedicated to each of the three methods of observation that have been used; the charge coupled device (CCD) camera imaging and photometry, the aperture photometry and the spectroscopy.

In chapter 7 the data are analysed in conjunction with other information published in the literature in order to investigate the physical conditions of the galaxies in the sample. Sections of this chapter deal with the flux distribution and the spectral, morphological and polarimetric characteristics of the Seyfert galaxies studied. A sub-chapter is dedicated to the derivation of the extinction of the nucleus. Finally, the variability is investigated.

of the extinction of the nucleus. Finally, the variability is investigated.

In chapter 8 the most important results from this thesis, those relating to the flux distribution, the extinction and the flux variations, are discussed in more general terms. Objects are discussed individually in chapter 9.

Chapter 10 concludes the thesis.

2. Review of Theory used in this Thesis

Before proceding to the main body of this study it is useful to review some of the theory that is frequently applied in the analysis of Seyfert galaxies. This includes standard applied physics as well as established empirical relationships. Three topics of particular relevance to this thesis will be examined.

2.1. Thermal and Non-Thermal Continuum Emission

During discussions dealing with the shape of the flux distribution and the source of the ionising radiation the phrases thermal and non-thermal radiation are frequently used. Thermal blackbody radiation results from the emission of energy by a body that absorbs and re-radiates radiation that falls on it. Non-thermal radiation is any form of flux emission that cannot even approximately be described as thermal radiation.

Thermal blackbody radiation is the chief energy emitting process in stars and dust clouds. Its spectral flux distribution is given by Planck's radiation law and has the form

$$F(\nu) \propto \nu^3/[\exp(h\nu/kT)-1] \ .$$

At the low frequency limit this becomes

$$F(\nu) \propto \nu^2 \ .$$

A form of flux distribution commonly encountered in astrophysics is the power law. The spectral index α of a power law flux distribution is defined by the relationship

$$F(\nu) \propto \nu^{-\alpha}.$$

(Note that several authors use a definition of α without the minus-sign in the above expression). The spectral index of the low-frequency part of the blackbody spectrum is therefore $\alpha = -2$. Wien's law tells us that this spectrum peaks at

$$\lambda_{max}(\text{Å}) = 5.1\ 10^7/T(K)$$

Thermal emission is also important in the study of Seyfert galaxies. The gas

surrounding the nucleus may be heated by the central energy source and it would then radiate thermally. Thermal flux components at T ~ 26000 K and T ~ 60 K have been identified in many Seyfert galaxies (Edelson and Malkan, 1986). Stellar spectra can generally be approximated by a blackbody distribution. The radiation from the host galaxy, a combination of stellar light and radiation from interstellar matter, is also of thermal origin.

The flux distributions of Seyfert nuclei do not resemble blackbody spectra. An examination of the continuum reveals that its shape can usually be approximated by a power law (Oke and Sargent, 1968). The spectral index of this distribution is normally close to 1. For X-ray emission $\alpha = 0.7$ is typical (Mushotzky, 1982) while in the infrared α is about 1.2 (Glass et al, 1982).

A power law flux distribution is characteristic of synchrotron radiation, i.e., radiation given off by electrons moving with relativistic velocities in a magnetic field. It can be produced by an electron energy distribution of the form

$$N(E) \propto E^{-\gamma}$$

where γ is directly related to α

$$\gamma = 2\alpha + 1 \ .$$

At high electron densities the synchrotron spectrum becomes self-absorbed below a critical frequency ν_s. For frequencies lower than ν_s the flux distribution still resembles a power law, but with a spectral index of -2.5 (Lang, 1974).

2.2. Gaseous Nebulae and Emission Lines

Much of the physical theory of Seyfert galaxies has been based on the interpretation of the emission line spectra. Later in this work some physical parameters of the Seyfert nuclei studied will be derived from their spectra. It is therefore useful to review the theoretical work that has been devised in order to account for the formation of spectral lines. Much of this applies the principles of atomic physics to the conditions prevailing in gaseous nebulae. A recent review of the subject was given by Osterbrock (1988) and the

remainder of this sub-chapter follows his treatment.

Emission lines result from the photons created by the transition of an atom or ion from an excited state to a lower state. In order for photons to be emitted it is necessary for at least some atoms inside the gas to be in an excited state. Two mechanisms that would provide the energy needed to excite the atoms will be discussed.

2.2.1. Collisions between atoms and free electrons

This is the chief excitation process for O^+, O^{++}, N^+, S^+ and many other ions in typical nebulae. In order to have a significant number of free electrons arising out of photoionisation it is necessary to have a strong source of ultraviolet- or X-rays.

An atom may be excited to a higher energy level (labelled "1") out of the ground state (labelled "0") if the free electron's kinetic energy is greater than χ_{10}, the energy of level 1 above the ground state. The electron temperature T_e may be defined as follows

$$T_e = (2k)^{-1}\langle E_{ek}\rangle,$$

where k is the Boltzmann constant and $\langle E_{ek}\rangle$ is the average kinetic energy of an electron in the gas. If n_e is the number of electrons per unit volume and n_i (n_j) is the number of atoms in state i (j) then the number of atoms excited to level i from level j per second per unit volume is given by the formula

$$n_j n_e q_{ji}(T_e)$$

where $q_{ji}(T_e)$ is a cross section that depends on the atomic characteristics of the atom and on the maxwellian velocity of the free electrons. Similarly, collisions between the atoms in state 1 and free electrons can occur, which can have the effect of deexciting the atom. The number of atoms per second and per unit volume deexcited through collisions to the ground state is given by

$$n_i n_e q_{ij}(T_e).$$

It is also possible for state i to spontaneously decay back to state j, emitting a photon in the process. The rate for this process per unit volume is

$n_i A_{ij}$.

Eventually an equilibrium will be reached where equally many atoms are excited from state j to state i as are deexcited from state i to state j. For the ground state and level 1 this means that

$$n_0 n_e q_{01}(T) = n_1[A_{10}+n_e q_{10}(T)]$$

Therefore the rate of emission of line photons from level 1 to the ground state per ion per unit time interval is given by

$$n_1/n_0\ A_{10} = A_{10}\ q_{01}/q_{10}\ [1+A_{10}/(n_e q_{10})]^{-1}$$

$$= A_{10}\ g_1/g_0\ \exp(-\chi_{10}/kT_e)\ [1+A_{10}/(n_e q_{10})]^{-1}$$

because in the high density limit the ratio n_1/n_0 is described by a Boltzmann distribution. g_i is the statistical weight of level i.

The last equation shows that the rate of line photon emission is proportional to n_e at low free electron densities and independent of n_e at high electron densities. There is a critical density above which an increase in the free electron density has no effect on the line strength. There are metastable energy levels in some atoms where the probability of a spontaneous decay into a lower state is extremely low because of quantum mechanical effects. Emission lines resulting from such transitions are also known as "forbidden". Forbidden lines are almost unobservable under typical laboratory conditions, where collisional de-excitation is dominant because of the relatively high densities. They can however be extremely strong in nebulae. This is because the typical densities in nebulae, $\sim 10^6$ atoms/cm^3 (Osterbrock, 1989), are very much lower than can be achieved in laboratory conditions.

The intensity ratio between emission lines formed by transitions between the levels j and i, and k and j is

$$I_{ji}/I_{kj} = C\ A_{ji}/A_{kj}\ g_j^2/(g_i g_k)\ \exp((\chi_{kj}-\chi_{ji})/kT_e)\ [1+A_{kj}/(n_e q_{kj})]/[1+A_{ij}/(n_e q_{ji})]$$

where C is a factor that takes into account the possibility that transitions to other levels are possible. This factor can be estimated by modelling of the atomic processes. The last formula shows the line intensity ratio to be dependent on temperature and density only.

Line ratios are an important diagnostic tool in the study of emission line

objects. They are often used to classify objects according to their activity type (Baldwin et al, 1981). As shown above, certain emission line ratios provide the opportunity to determine some of the properties of the circumnuclear gas such as the electron density n_e and the electron temperature T_e. The relationships used in this work to determine these quantities, given in general form by Osterbrock (1989), were calculated using the list of atomic constants compiled by Mendoza (1983). The most useful of these for Seyfert galaxies, involving the ratios between the [O III] 4363, 4959 and 5007 Å lines, which are usually strong in high excitation gases, is given below

$$I(4959+5007)/I(4363) = [7.73\exp(3.29\ 10^4/T_e)]/(1+4.5\ 10^{-4}\ n_e T_e^{-1/2}) \ .$$

A similar formula can be used to estimate the electron density from the intensity ratio of the [S II] 6716 and 6731 Å lines. The solutions are represented graphically in figure 5.3 of Osterbrock (1989). The values for n_e and T_e, derived using different sets of lines often disagree with each other. The reason for this is that the emission lines for different atoms and stages of ionisation can originate in different regions of the gas.

The intensity ratio of two emission lines originating from transitions involving the same upper levels is simply the ratio of their A_{ij} values, i.e., the ratio is constant provided that there is no self-absorption. The values of these ratios in optically thin gases for some common emission lines encountered are given in table 2.1 below. The A_{ij} values were taken from Mendoza (1983).

Table 2.1. Some intrinsic emission line ratios.

Ion	λ_{ij}	λ_{ik}	A_{ij}	A_{ik}	I_{ij}/I_{ik}
Ne III	3868.7	3967.5	0.171	0.0542	3.15
O III	5006.8	4958.9	0.0196	0.00674	2.91
Ca V	5308.9	6085.9	1.90	0.426	4.46
O I	6300.2	6363.9	0.00634	0.00211	3.00
N II	6583.6	6548.1	0.00299	0.00101	2.96
S III	9532.1	9069.4	0.0576	0.0221	2.61

2.2.2. Photoionisation and recombination

Photoionisation and recombination is the process that is largely responsible for the formation of the Balmer and helium lines. The photoionisation of the gas has already been discussed. Recombination occurs when a free electron collides with a proton to form a neutral hydrogen atom. The electron will

cascade down through a series of excited states to the ground state. During each jump a photon of the energy characteristic of the energy difference between the energy levels is emitted. The relative intensity of an emission line will depend on the probability that an atom de-excites through that particular transition during the recombination process. The recombination spectra of hydrogen under typical nebular conditions were calculated by Brocklehurst (1972). The case where the gas is optically thick in Lyman alpha, called "case B" by Baker and Menzel (1938), has been used by most investigators studying the conditions inside gaseous nebulae.

The most up-to-date "case B" calculations of intensity ratios between the hydrogen emission lines have been performed by Hummer and Storey (1987). They determine the ratio $H\alpha:H\beta:H\gamma:H\delta$ to be 2.85:1.00:0.47:0.26. Transitions of electrons from free states to bound states form the Balmer continuum which is strongest below 3646 A. Edelson and Malkan (1986) empirically found the Balmer continuum in Seyfert galaxies to be $I(Ba_c) = 2.1\ I(H\alpha)$.

2.3. Photometry of Galaxies

Photometric observations of Seyfert galaxies have to be corrected for a number of factors in order to extract information about the nuclear luminosity and flux distribution. The three most important of these are the contamination by extra-nuclear starlight, the redshift of the flux distribution and obscuration of the nucleus.

2.3.1. Measurement of galaxy intensity profiles

Knowledge of the intensity profile of a Seyfert galaxy is important for two reasons. Firstly, the extra-nuclear component has to be subtracted from the total flux in order to study the radiation of the nucleus. Secondly, the morphological characteristics of the galaxy could be related to its nuclear activity. There are several components that contribute to the flux that we measure.

a) The nucleus:- the central source of the power in Seyfert galaxies is known to be confined to a relatively small region that appears to be stellar to the observer. In the derivation of the galaxy intensity profile the nucleus will be assumed to be point-like. Its measured intensity profile will however be that of a star, i.e. it is effectively a delta function convolved by the point

spread function, which describes the effect of the seeing. This is normally assumed to have a Gaussian shape. The measured intensity profile may therefore be steeper than the real profile.

Apart from the central power source there may still be other sources, such as H II regions, too close to the Seyfert nucleus to be resolved with ground based telescopes.

b) The host galaxy:- Seyfert galaxies are almost always spirals. It is expected that the intensity profiles of Seyfert galaxies resemble the profiles of normal spiral galaxies. Spiral galaxies can be described as a superposition of a disk component, which dominates the outer regions, and a bulge component. The intensity profile of the disk component is best described by an exponential law. In a set direction θ

$$I_{disk}(r) \propto \exp(-\alpha(\theta)r).$$

The bulge component intensity profile resembles that of elliptical galaxies, whose profiles can be approximated by an

$$I_{bulge}(r) \propto \exp(-\beta r^{1/4})$$

law (De Vaucouleurs and De Vaucouleurs, 1964).

c) Foreground stars:- the effect that foreground stars may have on the photometric measurements of some galaxies will be taken into account in the analysis in later chapters. In the discussion below, however, their possible contribution to the intensity profile will be ignored.

An important quantity in the study of galaxy intensity profiles is the surface magnitude μ, which is a function of position. It is defined as

$$\mu(r,\theta) = -2.5 \log(I(r,\theta)) ,$$

where $I(r,\theta)$ is the flux per square arcsecond (at a distance r from the nucleus in a direction θ from the major axis) relative to the flux of a zero magnitude object. The central surface magnitude (i.e., $\mu(0,\theta)$) is also written as μ_o.

In the direction θ the surface brightness at a distance $r>0$ is therefore given by the relation

$\mu(r) = -2.5 \log(I_{disk}(r)+I_{bulge}(r))$.

In the outer regions of spiral galaxies the disk component is dominant. It follows that at these radii

$\mu(r) = 1.086\ \alpha(\theta)r + \mu_o$.

For an inclined galaxy the observed flux per unit solid angle will be higher than for a galaxy seen face-on. The increased inclination will however also diminish the observed flux because of the greater obscuration. If one takes the case where this obscuration is negligible one derives that the true surface magnitude is given by

$\mu'(r) = 1.086\ \alpha' r + \mu_o'$

$\mu_o' = \mu_o - 2.5 \log(b/a)$

where α' is the value of α along the galaxy major axis, $\mu'(r)$ and μ_o' are the true face-on surface magnitudes and b/a is the ratio of the minor to major axis diameters.

The parameters α' and μ_o' are extensively used in morphological studies of galaxies. They can be measured relatively easily from plots of $\mu'(r)$ versus r. Freeman (1970) found that for spirals μ_o' is nearly always close to 21.65 in the B band.

From these parameters the total brightness of the disk component of a galaxy may be derived. From this the nuclear magnitude can be estimated by subtracting the disk contribution from the measured brightness, if one can assume that the bulge component is small.

Measuring the bulge component is far more problematic, as it is strongest near the nucleus, where it can be difficult to see if the nucleus is bright.

2.3.2. Redshift corrections

When doing photometry of two otherwise identical galaxies at different redshifts, the filters will sample different regions of the spectrum. The correction for this effect is known as the K correction. For early type spirals this correction has been estimated by Griersmith (1980) to be approximately equal to 2z mag for V, B-V and U-V.

For the nucleus the K correction is more complicated. It depends, amongst

other things, on nuclear reddening and on relative emission line strength. The correction to component with a power law distribution is given by $K = -2.5\log(1+z)^{1-\alpha}$ (Veron-Cetty and Veron, 1989). For typical non-thermal component α-values the power law K correction will be smaller than 0.05 mag for $z < 0.06$. The K correction for the power law resembling low-frequency tail of a 26000 K blackbody could become as large as 0.2 mag for $z = 0.06$. The colours are not be affected for a power law. Models by Kalinkov et al (1989) suggest that the K correction for Seyfert 1 galaxies at $z < 0.3$ is small.

2.3.3. Extinction

The observed luminosities of Seyfert nuclei are lower than the true luminosities because of obscuration by interstellar gas and dust. In order to obtain the true luminosities it is necessary to correct the observed magnitudes for interstellar extinction, both in our Galaxy and in the Seyfert galaxy itself. R, the ratio of the extinction in the V band, A_v, to the reddening, E(B-V), is close to 3.1 for most of the interstellar medium in the Galaxy. This value is however by not universal. Regions in our Galaxy associated with star formation have higher R values (e.g., The and Groot, 1983), possibly because of the destruction of interstellar grains by the strong UV-flux in the neighbourhood of hot stars. Dust grains in Seyfert galaxies may also be affected by their exposure to the intense high frequency radiation from the Seyfert nucleus. Indeed, Martin et al (1982) find the polarisation of the edge-on Seyfert IC 4329A to be anomalous and propose that this could be the result of an abnormal R-value. However until there is a reliable method for measuring R in Seyfert galaxies it seems best to assume a normal Galactic reddening law.

In this work optical fluxes are corrected using the Whitford reddening law (Miller and Mathews, 1972), while other fluxes and broad band magnitudes are dereddened using the extinction curve for our Galaxy given by Savage and Mathis (1979).

a) Extinction in our galaxy

The question of the amount of extinction in our galaxy is controversial. The maps of Burstein and Heiles (1982) predict the reddening E(B-V) from hydrogen column density measurements. According to these maps the galactic caps are free of extinction. De Vaucouleurs and Buta (1983), however, find the galactic

extinction law to be of the form E(B-V) = 0.065 cosec b from aperture photometry of normal galaxies, implying that E(B-V) = 0.065 at the galactic poles.

In this thesis the reddening values of Burstein and Heiles will be used. If instead a cosec b law had been adopted the derived fluxes would have been fractionally larger and the colours slightly bluer. The discrepancy would however have been small in comparison to the errors associated with the nuclear extinction determination and would not have significantly affected the results.

b) Extinction of a Seyfert nucleus by the outer galaxy

The extinctions of the Seyfert nuclei by their outer galaxies are difficult to estimate. Various methods have been proposed.

The Balmer decrement.- The ratio $H\alpha/H\beta$ can be measured with reasonable accuracy. Extinction has a stronger effect on $H\beta$ than on $H\alpha$. If the theoretical Balmer decrement is well known, the reddening and extinction can be calculated from this ratio. Because of the many unknowns and the physical complexities of Seyfert nuclei the value of the Balmer decrement in these nuclei is uncertain. Some authors have tried to use the theoretical recombination theory "case B" ratio $H\alpha/H\beta$ = 2.85 (see chapter 2.2). Observational work suggests that this ratio is larger in Seyfert galaxies. Ward et al (1988) estimate its value to be 3.5 by assuming that the X-ray luminosity is proportional to the Balmer line strength.

X-ray and $H\beta$ line flux.- The $H\beta$ line flux is caused by recombination (see chapter 2.2.2) and could therefore be assumed to be proportional to the ionising flux, of which the X-ray flux forms part. As X-rays are largely unaffected by dust the X-ray to $H\beta$ luminosity ratio is expected to be a function of reddening. Ward et al (1988) found a good correlation between $A(H\beta)$, the extinction at 4861 Å, and the logarithm of the ratio of X-ray-to-$H\beta$ flux. They proposed the following formula for estimating $A(H\beta)$ from the total X-ray luminosity between 2 and 10 keV (L_X) and the $H\beta$ line luminosity:

$$A(H\beta) = 2.5\log(L_X/L(H\beta)) - 3.675 \ .$$

A drawback of this method is that the X-ray and $H\beta$ luminosities, which are

usually variable, are seldom measured simultaneously.

Power law spectral index.- The continua of the nuclear flux component in Seyferts are often described to have the form of a power law ($F(\nu) \propto \nu^{-\alpha}$). By comparing the flux distribution of the observed spectra to such a power law it is possible to estimate the obscuration, provided that the spectral index α and the wavelength dependence of the extinction are known.

In the infrared such a method was developed by Glass (1981), who estimated the extinction of Seyfert galaxy nuclei from their positions on infrared two-colour diagrams. The optically bluest nuclei, thus presumably the ones with the lowest nuclear extinction, were clustered around the normal galaxy to α = 1.5 power law mixing line. Other nuclei had larger J-H values. An E(J-H) value could be estimated by determining the displacement from this mixing line. The biggest problem is that the infrared flux distribution often does not look like a power law. Thermal components may be superimposed on the power law continuum. Another problem is that, as A_v is almost ten times as large as E(J-H), any error in E(J-H) tranlates into an A_v error an order of magnitude larger.

For X-ray spectra gas obscures the intrinsic flux distribution, found to obey a power law with α = 0.7 (Mushotzky, 1982), only at energies lower than about 4 keV. The amount of obscuration is related to the column density of any gas in the line of sight. The gas column density can be converted to an extinction measurement A_v if one makes the assumption that the material obscuring the X-rays is the same material that is obscuring the optical flux and that this material has a solar gas-to-dust ratio appropiate to the solar neighbourhood. In practice the optical extinction values obtained in this manner have been higher than those obtained by other means (Mushotzky, 1982). This may indicate an abnormally high gas-to-dust ratio in Seyfert galaxies.

Interstellar lines.- The strength of interstellar lines is a good indicator of the amount of material in the line of sight. The 2200 A feature is often used to estimate the extinction. However, this line is not strong in Seyferts and is sometimes not seen at all (e.g., Wu et al, 1983). Calcium H and K lines and Sodium D lines are formed by interstellar dust and can be used to estimate the extinction, provided that the extinction is not too great, as these lines saturate quickly. They do however also occur in the spectra of normal stars and galaxies. As spectra of Seyfert nuclei are usually contaminated by starlight from the underlying galaxy one can expect difficulties in deblending

the interstellar lines from the stellar lines. There are two other problems associated with this method of reddening determination. Firstly, the measuring of the interstellar lines is in practice only possible in the highest signal-to-noise ratio spectra. Secondly, the physical conditions near a Seyfert nucleus (high temperature, X-rays) may have an effect on the interstellar medium in the host galaxy. The relationship between interstellar line strength and extinction determined for our own galaxy is not necessarily the same in Seyferts.

Forbidden line ratios.- Allen (1979) devised a method to calculate the reddening of an emission line region using [O II] and [S II] line fluxes. The ratios [S II] 6725/4072 Å and [O II] 3727/7325 Å are both dependent on n_e and T_e, and are therefore related. Reddening will increase the first and decrease the second of these ratios and the extinction may be estimated graphically from these (see Allen, 1979). However, as some of these lines are weak, this method can only be employed with high quality spectra. Other methods to determine the reddening from forbidden line ratios are reviewed by Grandi (1983).

More will be said about these methods in later chapters.

3. The Sample

The aim of this work was to study the variations of Seyfert galaxies. In order to do this a sample of candidates for observation had to be chosen. The results of the analysis of the sample can then later be generalised to all Seyfert galaxies.

3.1. Selection Criteria

29 objects were chosen according to the following criteria:-
- their classification as Seyfert galaxies had to be beyond doubt.
- they had to be in the southern hemisphere.
- they had to be bright enough to be observed with the Sutherland 0.5 m telescope (i.e., a limit of about V = 15).

Preference was given to Seyfert 1 galaxies because:-
- they are known to be the most likely to vary (see, e.g., Hamuy and Maza, 1987).
- the high luminosity of their nuclei makes the contamination of the nuclear light by starlight less of a problem.

Some of the galaxies chosen are well studied, while others are relatively unknown. They are listed in table 3.1 below. Also listed in the table are the adopted values of the interstellar reddening in our Galaxy in the direction of the Seyferts, derived from the radio maps of Burstein and Heiles (1982), and the distances of the objects, calculated with a Hubble constant of 50 km s^{-1} Mpc^{-1}.

Table 3.1. The galaxies investigated for this thesis, with their right ascention and declination (1950 epoch), their galactic co-ordinates, the galactic extinctions at these co-ordinates and their distances.

Name	R.A. h m s	Dec ° '	l °	b °	E(B-V) mag	d Mpc
ESO 12-G21	00 39 14	-79 30.7	303.6	-37.9	0.07	196.8
Ton S180	00 54 42	-22 38.0	138.5	-85.1	0.00	372.0
NGC 526a	01 21 37	-35 19.5	263.8	-79.5	0.00	113.4
Fairall 9	01 21 51	-59 04.0	295.1	-57.8	0.00	282.2
IC 1816	02 29 48	-36 53.5	243.4	-66.7	0.00	102.0
H 0307-730	03 07 40	-73 01.5	290.3	-40.8	0.03	167.9
Fairall 1116	03 49 54	-40 37.5	244.6	-50.7	0.00	348.8
NGC 1566	04 18 54	-55 03.5	264.3	-43.4	0.00	27.9
MCG -5-13-17	05 17 44	-32 42.5	236.0	-32.6	0.00	75.5
3A 0557-383	05 56 21	-38 20.2	244.5	-26.4	0.03	200.0
Fairall 265	06 56 19	-65 29.5	276.0	-24.0	0.08	179.8
NGC 2992	09 43 18	-14 05.7	249.7	+28.8	0.03	48.9[a]
MCG -5-23-16	09 45 30	-30 43.0	262.7	+17.2	0.10	48.0
ESO 438-G9	11 08 22	-28 13.7	277.5	+29.4	0.06	147.0
NGC 3783	11 36 34	-37 28.0	287.5	+22.9	0.09	60.7
H 1143-182	11 43 08	-18 10.6	281.9	+41.7	0.02	197.8
MCG -2-33-34	12 49 35	-13 08.6	303.2	+49.5	0.01	82.8[b]
ESO 323-G77	13 03 37	-40 08.7	306.0	+22.4	0.10	88.6
MCG -6-30-15	13 33 02	-34 02.7	313.3	+27.7	0.06	48.6
IC 4329A	13 46 28	-30 03.8	317.5	+30.9	0.07	97.1
I 1509-211	15 09 06	-21 07.0	341.6	+30.8	0.11	264.4
ESO 103-G35	18 33 22	-65 28.2	329.8	-23.2	0.06	80.0
Fairall 51	18 40 08	-62 25.0	333.2	-23.1	0.08	86.1
ESO 141-G55	19 16 57	-58 45.8	338.2	-26.7	0.05	220.6
NGC 6814	19 39 56	-10 26.6	29.4	-16.0	0.15	30.8[c]
NGC 6860	20 04 30	-61 15.0	335.8	-32.8	0.02	89.6
H 2106-099	21 06 28	-09 52.5	40.3	-34.9	0.06	160.8[d]
NGC 7213	22 06 12	-47 25.0	349.6	-52.6	0.00	35.4
MCG -2-58-22	23 02 07	-08 57.3	64.1	-58.8	0.02	284.8[e]

References for distance measurements:- a) Shuder (1980), b) Carter (1984), c) Ulrich (1971), d) Remillard et al (1986), e) Ward et al (1978), all others are from Fairall and Jones (1988).

3.2. Introduction of the Candidates chosen for Observation

This sub-chapter gives a brief description of the galaxies that were investigated in this work. It describes the discovery of the Seyfert nature of the galaxies. It is written from a semi-historical perspective and therefore only gives the most important characteristics of each object. A more detailed

discussion of each galaxy will follow in chapter 9.

The first Seyfert galaxies were discovered by accident. Seyfert (1943) was the first to recognise them to be a separate class of objects. *NGC 6814* was proposed to be a possible Seyfert in this original paper. Ulrich (1971) confirmed this when she found broad emission lines in its spectrum.

While investigators systematically observe more and more galaxies, they occasionally discover new Seyferts. *NGC 1566* is a large nearby galaxy whose relatively faint Seyfert 1 nucleus was first described by De Vaucouleurs and De Vaucouleurs (1961). *NGC 3783* is a Seyfert 1 galaxy with a peculiar theta shape. Page (1967) took the first spectrum of this object and discovered its strong emission lines. A spectrum of the galaxy *NGC 2992*, which forms an interacting pair with NGC 2993, was obtained by Burbidge et al (1972). What had aroused interest in this galaxy was Weedman 2, a blue, starlike object, possibly a quasar or a BL Lac object, which was thought to be associated with NGC 2992. *IC 4329A* was first described by Disney (1973) and has had much interest shown in it after its Seyfert 1 nucleus was claimed to be the nearest quasar. It is a highly inclined (i=90°) spiral with a dust lane obscuring its nucleus (Wilson and Penston, 1979). *NGC 7213* received some attention after a paper by Phillips (1979), in which the peculiarities of its spectrum were pointed out. Its emission lines are of a low excitation, but Hα has a very broad component. It is also a relatively strong radio source and its spectrum exhibits features of broad line radio galaxies as well as LINERs. Kollatschny and Fricke (1983) found a Seyfert 1 nucleus in *ESO 438-G9* during a study of nuclear activity in barred spirals. The bright Seyfert 1 galaxy *ESO 323-G77* was discovered during the course of a redshift survey of the Hydra-Centaurus supercluster (Fairall, 1986).

It was soon noted that active galaxies could be distinguished from normal galaxies by properties other than their nuclear spectra. The realisation that active galaxies often have strong blue continua prompted investigators to search the sky for blue objects in the hope of discovering new AGN's. Markarian's survey found over 1000 such blue galaxies. *Ton S180*, the most distant object in the sample, appears in a list of blue objects in the south polar cap region discovered at the Tonantzintla y Tacubaya observatories (Chavira, 1958). A spectrum published by Veron-Cetty and Veron (1986) shows this to be a Seyfert 1 galaxy.

The fact that Seyferts usually have bright starlike nuclei prompted Fairall to

investigate a sample of over 1000 compact and bright nucleus galaxies. This survey yielded a number of interesting objects. *Fairall 9 (=ESO 113-IG45)* and *Fairall 51 (=ESO 140-G43)* were reported to be Seyferts (type 1) in the first paper of a series (Fairall, 1977). Fairall 9 has since then become one of the most studied Seyferts, largely because of its very high luminosity, which is comparable to some of the fainter quasars. It is also strongly variable, it having faded by nearly two magnitudes between 1978 and 1984. *Fairall 265* is described as being a near Seyfert, with no obvious spiral structure (Fairall, 1980). Spectra discussed later reveal this to be a type 1 Seyfert. *Fairall 1116* is described in the last paper of the series (Fairall, 1988). Its Seyfert 1 nature was independently discovered during the Calan-Tololo objective prism survey (Maza et al, 1989), where the object was called *B25.01*.

The advent of X-ray astronomy led to the discovery of a large number of X-ray sources. Much work has been done in trying to identify the optical counterparts of these sources. In many cases investigators observing galaxies within the X-ray position error boxes discovered Seyfert galaxies, which were then assumed to be the source of the X-ray radiation. Major X-ray surveys were carried out by the Ariel V, UHURU and HEAO-1 satellites. The Seyfert 1's *ESO 141-G55*, *MCG -2-58-22* (discovered by Ward et al (1978)), *ESO 12-G21* (Hayes et al, 1980), *3A 0557-383* (Fairall et al, 1982) and the Seyfert 1.8 *NGC 526a* (Griffiths et al, 1979) are all X-ray sources detected by the Ariel V mission. The Seyfert 1 *MCG -6-30-15* and the Seyfert 2 *MCG -5-23-16* were identified by Pineda et al (1980) and Schnopper et al (1978) respectively after their X-ray discovery by UHURU. The more recent HEAO-1 mission greatly increased the known number of X-ray sources. *H 0307-730*, *H 1143-182* and *H 2106-099* were three of these that were found to be Seyfert 1's by Remillard et al (1986). H 1143-182 was independently discovered in the Calan-Tololo objective prism survey (Maza et al, 1989), as photometry of the object is included in a paper by Hamuy and Maza (1987), where it is called *J17.02*.

The Infrared Astronomical Satellite (IRAS) has surveyed the whole sky in four colour bands between 12 μm and 100 μm. At these wavelengths Seyferts are bright and usually have a relatively flat flux distribution which sometimes peaks near 60 μm. IRAS sources with such colours are rare. Investigators therefore suspected that sources with such spectra would include many new Seyferts. *MCG -2-33-34 (=IRAS 1249-131)* and *IRAS 1509-211* were two of the 54 infrared sources with flat spectra listed in IRAS circular 11. Carter (1984), Osterbrock and De Robertis (1985) and De Grijp et al (1985) independently discovered these to be Seyfert 1 galaxies. *IC 1816*, *MCG -5-13-17 (=ESO 362-*

G18) and *NGC 6860* were galaxies picked by their IRAS colours to be observed by De Grijp et al (1987). IC 1816 is a Seyfert 1.8 while the others are Seyfert 1's. They were independently discovered to be Seyferts by Maia et al (1987).

4. The CCD Imaging

All CCD observations were made with the 1.0 m telescope at the Sutherland field station of the South African Astronomical Observatory (SAAO). Details of the observing runs that led to this work are given in Table 4.1.

Table 4.1. The observation log.

Dates from	to	Observer
6 Feb 86	9 Feb 86	I. Glass
15 Jun 87	23 Jun 87	H. Winkler
29 Dec 87	4 Jan 88	"
21 Jun 88	27 Jun 88	"
23 Aug 88	27 Aug 88	"
20 Sep 88	27 Sep 88	"

4.1 The Instrument

The 1 m telescope works in a Cassegrain mode and has a focal ratio f/15.8. It was mounted with the charge coupled device (CCD) imaging camera.

The CCD chip used has an effective size of 512 by 320 pixels and was made by RCA. The pixel size corresponds to 0.39x0.39 arcsec, giving the chip a field size of 3 by 2 arcminutes. It is possible to add the amount of light detected in squares of 2x2 pixels and record these as one data point. This mode of recording, also known as prebinning, was used for the December 1987-January 1988 observing run. It reduces the frame size to 256 by 160 pixels. This loss resolution is compensated by the saving of storage space.

The readout noise is 73 e^- rms. One count is recorded by the electronics for every 11.5 electrons detected. The normal operating temperature is 160 K. On average the chip records about 300 cosmic ray events per hour. A few bad pixels and one dud column are present on the chip. An autoguider sensitive to guide stars down to 12.5 mag was used for tracking.

The chip readout is not linear if the number of photons detected per pixel is below a threshold of 500 e^- per pixel. For short exposure frames it is therefore necessary to artificially illuminate the chip in order to raise the number of counts to above the threshold (also called preflashing).

The photometry was made using standard $BV(RI)_c$ filters. The liquid U filter could have a slightly different transmission to a standard U glass filter

(Walker, 1984). The transformation of the U magnitudes to the standard system derived by Walker (1984) from E-region standard stars was adopted, although this is probably not optimal for objects with emission line spectra, as a photomultiplier and a CCD have dissimilar responses at short wavelengths. The quantum efficiency of the CCD chip is about 80% from 4500 Å to 8000 Å, but outside these limits the sensitivity drops fairly smoothly until it reaches zero below 3400 Å and above 10000 Å.

4.2 Imaging and Photometry

These observations were made with the 1 m telescope. A list of all the CCD images recorded is given in table 4.2. Three sets of flatfields for each filter were obtained during an observing week. This was done by making short exposures of the twilight sky. On photometric nights E- region standard stars from the list of Menzies et al (1989) were observed regularly throughout the night. Because of the relatively long time required to make a standard star observation only a limited number of these could be observed per night. Due to the short exposure times these images had to be preflashed. In order to be able to correct for this long preflash frames were recorded as well.

As the blue-sensitivity of the chip is very poor, the integration times in the U band had to be very long. Even after that, the number of counts recorded were usually quite low. To compound this, many of the observations had to be done in the presence of a bright moon, whose effects are felt particularly severely at the shorter wavelengths. Consequently, the U magnitudes are prone to relatively large errors.

Observations could be made in non-photometric conditions if there were other stars on the frame, provided that the brightness of these stars could be determined from frames taken in photometric conditions.

Table 4.2. Log of the CCD Observations.

Date	integration time (s)					photom?	moon
	U	B	V	R	I	UBVRI	phase
ESO 12-G21							
22-09-88	2400	1500	1200	1200	1200	YYYYY	.78
Ton S180							
24-06-88	2100	-	1200	1000	600	Y NNY	-
21-09-88	1500	1500	1000	800	800	YYYYY	.67
NGC 526a							
25-06-88	2400	1800	1200	1000	1000	YYYYY	-
23-09-88	-	1500	1200	1000	1000	YYYY	.94
Fairall 9							
6-02-86	-	300	300	-	-	YY	-
19-06-87	2400	-	-	-	1200	Y Y	.53
22-06-87	-	1500	1200	-	1200	NN N	.22
2-01-88	1000	150	150	100	150	YYYYY	.99
23-06-88	2400	1400	1200	900	1000	NNNNN	-
26-08-88	2400	1200	1000	900	900	NNNNN	.96
21-09-88	1800	900	500	300	300	YYYYY	.78
IC 1816							
2-01-88	1200	800	600	750	400	YYYYY	.99
25-08-88	-	-	513	1000	900	NNN	.90
24-09-88	2400	1500	1200	900	900	YYYYY	.94
H 0307-730							
30-12-87	1200	500	500	500	500	YYYYY	.83
25-09-88	-	1800	1200	1000	1000	NYYN	.99
Fairall 1116							
30-12-87	800	400	300	400	500	YYYYY	.83
26-08-88	2400	1500	1200	1000	1000	NNNNN	.96
21-09-88	2000	1500	1200	1000	1000	YYYYY	.67
NGC 1566							
6-02-86	-	1200	600	-	-	YY	-
3-01-88	1200	400	400	250	250	YYYYY	.99
24-09-88	-	1500	1200	-	-	YY	.94
25-09-88	2400	-	-	800	800	N NN	.99
MCG -5-13-17							
31-12-87	800	400	300	400	400	YYYYY	.83
23-09-88	1800	1200	1200	1000	1000	YYYYY	.87
3A 0557-383							
31-12-87	-	500	400	400	400	YYYY	.83
22-09-88	-	1500	1200	-	-	YY	.78

Table 4.2. (continued)

Date	integration time (s) U	B	V	R	I	photom? UBVRI	moon phase
Fairall 265							
3-01-88	-	750	600	400	400	YYYY	1.0
NGC 2992							
7-02-86	-	1200	600	-	600	YY Y	-
MCG -5-23-16							
9-02-86	-	600	600	600	600	YYYY	-
31-12-87	-	600	600	500	500	YYYY	T?
ESO 438-G9							
23-06-88	2400	1500	1200	-	-	YYY	.62
NGC 3783							
6-02-86	600	600	600	600	600	YYYYY	-
20-06-87	1500	1000	800	600	600	YYYYY	-
3-01-88	-	250	250	150	200	NNNN	.99
22-06-88	1800	800	500	500	600	NNNNN	.53
H 1143-182							
30-12-87	700	-	800	400	400	Y YYY	T
31-12-87	-	500	-	-	-	Y	T
21-06-88	-	1800	1800	-	-	YY	.43
ESO 323-G77							
18-06-87	1800	-	-	-	250	Y Y	-
21-06-87	-	1500	1200	300	-	YYY	-
MCG -6-30-15							
8-02-86	-	400	400	-	-	YY	-
22-06-87	2120	-	1000	750	750	N NNN	-
24-06-88	2400	1500	900	600	600	YYYYY	.72
IC 4329A							
8-02-86	-	400	400	-	-	YY	-
21-06-87	-	1800	900	500	500	YYYN	-
22-06-88	-	-	1200	1000	-	NN	-
23-06-88	2400	1200	400	-	1000	YYY Y	.62
IRAS 1509-211							
20-06-87	-	-	1200	1200	1200	YYY	-
21-06-87	2400	1800	-	-	-	NN	-
21-06-88	2400	2400	1800	-	-	YYY	.43
22-06-88	-	-	-	1000	1200	NN	.53
26-08-88	-	1500	1200	-	-	YY	1.0
ESO 103-G35							
22-06-87	1800	1200	1200	1000	1000	NNNNN	-
24-06-88	2400	1500	1200	900	900	NNNNN	.67
25-08-88	-	1200	1000	900	900	YYYY	.96

Table 4.2. (continued)

Date	integration time (s)					photom?	moon
	U	B	V	R	I	UBVRI	phase
Fairall 51							
21-06-87	2400	2400	1500	1000	1000	YYYYY	-
22-06-88	2400	1800	1200	600	600	NNNNN	.53
25-08-88	2400	1200	1200	900	900	YYYYY	.96
22-09-88	-	1800	1200	1000	1000	YYYY	.87
ESO 141-G55							
19-06-87	2400	2400	1366	-	1200	YYN Y	.53
21-06-87	-	-	1500	-	1000	Y Y	.31
22-06-87	-	1000	-	1200	-	N N	-
23-06-88	2400	1500	900	600	750	NNNNN	-
23-08-88	600	2400	1200	1000	600	NNNNN	.82
20-09-88	1800	1000	800	600	600	YYYYY	.67
NGC 6814							
23-06-87	-	1500	1000	-	-	NN	-
22-06-88	-	1500	800	600	800	YYYY	-
23-09-88	-	1600	1200	800	750	YYYY	.94
NGC 6860							
21-09-88	2400	1500	1200	1650	750	YYYYY	.78
H 2106-099							
24-06-88	2400	1200	800	-	-	YYY	-
25-06-88	-	-	800	800	800	YYY	.72
24-09-88	2400	1800	1200	1000	1000	YYYYY	.99
NGC 7213							
21-06-87	1800	1200	1000	500	500	YYYYY	.31
23-06-88	-	1200	750	500	500	NNNN	-
23-09-88	-	1200	750	500	500	YYYY	.94
MCG -2-58-22							
23-06-87	2400	1500	1200	-	-	YYY	.14
22-06-88	2400	1800	1200	1200	1200	YYYYY	-
20-09-88	1800	1200	900	500	600	YYYYY	.67

Notes:- The first column gives the date of the observation. Columns 2-6 give the integration times for the U, B, V, R and I exposures. Column 7 describes if the conditions were photometric (Y) or not photometric (N) during the observation with the U, B, V, R and I filters respectively. The last column gives the phase of the moon, if it was above the horizon at the time of the observation.

4.3 Reductions

The CCD images were reduced on the SAAO computer. First of all, the images had to be corrected for differences in sensitivity between individual pixels by dividing each image by a normalised flatfield measured with the same filter. Where necessary the light contribution from the preflash had to be subtracted. The zero points were determined from the E-region standard stars. The colour and extinction equations of Walker (1984) were used. The extinction at Sutherland is known to be relatively stable. However for one particularly dusty night (24 June 1988) it was necessary to calculate separate extinction equations.

There are two major problems when calculating the magnitudes from the CCD photometry. One is that numerous flaws (bad pixels or cosmic ray events) are usually found on the image. Removing these computationally from a frame can be difficult, even if done interactively. Flaws will often be missed, particularly when these coincide with extended objects like galaxies. The second problem arises out of the difficulty in determining the sky background radiation. It is often almost impossible to define the outer edges of galaxies. The faint, outermost regions can easily be mistaken for sky background, especially if the images were recorded in bright moon conditions.

The position angle of the galaxy's major axis and the ratio of minor to major axis length, b/a, were estimated from the CCD images. A program was written for determining the galaxy intensity profiles in order to extract the nuclear magnitudes and extra-nuclear components. It worked as follows. The CCD frame was divided into blocks of 8x8 pixels. For each block the mean pixel value and the scatter of individual pixel values around this mean were calculated. The scatter would be particularly large if the block coincided with stars, galaxies, cosmic ray events or bad pixels. Pixels responsible for the large scatter could be identified. If the large scatter was because of the effect of three or less pixels then these would be assumed to be faults. Blocks that showed significant scatter for more than three pixels were displayed. Such blocks contained either stars and galaxies or numerous faulty pixels and cosmic rays. The last two could then be flagged and excluded from further analysis.

Blocks representing the sky background were expected to have the lowest internal scatter. Such low-scatter blocks within an annulus centered on the galaxy were used to determine the sky background for that galaxy by fitting a

least square plane to them. After that the sky background could be subtracted and the flux of the object measured. The next step was to measure the flux within successive annuli centered on the nucleus. The same colour and extinction equations as for the standard stars were used for this. These data will be used in chapter 5 to convert all aperture photometry to one standard size (20"). After this the magnitude through a 20" circular aperture could be calculated. All magnitudes and colours are listed in table 4.4. Some of these could not be measured because the count rate was too low. The magnitudes of the brighter stars on each frame were also calculated. These were used to calibrate some of the frames recorded in non-photometric conditions.

The images also enable one to derive the brightness and intensity profile of the underlying galaxy outside the Seyfert nucleus. This was done by measuring the average surface V-magnitudes for successive circular annuli centred on the nucleus with diameters ranging from 8" to 40". Although many of the galaxies are not observed face-on, the relationship between this average surface magnitude and the distance from the centre is still approximately linear. The central surface magnitude of the disk component μ_o was derived by extrapolating this relationship. The V-magnitude of the disk component of the galaxy could then be calculated with the formula

$$m = \mu_o + 5 \log \alpha^* - 2.175 \ ,$$

which follows from the formulae given in chapter 2, where α^* is the measured slope of the μ_o vs r graph. The colours of the galaxies were derived from the flux differences between the B, V and I images between 4 and 20" from the nucleus. The morphological parameters of each galaxy are listed in table 4.3. α^* is given in units of mag arcsec^{-1}.

Table 4.3. The parameters describing the host galaxy.

Name	b/a	α^*	μ_o(V)	V	B-V	V-I
ESO 12-G21	0.6	0.39	19.93	15.71	0.65	1.22
Ton S180	1.0*	0.43	20.66	16.64	-	-
NGC 526a	0.8	0.33	19.92	15.35	0.96	1.15
Fairall 9	0.7	0.32	20.24	15.79	0.89	1.21
IC 1816	1.0	0.19	20.09	14.26	0.88	1.18
H 0307-730	1.0	0.32	20.29	15.63	0.94	1.15
Fairall 1116	0.5	0.39	20.16	15.94	0.84	1.23
NGC 1566	1.0	0.10	19.15	12.06	0.97	1.27
MCG -5-13-17	1.0	0.24	19.38	14.14	0.68	1.04
3A 0557-383	0.25	0.42	20.14	16.08	-	-
Fairall 265	0.6	0.41	19.77	15.64	0.71	0.85
NGC 2992	0.3	0.14	19.57	13.22	-	-
MCG -5-23-16	0.35	0.22	19.80	14.33	1.04	1.29
ESO 438-G9	0.6	0.26	20.25	15.03	0.76	-
NGC 3783	0.9	0.12	20.10	13.41	1.01	1.31
H 1143-182	1.0	0.33	20.13	15.52	-	0.66
ESO 323-G77	1.0	0.20	19.95	14.31	0.98	1.62
MCG -6-30-15	0.5	0.36	18.45	14.05	0.93	1.16
IC 4329A	0.25	0.17	20.39	14.41	-	1.52
I 1509-211	1.0*	0.26	21.19	16.07	-	-
ESO 103-G35	0.3	0.21	20.63	15.02	1.08	1.32
Fairall 51	0.5	0.21	20.62	15.02	1.03	1.29
ESO 141-G55	1.0	0.33	19.90	15.34	0.65	1.09
NGC 6814	1.0	0.10	20.42	13.27	1.10	1.51
NGC 6860	0.6	0.20	19.40	13.69	1.01	1.18
H 2106-099	1.0*	0.20	21.14	15.52	-	-
NGC 7213	1.0	0.15	18.00	11.72	0.97	1.27
MCG -2-58-22	1.0	0.27	20.19	15.19	-	-

The galaxy component may then be subtracted from the total intensity profile, so to derive the nuclear component. In order to do this it was assumed that the galaxy profile at the nucleus can be described by the same exponential law found further out.

Table 4.4. 20" aperture photometry from the CCD Observations.

Date	V	B-V	U-B	V-R	V-I
ESO 12-G21					
22-09-88	14.44	0.67	-0.22	0.53	1.13
Ton S180					
24-06-88	14.32	0.18	-0.97	0.20	0.44
21-09-88	14.37	0.18	-0.90	0.22	0.47
NGC 526a					
25-06-88	14.48	1.01	-	0.55	1.19
23-09-88	14.55	1.03	-	0.59	1.20
Fairall 9					
6-02-86	14.13	0.57	-	-	-
22-06-87	13.66	0.40	-0.90	-	0.79
2-01-88	13.66	0.35	-0.86	0.41	0.80
23-06-88	13.76	0.48	-0.87	0.40	0.91:
26-08-88	13.77	0.46	-0.86	0.38	0.87:
21-09-88	13.72	0.40	-0.82	0.39	0.82
IC 1816					
2-01-88	13.95	0.91	-	0.55	1.16
24-09-88	13.91	0.89	-	0.50	1.12
H 0307-730					
30-12-87	14.90	0.77	0.01	0.53	1.09
25-09-88	14.82	0.74	-	0.49	1.07
Fairall 1116					
30-12-87	14.72	0.51	-0.68	0.45	0.95
26-08-88	14.59	0.50	-	0.42	0.90
21-09-88	14.71	0.47	-0.64	0.41	0.89
NGC 1566					
6-02-86	12.39	0.95	-	-	-
3-01-88	12.33	0.94	0.26	0.62	1.29
25-09-88	12.30	0.97	-	0.62	1.27
MCG -5-13-17					
31-12-87	13.34	0.61	-0.33	0.50	0.97
23-09-88	13.25	0.56	-0.35	0.44	0.92
3A 0557-383					
31-12-87	15.06	1.08	-	0.83	1.43
22-09-88	15.00	1.05	-	-	-
Fairall 265					
3-01-88	14.54	0.57	-0.36	0.52	1.02
NGC 2992					
7-02-86	13.45	1.07	-	-	1.47
MCG -5-23-16					
9-02-86	13.54	1.00	-	0.69	1.34
31-12-87	13.56	1.07	-	0.62	1.33

Table 4.4. (continued)

Date	V	B-V	U-B	V-R	V-I
ESO 438-G9					
23-06-88	14.02	0.53	-0.36	-	-
NGC 3783					
6-02-86	12.92	0.53	-0.82	0.63	1.06
20-06-87	13.16	0.73	-0.47	0.65	1.18
3-01-88	13.07	0.59	-0.58	0.62	1.12
22-06-88	13.07	0.66	-	0.60	1.15:
H 1143-182					
30-12-87	14.22	0.52	-1.04	0.35	0.63
21-06-88	14.43	0.57	-	-	-
ESO 323-G77					
21-06-87	13.29	0.88	0.04	0.65	1.33
MCG -6-30-15					
8-02-86	13.42	0.95	-	-	-
24-06-88	13.40	0.94	0.24	0.62	1.23
IC 4329A					
8-02-86	13.59	1.05	-	-	-
21-06-87	13.68	1.14	0.65	0.85	1.54
23-06-88	13.56	1.14	0.58	0.86	-
IRAS 1509-211					
20-06-87	14.94	1.15	-	0.64	1.28
21-06-88	14.84	0.92	-	0.59	1.26
26-08-88	14.90	0.95	-	-	-
ESO 103-G35					
22-06-87	14.30	1.04	-	0.62	1.25
24-06-88	14.31	1.05	-	0.62	1.27
25-08-88	14.39	1.09	-	0.64	1.33
Fairall 51					
21-06-87	14.18	0.84	-0.09	0.68	1.26
22-06-88	14.10	0.78	-	0.65	1.25
25-08-88	14.18	0.79	0.07	0.65	1.30
22-09-88	14.19	0.85	-	0.67	1.25
ESO 141-G55					
19-06-87	13.90	0.38	-0.82	0.46	0.88
23-06-88	14.19	0.56	-0.70	0.49	0.94
20-09-88	13.99	0.38	-0.84	0.45	0.87
NGC 6814					
23-06-87	13.60	1.12	-	-	-
22-06-88	13.52	1.17	-	0.73	1.50
23-09-88	13.56	1.19	-	0.74	1.54

Table 4.4. (continued)

Date	V	B-V	U-B	V-R	V-I
NGC 6860					
21-09-88	13.51	0.90	0.15	0.58	1.21
H 2106-099					
24-06-88	14.34	0.64	-0.69	0.57	1.12
24-09-88	14.34	0.58	-0.70	0.58	1.16
NGC 7213					
21-06-87	11.81	1.00	0.51	0.62	1.30
23-09-88	11.82	1.03	-	0.60	1.28
MCG -2-58-22					
23-06-87	14.45	0.70	-0.59	-	-
22-06-88	14.42	0.71	-0.66	0.58	1.02
20-09-88	14.40	0.70	-0.61	0.55	0.99

5. UBVRI Aperture Photometry

The 0.5 m telescope at Sutherland was used for all observations. Details of the observing runs are listed in table 5.1.

Table 5.1. The UBVRI aperture photometry observation log.

Dates from	to	Seeing (") Tu	We	Th	Fr	Sa	Su	Mo	Observer
31 Aug 86	2 Sep 86	-	-	-	-	-	2-3	1-2	H.Winkler
27 Jan 87	3 Feb 87	3	-	2-5	2-3	1	3	3	"
24 Feb 87	2 Mar 87	1	3	4	2	2-6	3	-	"
31 Mar 87	7 Apr 87	2	2-5	1-2	-	3-4	2-5	3	"
19 Aug 87	25 Aug 87	-	2	2	2-4	-	4	3-4	"
25 Aug 87	30 Aug 87	2-3	2	-	1-2	4	-	-	"
13 Oct 87	20 Oct 87	2	2-3	2	2	1-2	8	6	"
17 Nov 87	24 Nov 87	2-4	3	3	1-2	1-2	2	3	"
17 Feb 88	23 Feb 88	-	1-2	-	-	2-3	2-3	1-2	"
4 May 88	10 May 88	-	5	1-2	2	1-2	2	2	"
1 Nov 88	8 Nov 88	1-2	-	3	1-2	-	2	-	"
6 Dec 88	13 Dec 88	2-3	-	-	-	4	1-2	1-3	I.Glass
3 Jan 89	10 Jan 89	1-2	1	1-2	1-2	2-3	3	2	J.Sp-Jones
7 Feb 89	14 Feb 89	2	1-2	2-4	-	-	2-4	2-3	H.Winkler
7 Mar 89	14 Mar 89	1.5	-	-	-	-	5?	-	I.Glass
28 Mar 89	3 Apr 89	-	-	-	2-4	1-2	2-3	2	F.Van Wyk
23 May 89	30 May 89	-	-	-	-	2-3	1-3	1-3	D.Buckley
30 May 89	6 Jun 89	3	-	-	-	2	2-3	2-3	H.Winkler
27 Jun 89	4 Jul 89	2-3	-	-	-	3-5	-	3-4	J.Sp-Jones
25 Jul 89	1 Aug 89	-	-	2-3	2-3	2-3	-	-	H.Winkler
29 Aug 89	5 Sep 89	-	2-6	-	1-2	-	-	-	I.Glass
26 Sep 89	3 Oct 89	1-2	1-3	-	2-3	-	-	-	H.Winkler
24 Oct 89	31 Oct 89	1-2	-	-	-	-	-	-	I.Glass

5.1 The Instrument

The SAAO 0.5 m telescope is a reflector that works in the Cassegrain mode. It is fitted out with the SAAO modular photometer. This instrument uses a Hamamatsu GaAs tube, whose sensitivity extends from below 3500 Å to above 9000 Å. The observations were made with a set of Johnson U, B and V filters and Cousins R and I filters. In order to be able to see faint objects (such as the galaxies investigated in this work) a VARO image intensifying tube needed to be used. A set of eight circular apertures with diameters ranging from 10" to 90" are available. It is possible to illuminate the field of view in order to see the outline of the aperture, something of crucial importance as the galaxies needed to be placed into the exact centre of the aperture.

5.2 The Observations

The main reason for making the photometric measurements was to record the luminosity changes of the Seyfert nuclei. In order to do this one would ideally like to use an aperture small enough to only include the Seyfert nucleus and exclude the extra-nuclear parts of the galaxy. There are practical problems that make this difficult. It is not easy to position a star at the exact centre of the aperture. It is estimated that the error in centring of a bright star is of the order of 2 arcseconds. For a galactic nucleus, which is often faint and fuzzy, this error, which results in a net loss of flux, could be larger.

An additional source of light loss can be poor quality seeing. This affects galaxies more than stars because light from the outer galaxy falls close to the aperture edge. In retrospect it can be said that seeing errors are small compared to other errors provided that the seeing is better than 3". Repeated observations made during a week usually agree very well with each other. This showed that the errors associated with a particular measurement were about 0.04 mag in V and U-B and 0.03 in the other colours.

Three circular apertures were used, with diameters of 15, 20 and 30 arcseconds. The 15" aperture was only used in good seeing. The problems described above make the use of smaller aperture sizes prohibitive. Therefore there are some galaxies for which the extra-nuclear flux dominates the total flux, even when using a 15" diameter aperture.

The change in the sky transparency was monitored by making regular observations of E-region standard stars from the list of Menzies et al (1989). Observations were also carried out of stars from the SAO catalogue positioned within 1° of many of the Seyferts studied in this thesis. They were observed repeatedly over a period of months to check their stability. The magnitudes and colours determined for these have been published elsewhere (Winkler, 1989, and Winkler et al, 1990). In all but the earliest observations a Seyfert galaxy was measured in conjunction with two of these local standards. Standard stars were always observed through the 30" aperture.

The integration times used were as follows. Standard stars were observed for 10 s in V, R and I, 10 s or 20 s in B, and 20 s or 30 s in U. The sky brightness was measured at a clear-looking patch within about 5′ of the star immediately after the star. The integration times used for this were 5 s or 10

s in B, V, R and I and 10 s in U. For galaxies brighter than V = 14 the sky was first measured for 30 s in U and B and 15 s in V, R and I a few arcminutes to the east of the object. Then two sets of integrations of the object were made, each with 60 s in U, 30 s in B and 15 s in V, R and I. The object was recentred after the first set. The sequence was finished with another measurement of the sky (same integration times) a few arcminutes to the west of the object. For objects fainter than V = 14 the same procedure was followed, but the integration times were longer (30 s for all sky measurements and the object VRI observations, and 60 s for the object U and B integrations).

5.3 The Reductions

Primary reductions were made by staff of the SAAO in Cape Town. This included applying colour and extinction equations and dead time corrections. All these are known very accurately as a result of the intensive standard star observations carried out with the same system and telescope by astronomers at the SAAO. Variations in the zero points due to the changing of the aperture were determined by comparing the observations of stars through different aperture sizes. In a few cases for which no such measurements were done it was still possible to make this correction by taking into account the seeing on the night in question. An inspection of the photometric data shows that for seeing of 2" or less the corrections are -0.01 and -0.02 in the 20" and 15" apertures respectively. For seeing of 2-4" they are -0.02 for the 20" and -0.04 for the 15" apertures.

The results of the UBVRI photometry are presented in table 5.2. The values given normally represent weekly averages, with the errors calculated from the scatter in the individual measurements. The Julian days given for each point are therefore also averages. Within a week there was generally no sign of variability greater than the typical measurement errors. If only one observation was obtained during the week, the error was assumed to be $\sigma_V = \sigma_{UB} = 0.04$ and $\sigma_{BV} = \sigma_{VR} = \sigma_{VI} = 0.03$.

A literature search has been made in order to collect more photoelectric measurements of the galaxies studied here. These additional magnitudes and colours are listed in tables A1 and A2 in the appendix.

All photometric measurements listed in table 5.2 were converted to a 20"

aperture using the intensity profiles derived from the CCD images. The same was done for the data from tables A1 and A2, provided that the aperture sizes were known and the errors of measurement were less than 0.08 magnitudes. If no CCD image was available with a particular filter then only the magnitudes measured with a 20" aperture were used for further analysis.

The 20" aperture light curves of all objects for the period February 1986 to October 1989 are shown in figure 5.1.

The magnitudes may be converted to fluxes using a calibration described more fully later. Figure 5.2 shows the fluxes in various filters plotted against each other for four Seyfert galaxies with extensive photometric coverage. Different symbols are used to show the data gathered by different groups of investigators. It will later be shown that fluxes vary in such a way that the relationship between flux measurements in different filters is linear, a fact first noted by Choloniewski (1981).

The plots displayed in figure 5.2 therefore show that the aperture photometry made in this work (marked by squares in the figure) is in very good agreement with other studies. The results of the CCD observations (marked by triangles) are usually of good quality, although some of the I-band fluxes appear to disagree with the other points. Note that the U and I fluxes measured bu Hamuy and Maza (1987), marked as crosses, seem to be systematically higher than other fluxes observed in these wavebands, although the discrepancy is too small to affect the light curves in any significant way.

Table 5.2 UBVRI aperture photometry. ϕ is the aperture diameter, measured in arcseconds.

HJD 244+	log(ap) "	V	σ_V	B-V	σ_{BV}	U-B	σ_{UB}	V-R	σ_{VR}	V-I	σ_{VI}
ESO 12-G21											
7033	1.18	14.41	02	0.63	03	-.38	04	0.51	03	1.07	03
7033	1.30	14.31	04	0.68	03	-.36	04	0.51	03	1.07	03
7033	1.48	14.25	02	0.67	03	-.34	04	0.49	03	1.05	03
7084	1.30	14.47	01	0.68	01	-.30	02	0.54	02	1.11	01
7084	1.48	14.39	02	0.69	02	-.18	05	0.55	02	1.08	02
7122	1.18	14.54	04	0.74	03	-.35	04	0.54	03	1.17	03
7122	1.30	14.46	01	0.70	01	-.26	01	0.53	02	1.08	03
7122	1.48	14.40	02	0.68	02	-.20	02	0.55	02	1.14	02
7470	1.18	14.50	04	0.64	03	-.32	04	0.51	03	1.06	03
7470	1.30	14.39	04	0.69	03	-.33	04	0.48	03	1.06	03
7470	1.48	14.36	04	0.57	03	-.24	04	0.51	03	1.12	03
7507	1.18	14.50	04	0.60	03	-.33	04	0.54	03	1.10	03
7507	1.48	14.37	04	0.59	03	-.20	04	0.59	03	1.14	03
7679	1.30	14.50	01	0.68	02	-.28	02	0.56	01	1.11	01
7681	1.18	14.61	04	0.65	03	-.25	04	0.56	03	1.12	03
7735	1.18	14.58	04	0.65	03	-.26	04	0.52	03	1.08	03
7735	1.48	14.43	04	0.68	03	-.21	04	0.56	03	1.09	03
7799	1.30	14.54	04	0.73	03	-.31	04	0.51	03	1.12	03
7799	1.48	14.42	04	0.66	03	-.21	04	0.53	03	1.15	03
7824	1.30	14.51	04	0.67	03	-.20	04	0.58	03	1.17	03
Ton S180											
7123	1.48	14.48	04	0.24	03	-.86	04	0.24	03	0.48	03
7467	1.18	14.59	04	0.17	03	-.86	04	0.27	03	0.48	03
7467	1.48	14.46	04	0.23	03	-.87	04	0.18	03	0.42	03
7507	1.30	14.46	04	0.17	03	-.84	04	0.24	03	0.51	03
7736	1.48	14.36	04	0.21	03	-.89	04	0.20	03	0.44	03
7737	1.30	14.36	01	0.20	02	-.87	02	0.19	03	0.45	02
7771	1.18	14.36	04	0.19	03	-.86	04	0.19	03	0.43	03
7771	1.30	14.37	04	0.20	03	-.87	04	0.18	03	0.40	03
7796	1.18	14.42	04	0.19	03	-.86	04	0.22	03	0.46	03
7796	1.30	14.42	04	0.21	03	-.88	04	0.20	03	0.48	03
7824	1.30	14.43	04	0.25	03	-.89	04	0.18	03	0.45	03
NGC 526a											
7034	1.30	14.42	04	1.00	03	0.24	04	0.55	03	1.17	03
7034	1.48	14.26	04	0.96	03	0.21	04	0.58	03	1.15	03
7122	1.48	14.25	01	0.98	03	0.21	02	0.55	02	1.15	02
7507	1.48	14.23	01	0.97	02	0.19	04	0.55	01	1.14	03
7531	1.30	14.44	04	1.06	03	0.16	04	0.57	03	1.18	03
7531	1.48	14.26	04	1.00	03	0.13	04	0.57	03	1.18	03
7736	1.30	14.45	04	1.00	03	0.15	04	0.53	03	1.12	03
7736	1.48	14.24	04	0.97	03	0.15	04	0.50	03	1.11	03
7769	1.30	14.43	04	1.01	03	0.19	04	0.56	03	1.12	03
7769	1.48	14.23	04	0.98	03	0.18	04	0.54	03	1.14	03
7824	1.30	14.45	04	1.05	03	0.19	04	0.59	03	1.17	03

Table 5.1. (continued)

HJD 244+	log(ap) "	V	σ_V	B-V	σ_{BV}	U-B	σ_{UB}	V-R	σ_{VR}	V-I	σ_{VI}
Fairall 9											
6675	1.18	13.83	05	0.43	05	-.88	05	0.41	05	0.76	05
6675	1.30	13.77	05	0.44	04	-.84	05	0.42	04	0.77	04
6675	1.48	13.70	02	0.50	02	-.76	05	0.42	02	0.87	02
6827	1.48	13.65	03	0.46	03	-.80	04	0.42	03	0.84	03
7036	1.18	13.77	03	0.39	03	-.90	04	0.37	03	0.77	03
7036	1.48	13.64	03	0.44	03	-.82	04	0.44	03	0.92	03
7083	1.18	13.78	03	0.35	03	-.91	04	0.39	03	0.78	03
7083	1.30	13.66	03	0.40	03	-.87	04	0.39	03	0.80	03
7083	1.48	13.60	03	0.41	03	-.82	04	0.44	03	0.89	03
7122	1.18	13.69	03	0.34	03	-.90	04	0.37	03	0.75	03
7122	1.30	13.64	03	0.36	03	-.89	04	0.38	03	0.79	03
7122	1.48	13.54	03	0.41	03	-.85	04	0.42	03	0.82	03
7469	1.18	13.79	01	0.41	02	-.89	02	0.39	01	0.81	02
7469	1.30	13.72	02	0.42	03	-.87	02	0.39	03	0.80	02
7469	1.48	13.61	01	0.49	02	-.85	01	0.39	02	0.84	01
7507	1.18	13.88	01	0.45	02	-.86	01	0.39	02	0.81	02
7507	1.48	13.72	02	0.51	02	-.79	03	0.46	01	0.94	02
7530	1.18	13.79	04	0.35	03	-.86	04	0.43	03	0.79	03
7530	1.30	13.71	04	0.43	03	-.87	04	0.41	03	0.84	03
7530	1.48	13.63	04	0.46	03	-.83	04	0.40	03	0.86	03
7567	1.48	13.69	04	0.53	03	-.78	04	0.41	03	0.88	03
7681	1.18	13.89	04	0.46	03	-.86	04	0.37	03	0.76	03
7681	1.30	13.85	04	0.46	03	-.83	04	0.44	03	0.84	03
7709	1.48	13.67	04	0.47	03	-.78	04	0.40	03	0.89	03
7735	1.30	13.81	04	0.40	03	-.83	04	0.43	03	0.84	03
7735	1.48	13.71	04	0.46	03	-.82	04	0.44	03	0.92	03
7769	1.18	13.88	04	0.42	03	-.88	04	0.42	03	0.87	03
7769	1.48	13.69	04	0.47	03	-.78	04	0.43	03	0.90	03
7770	1.30	13.77	03	0.47	05	-.84	01	0.42	02	0.85	03
7799	1.30	13.88	04	0.50	03	-.82	04	0.45	03	0.88	03
7799	1.48	13.70	04	0.57	03	-.79	04	0.40	03	0.91	03
7824	1.30	13.81	04	0.48	03	-.82	04	0.42	03	0.85	03
IC 1816											
6827	1.48	13.62	02	0.81	02	0.22	04	0.54	02	1.11	04
7028	1.18	14.26	04	0.93	03	0.19	04	0.52	03	1.13	03
7028	1.48	13.57	04	0.86	03	0.17	04	0.50	03	1.07	03
7122	1.48	13.61	01	0.86	01	0.13	01	0.52	02	1.10	02
7507	1.18	14.26	01	0.94	02	0.21	04	0.54	01	1.14	02
7507	1.48	13.63	04	0.82	03	0.17	04	0.55	03	1.15	03
7736	1.30	13.92	04	0.90	03	0.18	04	0.55	03	1.08	03
7736	1.48	13.57	04	0.87	03	0.15	04	0.51	03	1.11	03
7771	1.30	13.93	04	0.90	03	0.19	04	0.51	03	1.06	03
7771	1.48	13.60	04	0.83	03	0.15	04	0.50	03	1.10	03
7824	1.30	13.92	04	0.90	03	0.18	04	0.55	03	1.09	03

Table 5.1. (continued)

HJD 244+	log(ap) "	V	σ_V	B-V	σ_{BV}	U-B	σ_{UB}	V-R	σ_{VR}	V-I	σ_{VI}
H 0307-730											
7123	1.48	14.68	04	0.73	03	-.16	04	0.57	03	1.08	03
7469	1.48	14.61	04	0.61	03	-.25	04	0.51	03	1.00	03
7507	1.18	14.98	04	0.69	03	-.35	04	0.50	03	1.10	03
7507	1.48	14.61	04	0.69	03	-.19	04	0.52	03	0.99	03
7567	1.30	14.78	04	0.71	03	-.21	04	0.51	03	1.04	03
7567	1.48	14.64	04	0.68	03	-.23	04	0.52	03	1.09	03
7797	1.30	14.65	04	0.72	03	-.35	04	0.42	03	0.94	03
7797	1.48	14.52	04	0.72	03	-.29	04	0.44	03	0.93	03
Fairall 1116											
6826	1.30	14.60	04	0.50	03	-.75	04	0.44	03	1.02	03
6826	1.48	14.51	03	0.50	05	-.76	04	0.43	03	-	
6855	1.48	14.53	01	0.46	01	-.70	01	0.44	01	0.88	02
7028	1.48	14.63	04	0.52	03	-.74	04	0.48	03	0.92	03
7086	1.48	14.63	04	0.54	03	-.71	04	0.43	03	0.90	03
7122	1.18	14.79	04	0.46	03	-.78	04	0.40	03	0.86	03
7122	1.30	14.73	04	0.45	03	-.69	04	0.43	03	0.87	03
7122	1.48	14.61	02	0.53	02	-.69	02	0.40	03	0.86	01
7470	1.18	14.72	04	0.36	03	-.81	04	0.43	03	0.80	03
7470	1.30	14.59	04	0.44	03	-.76	04	0.37	03	0.80	03
7470	1.48	14.51	01	0.45	01	-.72	03	0.41	01	0.84	04
7502	1.30	14.62	04	0.43	03	-.70	04	0.42	03	0.85	03
7502	1.48	14.54	04	0.49	03	-.73	04	0.44	03	0.80	03
7533	1.30	14.72	04	0.46	03	-.68	04	0.46	03	0.94	03
7533	1.48	14.58	04	0.51	03	-.68	04	0.40	03	0.73	03
7796	1.18	14.52	04	0.35	03	-.84	04	0.36	03	0.76	03
7796	1.48	14.34	04	0.42	03	-.77	04	0.34	03	0.77	03
7798	1.30	14.45	01	0.39	02	-.82	03	0.37	01	0.80	01
NGC 1566											
7123	1.30	12.25	04	0.90	03	0.12	04	0.58	03	1.20	03
7123	1.48	11.83	04	0.89	03	0.23	04	0.60	03	1.20	03
7214	1.18	12.62	04	0.95	03	0.28	04	0.58	03	1.23	03
7214	1.30	12.33	04	0.96	03	0.28	04	0.60	03	1.25	03
7214	1.48	11.87	04	0.92	03	0.34	04	0.60	03	1.23	03
7470	1.18	12.69	04	0.93	03	0.38	04	0.61	03	1.25	03
7473	1.48	11.90	04	0.95	03	0.38	04	0.59	03	1.22	03
7506	1.18	12.70	04	0.95	03	0.32	04	0.61	03	1.22	03
7506	1.48	11.90	04	0.95	03	0.38	04	0.59	03	1.22	03
7533	1.30	12.34	04	0.97	03	0.33	04	0.56	03	1.21	03
7533	1.48	11.91	04	0.95	03	0.38	04	0.59	03	1.23	03
7570	1.30	12.38	04	0.97	03	0.35	04	0.60	03	1.25	03
7570	1.48	11.93	04	0.95	03	0.39	04	0.61	03	1.25	03
7735	1.48	11.93	04	0.96	03	0.38	04	0.58	03	1.23	03
7736	1.18	12.72	04	0.96	03	0.37	04	0.59	03	1.24	03
7736	1.30	12.37	01	0.97	01	0.36	01	0.60	01	1.25	01
7799	1.30	12.35	04	0.98	03	0.36	04	0.58	03	1.24	03
7799	1.48	11.89	04	0.95	03	0.39	04	0.60	03	1.23	03

Table 5.1. (continued)

HJD 244+	log(ap) "	V	σ_V	B-V	σ_{BV}	U-B	σ_{UB}	V-R	σ_{VR}	V-I	σ_{VI}
MCG -5-13-17											
6827	1.30	13.37	05	0.63	01	-.24	02	0.47	01	0.92	02
6827	1.48	13.15	02	0.64	02	-.18	05	0.47	02	0.92	04
6854	1.18	13.54	04	0.64	03	-.22	04	0.49	03	0.98	03
6854	1.48	13.17	04	0.63	03	-.13	04	0.46	03	0.93	03
6889	1.18	13.54	04	0.66	03	-.14	04	0.47	03	0.95	03
6889	1.30	13.38	02	0.66	01	-.14	03	0.47	02	0.98	04
6889	1.48	13.18	02	0.64	02	-.11	02	0.47	02	0.97	01
7082	1.18	13.49	04	0.55	03	-.44	04	0.46	03	0.89	03
7082	1.30	13.26	04	0.57	03	-.39	04	0.44	03	0.93	03
7082	1.48	13.09	04	0.56	03	-.32	04	0.48	03	0.95	03
7122	1.18	13.49	01	0.61	02	-.37	01	0.46	02	0.93	02
7122	1.30	13.32	01	0.61	02	-.29	02	0.47	01	0.93	02
7122	1.48	13.11	01	0.61	02	-.22	03	0.47	01	0.93	02
7212	1.18	13.55	02	0.63	02	-.29	02	0.48	02	0.95	02
7212	1.30	13.35	01	0.62	01	-.23	02	0.47	01	0.93	02
7212	1.48	13.17	01	0.61	01	-.16	01	0.48	01	0.94	03
7469	1.18	13.55	01	0.65	01	-.21	05	0.45	01	0.94	01
7469	1.30	13.39	02	0.63	02	-.20	04	0.49	04	0.94	05
7469	1.48	13.17	01	0.63	01	-.12	02	0.46	02	0.94	04
7502	1.18	13.46	04	0.61	03	-.36	04	0.45	03	0.93	03
7502	1.30	13.32	04	0.60	03	-.32	04	0.46	03	0.97	03
7502	1.48	13.11	04	0.60	03	-.24	04	0.46	03	0.95	03
7534	1.18	13.48	02	0.58	02	-.39	01	0.48	01	0.92	01
7534	1.30	13.29	03	0.58	02	-.30	03	0.47	03	0.92	04
7534	1.48	13.10	01	0.60	02	-.27	01	0.47	01	0.93	02
7566	1.18	13.55	04	0.69	03	-.02	04	0.50	03	0.98	03
7568	1.30	13.43	03	0.72	06	-.07	01	0.45	01	0.96	02
7568	1.48	13.18	01	0.69	03	-.03	02	0.48	02	0.97	01
7596	1.18	13.57	04	0.66	03	-.14	04	0.45	03	0.93	03
7596	1.30	13.37	04	0.67	03	-.12	04	0.45	03	0.97	03
7596	1.48	13.16	04	0.66	03	-.11	04	0.46	03	0.95	03
7796	1.18	13.58	04	0.70	03	-.08	04	0.45	03	0.95	03
7798	1.30	13.41	02	0.69	01	-.07	01	0.45	02	0.93	03
7799	1.48	13.18	04	0.67	03	0.01	04	0.46	03	0.93	03
3A 0557-383											
6827	1.48	14.92	03	1.01	02	0.15	03	0.80	10	1.36	04
6854	1.30	14.98	02	1.09	04	0.21	03	0.80	01	1.44	05
6854	1.48	14.94	05	1.05	02	0.29	04	0.81	03	1.41	02
6889	1.18	15.05	04	1.09	03	0.16	04	0.84	03	1.41	03
6889	1.30	14.98	01	1.07	04	0.16	04	0.82	01	1.41	02
6889	1.48	14.91	03	1.09	04	0.15	06	0.79	04	1.37	02
7122	1.48	14.91	03	1.11	03	-		0.81	03	1.39	01
7212	1.30	15.00	01	1.11	03	-		0.80	02	1.39	03
7507	1.18	15.10	04	1.06	03	0.12	04	0.81	03	1.36	03
7507	1.48	14.89	04	0.95	03	0.29	04	0.77	03	1.28	03
7533	1.30	14.96	04	1.13	03	0.13	04	0.78	03	1.36	03
7570	1.30	14.99	04	1.08	03	0.04	04	0.83	03	1.39	03
7797	1.30	14.99	04	1.06	03	0.13	04	0.84	03	1.39	03

Table 5.1. (continued)

HJD 244+	log(ap) "	V	σ_V	B-V	σ_{BV}	U-B	σ_{UB}	V-R	σ_{VR}	V-I	σ_{VI}
Fairall 265											
6827	1.30	14.46	02	0.57	05	-.48	04	0.45	01	0.86	07
6827	1.48	14.36	02	0.56	02	-.40	05	0.47	03	0.95	04
6854	1.18	14.55	04	0.52	03	-.49	04	0.43	03	0.90	03
6854	1.48	14.34	04	0.56	03	-.42	04	0.48	03	1.01	03
6889	1.18	14.59	04	0.55	03	-.42	04	0.41	03	0.93	03
6889	1.30	14.48	03	0.55	04	-.43	04	0.45	05	0.97	01
6889	1.48	14.40	01	0.59	01	-.39	01	0.46	02	-	
7122	1.30	14.44	01	0.56	01	-.40	01	0.45	01	0.93	04
7122	1.48	14.31	04	0.61	03	-.40	04	0.45	03	0.97	03
7214	1.30	14.48	02	0.54	02	-.41	02	0.46	02	0.97	04
7469	1.48	14.44	04	0.64	03	-.46	04	0.47	03	0.94	03
7502	1.48	14.40	04	0.57	03	-.46	04	0.46	03	0.99	03
7534	1.18	14.58	01	0.56	01	-.46	02	0.43	02	0.88	01
7534	1.30	14.50	03	0.50	01	-.44	03	0.52	03	0.94	07
7534	1.48	14.42	03	0.54	04	-.47	01	0.47	01	0.93	01
7567	1.30	14.53	04	0.51	03	-.39	04	0.53	03	0.97	03
7567	1.48	14.39	04	0.60	03	-.39	04	0.44	03	0.97	03
7594	1.48	14.43	04	0.62	03	-.37	04	0.49	03	0.97	03
7596	1.18	14.64	03	0.56	01	-.40	01	0.43	01	0.94	02
7596	1.30	14.51	01	0.58	01	-.38	02	0.46	02	0.94	05
7797	1.48	14.39	04	0.55	03	-.39	04	0.44	03	0.96	03
7798	1.30	14.48	01	0.56	02	-.38	01	0.48	01	0.99	02
NGC 2992											
6827	1.48	13.07	04	1.04	04	0.37	08	0.67	02	1.34	02
7288	1.30	13.45	01	1.07	01	0.36	05	0.69	03	1.44	01
7288	1.48	13.00	01	1.02	02	0.34	02	0.65	02	1.35	02
7532	1.30	13.47	04	1.10	03	0.36	04	0.69	03	1.44	03
7532	1.48	13.01	04	1.04	03	0.37	04	0.63	03	1.34	03
7568	1.30	13.49	04	1.10	03	0.37	04	0.71	03	1.42	03
7568	1.48	13.04	04	1.07	03	0.29	04	0.66	03	1.35	03
7596	1.30	13.42	03	1.13	03	0.37	03	0.68	01	1.41	02
7597	1.48	13.04	04	1.04	02	0.34	03	0.67	01	1.38	02
7619	1.30	13.41	04	1.09	03	0.35	04	0.70	03	1.43	03
7619	1.48	12.99	04	1.03	03	0.32	04	0.66	03	1.35	03
7681	1.30	13.45	04	1.08	03	0.43	04	0.73	03	1.4	03
7681	1.48	13.00	04	1.05	03	0.30	04	0.63	03	1.32	03

Table 5.1. (continued)

HJD 244+	log(ap) "	V	σ_V	B-V	σ_{BV}	U-B	σ_{UB}	V-R	σ_{VR}	V-I	σ_{VI}
MCG -5-23-16											
6826	1.30	13.60	04	1.03	02	0.66	01	0.63	01	1.29	02
6826	1.48	13.39	04	1.05	03	0.43	04	0.62	03	1.27	04
6854	1.48	13.35	02	1.02	01	0.50	02	0.63	03	1.30	03
6892	1.18	13.83	04	1.02	03	0.49	04	0.63	03	1.34	03
6892	1.30	13.57	04	1.08	03	0.52	04	0.63	03	1.32	03
6892	1.48	13.41	04	1.01	03	0.47	04	0.62	03	1.31	03
7122	1.30	13.55	02	1.05	02	0.49	02	0.60	02	1.28	02
7122	1.48	13.35	02	1.05	01	0.51	04	0.62	01	1.27	02
7212	1.30	13.57	02	1.06	01	0.45	01	0.61	02	1.31	01
7212	1.48	13.38	02	1.03	02	0.49	02	0.64	01	1.32	01
7288	1.30	13.59	01	1.02	01	0.50	05	0.63	02	1.33	03
7288	1.48	13.32	01	1.05	01	0.48	01	0.60	01	1.27	01
7533	1.30	13.58	04	1.03	03	0.43	04	0.63	03	1.30	03
7533	1.48	13.35	04	1.00	03	0.54	04	0.65	03	1.34	03
7567	1.30	13.58	04	1.04	03	0.49	04	0.63	03	1.30	03
7567	1.48	13.40	04	1.04	03	0.49	04	0.62	03	1.30	03
7596	1.30	13.57	02	1.06	01	0.48	03	0.62	01	1.30	02
7596	1.48	13.34	01	1.02	01	0.50	01	0.62	02	1.28	01
7620	1.48	13.31	04	1.06	03	0.47	04	0.60	03	1.27	03
ESO 438-G9											
7214	1.18	14.17	01	0.48	01	-.50	01	0.45	01	0.96	01
7214	1.30	13.99	01	0.54	01	-.44	01	0.45	01	0.94	03
7214	1.48	13.86	01	0.56	01	-.39	01	0.45	01	0.96	01
7288	1.18	14.14	02	0.50	02	-.47	01	0.42	02	0.91	02
7288	1.30	13.98	02	0.54	01	-.40	01	0.44	01	0.94	01
7288	1.48	13.82	01	0.57	02	-.36	01	0.41	03	0.89	01
7534	1.30	14.07	01	0.53	01	-.40	01	0.48	01	1.00	02
7534	1.48	13.87	04	0.56	03	-.31	04	0.44	03	0.92	03
7566	1.18	14.24	04	0.52	03	-.44	04	0.48	03	0.96	03
7566	1.30	14.08	04	0.57	03	-.32	04	0.47	03	0.95	03
7566	1.48	13.94	04	0.57	03	-.36	04	0.48	03	0.97	03
7596	1.30	14.13	04	0.54	03	-.32	04	0.49	03	0.97	03
7596	1.48	13.96	04	0.57	03	-.31	04	0.49	03	0.97	03
7681	1.18	14.15	04	0.52	03	-.49	04	0.46	03	0.90	03
7682	1.30	14.03	01	0.53	02	-.43	02	0.46	01	0.94	04
7683	1.48	13.88	04	0.55	03	-.38	04	0.46	03	0.94	03

Table 5.1. (continued)

HJD 244+	log(ap) "	V	σ_V	B-V	σ_{BV}	U-B	σ_{UB}	V-R	σ_{VR}	V-I	σ_{VI}
NGC 3783											
6826	1.18	13.23	04	0.60	03	-.73	04	0.56	03	0.96	03
6826	1.30	13.05	02	0.64	02	-.66	02	0.60	01	1.04	03
6826	1.48	12.71	02	0.71	02	-.50	02	0.59	01	1.09	01
6854	1.18	13.20	01	0.59	02	-.71	02	0.59	01	1.03	01
6854	1.30	13.00	01	0.66	01	-.62	01	0.59	01	1.07	01
6854	1.48	12.70	01	0.71	01	-.47	01	0.59	01	1.12	01
6889	1.18	13.09	01	0.54	01	-.78	02	0.55	01	0.98	02
6889	1.30	12.93	01	0.59	01	-.70	02	0.56	01	1.03	02
6889	1.48	12.63	01	0.66	01	-.58	02	0.56	01	1.06	01
7212	1.18	13.24	01	0.65	02	-.64	04	0.56	01	1.01	02
7212	1.30	13.05	04	0.66	03	-.53	04	0.56	03	1.05	03
7212	1.48	12.73	01	0.73	01	-.40	01	0.57	01	1.10	02
7261	1.48	12.68	04	0.71	03	-.46	04	0.57	03	1.10	03
7283	1.48	12.82	04	0.81	03	-.36	04	0.63	03	1.17	03
7284	1.48	12.83	04	0.78	03	-.19	04	0.63	03	1.15	03
7288	1.18	13.43	01	0.76	03	-.50	04	0.60	01	1.08	01
7288	1.30	13.17	01	0.81	01	-.37	01	0.59	01	1.12	03
7288	1.48	12.81	02	0.81	01	-.24	01	0.59	01	1.13	02
7507	1.18	13.25	04	0.66	03	-.63	04	0.53	03	1.00	03
7507	1.48	12.76	02	0.74	01	-.40	01	0.55	01	1.08	01
7534	1.18	13.07	03	0.53	01	-.76	02	0.49	01	0.91	02
7534	1.30	12.89	01	0.56	02	-.66	02	0.52	02	0.99	01
7534	1.48	12.60	01	0.64	01	-.53	01	0.53	01	1.03	02
7565	1.30	12.86	04	0.56	03	-.67	04	0.55	03	1.00	03
7565	1.48	12.59	03	0.62	02	-.57	02	0.56	03	1.05	03
7566	1.18	13.02	04	0.53	03	-.77	04	0.52	03	0.91	03
7595	1.30	12.84	02	0.57	01	-.71	03	0.53	01	0.99	01
7595	1.48	12.58	02	0.63	01	-.59	04	0.55	02	1.04	01
7596	1.18	12.99	01	0.52	01	-.79	01	0.52	02	0.93	02
7619	1.30	12.75	01	0.49	04	-.74	02	0.51	02	0.95	03
7619	1.48	12.51	01	0.57	03	-.61	02	0.54	02	1.04	03
7670	1.18	12.95	04	0.46	03	-.83	04	0.52	03	0.94	03
7670	1.30	12.78	04	0.53	03	-.76	04	0.53	03	0.96	03
7670	1.48	12.53	04	0.60	03	-.63	04	0.55	03	1.02	03
7681	1.18	12.99	04	0.54	03	-.80	04	0.50	03	0.92	03
7682	1.30	12.84	01	0.56	01	-.72	01	0.55	01	1.00	01
7683	1.48	12.55	04	0.64	03	-.59	04	0.54	03	1.03	03
7707	1.30	12.83	03	0.57	01	-.71	01	0.55	01	1.02	02
7707	1.48	12.56	02	0.63	01	-.59	01	0.55	01	1.05	02
7709	1.18	13.02	04	0.52	03	-.78	04	0.56	03	0.96	03
7735	1.30	12.89	04	0.61	03	-.67	04	0.53	03	1.00	03
7735	1.48	12.62	04	0.66	03	-.55	04	0.55	03	1.05	03

Table 5.1. (continued)

HJD 244+	log(ap) "	V	σ_V	B-V	σ_{BV}	U-B	σ_{UB}	V-R	σ_{VR}	V-I	σ_{VI}
H 1143-182											
7214	1.18	14.29	03	0.34	03	-.99	01	0.37	02	0.65	01
7214	1.30	14.18	02	0.42	01	-.99	01	0.34	01	0.62	03
7214	1.48	14.02	04	0.52	03	-.97	04	0.29	03	0.60	03
7289	1.18	14.43	01	0.50	01	-1.01	01	0.41	02	0.71	03
7289	1.30	14.32	02	0.51	02	-.95	02	0.37	03	0.66	02
7289	1.48	14.19	04	0.57	03	-.93	04	0.34	03	0.73	03
7535	1.18	14.47	04	0.45	03	-1.09	04	0.43	03	0.69	03
7535	1.30	14.29	04	0.47	03	-.93	04	0.35	03	0.64	03
7535	1.48	14.15	03	0.53	03	-.89	01	0.33	03	0.68	02
7566	1.18	14.28	04	0.43	03	-1.00	04	0.35	03	0.61	03
7566	1.30	14.21	02	0.46	01	-.95	01	0.34	01	0.65	03
7568	1.48	14.09	02	0.52	02	-.93	04	0.31	03	0.63	04
7595	1.18	14.24	01	0.40	01	-.99	01	0.33	01	0.64	02
7595	1.30	14.16	01	0.46	01	-.99	02	0.34	01	0.63	03
7595	1.48	14.08	04	0.48	03	-.94	03	0.34	03	0.64	01
7618	1.48	14.09	04	0.54	03	-.92	04	0.35	03	0.63	03
7674	1.18	14.30	04	0.42	03	-.99	04	0.35	03	0.60	03
7674	1.48	14.09	04	0.48	03	-.92	04	0.31	03	0.59	03
7679	1.30	14.16	01	0.45	02	-.96	02	0.31	01	0.58	02
MCG -2-33-34											
6854	1.30	13.87	01	0.80	03	-.33	04	0.54	03	1.11	02
6854	1.48	13.54	02	0.80	03	-.19	04	0.56	03	1.15	02
6889	1.30	13.88	02	0.78	01	-.34	01	0.54	01	1.11	03
6889	1.48	13.55	03	0.78	03	-.16	04	0.57	03	1.16	03
7212	1.18	14.03	04	0.70	03	-.47	04	0.51	03	1.04	03
7212	1.30	13.81	01	0.72	01	-.34	05	0.52	01	1.08	01
7212	1.48	13.50	03	0.74	02	-.26	03	0.57	01	1.14	01
7288	1.30	13.88	03	0.77	01	-.29	04	0.58	02	1.14	04
7288	1.48	13.54	05	0.80	02	-.24	02	0.56	04	1.17	05
7565	1.30	13.91	04	0.76	03	-.37	04	0.55	03	1.14	03
7565	1.48	13.56	04	0.83	03	-.23	04	0.58	03	1.15	03
7596	1.30	13.86	02	0.74	01	-.39	01	0.54	02	1.10	01
7596	1.48	13.53	01	0.76	01	-.24	01	0.56	02	1.14	03
7617	1.30	13.89	04	0.74	03	-.36	04	0.55	03	1.12	03
7617	1.48	13.55	04	0.79	03	-.28	04	0.54	03	1.05	03
7682	1.30	13.91	01	0.80	03	-.21	03	0.56	03	1.10	03
7682	1.48	13.58	01	0.83	01	-.13	01	0.57	03	1.15	03
7737	1.30	13.91	01	0.79	01	-.25	01	0.52	02	1.13	02
7736	1.48	13.55	04	0.81	03	-.15	04	0.54	03	1.20	03

Table 5.1. (continued)

HJD 244+	log(ap) "	V	σ_V	B-V	σ_{BV}	U-B	σ_{UB}	V-R	σ_{VR}	V-I	σ_{VI}
ESO 323-G77											
6827	1.18	13.41	04	0.84	03	-.01	04	0.68	03	1.29	03
6827	1.30	13.30	02	0.89	02	0.02	03	0.67	02	1.29	01
6827	1.48	13.09	02	0.89	01	0.10	02	0.66	01	1.29	01
6854	1.18	13.40	02	0.85	03	0.02	04	0.66	03	1.30	03
6854	1.30	13.27	02	0.89	01	0.03	01	0.69	03	1.33	03
6854	1.48	13.08	02	0.91	01	0.08	03	0.67	03	1.31	03
6889	1.18	13.41	02	0.86	02	-.03	02	0.67	01	1.30	02
6889	1.30	13.29	02	0.88	01	0.02	02	0.67	02	1.33	02
6889	1.48	13.11	02	0.90	01	0.07	02	0.66	01	1.32	04
7209	1.18	13.43	04	0.87	03	-.04	04	0.69	03	1.32	03
7209	1.30	13.27	04	0.88	03	0.04	04	0.66	03	1.32	03
7209	1.48	13.09	04	0.91	03	0.07	04	0.65	03	1.26	03
7288	1.18	13.43	03	0.89	02	-.02	02	0.67	01	1.30	01
7288	1.30	13.29	02	0.87	02	0.01	03	0.68	02	1.31	01
7288	1.48	13.14	04	0.87	03	0.11	04	0.66	03	1.31	03
7594	1.18	13.46	04	0.86	03	-.01	04	0.69	03	1.32	03
7595	1.30	13.32	01	0.88	01	0.04	01	0.66	01	1.32	02
7595	1.48	13.12	01	0.90	03	0.12	01	0.66	02	1.30	01
7618	1.30	13.28	04	0.88	03	0.03	04	0.66	03	1.31	03
7618	1.48	13.08	04	0.90	03	0.09	04	0.64	03	1.29	03
7681	1.30	13.34	04	0.89	03	0.06	04	0.66	03	1.34	03
7681	1.18	13.47	04	0.89	03	0.00	04	0.64	03	1.30	03
7681	1.48	13.15	04	0.94	03	0.08	04	0.65	03	1.28	03
MCG -6-30-15											
6826	1.30	13.48	03	0.99	01	0.36	02	0.63	01	1.24	01
6826	1.48	13.25	01	0.95	01	0.36	03	0.61	01	1.19	02
6854	1.18	13.76	06	0.96	05	0.27	05	0.66	03	1.30	03
6854	1.30	13.39	02	1.00	01	0.32	01	-		-	
6854	1.48	13.25	02	0.95	01	0.34	01	0.59	03	1.20	03
6889	1.18	13.67	05	0.95	03	0.38	04	0.62	04	1.26	04
6889	1.30	13.41	01	0.96	01	0.41	01	0.62	02	1.23	03
6889	1.48	13.25	01	0.94	01	0.38	03	0.59	01	1.21	02
7214	1.30	13.44	04	0.98	03	0.41	04	0.63	03	1.22	03
7288	1.30	13.38	02	0.97	03	0.37	07	0.62	01	1.22	02
7288	1.48	13.28	04	0.94	03	0.38	04	0.62	03	1.23	03
7595	1.48	13.23	04	1.02	03	0.33	04	0.57	03	1.23	03
7619	1.48	13.22	04	0.95	03	0.36	04	0.58	03	1.20	03
7705	1.48	13.24	04	0.97	03	0.32	04	0.61	03	1.20	03

Table 5.1. (continued)

HJD 244+	log(ap) "	V	σ_V	B-V	σ_{BV}	U-B	σ_{UB}	V-R	σ_{VR}	V-I	σ_{VI}
IC 4329A											
6826	1.30	13.61	02	1.16	02	0.45	02	0.85	02	1.49	02
6826	1.48	13.41	02	1.12	07	0.42	05	0.82	02	1.47	03
6854	1.18	13.80	01	1.19	01	0.41	03	0.84	03	1.52	03
6854	1.30	13.63	04	1.18	03	0.37	04	-		-	
6854	1.48	13.44	01	1.14	02	0.44	04	0.79	03	1.49	03
6889	1.18	13.93	04	1.25	04	0.42	03	0.87	02	1.55	02
6889	1.30	13.73	01	1.16	01	0.47	02	0.84	01	1.51	01
6889	1.48	13.47	01	1.20	01	0.44	02	0.78	01	1.48	01
7028	1.30	13.62	04	1.17	03	0.41	04	0.84	03	1.49	03
7028	1.48	13.39	04	1.15	03	0.51	04	0.76	03	1.46	03
7212	1.18	13.79	02	1.17	02	0.40	02	0.87	02	1.53	02
7212	1.30	13.60	02	1.16	02	0.37	03	0.82	02	1.50	01
7212	1.48	13.42	02	1.15	02	0.39	02	0.79	02	1.47	02
7288	1.18	13.78	:	1.18	:	0.22	:	0.86	:	1.53	:
7288	1.30	13.58	03	1.17	04	0.37	03	0.82	04	1.49	03
7288	1.48	13.42	01	1.15	03	0.29	10	0.83	02	1.50	01
7566	1.18	13.83	04	1.16	03	0.44	04	0.88	03	1.55	03
7566	1.30	13.65	04	1.20	03	0.43	04	0.84	03	1.52	03
7566	1.48	13.48	04	1.13	03	0.45	04	0.83	03	1.48	03
7596	1.18	13.75	02	1.16	02	0.40	03	0.86	01	1.54	01
7596	1.30	13.58	03	1.16	03	0.38	01	0.83	01	1.52	01
7597	1.48	13.39	04	1.14	03	0.37	04	0.81	03	1.50	03
7619	1.30	13.60	03	1.17	01	0.40	03	0.84	02	1.51	03
7619	1.48	13.42	01	1.16	03	0.41	01	0.81	02	1.49	01
7675	1.48	13.38	04	1.14	03	0.41	04	0.80	03	1.46	03
7678	1.30	13.54	02	1.18	02	0.41	04	0.81	01	1.50	01
7681	1.18	13.76	04	1.14	03	0.40	04	0.88	03	1.52	03
7707	1.30	13.52	01	1.15	01	0.38	02	0.82	01	1.49	01
7707	1.48	13.33	01	1.13	01	0.40	02	0.79	01	1.45	01
7709	1.18	13.68	04	1.17	03	0.37	04	0.84	03	1.49	03
7736	1.30	13.48	01	1.16	01	0.38	01	0.82	01	1.50	01
7736	1.48	13.31	01	1.11	01	0.38	03	0.81	02	1.48	02
7737	1.18	13.63	01	1.16	01	0.32	02	0.84	02	1.50	01
IRAS 1509-211											
6854	1.30	14.82	01	0.90	01	0.04	04	0.63	02	1.26	01
6854	1.48	14.64	02	0.95	01	-.04	04	0.60	01	1.22	01
6889	1.30	14.82	03	0.96	01	0.00	04	0.61	01	1.22	01
6889	1.48	14.64	01	0.96	01	0.05	05	0.63	03	1.22	03
7035	1.30	14.92	04	1.03	03	0.01	04	0.63	03	1.25	03
7035	1.48	14.78	04	1.03	03	-.22	04	0.72	03	1.25	03
7212	1.30	14.91	04	0.98	03	-.09	04	0.65	03	1.21	03
7212	1.48	14.70	04	0.92	03	0.07	04	0.60	03	1.19	03
7595	1.30	14.85	04	0.89	03	-.07	04	0.66	03	1.21	03
7683	1.30	14.78	04	0.93	03	0.05	04	-		-	
7707	1.30	14.79	01	0.96	03	-.02	03	0.64	02	1.23	01

Table 5.1. (continued)

HJD 244+	log(ap) "	V	σ_V	B-V	σ_{BV}	U-B	σ_{UB}	V-R	σ_{VR}	V-I	σ_{VI}
ESO 103-G35											
7034	1.48	14.11	02	1.01	02	0.46	03	0.60	02	1.23	02
7683	1.30	14.33	04	1.07	03	0.42	04	0.60	03	1.23	03
7683	1.48	14.13	04	1.00	03	0.38	04	0.63	03	1.28	03
7707	1.30	14.34	03	1.06	03	0.45	:	0.59	01	1.24	03
7707	1.48	14.13	02	1.01	02	0.43	01	0.60	02	1.22	03
7799	1.30	14.36	04	1.01	03	0.40	04	0.62	03	1.29	03
7799	1.48	14.10	04	1.02	03	-		0.68	03	1.35	03
Fairall 51											
6889	1.18	14.33	01	0.84	03	-.07	03	0.66	01	1.22	02
6889	1.30	14.17	01	0.86	02	-.05	02	0.66	01	1.23	03
6889	1.48	13.94	03	0.83	01	0.01	02	0.65	03	1.23	02
7035	1.18	14.24	04	0.83	03	-.21	04	0.64	03	1.22	03
7035	1.30	14.07	04	0.85	03	-.17	04	0.63	03	1.20	03
7035	1.48	13.87	04	0.85	03	-.05	04	0.61	03	1.22	03
7596	1.18	14.25	04	0.89	03	-.14	04	0.62	03	1.18	03
7596	1.30	14.12	04	0.88	03	-.10	04	0.60	03	1.17	03
7596	1.48	13.90	04	0.87	03	0.04	04	0.63	03	1.20	03
7620	1.30	14.13	01	0.81	02	-.11	06	0.67	02	1.21	02
7620	1.48	13.90	01	0.83	03	-.07	03	0.63	03	1.20	01
7681	1.18	14.27	04	0.82	03	-.16	04	0.64	03	1.21	03
7682	1.30	14.11	01	0.85	01	-.09	02	0.62	03	1.16	03
7683	1.48	13.91	04	0.84	03	-.01	04	-		-	
7707	1.30	14.04	03	0.83	01	-.15	03	0.61	03	1.18	01
7707	1.48	13.85	01	0.82	01	-.08	02	0.61	02	1.16	02
7736	1.30	14.14	02	0.82	01	-.09	01	0.64	01	1.24	02
7736	1.48	13.92	03	0.83	01	-.05	02	0.64	01	1.21	01
7737	1.18	14.29	02	0.82	01	-.14	04	0.67	01	1.22	01
7771	1.18	14.34	04	0.86	03	-.12	04	0.65	03	1.22	03
7771	1.30	14.18	04	0.85	03	-.09	04	0.66	03	1.22	03
7771	1.48	13.94	04	0.89	03	-.04	04	0.62	03	1.21	03
7797	1.30	14.24	04	0.86	03	0.01	04	0.62	03	1.20	03
7797	1.48	14.04	04	0.84	03	0.00	04	0.65	03	1.24	03
7824	1.30	14.15	04	0.85	03	-.01	04	0.65	03	1.18	03

Table 5.1. (continued)

HJD 244+	log(ap) "	V	σ_V	B-V	σ_{BV}	U-B	σ_{UB}	V-R	σ_{VR}	V-I	σ_{VI}
ESO 141-G55											
6889	1.18	13.67	01	0.29	02	-.90	04	0.36	01	0.68	01
6889	1.30	13.63	02	0.30	02	-.87	02	0.39	01	0.74	02
6889	1.48	13.55	02	0.34	02	-.85	02	0.38	02	0.73	05
7033	1.18	13.98	04	0.34	03	-.90	04	0.41	03	0.78	03
7033	1.30	13.83	01	0.37	03	-.86	04	0.43	03	0.83	03
7033	1.48	13.77	01	0.37	03	-.82	04	0.46	03	0.85	03
7082	1.18	13.85	04	0.32	03	-.90	04	0.41	03	0.78	03
7082	1.30	13.78	04	0.35	03	-.88	04	0.41	03	0.80	03
7082	1.48	13.74	04	0.36	03	-.86	04	0.45	03	0.82	03
7471	1.30	13.94	02	0.42	02	-.86	01	0.44	02	0.83	02
7597	1.18	14.07	04	0.36	03	-.88	04	0.46	03	0.84	03
7596	1.30	13.96	02	0.40	05	-.77	03	0.48	05	0.82	05
7596	1.48	13.84	04	0.44	01	-.79	01	0.45	03	0.92	02
7619	1.30	13.89	02	0.39	02	-.82	01	0.45	02	0.80	02
7619	1.48	13.82	01	0.40	02	-.80	01	0.50	01	0.90	02
7676	1.48	13.80	04	0.43	03	-.79	04	0.44	03	0.83	03
7679	1.18	13.99	01	0.34	03	-.85	03	0.41	01	0.79	03
7679	1.30	13.90	01	0.41	02	-.85	02	0.43	02	0.81	02
7707	1.30	13.80	02	0.37	02	-.85	01	0.39	01	0.78	02
7707	1.48	13.69	03	0.38	01	-.80	01	0.41	01	0.80	01
7736	1.30	13.77	02	0.34	02	-.88	01	0.39	03	0.82	05
7737	1.18	13.86	02	0.30	03	-.90	01	0.39	02	0.76	02
7737	1.48	13.69	03	0.37	04	-.83	01	0.45	02	0.84	01
7769	1.18	13.83	04	0.33	03	-.90	04	0.39	03	0.70	03
7769	1.48	13.70	04	0.38	03	-.85	04	0.45	03	0.86	03
7771	1.30	13.76	04	0.31	03	-.88	04	0.43	03	0.80	03
7797	1.18	13.79	04	0.30	03	-.92	04	0.40	03	0.76	03
7797	1.30	13.72	04	0.33	03	-.90	04	0.45	03	0.82	03
7824	1.30	13.82	04	0.40	03	-.86	04	0.44	03	0.83	03
NGC 6814											
6675	1.65	12.63	04	1.08	03	0.40	04	0.68	03	1.42	03
7033	1.18	13.75	04	1.05	03	0.13	04	0.70	03	1.43	03
7033	1.30	13.47	02	1.07	03	0.30	04	0.69	03	1.44	03
7033	1.48	13.12	02	1.09	03	0.35	04	0.71	03	1.44	03
7086	1.30	13.49	04	1.08	03	0.18	04	0.71	03	1.45	03
7086	1.48	13.08	04	1.12	03	0.30	04	0.70	03	1.43	03
7619	1.48	13.11	01	1.10	01	0.32	05	0.69	02	1.43	01
7620	1.30	13.50	04	1.10	01	0.36	05	0.71	02	1.46	01
7679	1.30	13.54	03	1.07	01	0.45	04	0.74	01	1.47	02
7679	1.48	13.11	02	1.09	03	0.41	02	0.73	01	1.46	01
7681	1.18	13.80	04	1.10	03	0.43	04	0.73	03	1.44	03
7716	1.30	13.52	04	1.07	03	0.36	04	0.71	03	-	
7716	1.48	13.10	04	1.08	03	0.45	04	0.71	03	-	
7736	1.18	13.82	04	1.13	03	0.38	04	0.70	03	1.44	03
7736	1.30	13.54	04	1.11	02	0.44	02	0.73	01	1.46	01
7736	1.48	13.13	02	1.11	02	0.43	01	0.72	01	1.43	01
7770	1.18	13.84	02	1.13	04	0.44	05	0.71	01	1.42	02
7770	1.30	13.53	03	1.14	02	0.43	02	0.72	03	1.46	02
7770	1.48	13.13	02	1.12	02	0.43	02	0.71	02	1.44	02
7797	1.30	13.53	04	1.12	03	0.39	04	0.72	03	1.48	03

Table 5.1. (continued)

HJD 244+	log(ap) "	V	σ_V	B-V	σ_{BV}	U-B	σ_{UB}	V-R	σ_{VR}	V-I	σ_{VI}
NGC 6860											
7083	1.30	13.53	04	0.87	03	0.07	04	0.58	03	1.17	03
7083	1.48	13.23	04	0.81	03	0.11	04	0.59	03	1.17	03
7470	1.30	13.54	04	0.88	03	0.18	04	0.57	03	1.16	03
7470	1.48	13.23	04	0.83	03	0.10	04	0.56	03	1.16	03
7619	1.48	13.19	04	0.82	03	0.15	04	0.56	03	1.15	03
7709	1.30	13.46	04	0.82	03	0.07	04	0.59	03	1.15	03
7709	1.48	13.17	04	0.78	03	0.08	04	0.60	03	1.13	03
7736	1.30	13.48	01	0.82	01	0.06	01	0.61	02	1.17	02
7736	1.48	13.19	01	0.81	01	0.07	01	0.58	01	1.16	02
7771	1.30	13.42	04	0.83	03	0.05	04	0.58	03	1.17	03
7771	1.48	13.14	04	0.82	03	0.03	04	0.58	03	1.12	03
H 2106-099											
7027	1.18	14.39	04	0.56	03	-.74	04	0.51	03	0.96	03
7027	1.30	14.31	04	0.57	03	-.70	04	0.55	03	1.04	03
7084	1.18	14.43	02	0.61	02	-.72	02	0.53	01	0.98	04
7084	1.30	14.35	02	0.63	05	-.66	01	0.57	01	1.03	02
7470	1.18	14.40	02	0.57	01	-.73	01	0.49	01	0.95	01
7470	1.30	14.31	02	0.59	02	-.69	02	0.49	01	0.96	05
7681	1.18	14.27	04	0.53	03	-.70	04	0.50	03	0.91	03
7682	1.30	14.18	01	0.56	02	-.67	02	0.50	03	0.93	03
7736	1.18	14.23	01	0.52	01	-.74	01	0.50	02	0.94	01
7736	1.30	14.16	01	0.52	01	-.70	01	0.51	01	0.96	02
7771	1.18	14.08	04	0.44	03	-.79	04	0.44	03	0.88	03
7771	1.30	13.99	04	0.49	03	-.77	04	0.46	03	0.89	03
7799	1.30	13.97	04	0.55	03	-.75	04	0.51	03	0.93	03
NGC 7213											
7033	1.18	12.14	04	1.00	03	0.44	04	0.62	03	1.24	03
7033	1.30	11.78	01	0.99	03	0.45	04	0.60	03	1.24	03
7033	1.48	11.36	01	0.97	03	0.46	04	0.59	03	1.21	03
7084	1.18	12.14	01	1.00	03	0.43	04	0.62	03	1.25	03
7084	1.30	11.79	01	0.99	03	0.46	04	0.60	03	1.24	03
7084	1.48	11.36	01	0.96	03	0.44	04	0.59	03	1.21	03
7122	1.18	12.12	04	0.99	03	0.44	04	0.61	03	1.26	03
7122	1.30	11.81	04	0.98	03	0.46	04	0.61	03	1.25	03
7122	1.48	11.37	04	0.97	03	0.47	04	0.59	03	1.22	03

Table 5.1. (continued)

HJD 244+	log(ap) "	V	σ_V	B-V	σ_{BV}	U-B	σ_{UB}	V-R	σ_{VR}	V-I	σ_{VI}
MCG -2-58-22											
6675	1.48	13.68	01	-		-		0.45	01	0.91	02
7033	1.18	14.50	01	0.62	03	-.76	04	0.57	03	0.94	03
7033	1.30	14.32	04	0.70	03	-.73	04	0.54	03	0.98	03
7033	1.48	14.14	04	0.70	03	-.58	04	0.60	03	1.05	03
7084	1.18	14.48	04	0.64	03	-.76	04	0.51	03	0.88	03
7084	1.30	14.35	02	0.64	01	-.68	03	0.58	01	1.01	01
7084	1.48	14.13	01	0.70	01	-.60	01	0.57	02	1.03	03
7122	1.30	14.39	02	0.74	02	-.61	02	0.56	02	0.98	04
7122	1.48	14.20	02	0.74	03	-.50	02	0.61	04	1.07	04
7469	1.18	14.51	01	0.62	03	-.78	03	0.56	02	0.95	01
7470	1.30	14.33	02	0.66	04	-.68	04	0.55	02	0.98	03
7470	1.48	14.13	02	0.73	05	-.62	04	0.55	03	1.03	03
7508	1.18	14.54	04	0.64	03	-.75	04	0.58	03	1.00	03
7681	1.18	14.67	04	0.63	03	-.63	04	0.60	03	0.98	03
7682	1.30	14.45	01	0.73	01	-.54	01	0.57	02	1.01	02
7736	1.18	14.73	02	0.78	01	-.57	04	0.57	01	1.00	01
7736	1.30	14.54	01	0.78	01	-.49	02	0.59	03	1.06	02
7737	1.48	14.31	01	0.87	02	-.43	03	0.56	03	1.09	01
7769	1.18	14.79	04	0.81	03	-.52	04	0.59	03	1.00	03
7769	1.48	14.31	04	0.90	03	-.33	04	0.53	03	1.02	03
7770	1.30	14.58	04	0.81	02	-.43	02	0.60	04	1.05	03
7799	1.30	14.63	04	0.86	03	-.42	04	0.55	03	1.06	03
7799	1.48	14.37	04	0.86	03	-.29	04	0.57	03	1.08	03
7824	1.30	14.60	04	0.82	03	-.41	04	0.57	03	1.05	03

Figure 5.1(a). The light curves of ESO 12-G21 and Ton S180.

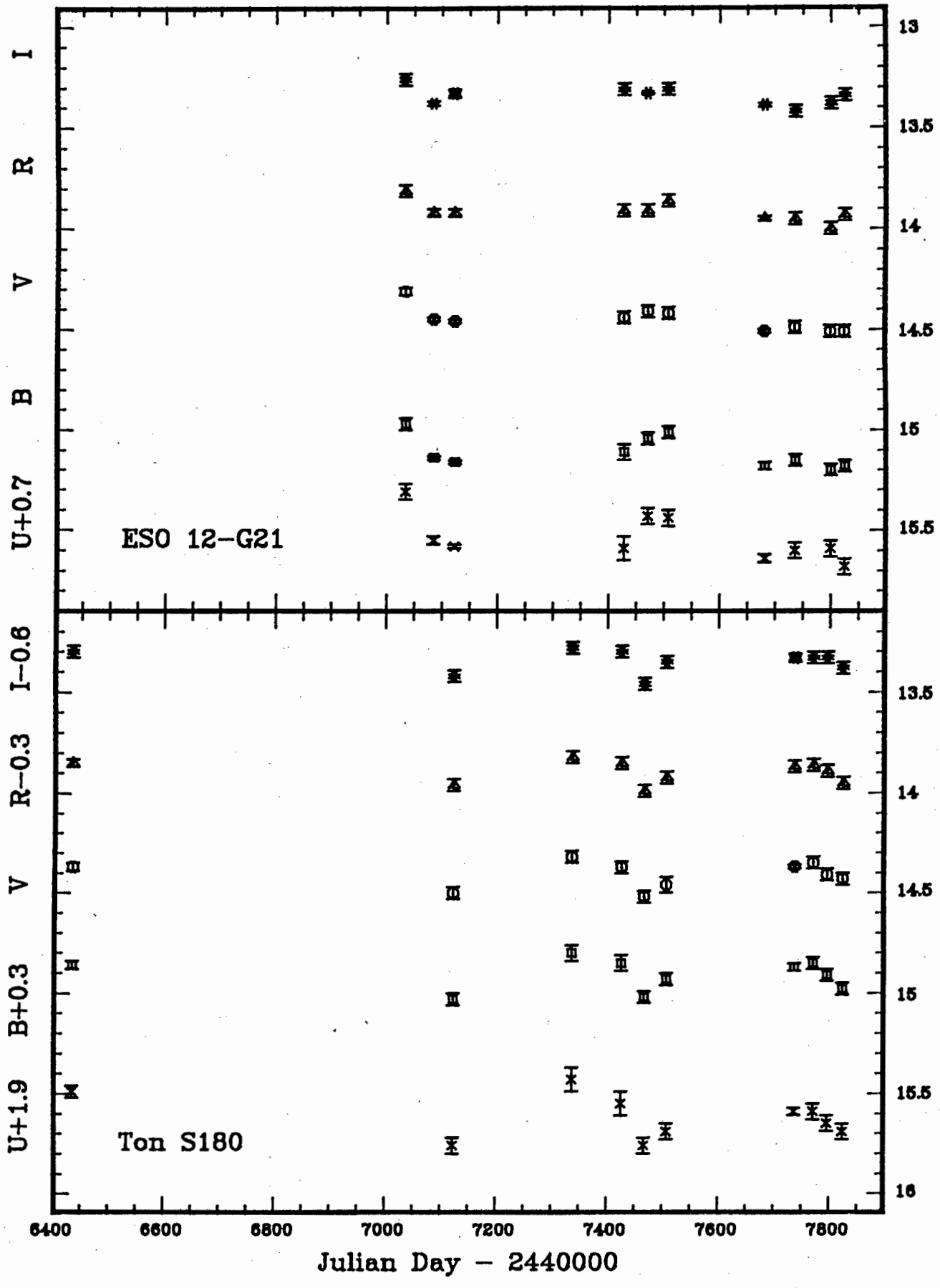

Figure 5.1(b). The light curves of NGC 526a and Fairall 9.

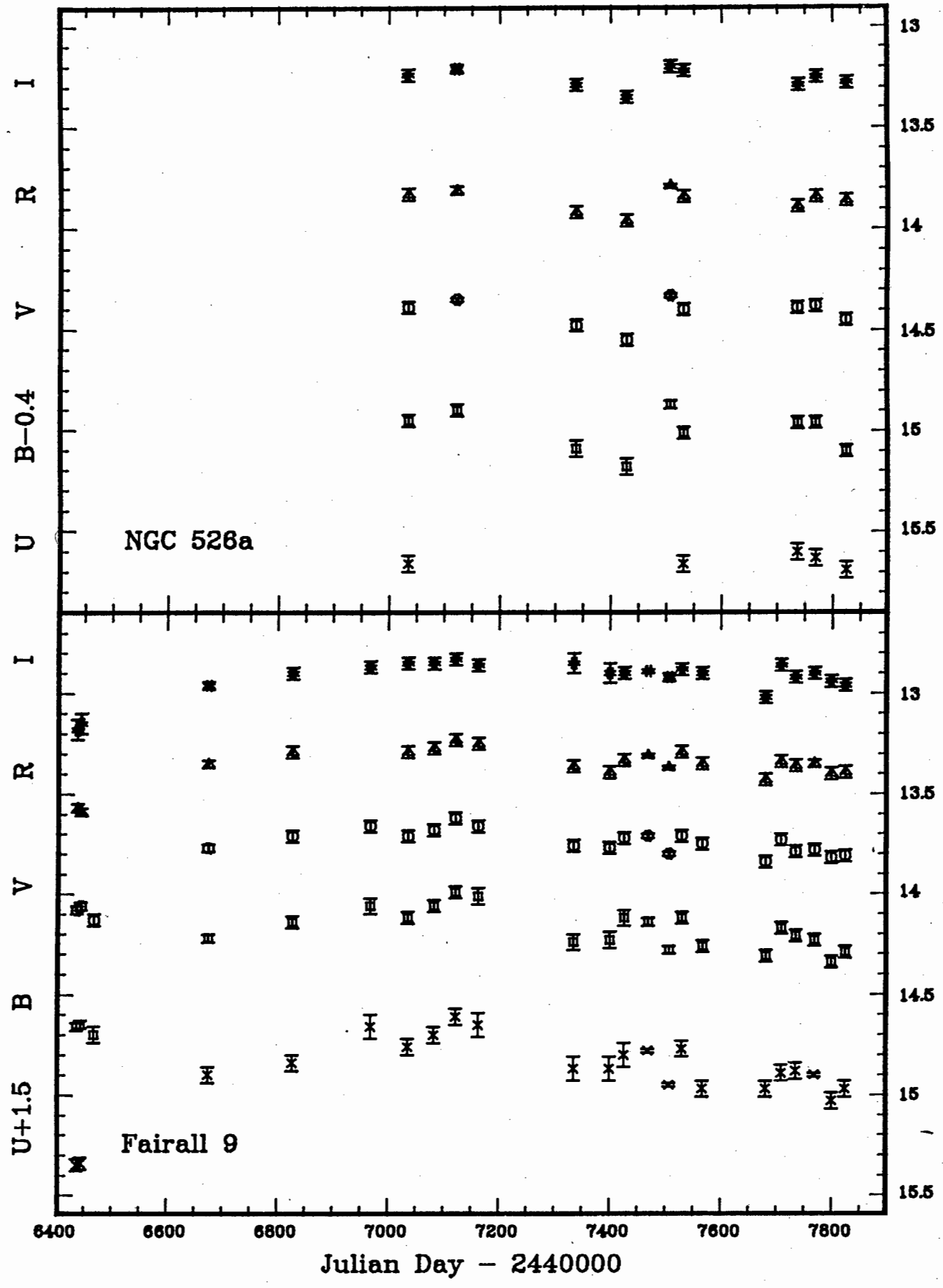

Figure 5.1(c). The light curves of IC 1816 and H 0307-730.

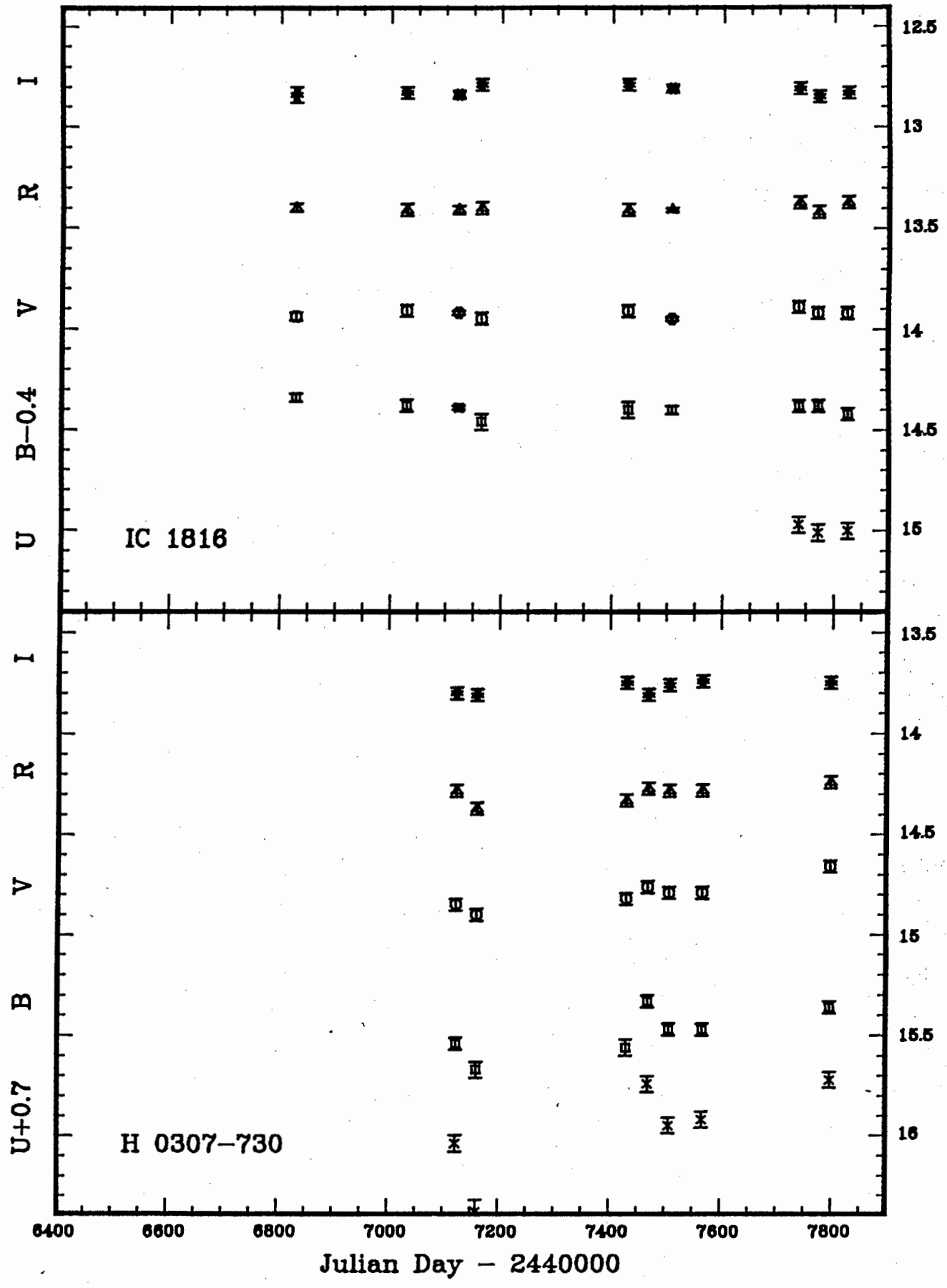

Figure 5.1(d). The light curves of Fairall 1116 and NGC 1566.

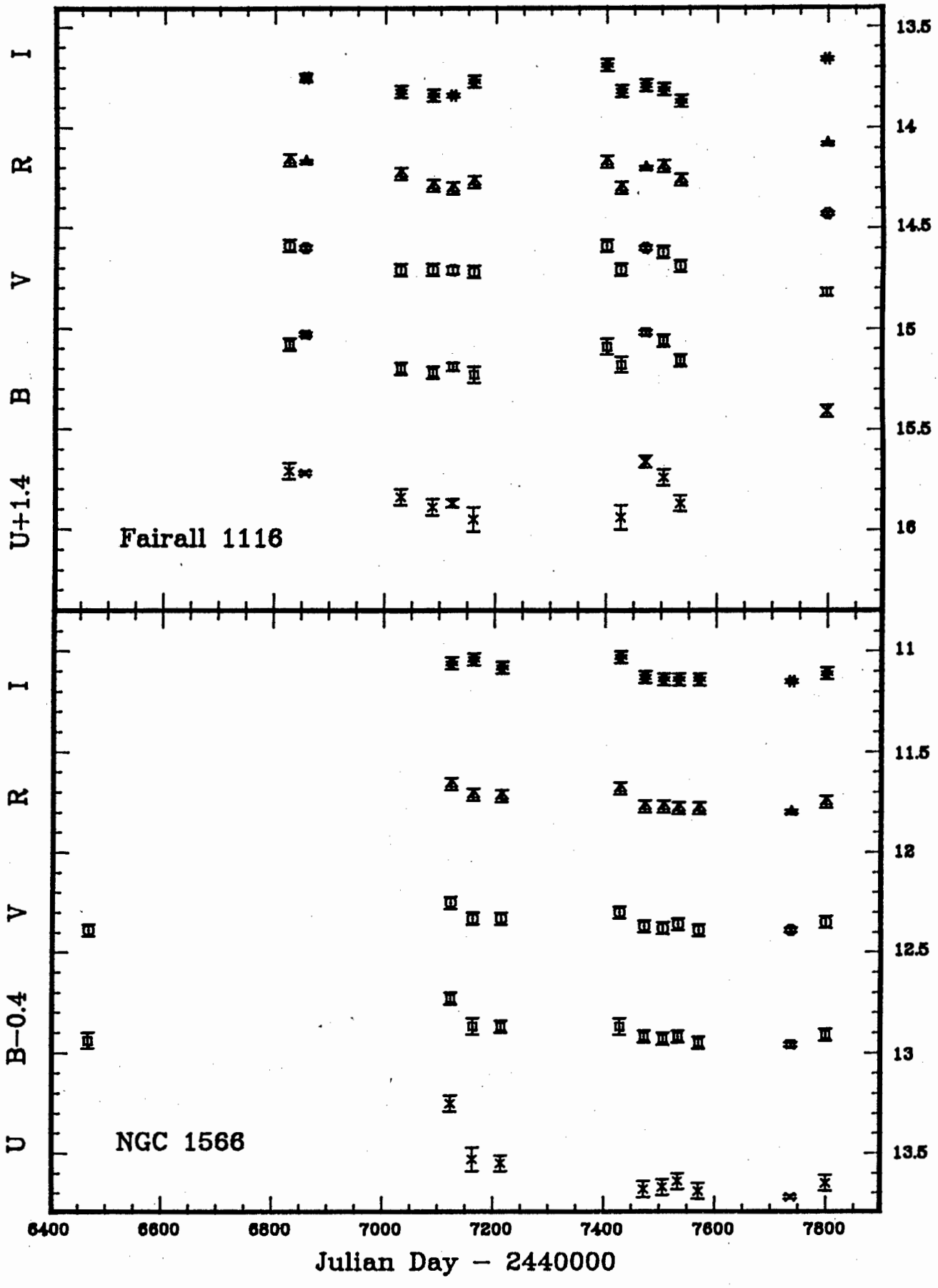

Figure 5.1(e). The light curves of MCG -5-13-17 and 3A 0557-383.

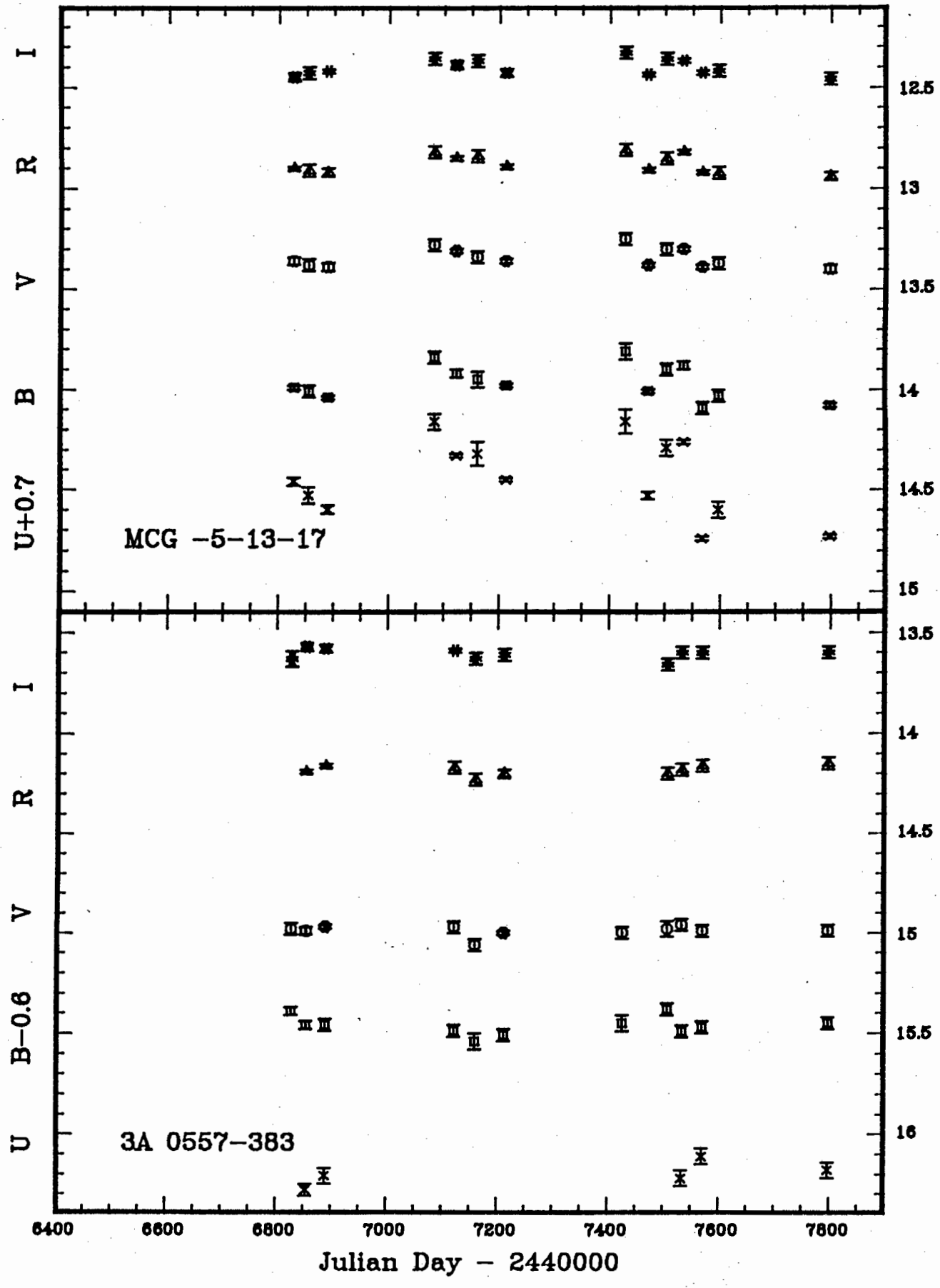

Figure 5.1(f). The light curves of Fairall 265 and NGC 2992.

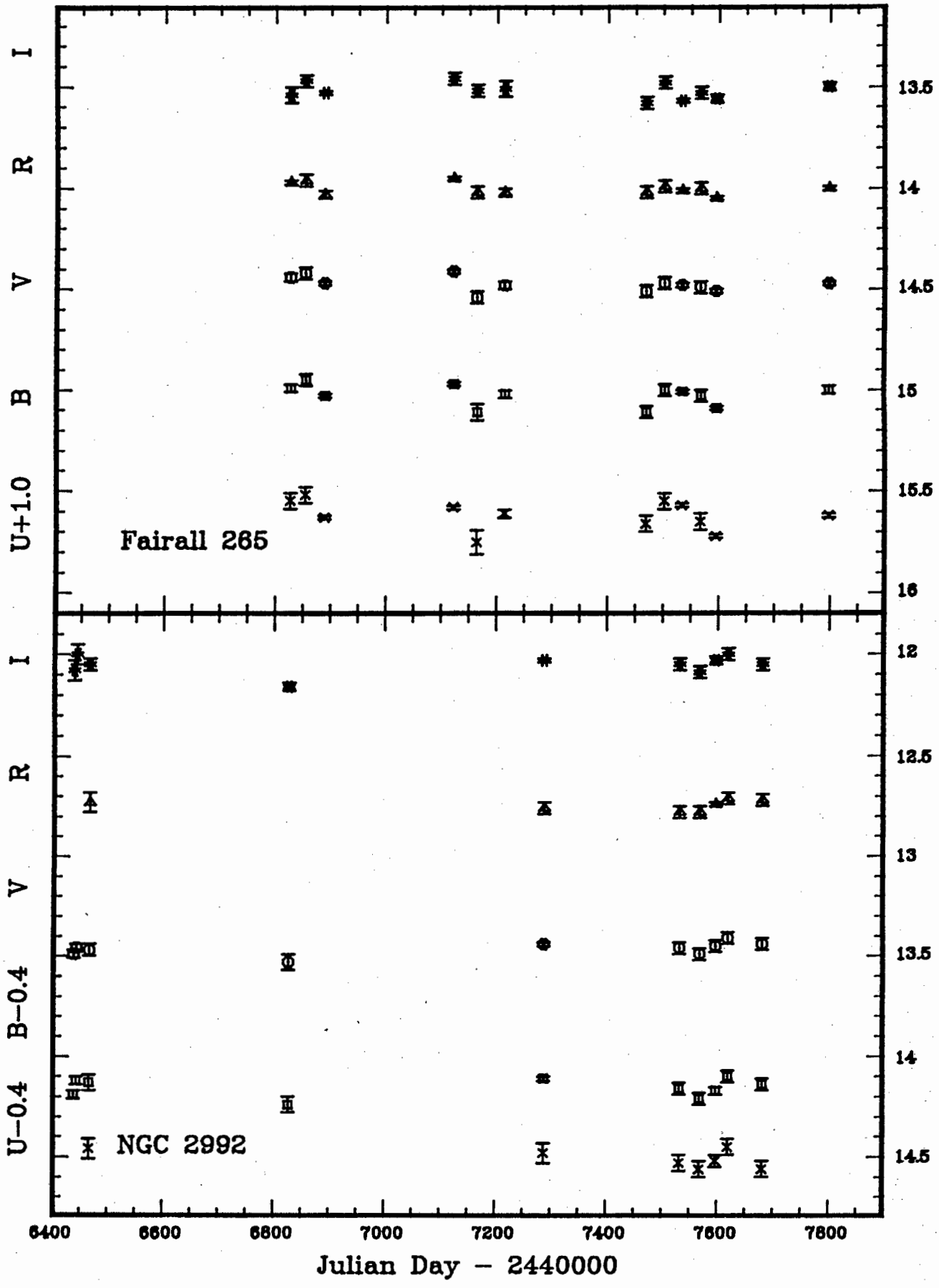

Figure 5.1(g). The light curves of MCG -5-23-16 and ESO 438-G9.

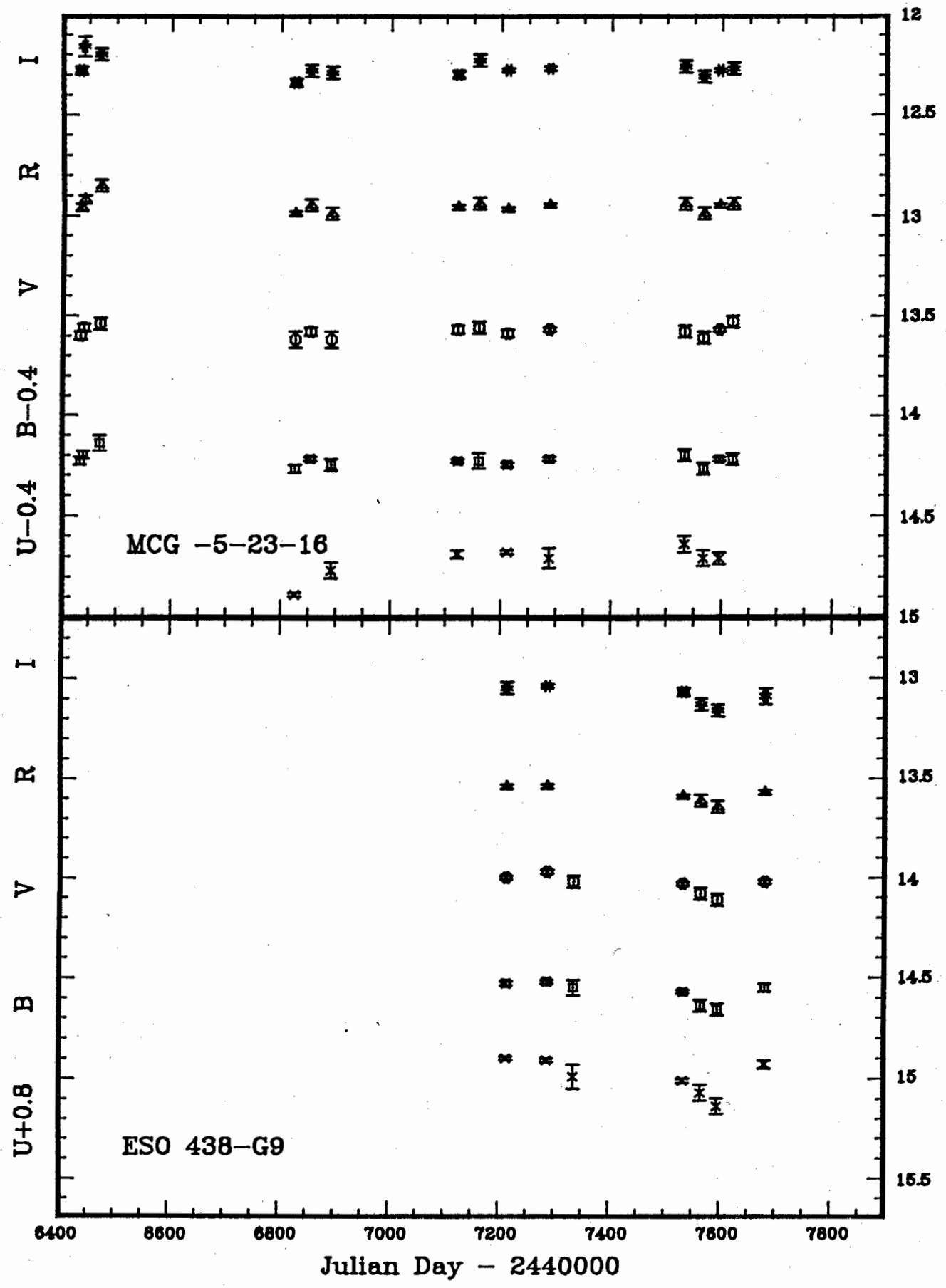

Figure 5.1(h). The light curves of NGC 3783 and H 1143-182.

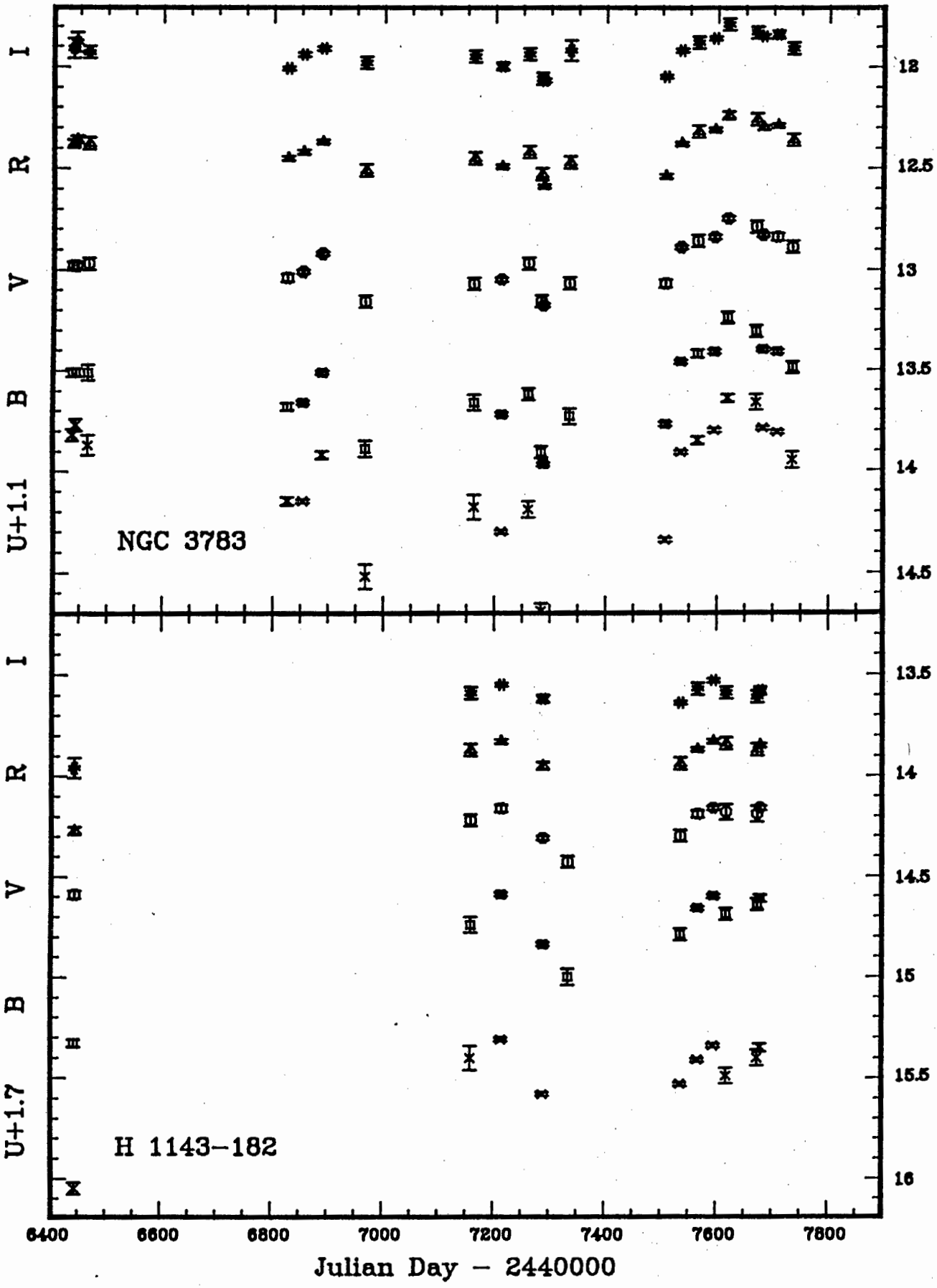

Figure 5.1(i). The light curves of MCG -2-33-34 and ESO 323-G77.

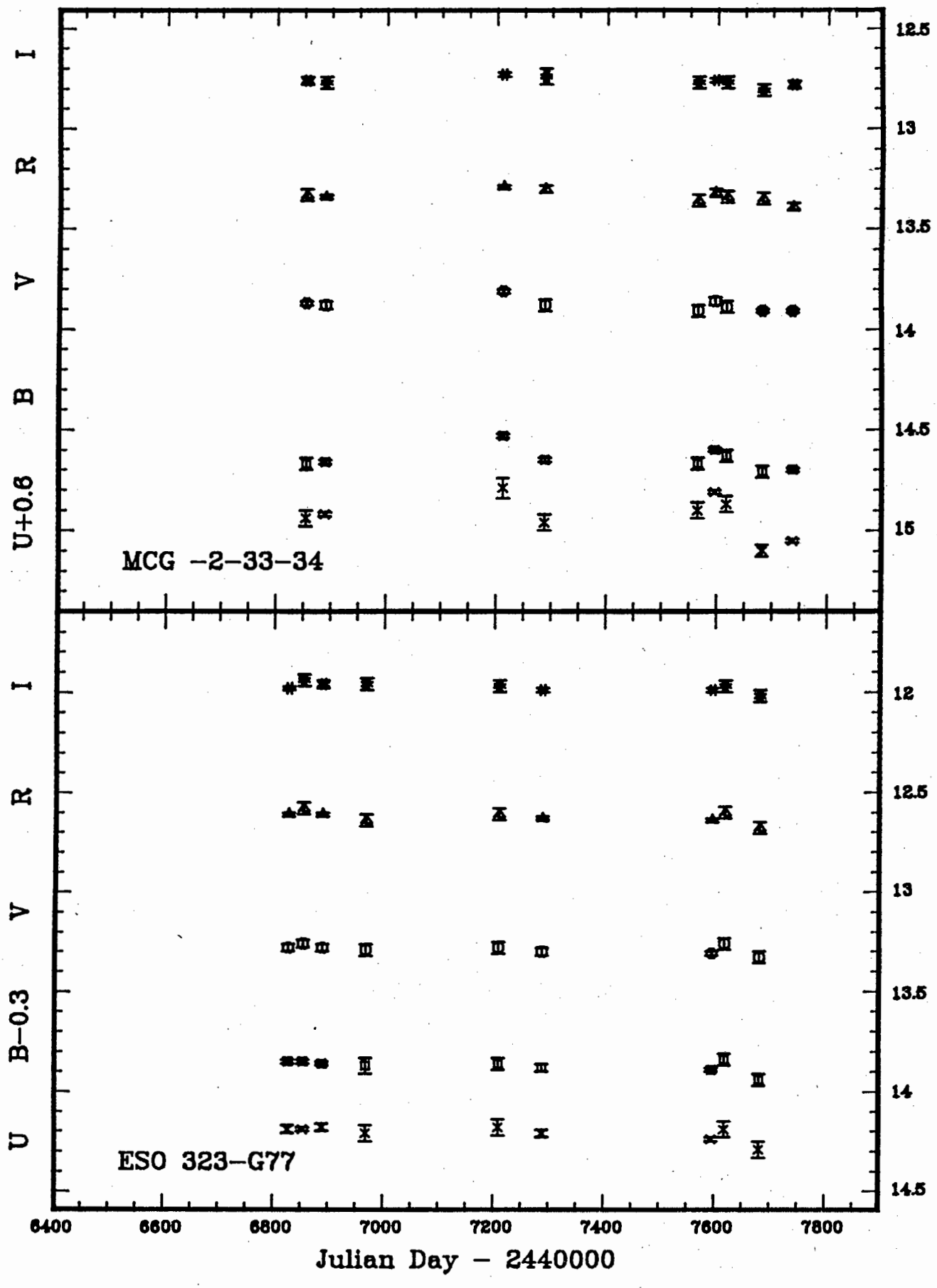

Figure 5.1(j). The light curves of MCG -6-30-15 and IC 4329A.

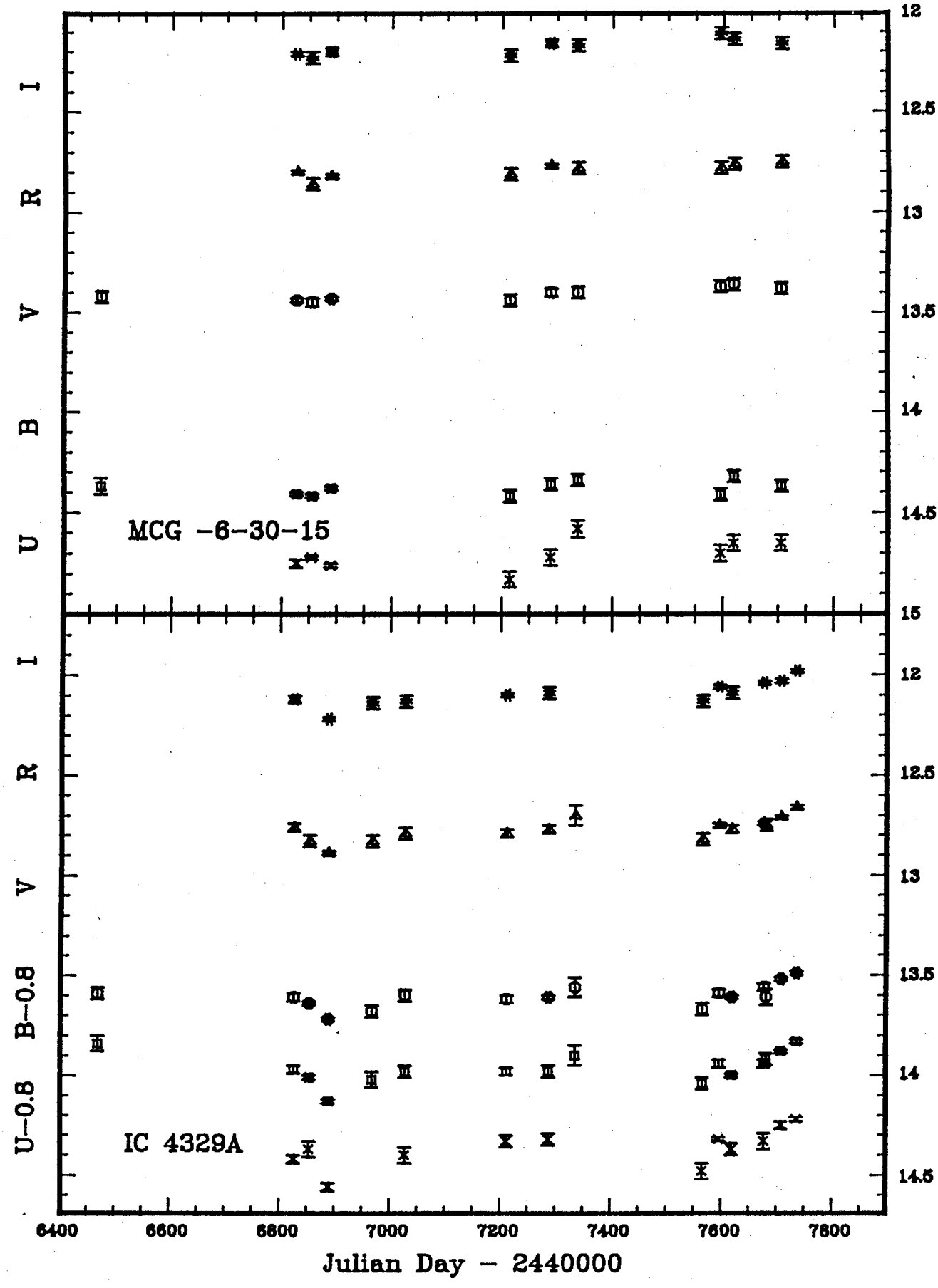

Figure 5.1(k). The light curves of IRAS 1509-211 and ESO 103-G35.

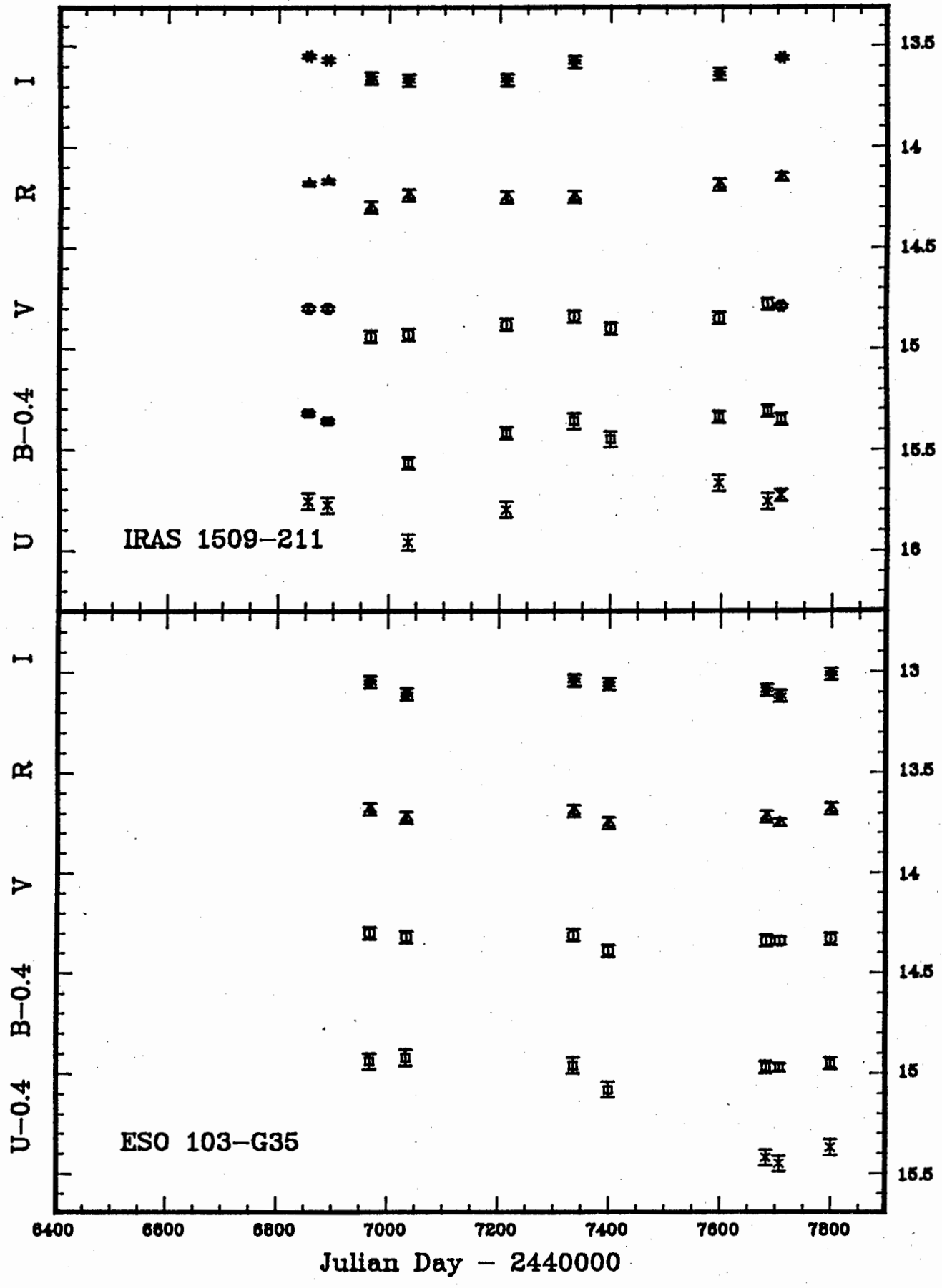

Figure 5.1(1). The light curves of Fairall 51 and ESO 141-G55.

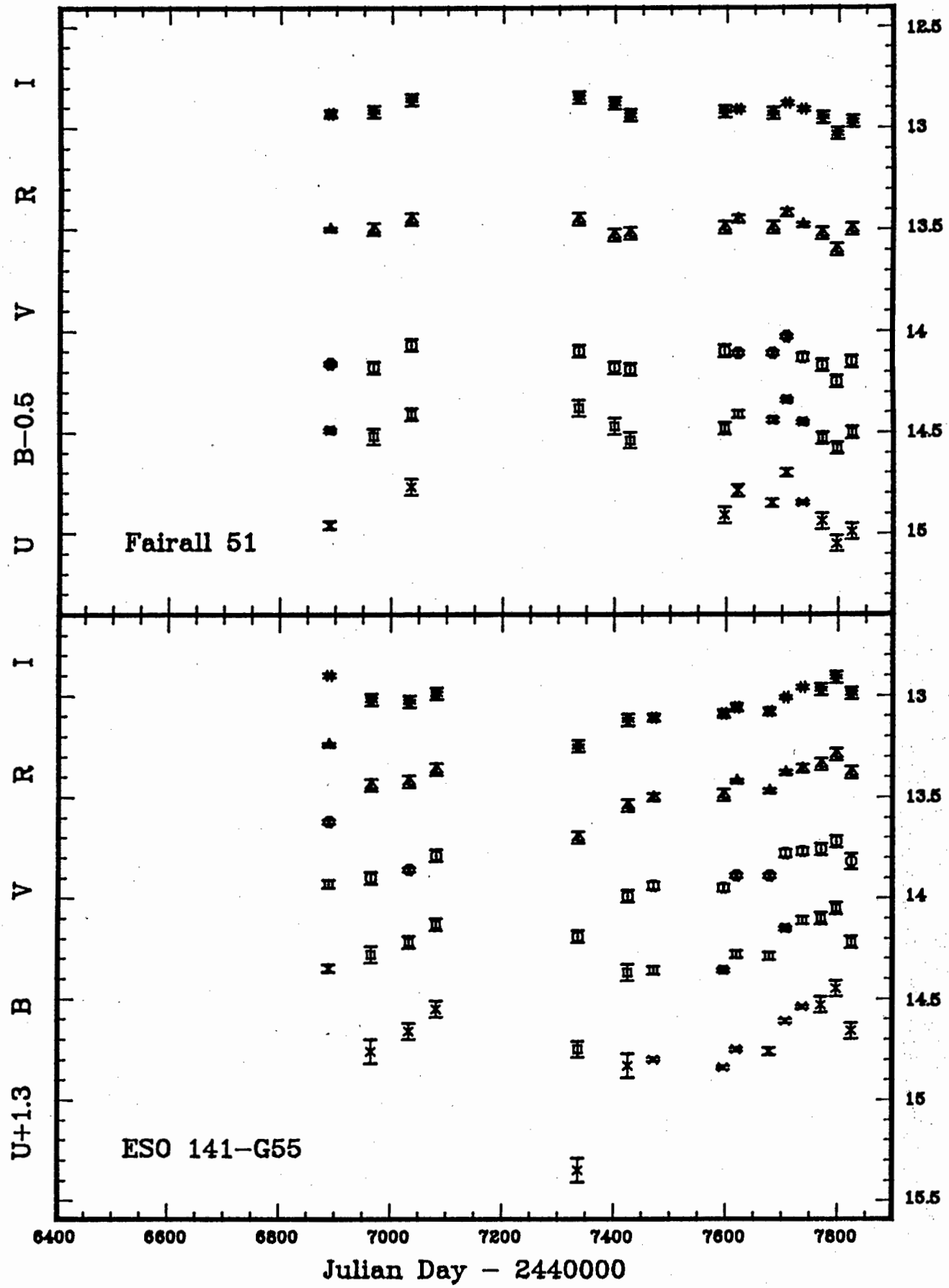

Figure 5.1(m). The light curves of NGC 6814 and NGC 6860.

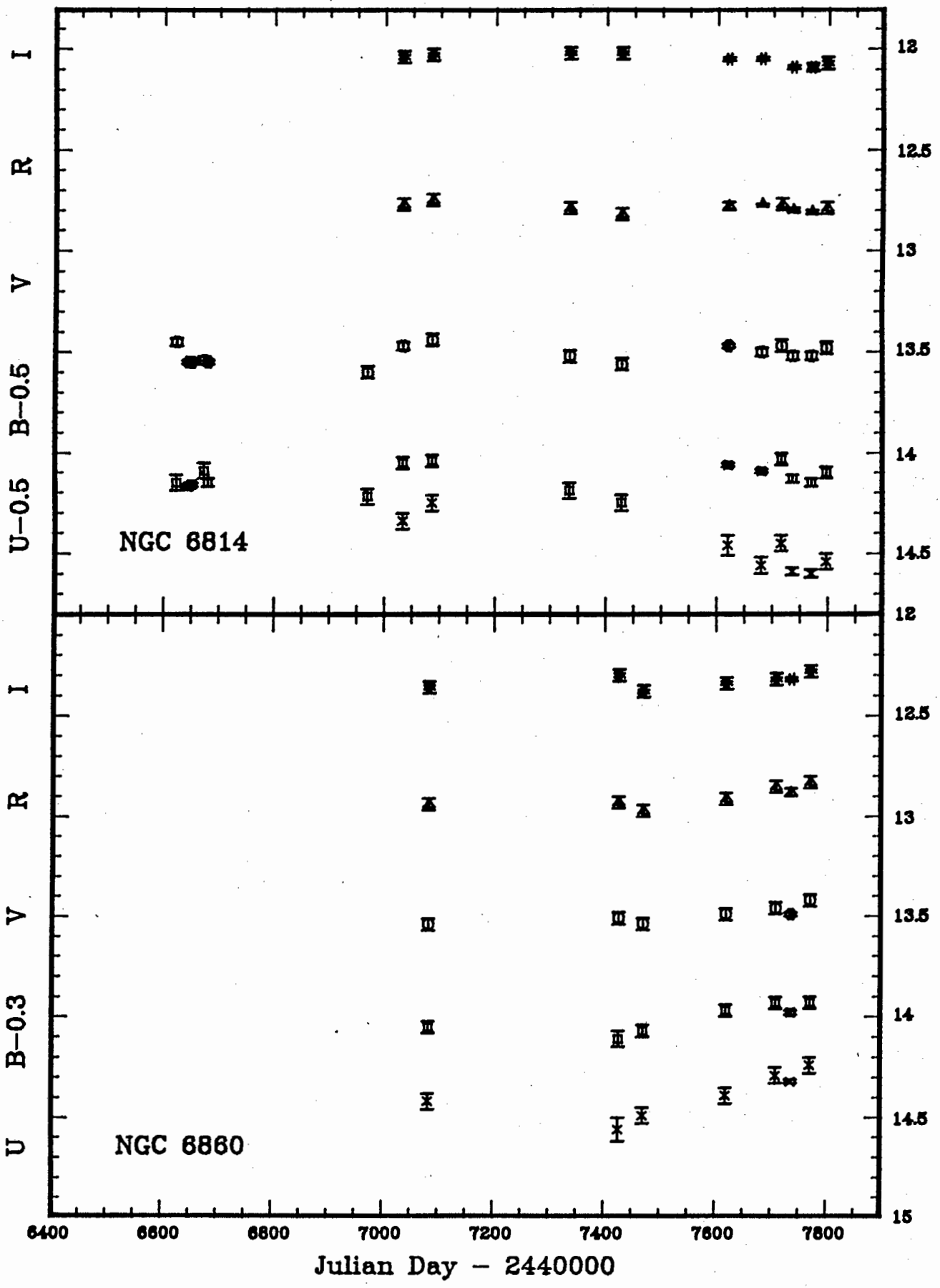

Figure 5.1(n). The light curves of H 2106-099 and NGC 7213.

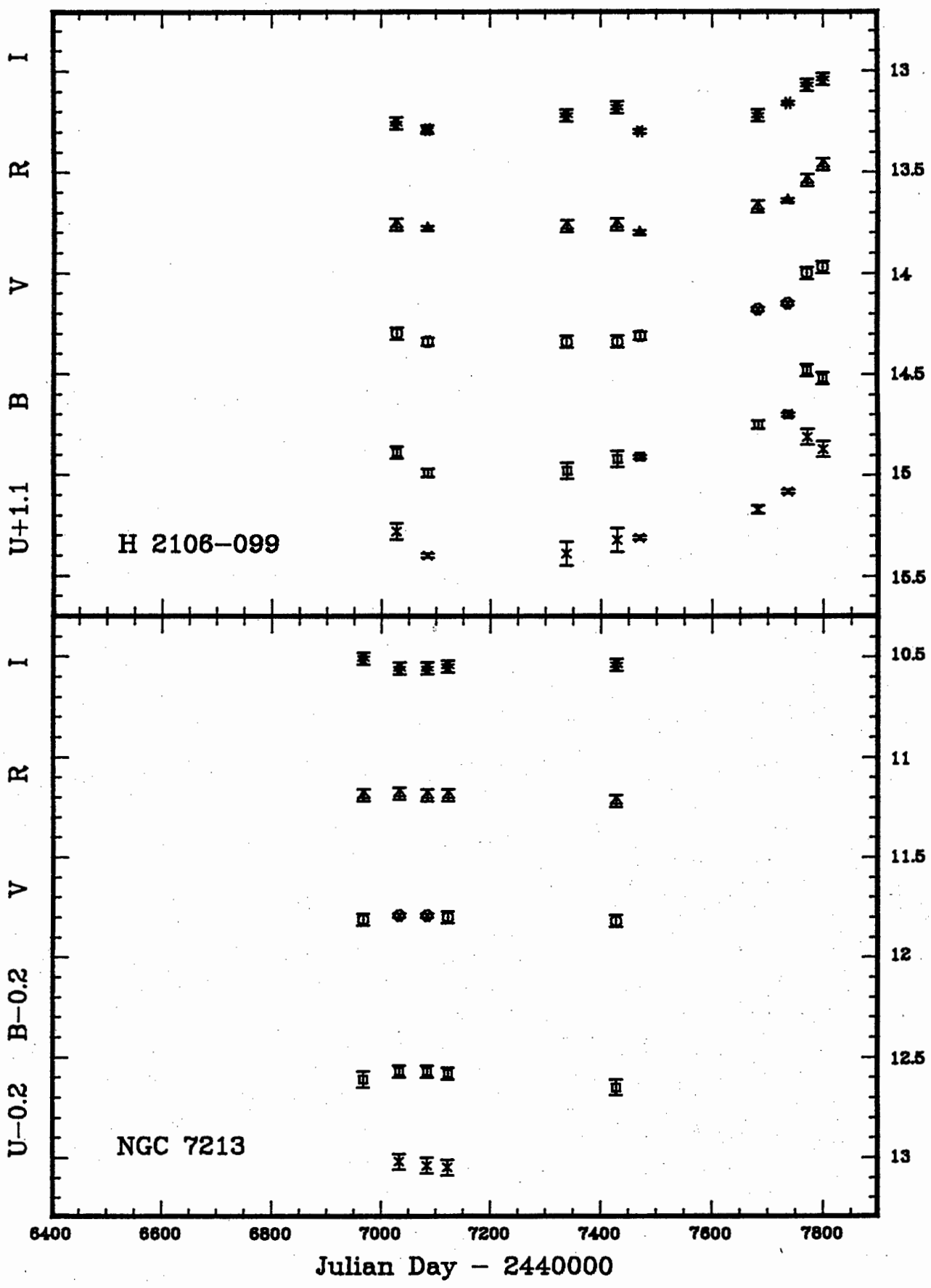

Figure 5.1(o). The light curve of MCG -2-58-22.

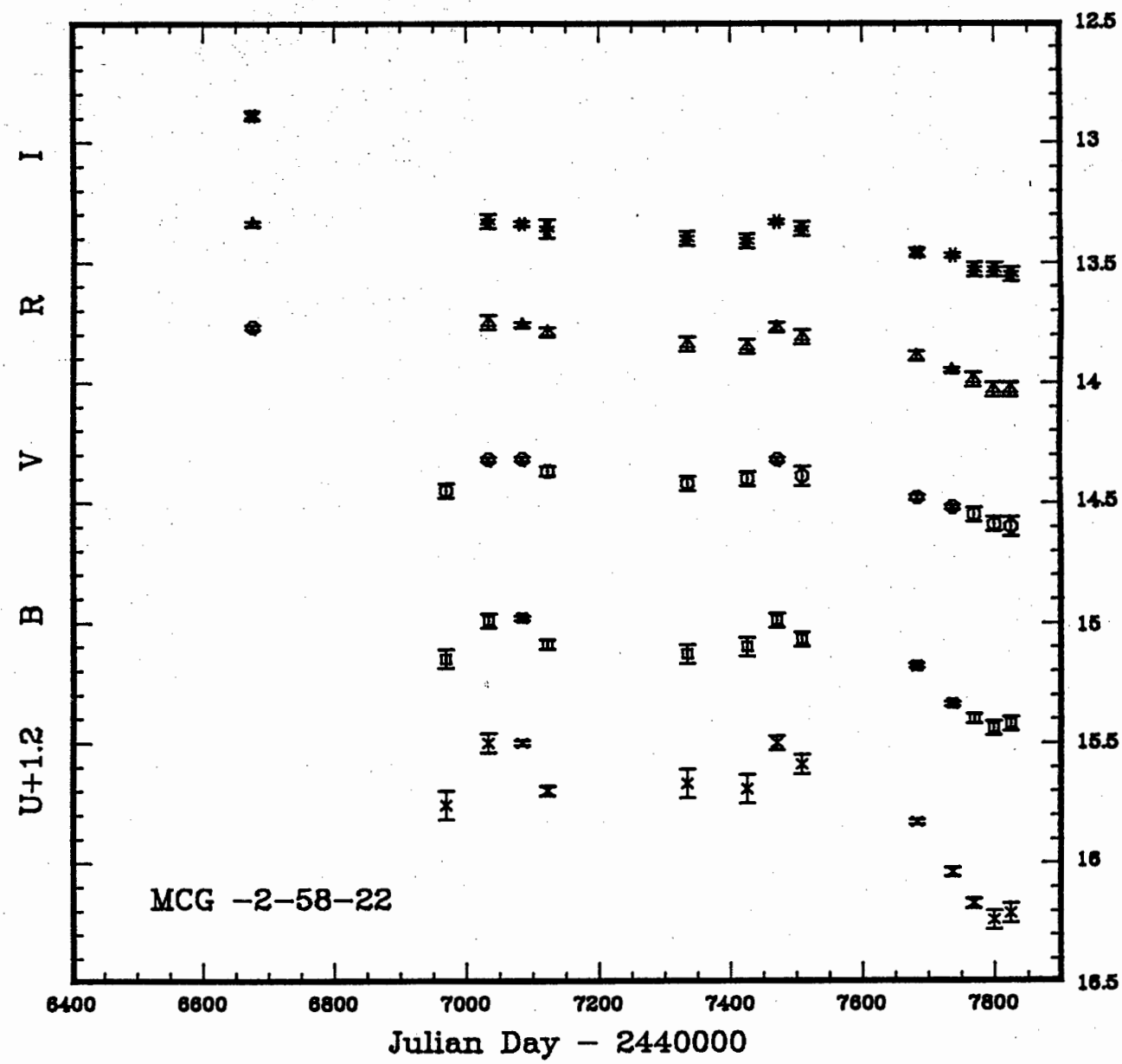

Figure 5.2(a). Plots of the U-band fluxes vs. the B-band fluxes for four galaxies. Different symbols are used to mark the fluxes measured by the different investigators. The aperture and CCD photometry from this work are marked by a square and a triangle respectively. Note that the axes are not the same for all objects.

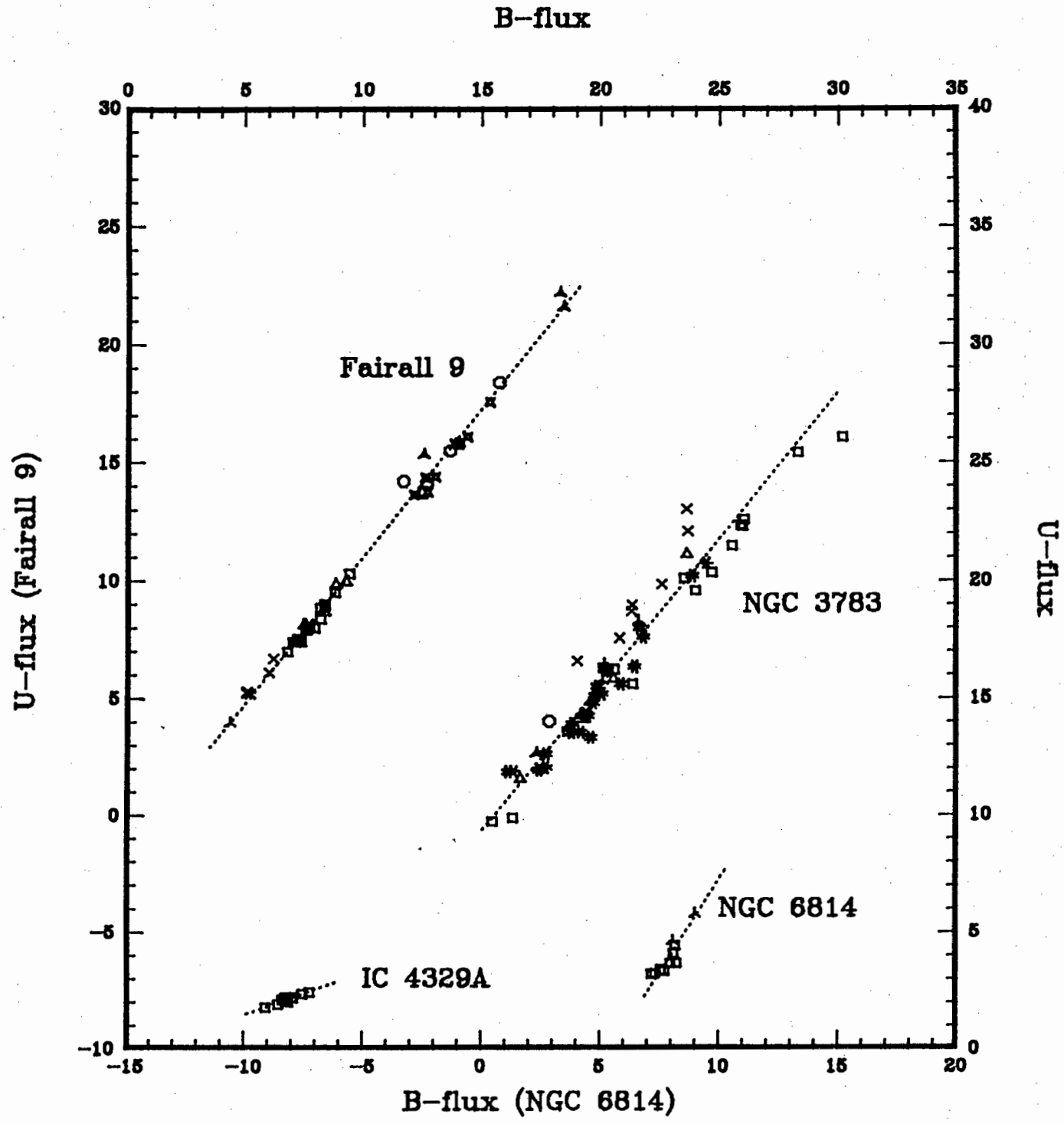

Figure 5.2(b). Plots of the B-band fluxes vs. the V-band fluxes for four galaxies.

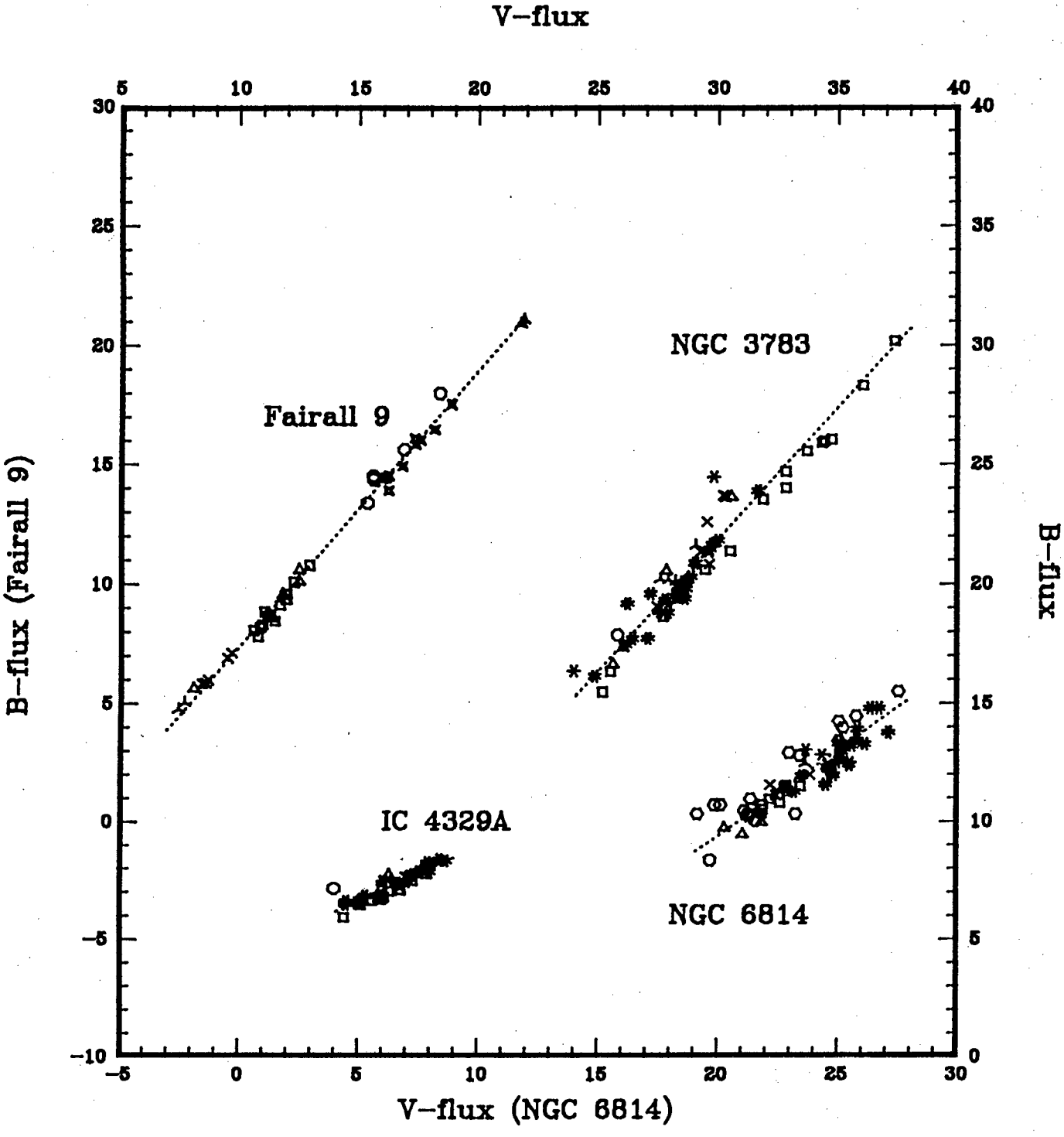

Figure 5.2(c). Plots of the V-band fluxes vs. the R-band fluxes for four galaxies.

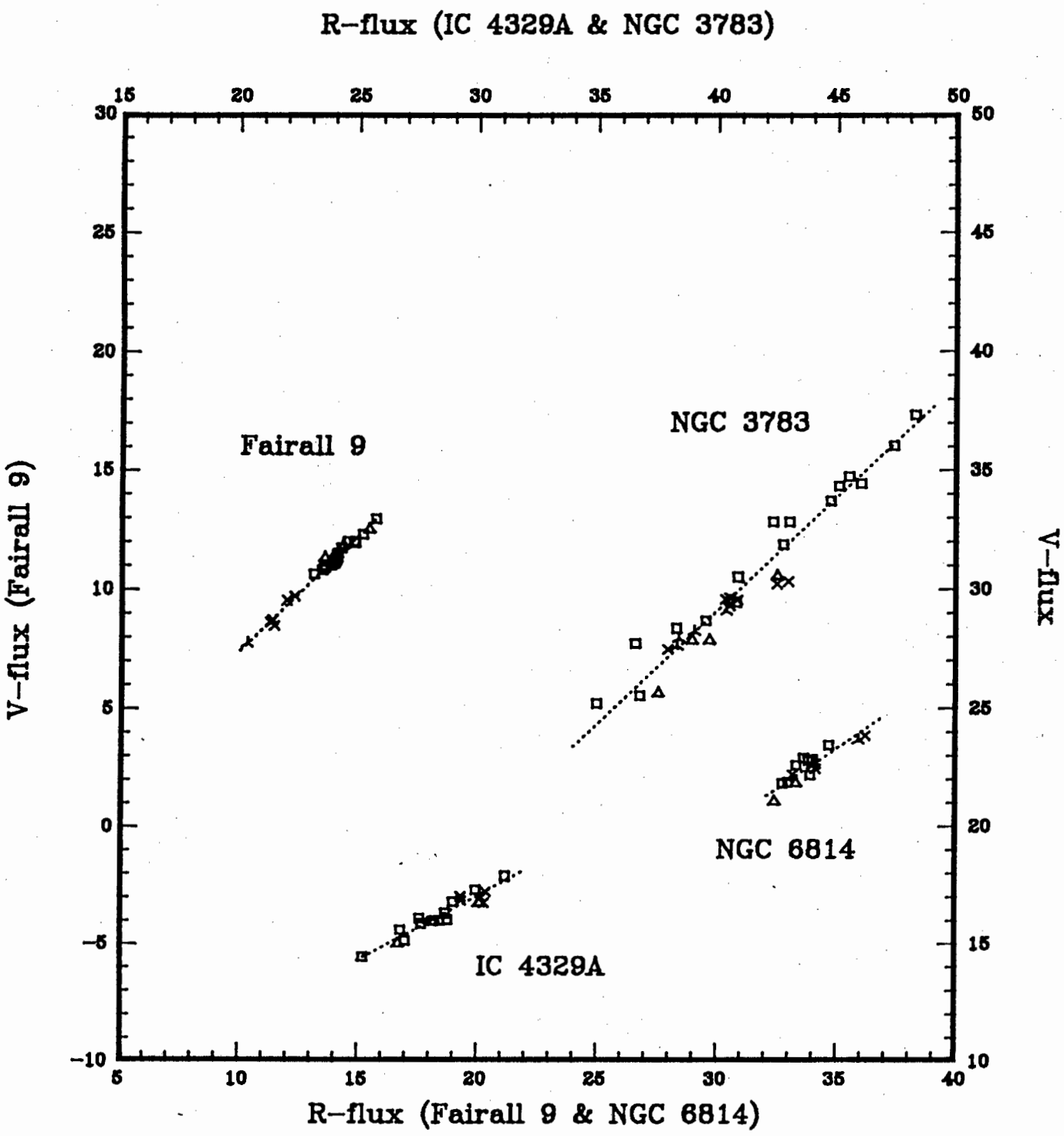

Figure 5.2(d). Plots of the V-band fluxes vs. the I-band fluxes for four galaxies.

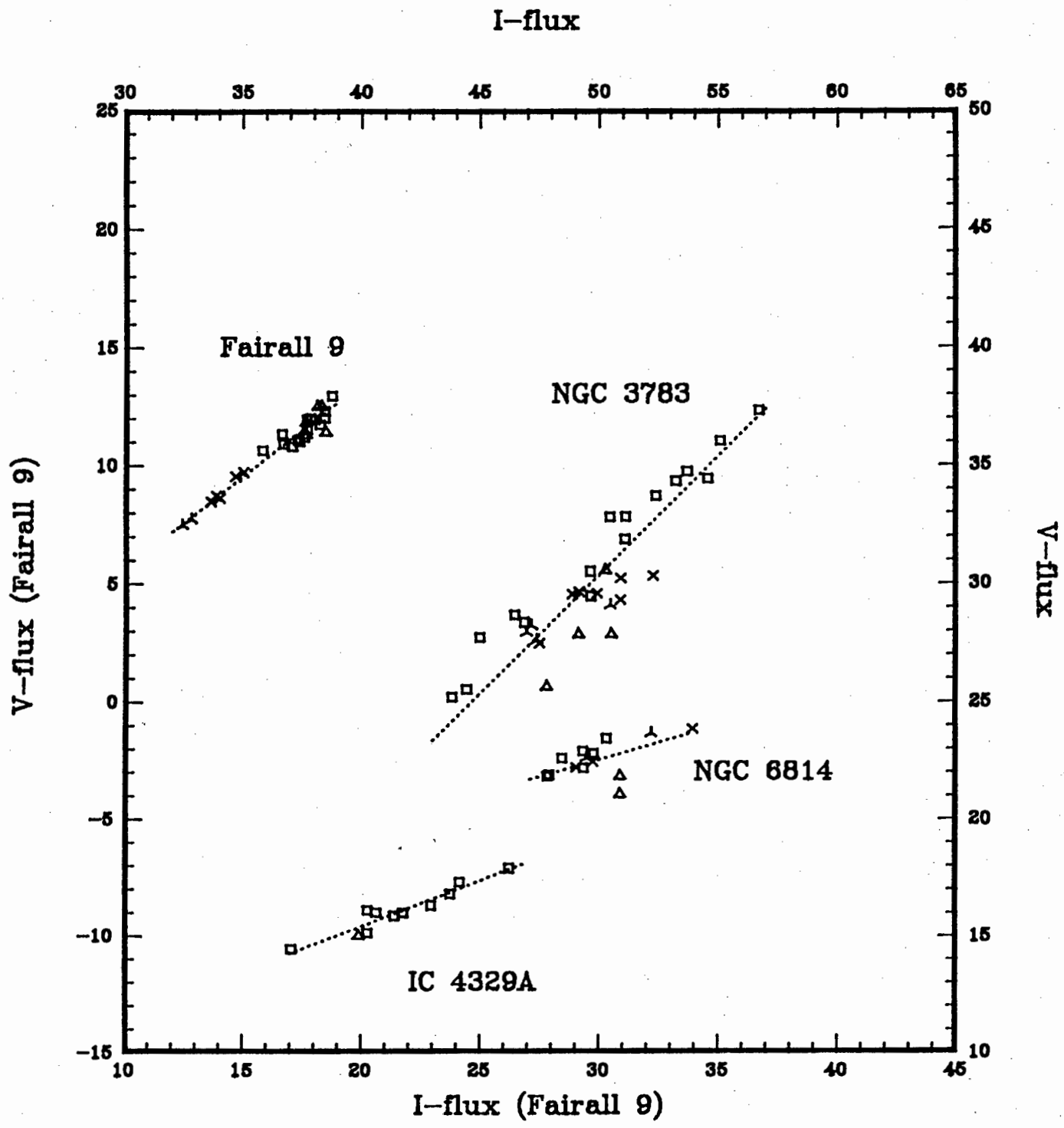

6. Spectroscopy

Spectroscopic measurements of most of the galaxies in the sample were made with two aims in mind. Firsty, a consistent data set was to be obtained in order to extract information about spectroscopic parameters such as the relative line intensities and line widths. To do this it was necessary to get one spectrum of the highest quality possible. Secondly, it was attempted to investigate the behaviour of the spectral features as a function of time. This required one to observe several spectra.

Table 6.1 lists the dates and other information relating to the spectroscopic observations.

Table 6.1. The spectroscopic observation log.

Dates from	to	Seeing (in ") Tu	We	Th	Fr	Sa	Su	Mo
18 Nov 86	25 Nov 86	3-4	3-4	2	1	3-4	2	2
3 Mar 87	6 Mar 87	2-6	2-3	2-3	1-2	-	-	-
15 Jun 87	16 Jun 87							2-3$^+$
28 Jul 87	2 Aug 87	2-3	1	1-2	1-2	1-2	-	-
4 Jan 88	5 Jan 88							2-3$^+$
11 Jan 88	12 Jan 88							2$^+$
2 Feb 88	3 Feb 88	1-2$^+$						
30 Nov 88	6 Dec 88	2-3	2	2	2-4	3-5	-	2-3

Note: a $^+$ indicates that only one night was allocated instead of the normal week.

6.1 The RETICON Spectrograph

The spectroscopic observations were made using the Image Tube Spectrograph (ITS) attached to the 1.9 m telescope at Sutherland. The detector used by this spectrograph is a Reticon Photon Counting System (RPCS), which has an EMI tube (S-20 photocathode) followed immediately by a Varo image intensifier, which in turn is followed by two linear RETICON arrays of 1872 pixels each. The slit width can be adjusted in 25 μm steps. 164 μm corresponds to a 1 arcsec angle in the sky. Dekkers are positioned orthogonally to the slit, so as to constrain the aperture to two smaller openings (slits) with slit lengths of 4 or 6 arcseconds, depending on the dekker size. The dekker is adjusted until the light passing through one aperture registers on the first pixel array, and

the light going through the other aperture registers on the second array.

Spectral dispersion is achieved through the use of a diffraction grating. Two gratings were used, a low resolution grating (no. 1 in the SAAO collection), which gives a dispersion of 210 Å/mm, and a high resolution grating (no. 4), with a dispersion of 50 Å/mm. Grating 1 covers the entire spectral range of the S-20 photocathode (3300-7500 Å).

6.2 Observations

A list of all the spectra recorded is given in table 6.2. Most of these were observed with grating 1. This grating has a nominal resolution of 2.8 Å per pixel, but the real resolution with a slit width of 300 μm is about 7 Å. Grating 4 (nominal resolution 0.7 Å) was used to obtain higher resolution (about 2 Å) spectra in a 900 A wavelength interval centered at 5000 Å, which is approximately the wavelength of Hβ. The slit was always orientated in an east-west direction. One array was used to record the spectrum of the object observed while the other array recorded the sky background. After this a second spectrum was usually measured, with the object having been moved into the other array.

In order to determine the relationship between pixel number and wavelength, an emission line spectrum from an argon lamp was recorded. This had to be done immediately before and/or after each object integration with the telescope in the same position, as the ITS suffers from flexure effects. Corrections for an unequal sensitivity of individual pixels could be made by measuring the light from a lamp with a featureless spectrum (the "flatfield"). Flatfields were usually recorded both before and after each night's work, using exposure times of about 3 hours.

If conditions were photometric, spectrophotometric standard stars from the lists of Baldwin and Stone (1984) and Stone and Baldwin (1983) were also observed during the night. For these, and in rare cases for bright Seyferts, neutral density filters had to be used.

Table 6.2. A list of all the spectra measured. The seven columns give the name of the galaxy, the date and time of the observation (local time), the integration times of the galaxy for each of the two arrays, the slit width and the grating used.

Galaxy name	date dd-mm-yy	SAST hhss	t(A) (s)	t(B) (s)	slit (μm)	grating no.
ESO 12-G21	29-07-87	0410	400	400	300	1
	04-12-88	2325	1200	-	300	1
	05-12-88	2235	-	1200	300	1
Ton S180	05-12-88	2200	1200	830	300	1
NGC 526a	19-11-86	2230	500	500	300	1
	30-07-87	0320	500	500	300	1
Fairall 9	18-11-86	2145	1000	1000	300	1
	16-06-87	0600	600	600	225	1
	29-07-87	0430	400	400	300	1
	11-01-88	2140	1200	1200	300	1
	30-11-88	2200	1000	1000	600	1
IC 1816	18-11-86	2330	600	600	300	1
	01-08-87	0440	500	500	300	1
H 0307-730	06-12-88	0115	1200	-	300	1
F-1116	24-11-86	0000	300	300	300	1
	31-07-87	0550	500	500	300	1
	12-01-88	0005	1200	1200	300	1
NGC 1566	04-01-88	2305	1200	1200	300	1
MCG -5-13-17	04-03-87	2220	500	500	300	1
	05-03-87	2235	600	600	300	4
	04-01-88	2355	1200	1200	300	1
	03-02-88	0000	1200	1200	225	1
3A 0557-383	04-03-87	2310	500	500	300	1
	12-01-88	0145	1200	1200	300	1
Fairall 265	05-03-87	2345	600	600	300	4
	05-01-88	0055	1200	1200	300	1
NGC 2992	23-03-85	2340	-	712	900	1
	05-01-88	0150	1200	1200	300	1
MCG -5-23-16	22-03-85	2055	672	672	900	1
	06-03-87	0045	600	600	300	4
	12-01-88	0235	1200	1200	300	1
	03-02-88	0055	1200	1200	225	1

Table 6.2. (continued)

Galaxy name	date dd-mm-yy	SAST hhss	t(A) (s)	t(B) (s)	slit (μm)	grating no.
NGC 3783	23-03-85	2300	500	500	900	1
	05-03-87	0025	400	400	300	1
	06-03-87	0210	600	600	300	4
	15-06-87	1945	500	500	225	1
	05-01-88	0255	1200	1200	300	1
	03-02-88	0150	1200	1200	225	1
H 1143-182	12-01-88	0325	1200	1200	300	1
	03-02-88	0240	1200	1200	225	1
MCG -2-33-34	05-03-87	0105	500	500	300	1
	06-03-87	0535	600	600	300	4
	05-01-88	0345	1200	1200	300	1
ESO 323-G77	21-03-85	0240	-	400	300	1
	05-03-87	0130	-	600	300	1
	06-03-87	0235	-	600	300	4
	15-06-87	2010	-	600	225	1
	12-01-88	0400	-	1200	300	1
MCG -6-30-15	21-03-85	0255	-	200	300	1
	21-03-85	0305	-	1000	900	1
	05-03-87	0145	500	500	300	1
	06-03-87	0350	600	600	300	4
	15-06-87	2030	600	600	225	1
	03-02-88	0330	1200	1200	225	1
IC 4329A	05-03-87	0220	500	500	300	1
	06-03-87	0415	600	600	300	4
	15-06-87	2100	750	750	225	1
	31-07-87	1915	500	500	300	1
	03-02-88	0415	1200	1200	225	1
IRAS 1509-211	05-03-87	0415	500	500	300	1
	31-07-87	2015	500	500	300	1
Fairall 51	29-07-87	2225	400	400	300	1
ESO 141-G55	16-06-87	0300	500	500	225	1
	29-07-87	2245	500	500	300	1
NGC 6814	29-07-87	2310	500	500	300	1
H 2106-099	30-07-87	0005	500	500	300	1
NGC 7213	16-06-87	0515	600	600	225	1
MCG -2-58-22	22-11-86	2035	300	300	300	1
	30-07-87	0215	500	500	300	1
	05-12-88	2105	1200	1200	300	1

6.3 Spectroscopic Reductions

The spectroscopic data were calibrated using the SKIP reduction package on the SAAO VAX computer. The spectra were divided by the normalised flatfields in order to correct them for individual pixel sensitivity. They were then wavelength calibrated after determining the wavelength-pixel relationship from the argon spectra recorded in conjunction with them. The flux calibration was made after determining the instrumental response function of the system from the spectra of the spectrophotometric standard stars. The spectra are displayed in figure 6.1.

Many of the spectra were recorded in cloudy or bad seeing conditions. Further light losses are expected as a result of bad guiding (no auto-guider is available) and flexure, which in extreme cases can result in light from an object falling on the sky array. Because of these difficulties it is believed that the spectra analysed here will not give a very accurate indication of the absolute nuclear flux. Therefore relative fluxes have been derived. Only in some cases has the strength of the Hβ line flux been estimated.

Although the spectral features of Seyfert nuclei are known to vary the emission from the narrow line region is taken to be comparatively constant (see chapter 7). Therefore to determine the relative narrow line intensities all the available spectra for an object may be co-added. The improved signal-to-noise ratio allowed the detection and measurement of otherwise invisible features. In many cases it was then also possible to separate the broad and narrow line components of the Balmer lines.

Many spectral lines are compound or blended, i.e., they are in fact a superposition of two or more lines. Separating a line into its components can be difficult as assumptions have to be made about the shape, strength and position of at least some of the components. It will be assumed that the widths of all narrow lines are equal when measured in velocity units (i.e., $\Delta\lambda/\lambda$ units). Appenzeller and Ostreicher (1988) have shown that forbidden line widths usually increase with ionisation potential. However, the line widths of [O III], [N II], [O I] and HI_{narrow} are normally similar. The narrow line widths have been determined from the strong [O III] 5007 Å line. Below are descriptions of how some of the lines were deblended. The procedure makes use of the intrinsic line ratios listed in chapter 2.2.1.

- The narrow line component of Hβ could be separated from the broad line

component by identifying the points where the Hβ width coincided with the [O III] 5007 Å width, measuring the height of the line peak from these points and comparing these to the 5007 Å peak height.

- [O III] 4363 Å is often superimposed on Hγ. If this line was clearly visible its strength could be estimated by comparing its profile to the [O III] 5007 Å profile.

- [N II] 6548 Å and 6583 Å usually superimpose on the wings of Hα. Separating these from Hα was only possible if the strength of the 6583 Å line could be estimated using the same procedure as for the [O III] 4363 Å line. In gases with densities and temperatures of the order of magnitude expected in the narrow line region of Seyfert galaxies, the intensity of the 6583 Å line will be 2.96 times the intensity of the 6548 Å line.

- [Fe X] 6374 Å may be contaminated by [O I] 6363 Å. This was corrected for by assuming that the intensity of the 6363 Å line was 1/3 of the intensity of the [O I] 6300 Å line.

- The wavelength of Hε almost coincides with that of [Ne III] 3967 Å. The Hε intensity was calculated by assuming that the intensity ratio of the [Ne III] 3869 Å, 3967 Å doublet was 3.15.

- The 3889 Å line is a blend of H8 and He I. As these lines are expected to be formed in the same region and because they are not of special interest no attempt at separating them was made.

- Although there is a [Ca V] line at 6086 Å, its intensity must be very small, as the [Ca V] 5309 Å line, which is 4.46 times stronger, is normally not detected. Therefore the [Fe VII] 6087 Å line is not significantly blended.

The spectral line intensities measured relative to [O III] 5007 Å, corrected for blending effects and reddening in our galaxy, are given in table 6.3. The broad line intensities are also given, although their strengths are known to be variable. The nature of this variability will be discussed in chapter 7. The strength of the Fe II emission line bands is graded on a scale from 1 to 4 (corresponding to "not visible", "visible", "strong" and "very strong"; a 0 means "impossible to tell"). The measurement and analysis of the line widths

will also be discussed in chapter 7.

Additional spectral information is given in table A4 in the appendix, where the relative emission line strengths derived by other investigators have been listed.

Table 6.3. The spectral line intensities measured realtive to [O III] 5007 A.

Galaxy Name	[NeV] 3427	[OII] 3727	[FeVII] 3757	[NeIII] 3868	H8+HeI 3889	Hε 3968	[SII] 4068	Hδ 4102
ESO 12-G21	-	0.25	-	-	-	-	-	-
Ton S180	-	-	-	-	-	-	-	0.79
NGC 526a	-	0.48	-	0.15	-	-	-	-
Fairall 9	0.35	0.14	0.11	0.30	0.22	0.28	-	0.59
IC 1816	-	0.24	-	0.16	-	-	-	-
H 0307-730	-	-	-	-	-	-	-	-
Fairall 1116	1.55	0.50	0.25	0.22	-	0.18	-	1.50
NGC 1566	-	0.46	-	0.20	-	-	-	-
MCG-5-13-17	-	0.15	0.03	0.23	-	-	-	-
3A 0557-383	-	0.14	-	0.10	0.04	-	-	0.28
Fairall 265	-	0.76	-	-	-	-	-	1.15
NGC 2992	-	0.41	-	0.08	-	-	-	-
MCG-5-23-16	0.27	0.30	-	0.14	-	-	-	-
NGC 3783	0.42	0.14	0.13	0.20	0.13	0.17	-	0.47
H 1143-182	0.32	0.24	0.06	0.21	0.17	0.24	-	0.53
MCG-2-33-34	0.09	0.36	-	0.10	0.06	0.03	-	0.20
ESO 323-G77	-	0.23	-	0.20	0.13	-	-	0.64
MCG-6-30-15	0.44	0.40	-	0.14	-	-	-	0.17
IC 4329A	-	0.05	-	0.08	-	-	-	0.17
IRAS 1509-21	-	0.31	-	0.11	-	0.06	-	0.20
Fairall 51	-	0.42	-	0.24	-	-	-	0.58
ESO 141-G55	0.65	-	-	0.83	<--	0.57	-	0.78
NGC 6814	-	-	-	-	-	-	-	-
H 2106-099	-	-	-	-	-	0.72	-	1.18
NGC 7213	-	0.95	-	0.52	0.28	-	0.22	-
MCG-2-58-22	0.33	0.53	-	0.17	0.10	0.03	-	0.22

Table 6.3. (continued)

Galaxy Name	Hγ 4340	[OIII] 4363	HeII 4686	Hβwid 4861	Hβnar 4861	[OIII] 4959	[FeVI] 5673	[FeVII] 5721	HeI 5876
ESO 12-G21	0.86	<--	-	1.64	<--	0.22	-	-	0.32
Ton S180	1.68	<--	-	4.55	<--	0.18	-	-	-
NGC 526a	0.05	<--	-	-	0.10	0.37	-	-	-
Fairall 9	0.98	0.12	0.09	2.31	0.17	0.43	-	0.07	0.31
IC 1816	-	-	-	-	0.11	0.39	-	-	-
H 0307-730	0.45	<--	-	1.24	<--	0.25	-	-	-
Fairall 1116	2.16	0.13	0.25	6.52	0.08	0.34	-	0.16	0.30
NGC 1566	0.70	<--	-	0.53	0.18	0.39	-	-	0.06
MCG-5-13-17	0.17	0.07	0.04	0.49	0.09	0.35	-	0.03	0.06
3A 0557-383	0.82	<--	0.10	2.19	<--	0.33	-	-	0.20
Fairall 265	1.23	<--	-	2.40	<--	0.26	-	-	-
NGC 2992	0.08	0.06	-	-	0.12	0.36	-	-	0.03
MCG-5-23-16	-	-	-	-	0.04	0.40	-	-	-
NGC 3783	0.59	0.08	0.04	1.04	0.10	0.34	0.01	0.02	0.10
H 1143-182	0.96	0.06	0.39	1.44	0.09	0.36	-	-	0.18
MCG-2-33-34	0.35	<--	0.05	0.49	0.15	0.33	-	-	0.03
ESO 323-G77	1.20	<--	-	2.74	<--	0.30	-	-	0.19
MCG-6-30-15	0.60	<--	0.08	0.98	0.10	0.39	-	-	0.12
IC 4329A	0.48	0.06	0.06	1.65	0.10	0.34	-	0.04	0.36
IRAS 1509-21	0.36	<--	0.13	0.83	0.17	0.29	-	-	0.35
Fairall 51	0.86	<--	-	1.00	0.16	0.36	-	-	-
ESO 141-G55	2.05	0.05	-	4.24	<--	0.37	-	-	0.78
NGC 6814	-	-	-	0.35	<--	0.28	-	-	-
H 2106-099	2.02	<--	-	3.05	<--	0.42	-	-	0.35
NGC 7213	0.45	0.50	-	0.75	<--	0.58	-	-	-
MCG-2-58-22	0.43	0.04	-	0.48	0.11	0.38	-	-	-

Table 6.3. (continued)

Galaxy Name	[FeVII] 6087	[OI] 6300	[FeX] 6364	[NII] 6548	Hα 6563	[NII] 6584	[SII] 6716	[SII] 6731	FeII
ESO 12-G21	-	-	-	-->	8.82	<--	0.44	<--	4
Ton S180	-	-	-	-->	15.6	<--	-	-	4
NGC 526a	-	0.07	-	0.06+	0.30	0.20	0.08	0.08	1
Fairall 9	0.15	-	-	0.11+	7.62	0.33	-	-	2
IC 1816	-	0.07	-	0.15+	0.40	0.45	0.12	0.12	1
H 0307-730	-	-	-	-->	11.5	<--	-	-	0
Fairall 1116	0.16	-	-	-->	14.4	<--	-	-	3
NGC 1566	-	0.03	0.01	0.32+	2.56	0.96	0.18	0.22	2
MCG-5-13-17	0.03	0.08	0.03	0.10+	2.74	0.30	0.07	0.07	1
3A 0557-383	-	-	-	-->	21.8	<--	-	-	2
Fairall 265	-	-	-	0.45+	8.49	1.35	-	-	3
NGC 2992	-	0.10	0.05	0.26+	1.99	0.78	0.36	0.30	1
MCG-5-23-16	-	0.05	-	0.15	0.45	0.40	0.06	0.07	1
NGC 3783	0.05	0.05	0.04	0.03+	4.31	0.10	0.06	0.06	2
H 1143-182	-	0.04	0.03	-->	5.32	<--	0.04	0.03	1
MGC-2-33-34	0.02	0.04	-	0.19+	1.74	0.57	0.09	0.10	2
ESO 323-G77	-	-	-	-->	13.9	<--	0.32	<--	4
MCG-6-30-15	0.04	-	0.05	-->	7.60	<--	0.12	0.13	2
IC 4329A	0.08	0.23	-	-->	15.4	<--	-	-	3
IRAS 1509-21	-	0.13	-	0.09+	4.81	0.27	0.22	<--	2
Fairall 51	-	-	-	0.11+	4.01	0.33	-	-	2
ESO 141-G55	-	-	-	-->	16.6	<--	-	-	3
NGC 6814	-	-	-	-->	2.42	<--	-	-	0
H 2106-099	0.22	-	-	-->	8.31	<--	-	-	3
NGC 7213	-	0.75	-	0.25+	4.32	0.75	0.25	0.25	0
MCG-2-58-22	-	0.10	-	-->	4.36	<--	0.21	<--	1

Notes:-

--> (or <--): this signifies that the line could not be measured because of blending with the line tabled immediately to its left (right).

+: these intensities were not measured. They were derived by dividing the 6584 Å line intensity by 2.96.

Figure 6.1(a). The spectra of Fairall 1116, Ton S180, ESO 141-G55, H 2106-099 and Fairall 9. The Y-scale is not the same for all objects.

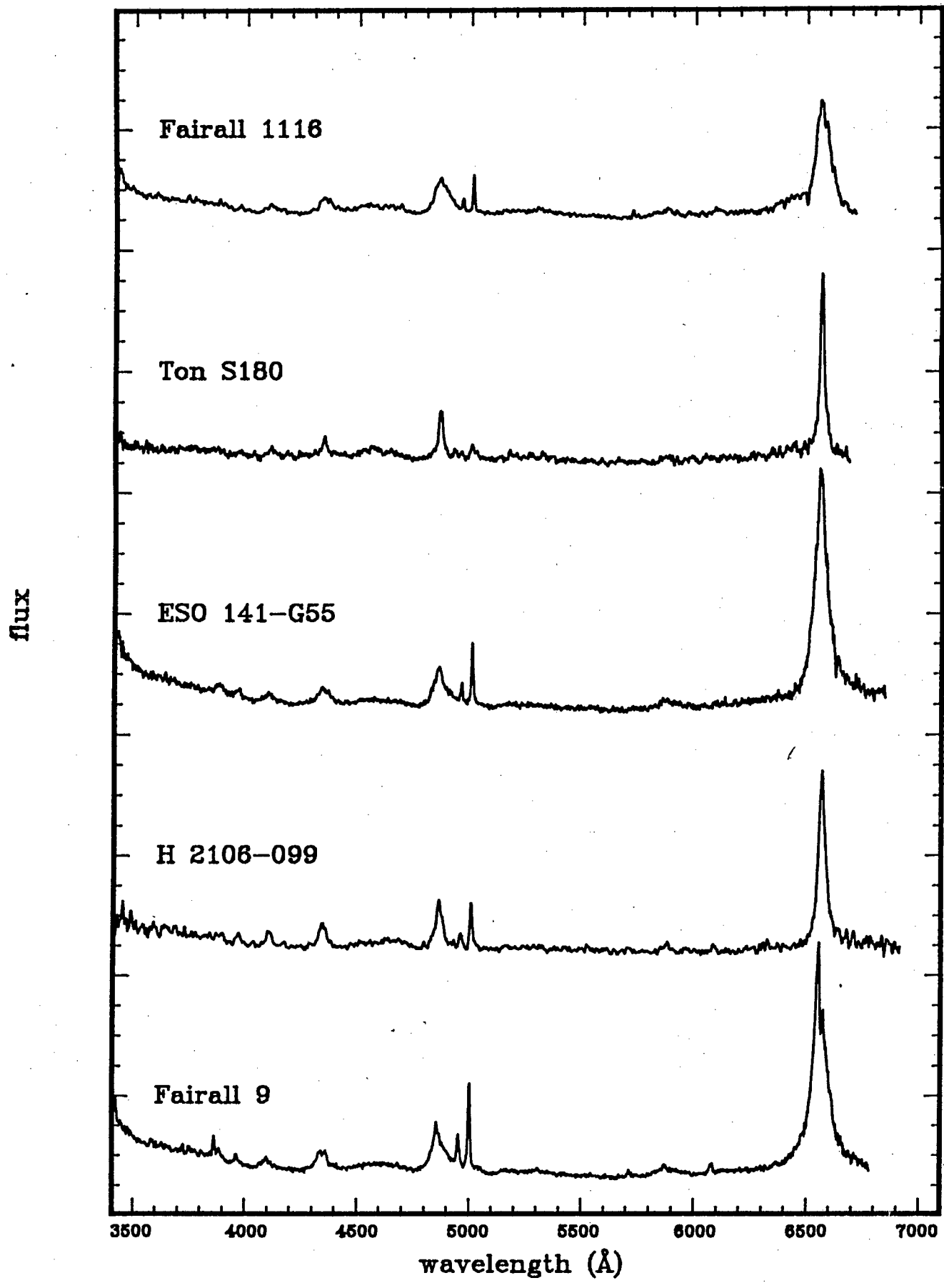

Figure 6.1(b). The spectra of Fairall 265, ESO 12-G21, H 1143-182, H 0307-730 and NGC 3783.

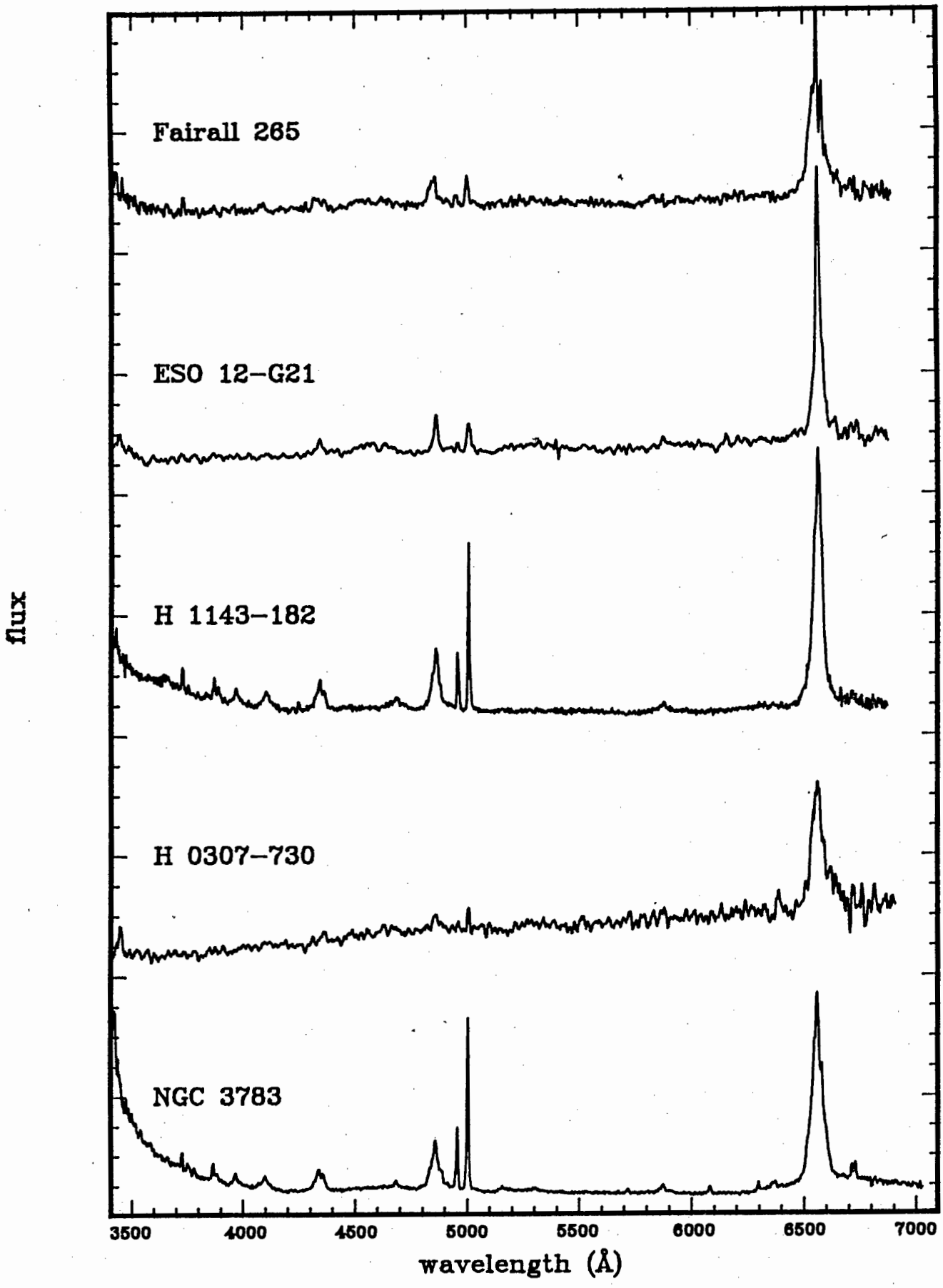

Figure 6.1(c). The spectra of 3A 0557-383, IC 4329A, ESO 323-G77, MCG -6-30-15 and MCG -2-58-22.

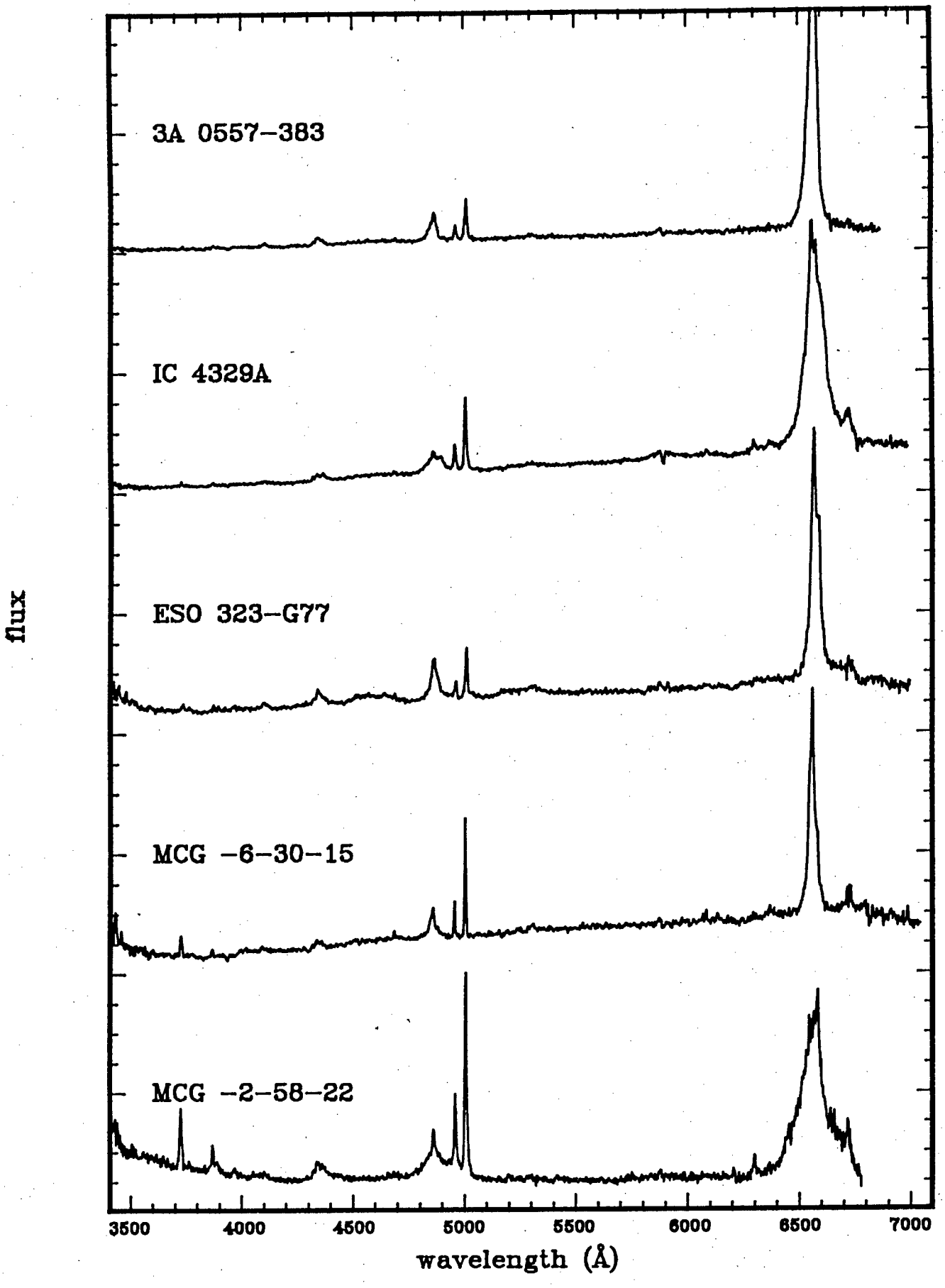

Figure 6.1(d). The spectra of NGC 1566, MCG -5-13-17, MCG -2-33-34, Fairall 51 and IRAS 1509-211.

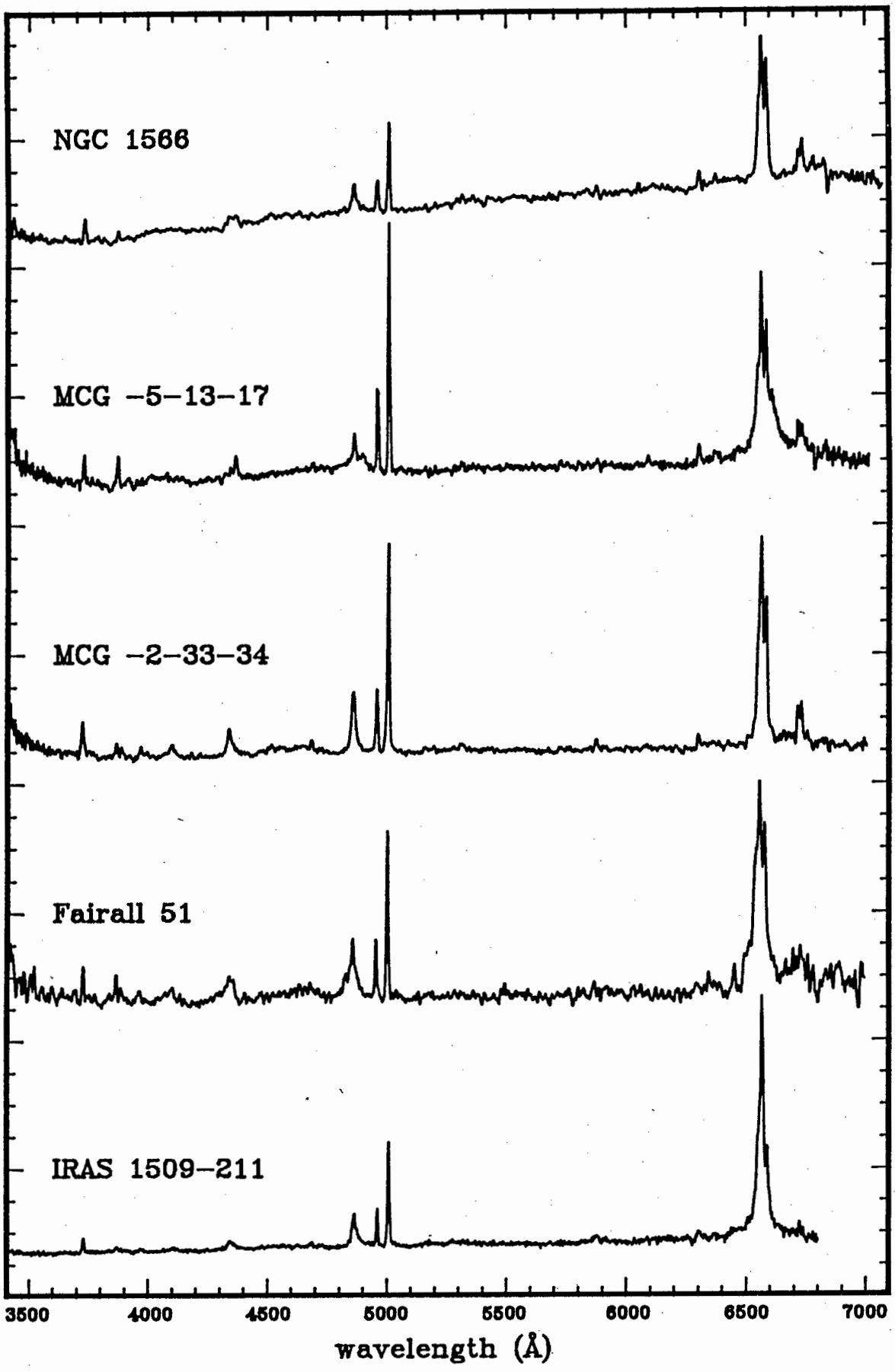

Figure 6.1(e). The spectra of MCG -5-23-16, NGC 2992, IC 1816, NGC 526a and NGC 6814.

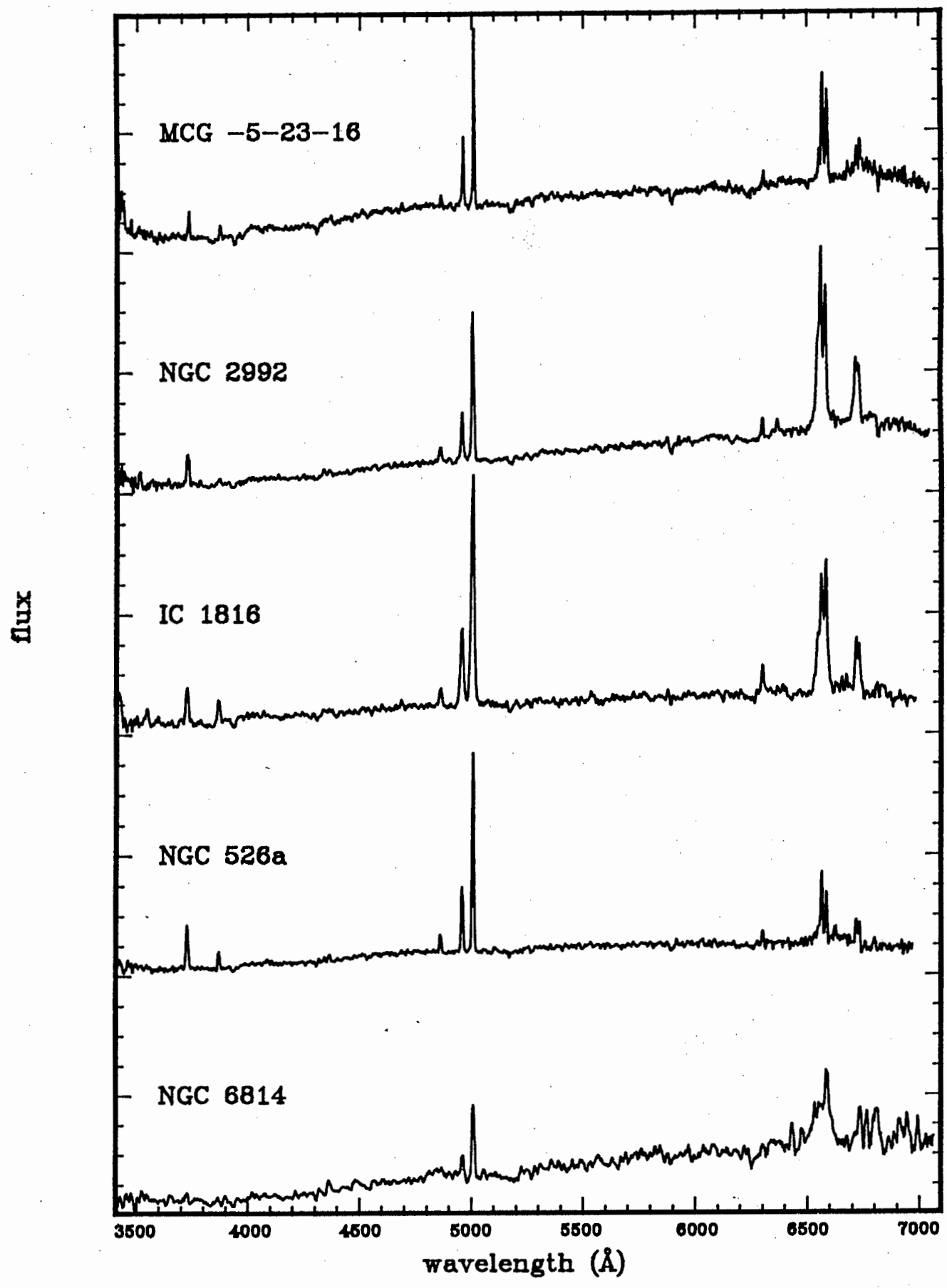

Figure 6.1(f). The spectrum of NGC 7213.

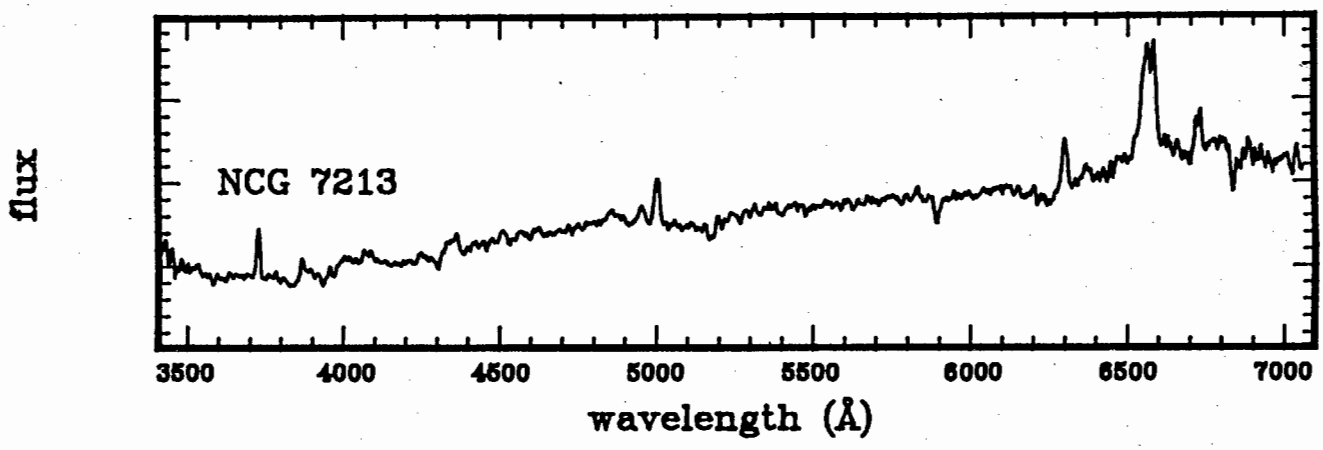

7. The general Properties of Seyfert Galaxies

7.1. Flux Distribution

A lot of effort has been put into mapping the spectral energy distribution of AGN's and identifying the flux components of the continuum (McAlary et al, 1983, Edelson and Malkan, 1986, Ward et al, 1987, Carleton et al, 1987, Sun and Malkan, 1989). There is general agreement about the existence of the following components:-

a) a non-thermal component described by a power law of the form $F(\nu) \propto \nu^{-\alpha}$ with a low frequency exponential cut-off. It has been suggested that the power law index varies depending on what part of the spectrum one is dealing with. In the infrared α is about 1.2 (Glass et al, 1982) while for X-ray spectra $\alpha \sim 0.7$ (Mushotzky, 1982).

b) an emission line spectrum, including iron emission line bands and a Balmer continuum.

c) an ultraviolet blackbody component with a temperature suggested by Edelson and Malkan (1986) to be ~ 26000 K.

d) thermal dust emission components in the infrared.

More components have been proposed in order to explain the complexity of some spectra. For example, a 5 μm excess has been suggested by Edelson and Malkan (1986). The possibility of the non-thermal radiation beaming in a preferred direction has been suggested by Ward (1989).

Different wavelength regimes will now be discussed. All fluxes given below have been corrected for extinction in our galaxy.

7.1.1. Ultraviolet

Ultraviolet flux measurements (given in columns 3 and 4 of table 7.6) were extracted from the literature (e.g., Wu et al, 1983). They have been estimated near rest wavelengths of 1450 Å and 2500 Å, two regions of the spectrum that are relatively free from emission lines, and these fluxes are therefore measures of the continuum strength. Stellar contamination in the ultraviolet is expected to be very small, hence the subtraction of a stellar component was not deemed necessary.

There are two factors responsible for a relatively large uncertainty of the ultraviolet nuclear flux. Firstly, the UV is the part of the spectrum most

affected by reddening. The errors in the nuclear flux estimates because of an uncertainty of A_v will be largest at these wavelengths. Secondly, the UV flux is also subject to intense luminosity changes. For example, Barr et al (1983) found that their ultraviolet flux measurements of NGC 3783 varied by a factor of 10. As the ultraviolet and optical observations were usually not made simultaneously, the flux distribution could have a discontinuity between these two wavelength regions, which could lead to an over- or underestimation of the ultraviolet excess.

7.1.2. Optical

The flux distribution in the optical was calculated from the $UBV(RI)_c$ aperture photometry and/or CCD photometry. In this part of the spectrum starlight from the underlying galaxy contributes a significant fraction of the total light measured. Corrections for reddening introduce further uncertainties, particularly at shorter wavelengths. The use of broadband photometry to define the flux distribution does not allow an accurate subtraction of emission lines. They will affect the various passbands as follows.

U - this will include the Balmer continuum.

B - this will include Hβ and Hγ.

V - just includes the Hβ and [O III] lines.

R - probably the most affected band, with Hα in its centre.

Accurate spectrophotometry would circumvent the problems of separating the continuum flux and the line flux, but a large aperture is required to avoid seeing and losses from bad guiding. This means that a substantial starlight component would be measured as well. The spectra from this work that were taken in photometric conditions are not suitable for spectrophotometric analysis because of the small slit width.

An advantage of using broadband photometry to study the flux distribution is that much data covering many years are often available. This enables one to monitor the changes in the various components of the flux distribution as a function of time. The B, V and I bands should show the behaviour of the power law and the UV thermal components. The R band will describe the relative strength of the broad emission lines. The U band can be used to gauge variations in the Balmer continuum.

The magnitudes and colours of the program galaxies at various epochs converted to the 20" aperture were derived in chapter 5. These values were changed to

fluxes per unit frequency (measured in Jansky) using the formula

$$F(m)\ (Jy) = a(m).10^{3-0.4(m-Am)}$$

where A_m is the extinction in the m filter in our galaxy. The calibration coefficients a(m) and the characteristic band frequencies ν_m were taken from Bessell (1979) and are listed in table 7.1. The table also lists the conversion factors between A_m and E(B-V) given by Savage and Mathis (1979).

Table 7.1. The specifications of the optical filters.

filter	a(m)	ν_m (Hz)	$A_m/E(B-V)$
U	1.81	$8.33\ 10^{14}$	4.80
B	4.26	$6.82\ 10^{14}$	4.10
V	3.64	$5.45\ 10^{14}$	3.10
R	3.08	$4.68\ 10^{14}$	2.50
I	2.55	$3.80\ 10^{14}$	1.85

The U, B, V, R and I fluxes, corrected for extinction in our galaxy, were then plotted against each other for various filter combinations. Figure 7.1 shows six examples of such plots. Where significant flux variations had taken place the relationship between fluxes in different filters was found to be linear. This important result has already been noted by Choloniewski (1981). It tells us that the flux changes through the optical filters are proportional to each other and happen nearly simultaneously. It means that the shape of the nuclear flux distribution does not change. This is also true for the R-filter; therefore Hα varies proportionally to the continuum as well. The slope of the best fitting least-squares line through the data points (the dotted lines in the figures) was determined using statistical methods. These slopes are listed in table 7.2. They will be called flux variation gradients (FVGs) after this and will be denoted by the symbol Γ. Only gradients derived from more than four data points with a good linear correlation ($r > 0.8$) have been included in the table. The last entry is the average gradient for Fairall 9, H 1143-182 and ESO 141-G55, three strongly variable Seyfert nuclei that will later be shown to have little or no obscuration.

Figure 7.1(a). Plots of the flux measurements for Fairall 9.

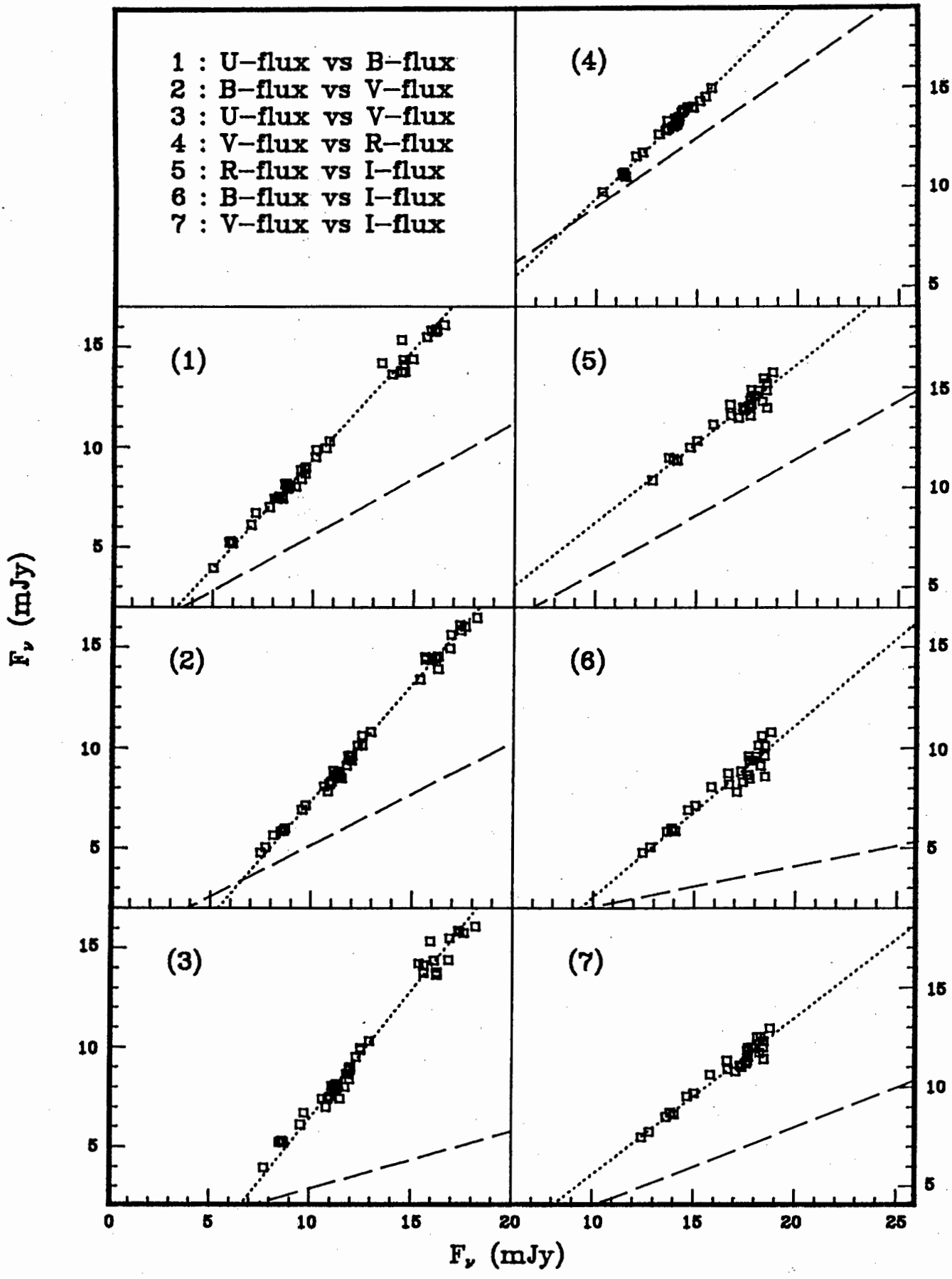

Figure 7.1(b). Plots of the flux measurements for NGC 3783.

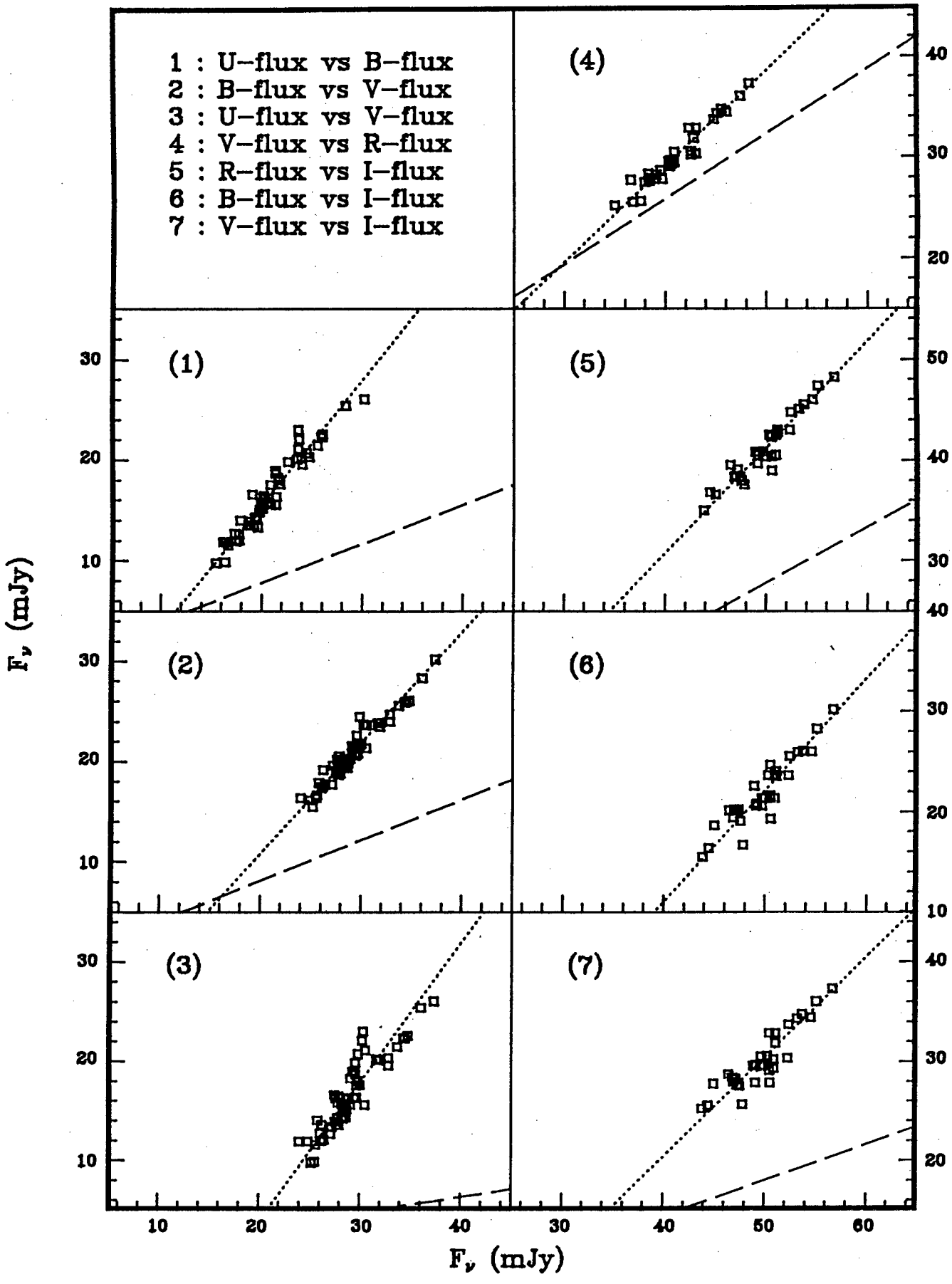

Figure 7.1(c). Plots of the flux measurements for Ton S180.

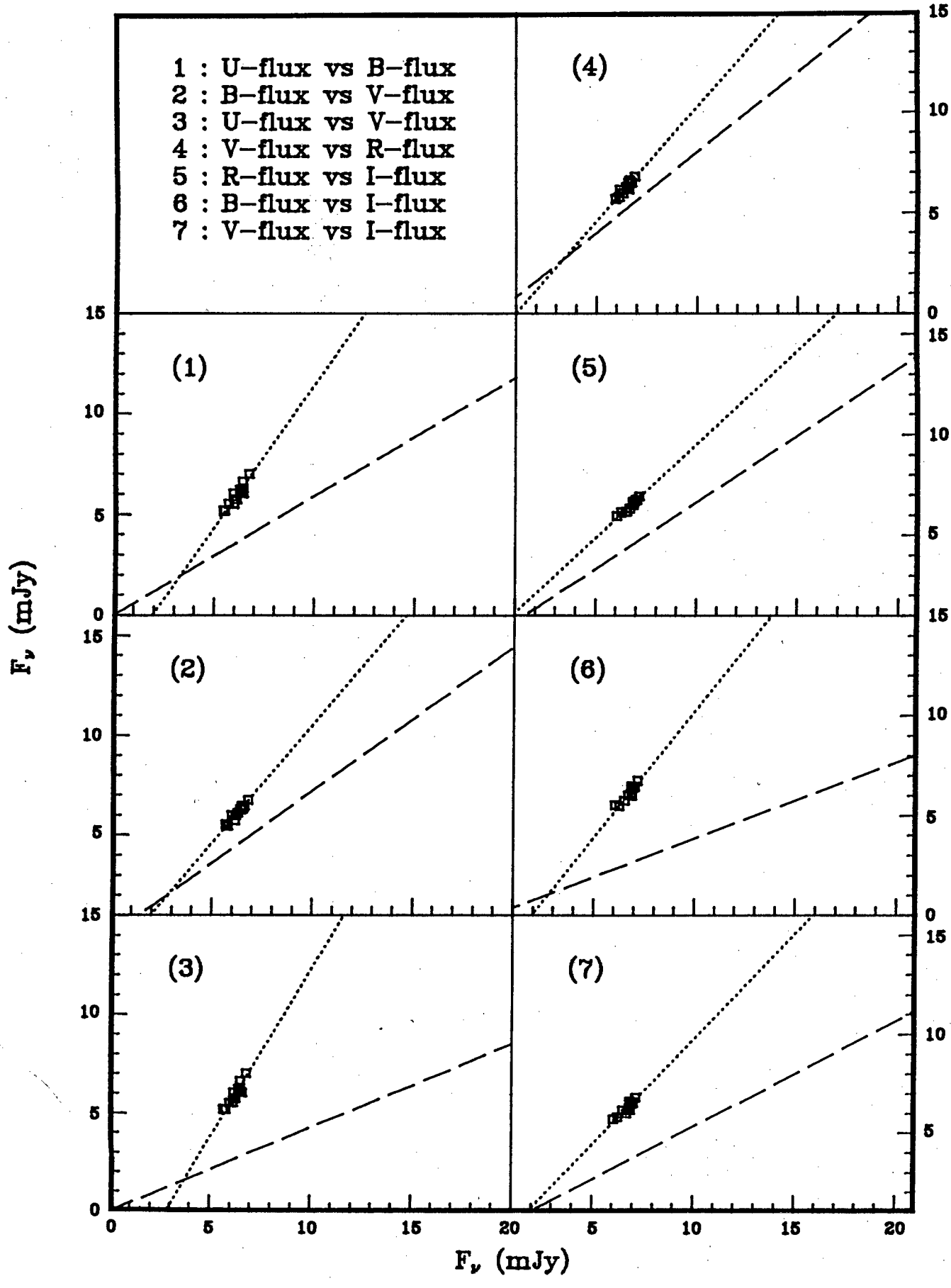

Figure 7.1(d). Plots of the flux measurements for MCG -5-13-17.

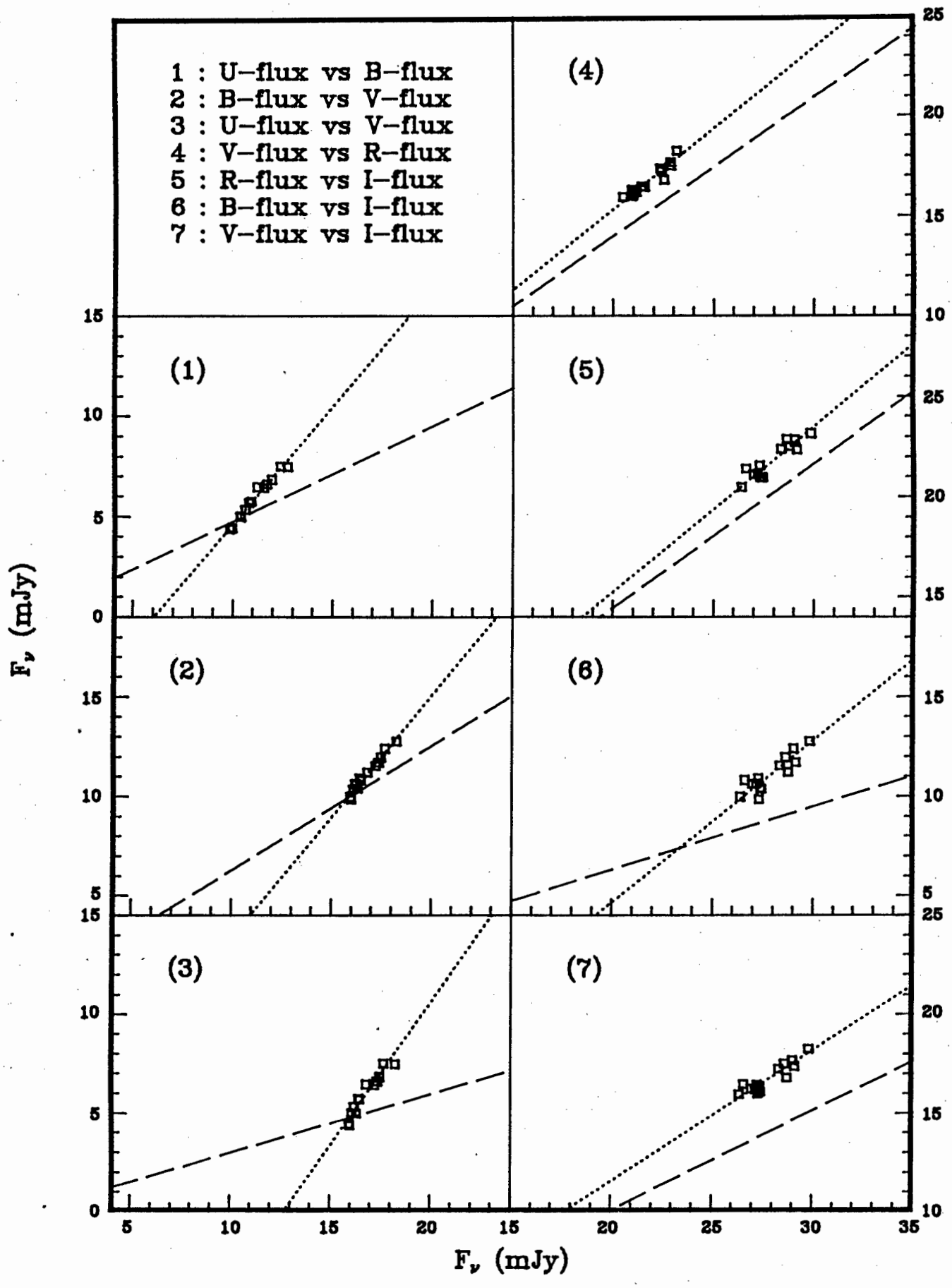

Figure 7.1(e). Plots of the flux measurements for ESO 323-G77.

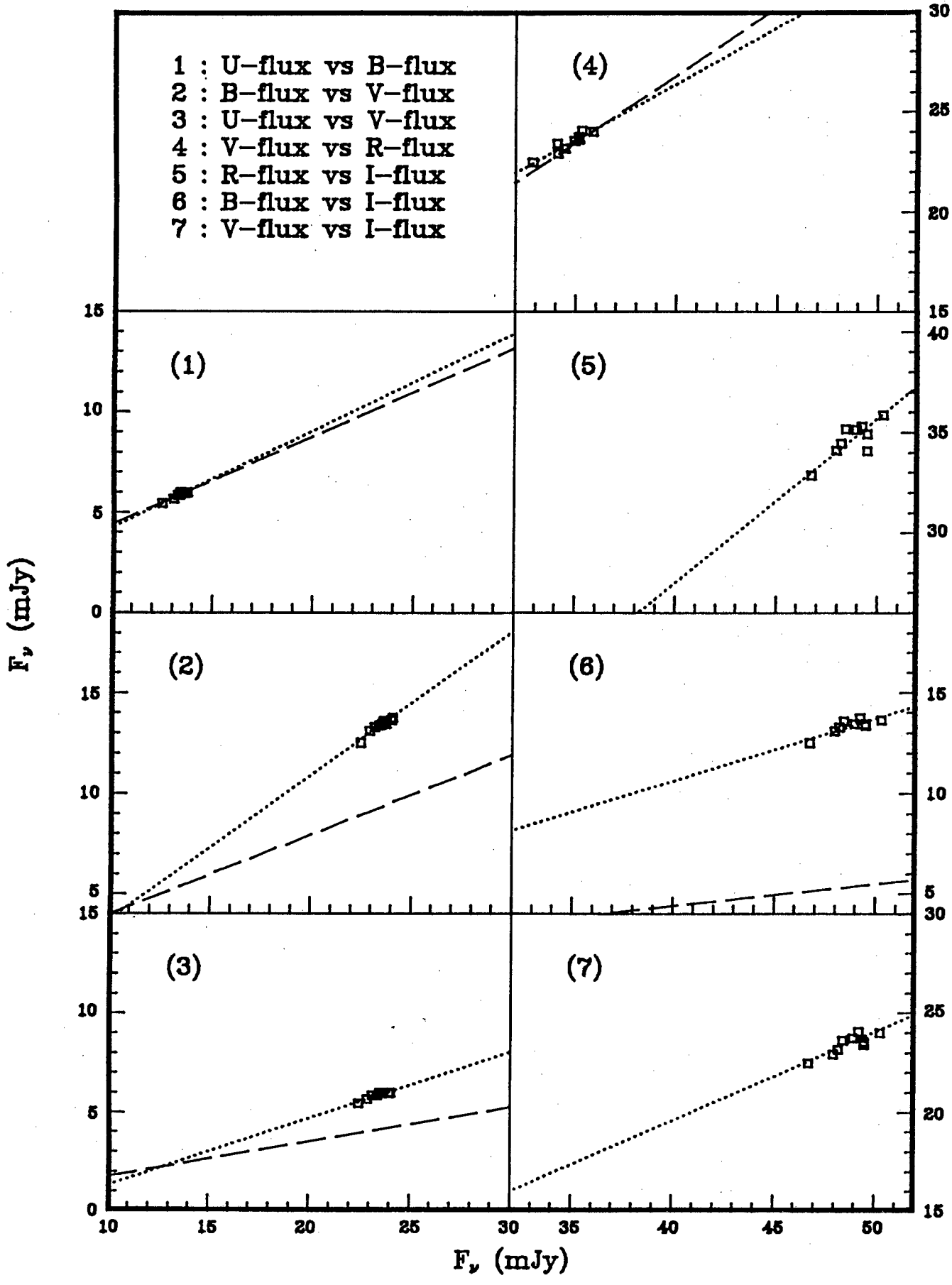

Figure 7.1(f). Plots of the flux measurements for NGC 2992.

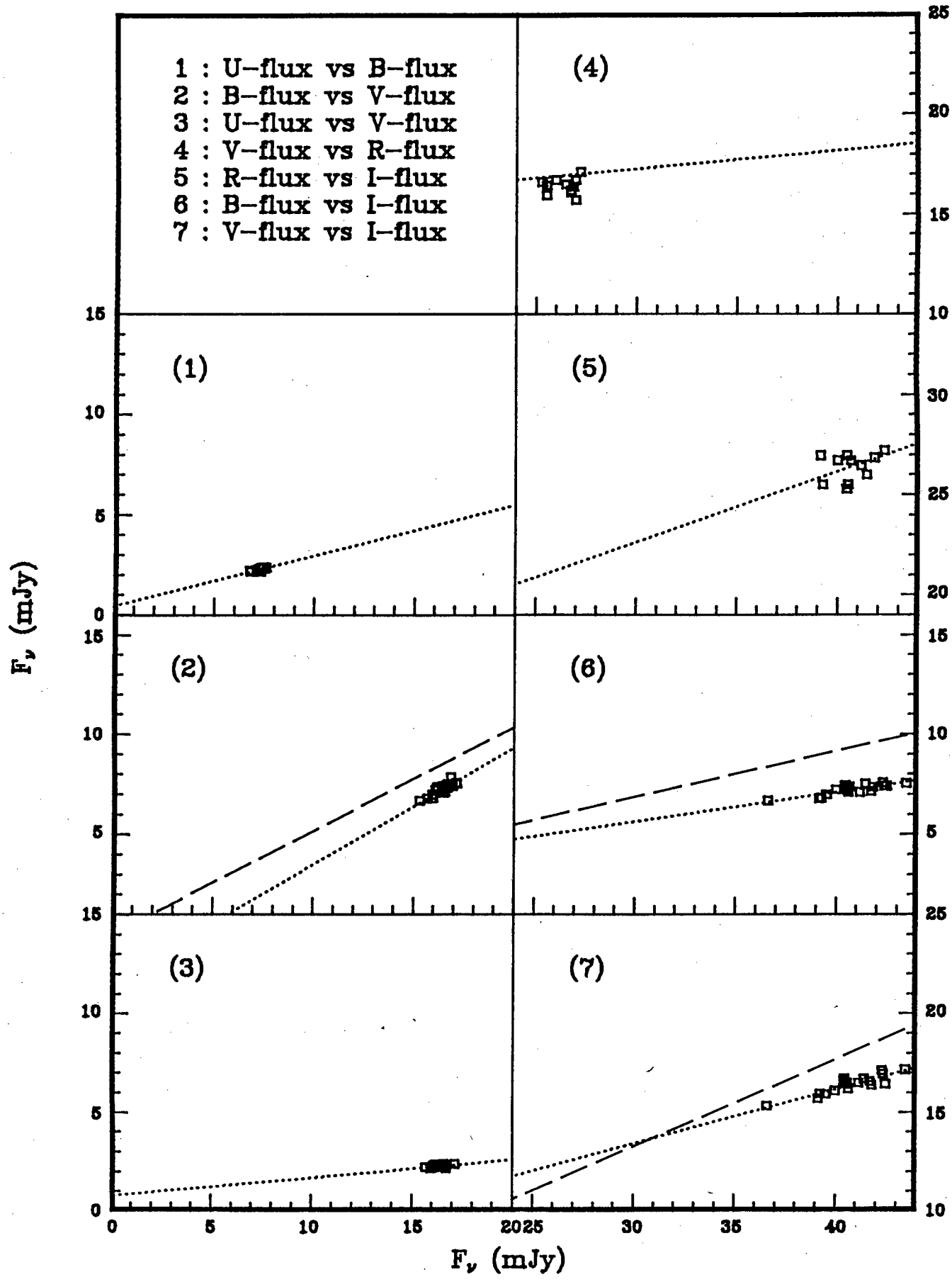

Table 7.2. The nuclear flux variation gradients.

Name	Γ_{UB}	Γ_{BV}	Γ_{VR}	Γ_{RI}	Γ_{UV}	Γ_{BI}	Γ_{VI}
ESO 12-G21	0.85	0.86	0.92	0.77	0.73	-	0.70
Ton S180	1.42	1.18	1.14	0.93	1.71	1.27	1.06
NGC 526a	-	0.67	0.80	0.75	-	0.39	0.59
Fairall 9	1.10	1.16	0.98	0.79	1.28	0.86	0.79
IC 1816	-	-	-	-	-	-	-
H 0307-730	0.98	0.96	1.44	-	0.91	-	-
Fairall 1116	1.11	1.07	1.00	-	1.20	-	-
NGC 1566	0.71	0.66	0.67	0.70	-	-	-
MCG -5-13-17	1.17	1.22	0.81	0.83	1.45	0.82	0.66
3A 0557-383	-	-	-	-	-	-	-
Fairall 265	0.86	1.02	1.05	-	0.87	-	-
NGC 2992	-	0.58	-	-	-	0.15	0.28
MCG -5-23-16	-	0.56	0.50	-	-	-	-
ESO 438-G9	1.01	0.86	1.05	0.66	0.87	0.60	0.70
NGC 3783	1.24	1.11	0.95	1.05	1.40	1.11	1.00
H 1143-182	1.04	1.14	0.87	1.04	1.20	1.05	0.91
MCG -2-33-34	1.03	1.01	0.73	-	-	-	-
ESO 323-G77	0.48	0.72	0.56	0.82	0.34	0.31	0.44
MCG -6-30-15	0.51	-	0.57	0.60	-	-	0.39
IC 4329A	0.36	0.47	0.55	0.64	0.18	0.19	0.39
I 1509-211	0.43	0.78	0.78	-	-	-	0.55
ESO 103-G35	-	-	-	-	-	-	-
Fairall 51	0.76	0.79	0.68	0.74	0.57	0.38	0.47
ESO 141-G55	1.26	1.16	1.00	1.10	1.48	1.29	1.10
NGC 6814	1.41	0.73	0.69	0.59	1.44	-	-
NGC 6860	0.61	0.95	0.58	-	0.55	-	0.56
H 2106-099	0.99	0.95	0.92	1.09	0.94	0.94	1.00
NGC 7213	-	0.62	0.57	-	-	-	-
MCG -2-58-22	1.19	1.06	0.93	0.90	1.26	0.95	0.84
A_v=0	1.13	1.15	0.95	0.98	1.32	1.07	0.93

The FVGs given in the table above allow one to study the reddening and extinction inside the Seyfert galaxy. Alternatively, conclusions about the shape of the flux distribution can be drawn. There are two approaches. Firstly, one can assume that all Seyfert nuclei can be described by an identical flux distribution and derive the extinction through various wavebands by comparing the FVGs for different objects. One could however also use the nuclear reddenings and extinctions obtained through other methods to calculate the power law index and the relative contribution by other nuclear components.

The extra-nuclear contributions to the total flux in each band were derived as follows. The CCD images were used to measure the flux and colours of an annulus between 4 and 20 arcseconds from the nucleus. These colours were then assumed to be those of the extra-nuclear component of the galaxy. Therefore in

figure 7.1 the extra-nuclear component lies somewhere along the dashed line, which has a slope defined by the extra-nuclear colours. As it has been found that the total fluxes through different filters have a linear relationship to each other (described by the dotted lines in figure 7.1), it may be assumed that the flux of the underlying galaxy through a 20 arcsec aperture corresponds to the intersection of the dashed and dotted lines, and that the remaining flux between this point and the measured points corresponds to the nuclear flux. From this the magnitude and range of the nuclear fluxes could be estimated. This method can give misleading results if the galactic and nuclear colours are similar, which is usually the case for the V vs R, R vs I and V vs I flux diagrams. It was therefore best to estimate the nuclear flux in only one filter (U, B or V) with the method given above, and calculate the fluxes for the other filters from this using the flux variation gradients. An alternative procedure was used if the uncertainty in the flux variation gradient was too large or the nuclear flux too weak (see, e.g. figure 7.1f). In such cases the nuclear fluxes were estimated from the CCD images by subtracting the extra-nuclear fluxes derived in chapter 4 from the total fluxes.

The average nuclear fluxes in the U, B, V, R and I bands are given in columns 2-6 of table 7.4.

7.1.3. Near-infrared

The nuclear near-infrared fluxes, calculated as for the optical fluxes with the formula

$$f(m)\ (Jy) = a(m).10^{3-0.4(m-Am)}\ ,$$

were derived from the photometric data obtained by Ian Glass, which are listed in table A3 in the appendix. The ratio between the extinction in the m filter and E(B-V), the calibration coefficients a(m), and characteristic frequencies for each filter (taken from Wilson et al ,1972) are listed in table 7.3.

Table 7.3. The specifications for the infrared bands.

filter	a(m)	ν_m (Hz)	$A_m/E(B-V)$
J	1.52	$2.40\ 10^{14}$	0.78
H	0.98	$1.82\ 10^{14}$	0.43
K	0.62	$1.36\ 10^{14}$	0.25
L	0.28	$8.57\ 10^{13}$	0.09

The isolation of the nuclear component was made using the method suggested by Glass (1981). After correcting the magnitudes for extinction in our galaxy the J-H and H-K colours were plotted on a two colour diagram. The mixing line of Glass (1981) was used to determine the ratio of galactic to nuclear luminosity in the K band. The starlight contamination in the J, H and L filters can be derived by assuming that the underlying galaxy has normal colours

$$H_{gal} = K_{gal} + 0.22$$

$$J_{gal} = K_{gal} + 1.00$$

$$L_{gal} = K_{gal} - 0.22$$

(see Glass and Moorwood, 1985). The nuclear magnitudes therefore are

$$J_{nuc} = -2.5 \log(10^{-0.4J} - 0.398g.10^{-0.4K})$$

$$H_{nuc} = -2.5 \log(10^{-0.4H} - 0.817g.10^{-0.4K})$$

$$L_{nuc} = -2.5 \log(10^{-0.4L} - 1.224g.10^{-0.4K})$$

where g is the fraction of the galactic component at K. The estimated values of g are listed in column 7 of table A3. The infrared nuclear fluxes are listed in columns 7-10 of table 7.4.

Table 7.4. The derived nuclear fluxes (in mJy) in the UBVRIJHKL bands.

Name	f(U)	f(B)	f(V)	f(R)	f(I)	f(J)	f(H)	f(K)	f(L)
ESO 12-G21	2.4	2.8	3.3	3.6	4.7[a]	1.3	7.4	14.4	22.4
Ton S180	4.5	3.2	2.6	2.3	2.5[a]	5.2	5.5	11.4	25.2
NGC 526a	-	0.7	1.1	1.4	1.9[b]	7.4	16.8	38.7	90.0
Fairall 9	11.3	10.3	8.8	9.0	11.2[a]	13.6	30.9	60.7	111.6
IC 1816	-	1.1	2.5	3.3	4.8[c]	0.8	1.0	2.1	2.4
H 0307-730	1.3	1.3	1.4	1.0	- [a]	0.8	1.5	3.5	-
Fairall 1116	2.9	2.6	2.4	2.4	- [a]	3.9	7.2	12.6	24.5
NGC 1566	4.9	6.9	10.5	15.6	22.3[a]	6.8	15.2	28.5	46.1
MCG -5-13-17	1.2	1.0	0.8	1.0	1.3[a]	5.1	4.0	7.1	15.4
3A 0557-383	-	-	2.1	3.8	5.3[c]	12.1	23.5	52.3	150.7
Fairall 265	2.6	3.0	3.0	2.8	- [a]	5.0	8.4	13.2	24.1
NGC 2992	-	2.1	3.6	-	12.9[b]	2.6	11.6	24.2	41.0
MCG -5-23-16	-	2.7	4.8	9.5	21.2[b]	9.6	16.0	29.3	61.6
ESO 438-G9	3.4	3.4	3.9	3.7	5.6[a]	8.1	13.5	23.9	33.7
NGC 3783	14.4	11.6	10.3	10.8	10.3[a]	22.3	37.3	62.4	121.7
H 1143-182	4.1	3.9	3.4	3.9	3.8[a]	4.1	6.2	11.0	16.6
MCG -2-33-34	2.1	2.0	2.0	2.8	- [a]	3.6	5.4	10.6	16.0
ESO 323-G77	3.5	7.3	10.3	18.4	23.4[a]	39.0	89.6	161.2	260.3
MCG -6-30-15	1.2	2.4	4.6	8.1	11.7[b]	11.2	10.2	35.9	82.1
IC 4329A	0.8	2.1	4.5	8.1	11.5[a]	28.0	53.2	97.2	193.2
I 1509-211	0.7	1.6	2.0	2.6	3.6[a]	8.4	15.0	25.6	42.5
ESO 103-G35	-	0.8	2.4	4.1	6.2[c]	0.8	2.3	4.2	26.3
Fairall 51	2.2	2.9	3.9	5.7	8.2[a]	14.3	23.6	40.1	68.1
ESO 141-G55	7.5	6.0	5.1	5.1	4.6[a]	10.3	19.6	43.6	98.5
NGC 6814	2.5	1.2	1.7	2.5	- [a]	4.2	8.9	16.4	21.3
NGC 6860	1.7	2.8	3.1	5.3	5.5[a]	10.6	19.3	36.2	65.9
H 2106-099	5.1	5.2	5.4	5.9	5.4[a]	10.3	17.3	30.7	46.7
NGC 7213	-	6.2	10.0	17.6	- [b]	20.2	30.1	50.5	98.9
MCG -2-58-22	5.8	4.9	4.6	4.9	5.5[a]	11.0	20.3	41.6	76.0

Notes:- the superscript after the I flux indicates the method used to derive the optical fluxes. a) using flux variation gradients and estimating the galactic background radiation from its intersection with the galactic colour vector; b) using nuclear flux gradients and at least one nuclear flux derived from CCD images; c) nuclear fluxes entirely derived from CCD images.

7.1.4. Far-infrared

The Infrared Astronomical Satellite (IRAS) has made an all-sky survey of infrared sources in four wavelength bands centered at 12 μm, 25 μm, 60 μm and 100 μm. A warm gas will emit most of its radiation in this wavelength range. Cool stars give off large quantities of radiation in the near-infrared, while the cool interstellar dust emits the bulk of its energy at longer wavelengths. Studies of the far infrared flux distribution showed that Seyferts are strong emitters at these wavelengths. The far infrared continuum is often relatively flat, which could be evidence of synchrotron emission, although warm dust may also give rise to a flux distribution of that shape. If one fits a power law

between 25 μm and 60 μm then the spectral index $\alpha(25\mu m, 60\mu m)$ is usually less than 1.5 (Miley et al, 1985). It was noticed that not many objects other than Seyferts have such infrared colours. It was therefore suspected that many sources with such a spectral index would be previously unchartered Seyferts. A list of 54 such sources was published in the IRAS circular 11. These were then examined by various observers (Carter, 1984, Osterbrock and De Robertis, 1985, De Grijp et al, 1985), who showed that 70% of the sources from this list were Seyferts, usually of activity type 2. Most of the remainder were starburst galaxies. Following this De Grijp et al (1987) prepared a complete list of 563 sources satisfying the above criteria. Many of these objects have been observed by them, and again a large number of new Seyferts were discovered.

The fluxes measured by the IRAS satellite are given in columns 5-8 of table 7.6. At these wavelengths interstellar extinction is negligibly small. In the shorter wavelength bands these fluxes are expected to be entirely nuclear. However an extra-nuclear component resulting from the cool dust radiation from the interstellar matter in the outer part of th galaxy can affect the fluxes measured in the 60 μm and 100 μm bands. No attempt was made to separate this component from the nuclear component because it is difficult to determine reliably the amount of interstellar dust in a galaxy. This must be born in mind when interpreting the flux distributions. NGC 1566, NGC 2992 and NGC 6814 are three galaxies for which the 60 μm and 100 μm fluxes are probably almost entirely extra-nuclear.

7.1.5. X-ray

X-ray astronomy has been an important tool in the study of Seyfert galaxies as it has shown that the non-thermal continuum emission extends to very high frequencies. Measurements of the total flux between two frequencies have been used to determine the X-ray luminosities of these objects (e.g., between 2 and 10 keV). X-ray spectroscopy has enabled investigators to study the shape of the X-ray continuum. Absorption by gas affects the continuum strength at frequencies lower than ~4 keV only. One can therefore, by making the assumption that the intrinsic X-ray continuum has the form of a power law, deduce the hydrogen column density N_H in the line of sight. The 2-10 keV X-ray fluxes and values for the hydrogen column densities derived by a range of investigators are listed in table 7.5. The N_H estimates show large discrepancies because of the high sensitivity of this parameter to slight

changes in the X-ray spectrum model fits.

Table 7.5. The 2-10 keV fluxes (in units of 10^{-13} erg.cm^{-2}.s^{-1}) and hydrogen column densities N_H (in units of 10^{21} cm^{-2}) derived by fitting the X-ray spectra of some of the galaxies.

Name	F_X	N_H by different investigators					
	2-10keV	h	i	j	k	other	adopted
ESO 12-G21	380[a]					0[a]	0.0
NGC 526a	387[b]	16.4	17.5	0	43		17.0
Fairall 9	290[b]	0.3			0		0.2
H 0307-730	165[c]						
3A 0557-383	394[b]	7					7.0
NGC 2992	805[b]	6.8	14.5	16	1.0		7.0
MCG -5-23-16	770[d]	10.6	17.5	17	11.4		13.0
NGC 3783	390[e]	1.1	24.5	29	0	22[e]	1.5
H 1143-182	145[c]						
MCG -2-33-34	108[f]					0[f]	0.0
MCG -6-30-15	511[b]	4.1	0.4		0.8		2.0
IC 4329A	774[b]	1.5			5.37		2.8
IRAS 1509-211	160[f]					3.9[f]	3.9
ESO 103-G35	265[b]	135					-
Fairall 51	245[g]						
ESO 141-G55	380[e]	0.12			1.39	0[e]	0.3
NGC 6814	550[e]	2.9				43[e]	4.0
H 2106-099	225[c]						
NGC 7213	315[b]	0.15	3.0	0	0.8		0.7
MCG -2-58-22	455[b]	0.19			0.39		0.3

References:- a) Hayes et al (1980), b) Piccinotti et al (1982), c) Wood et al (1984) using 2x10^{-3} LASS counts = 10^{-11} erg.cm^{-2}.s^{-1}, d) Schnopper et al (1980), e) Mushotzky et al (1980): HEAO-1 A2 2-20keV, f) Ward et al (1988): EXOSAT ME 1-20 keV, g) Marshall et al (1979), h) Turner and Pounds (1989): Einstein SSS 0.75-5 keV, i) quoted by Reichert et al (1985): Einstein MPC 2-10 keV, j) quoted by Reichert et al (1985), k) Reichert et al (1985) and Petre et al (1984): Einstein SSS 0.75-5 keV

In column 2 of table 7.6 the flux per unit frequency interval at 4 keV, usually estimated from X-ray spectra, has been given. Where only a 2-10 keV flux measurement was available the 4 keV flux was calculated from this by assuming that the X-ray continuum obeys a power law with an index of $\alpha = 0.7$. The 4 keV flux is only minimally affected by extinction, and it can be assumed that all the X-rays detected originate from the Seyfert nucleus.

7.1.6. Radio and sub-millimeter

In Seyfert galaxies the energy output at radio frequencies is much lower than in the infrared. This shows that the optical-infrared power law does not extend to radio wavelengths. Therefore the density of the source of the non-thermal emission is sufficiently high for synchrotron self-absorption to dominate at low frequencies. Edelson (1987) showed that the Seyfert flux distribution at radio wavelengths obeys an α(6cm,20cm) = -0.7 power law. This seems to be the result of another synchrotron component that is too weak to be observed at shorter wavelengths. NGC 7213 is an exception, as its spectral index α(6cm,20cm) is positive. In this case one is probably seeing the low frequency tail of the power law.

Studies of the flux distribution in the sub-millimeter regime of Seyfert galaxies have only recently been started. However the flux of quasars at these frequencies has been shown to be relatively weak by Chini et al (1989). This shows that the low-frequency turnover of the power law must be between 100 μm and 1 mm.

Six and 20 cm fluxes found in the literature are listed in columns 9 and 10 of table 7.6.

Table 7.6. The Seyfert flux in the X-ray, UV, medium IR and radio frequencies.

Name	4keV	1450A	2500A	12μm	25μm	60μm	100μm	6cm	20cm
	μJy	mJy				mJy			mJy
ESO 12-G21	2.19[a]	0.20	0.83[g]	-	330	1450	2940	-	-
Ton S180	-	-	-	-	-	-	-	-	-
NGC 526a	2.47[b]	-	-	240	520	-	-	4	6[l]
Fairall 9	0.82[b]	12.9	19.2[h]	380	590	590	730	-	-
IC 1816	-	-	-	250	430	1420	2400	-	-
H 0307-730	0.85[c]	-	-	-	-	-	-	-	-
Fairall 1116	-	-	-	-	-	-	-	-	-
NGC 1566	-	0.17	0.90[g]	530	890	12700	42200	-	204[m]
MCG -5-13-17	-	-	-	-	590	1490	.2020	-	-
3A 0557-383	0.82[b]	-	-	530	700	-	-	20	40[l]
Fairall 265	-	-	-	-	190	780	1130	-	-
NGC 2992	2.06[b]	-	-	590	1360	6870	14440	77	206[n]
MCG -5-23-16	3.29[b]	-	-	-	-	-	-	6	11[n]
ESO 438-G9	-	0.50	1.78[i]	-	560	3280	4260	-	-
NGC 3783	2.74[b]	1.78	5.00[j]	800	2450	3330	4930	13[n]	23[l]
H 1143-182	0.75[c]	-	-	-	-	-	-	-	6[o]
MCG -2-33-34	0.47[d]	-	-	-	500	1190	2310	-	-
ESO 323-G77	-	-	-	680	1240	5510	8940	-	-
MCG -6-30-15	2.47[e]	-	-	430	810	1110	-	1	2[n]
IC 4329A	3.29[b]	-	-	1050	2250	2040	1620	24	35[l]
I 1509-211	0.75[d]	-	-	-	640	1610	1750	-	-
ESO 103-G35	1.65[b]	-	-	580	2360	2270	:1240	-	-
Fairall 51	1.27[f]			380	860	2000	2620	-	-
ESO 141-G55	1.92[b]	5.04	8.00[k]	250	350	620	-	-	-
NGC 6814	1.92[b]	-	-	330	590	5690	18160	2	6[n]
NGC 6860	-	-	-	:240	350	1050	2580	-	-
H 2106-099	1.16[c]	-	-	-	-	-	-	-	4[o]
NGC 7213	2.74[b]	0.70[k]	-	640	750	2540	8280	228[p]	191[m]
MCG -2-58-22	3.29[b]	2.26[k]	-	-	-	-	-	9[q]	19[l]

References:- a) Hayes et al (1980), b) Turner and Pounds (1989), c) Wood et al (1984) using 2×10^{-3} LASS counts = 10^{-11} erg.cm^{-2}.s^{-1} as in Remillard et al (1986), d) Ward et al (1988), e) Piccinotti et al (1982), f) Marshall et al (1979), 2-10 keV, g) Clavel and Joly (1984), h) Masegosa et al (1986), i) calculated from figure 1 of Kollatschny and Fricke (1983), j) found by averaging the fluxes measured by Barr et al (1983), k) from Wu et al (1983), sometimes estimated from figures, l) Unger et al (1987), m) extrapolated to 20 cm using the fluxes and spectral indexes from Harnett (1987), n) Ulvestad and Wilson (1984b), o) Remillard et al (1986), p) Sadler (1984), q) Ulvestad and Wilson (1984a)

7.1.7. The nuclear continuum

The derived nuclear fluxes are plotted as a function of frequency in figure 7.2 (in the form log $\nu F\nu$ vs log ν). The objects have been reordered so that

Figure 7.2(a). The flux distributions of Ton S180, Fairall 9, Fairall 1116, H 1143-182, ESO 141-G55 and H 2106-099.

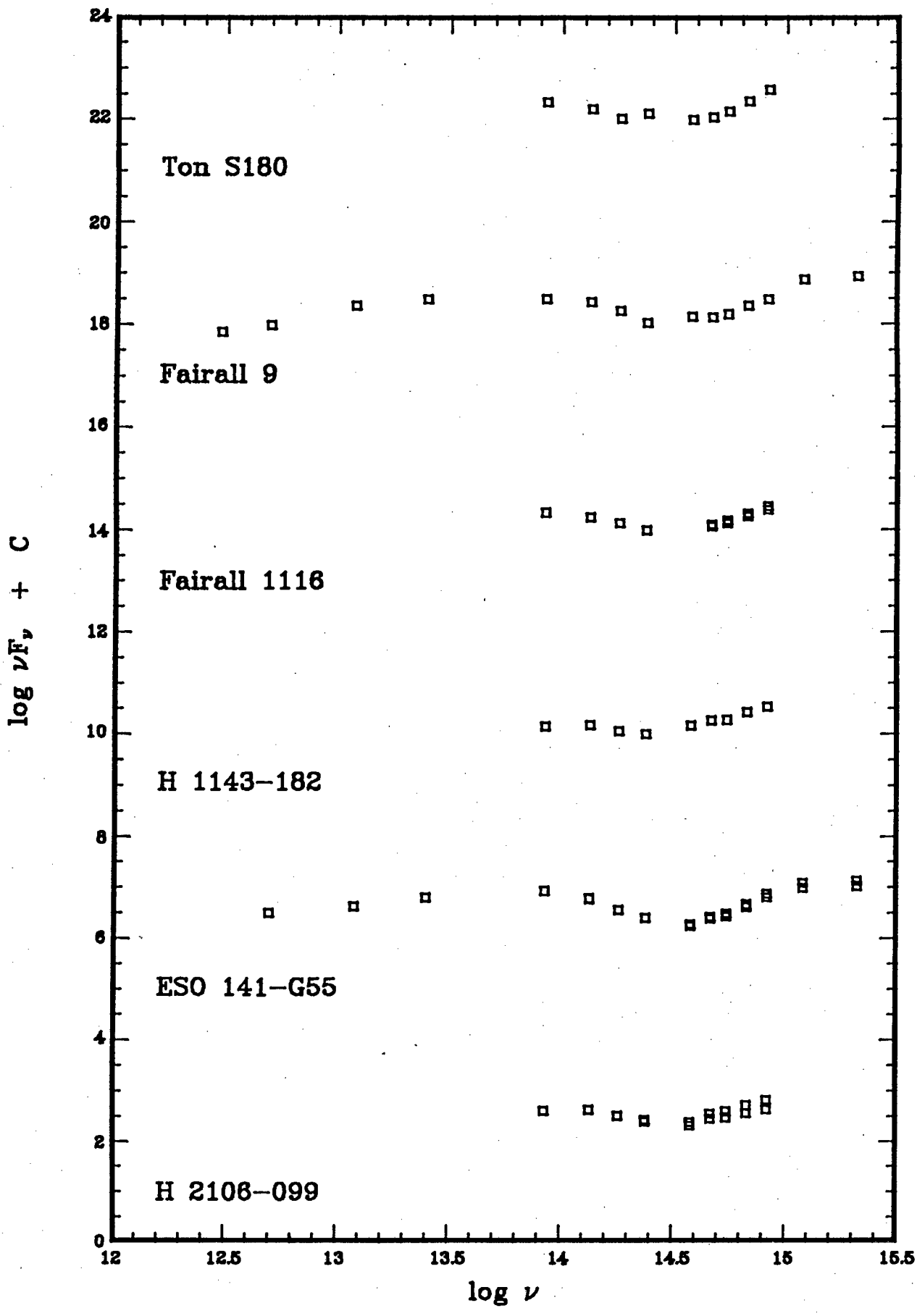

Figure 7.2(b). The flux distributions of ESO 12-G21, Fairall 265, ESO 438-G9, NGC 3783, MCG -2-33-34 and MCG -2-58-22.

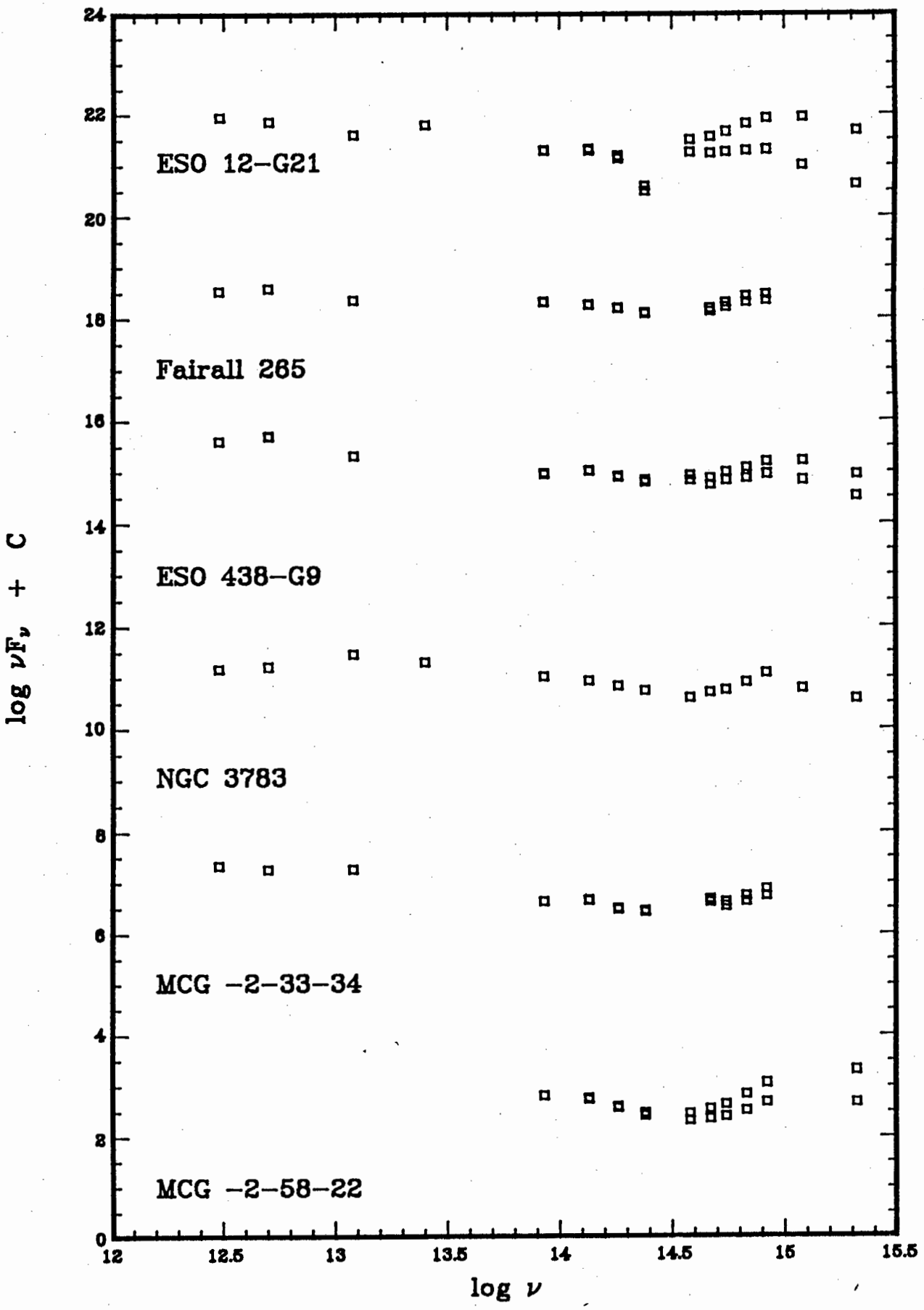

Figure 7.2(c). The flux distributions of 3A 0557-383, ESO 323-G77, IC 4329A, IRAS 1509-211, Fairall 51 and NGC 6860.

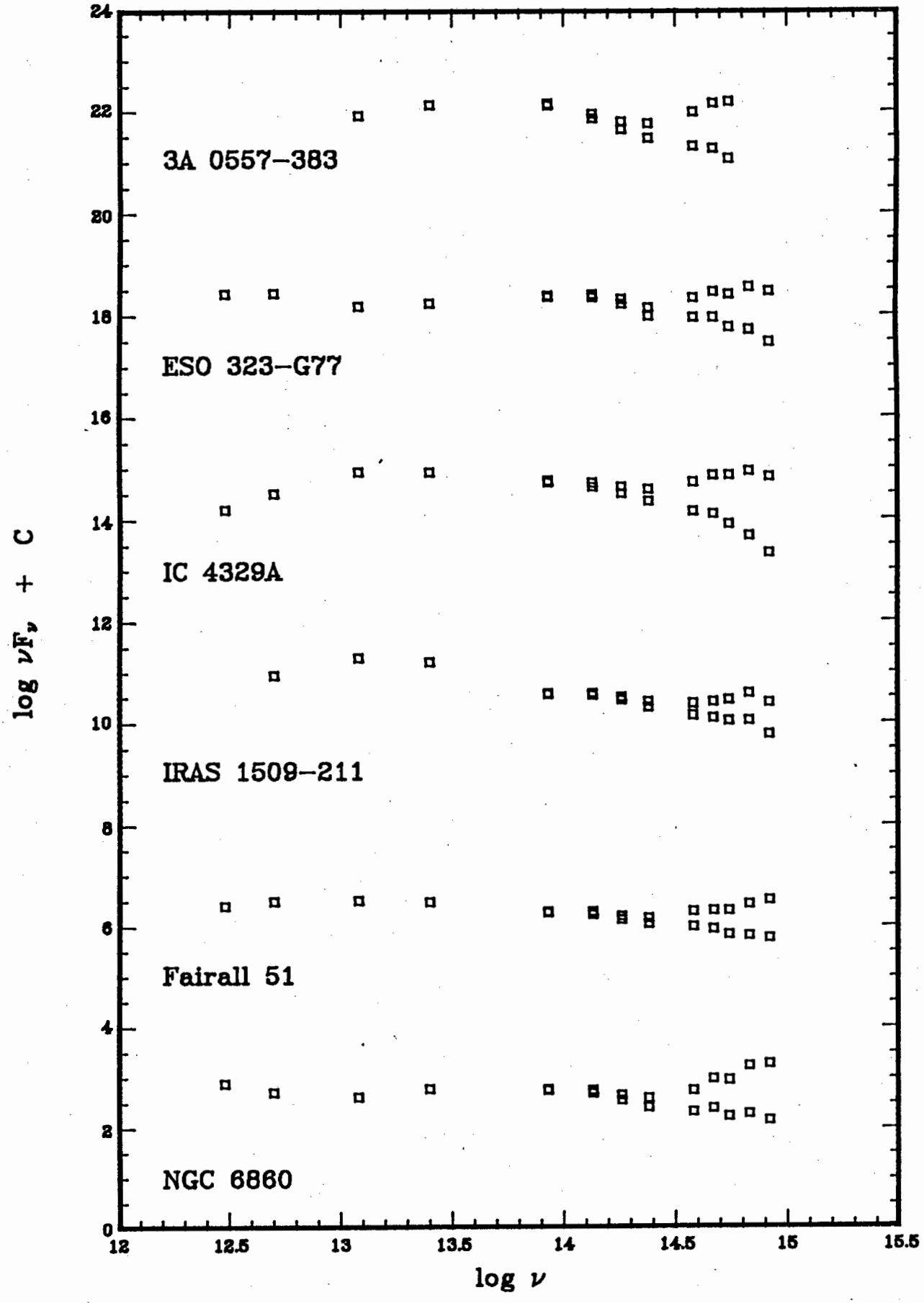

Figure 7.2(d). The flux distributions of H 0307-730, NGC 1566, MCG -5-13-17, MCG -6-30-15, NGC 6814 and NGC 7213.

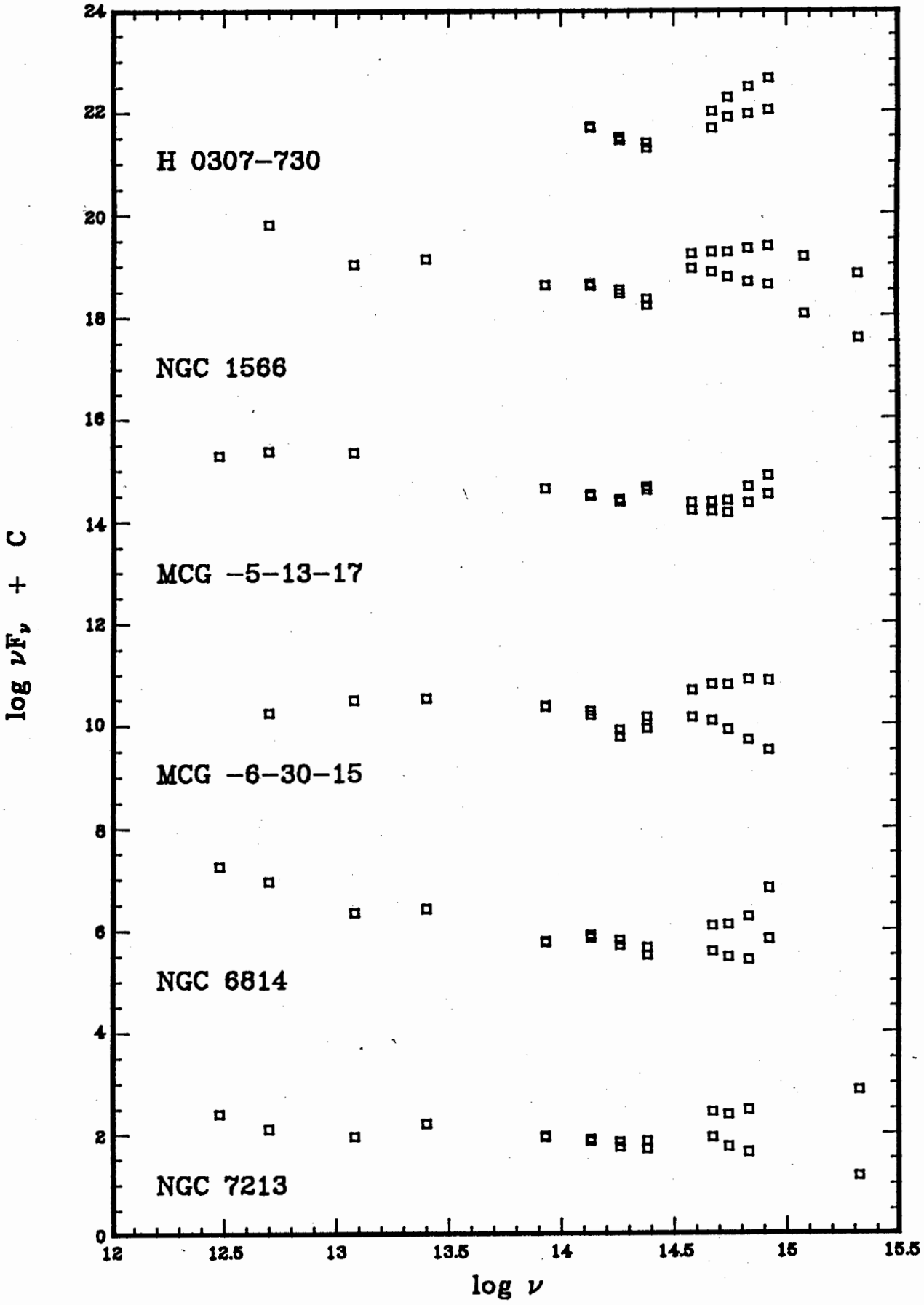

Figure 7.2(e). The flux distributions of NGC 526a, IC 1816, NGC 2992, MCG -5-23-16 and ESO 103-G35.

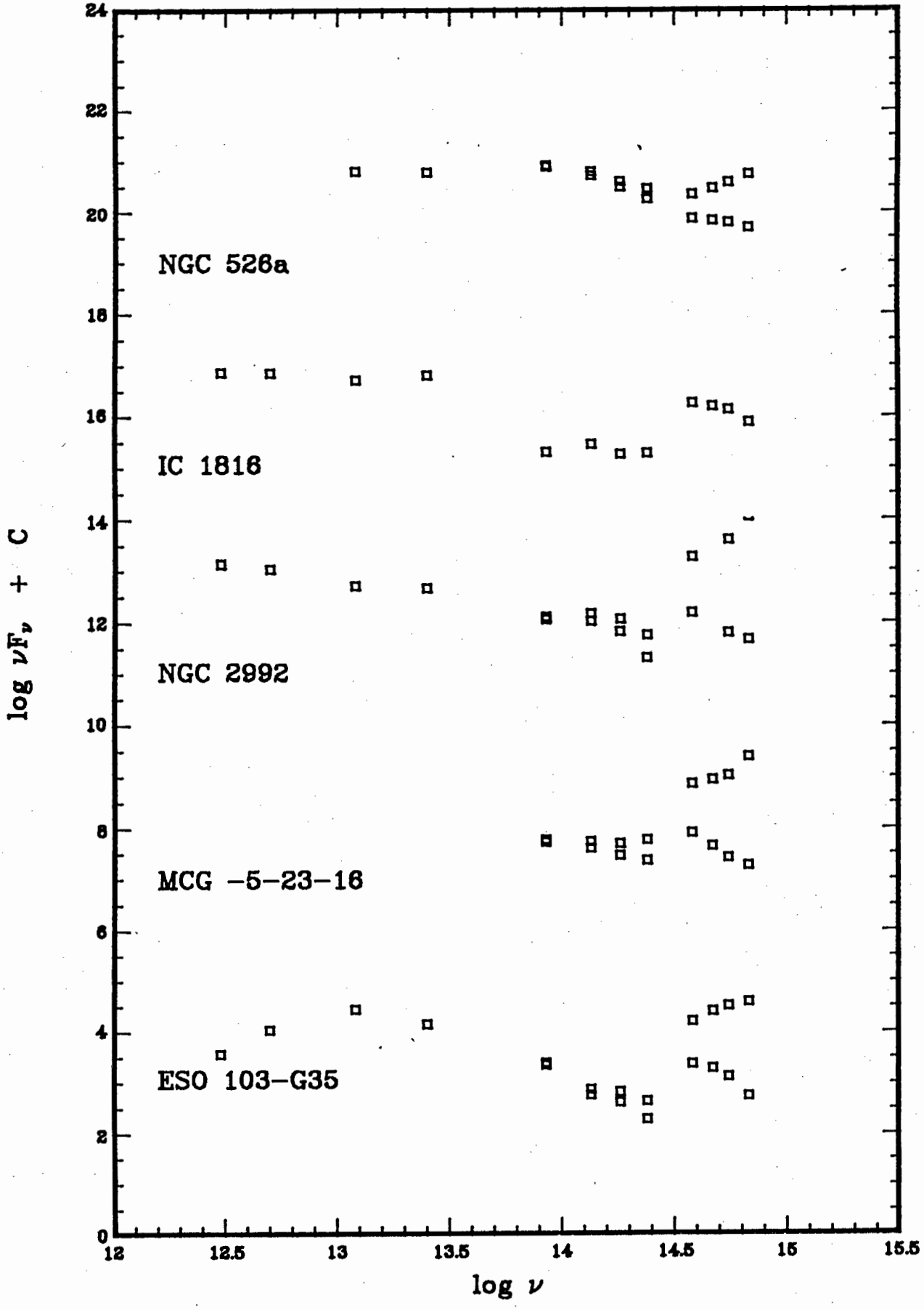

the Seyferts with the most clearly defined optical flux distributions have been plotted first while the galaxies with badly defined or undefined flux variation gradients have been left until last. In order to facilitate the representation these plots are limited to the fluxes between 0.1 and 100 μm. Two sets of points were drawn per object. In the lower curve the fluxes from tables 7.4 and 7.5 are plotted. In the upper curve the same fluxes are shown after corrections have been made for extinction of the nucleus using the A_V values derived later in chapter 7.4 in conjunction with the extinction curve from Savage and Mathis (1979).

It is apparent that most objects have similar flux distributions at these wavelengths. Two factors are chiefly responsible for deforming the flux continua in figures 7.2 (d) and (e). Firstly, the method of deducing the optical nuclear flux from the CCD images usually overestimates this quantity. This is likely to be the result of being unable to separate the nucleus from nearby sources of radiation. These could be a bulge component or H II regions. Secondly, faint infrared sources usually have large errors associated with them, particularly at J, as the contamination from starlight can be substantial at the shorter infrared wavelengths. The method used to determine the 1.2 μm and 1.6 μm nuclear fluxes is very sensitive to errors in the assumed galactic colours. An error in the estimated nuclear flux at K will translate to larger errors at J and H.

An examination of the flux distributions plotted in figure 7.2 reveals the following:-

- the ultraviolet bump dominates the optical and ultraviolet parts of the flux distribution.
- it extends to about the frequency of the I band.
- its shape is probably best explained by a superposition of a ~30000 K blackbody and other cooler and weaker thermal components.
- the near infrared flux distribution has a convex appearence and is steeper than suggested by an $\alpha = 1.2$ power law.
- there is no sign of a 5 μm bump.
- thermal dust emission components are prominent in the far infrared parts of the spectrum.
- the flux usually evens out and sometimes starts dropping before the wavelength reaches 100 μm. This could be due to a synchrotron self-absorption cut-off. It may however also be the low frequency tail of a warm thermal

component.

Nuclear luminosities per frequency unit at 4 keV, 1450 Å, 5500 Å, 2.2 μm, 25 μm and 20 cm were calculated from the fluxes using the distances given in table 3.1. They have been plotted against each other using a logarithmic scale in figure 7.3. If the flux distributions of all objects have the same shape then the points in this graph would lie along a straight line with a slope of 1. Note that the scatter in these diagrams is much smaller if one does not take into account the points for which the optical fluxes were derived from the CCD images only (the crosses in the figures).

If one neglects the points marked with crosses, for which, as mentioned earlier, the optical flux could have been overestimated, one finds that the slopes of the diagrams in which the X-ray, near infrared and radio luminosities are plotted against the optical luminosities do indeed seem to be 1. The ratio of 25 μm to optical luminosity seems to decrease for the most luminous objects, while the UV to optical luminosity ratio appears to increase with increasing luminosity. If a power law were fitted between the 4 keV and 2.2 μm fluxes then the spectral index between these is close to 1.2 for most objects.

No attempt was made to apply the K (redshift) correction to the fluxes. As shown in chapter 2.3.2, it will not affect the power law component as α is close to 1. The ultraviolet excess will be moved redwards. However this does not change the slope of the continuum in the optical significantly for $z < 0.06$. Therefore the flux variation gradients should not change much either. The redshifting of the emission lines is not expected to have a major effect on the flux recorded through a filter. For $z < 0.06$ Hα, the strongest line, will have a redshifted wavelength that still places it within the range of the R filter. Hγ and the lower Balmer lines are normally weak in relation to the continuum. The major effect will probably be that of the Balmer continuum spilling into the B filter and Hβ and the [O III] nebular lines being moved towards the V filter.

7.2. Spectroscopic Properties

Spectroscopic observations of the Seyfert galaxies in this sample have been used to determine a number of physical parameters that are expected to be in some way related to the properties of the central source. The widths and

Figure 7.3. A comparison of the fluxes from wide-ranging parts of the spectrum after they had been corrected for distance effects.

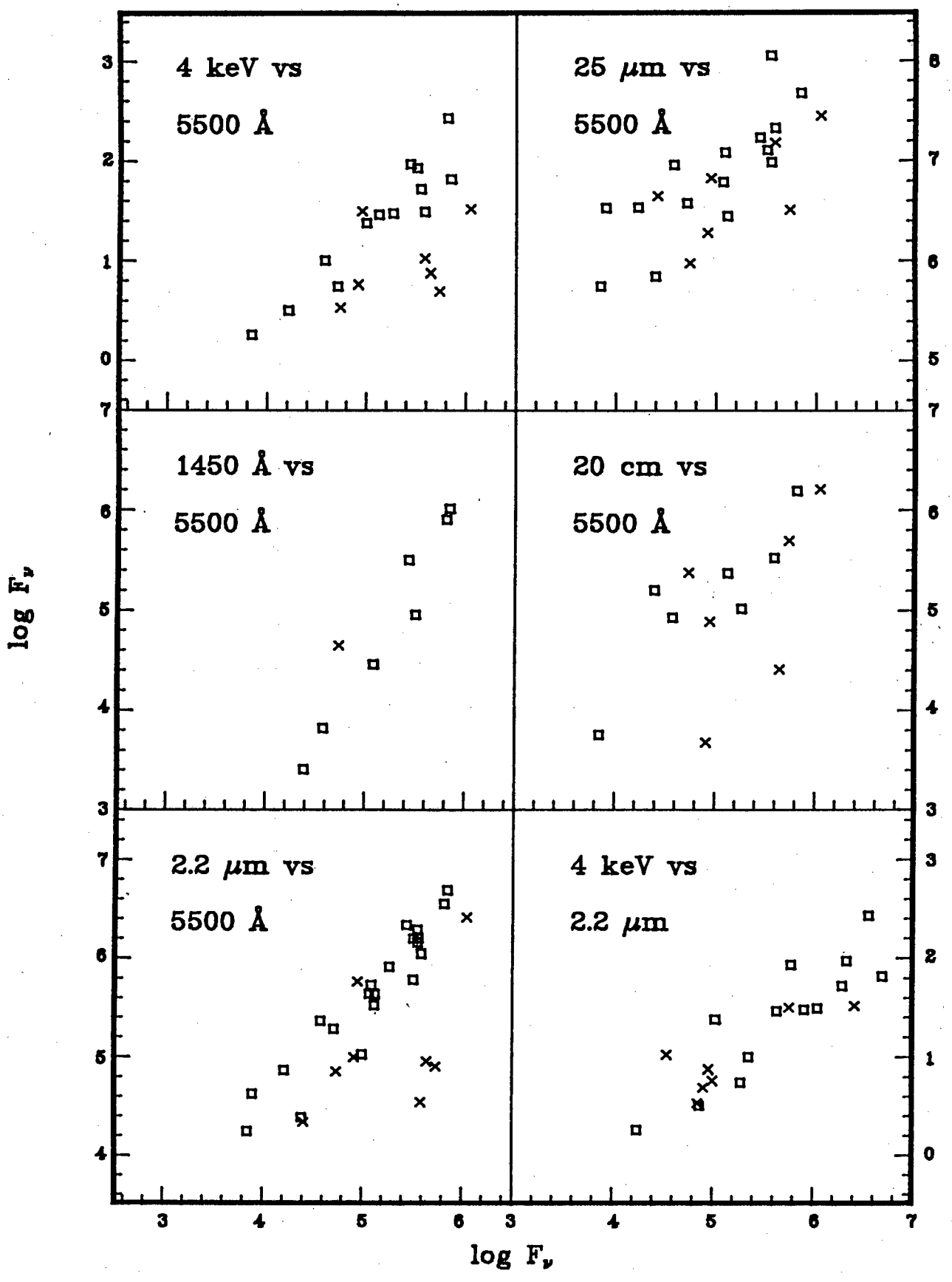

profiles of the spectral lines are a function of the dynamics of the emitting regions. Line intensity ratios can be used to investigate the excitation mechanisms or the extinction of the emitting gas. Some of these ratios are a function of the density or temperature of the emission line regions.

Table 7.7 lists some of these parameters derived for the sample objects. In determining the quantities derived from relative line intensities the values obtained for this work was compared with the data from table A5. Usually results from the two were averaged but if the one data set had a much better signal-to-noise ratio than the other the adopted mean would be closer to the values derived from the less noisy data.

Table 7.7. The spectral characteristics.

Name	$FWHM_n$ km/s	$FWZI_w$ km/s	FHβ #	Hα/Hβ	Fe	n_e cm^{-3}	T_e K
ESO 12-G21	-	4500	0.99	5.4	4	-	-
Ton S180	-	5000	1.28	3.2	4	-	-
NGC 526a	210[a]	-	0.85[f]	3.0	1	600	-
Fairall 9	425[b]	9500	80.40[g]	2.8	3	-	55000
IC 1816	980	4000	0.64	3.6	1	600	-
H 0307-730	-	10500	1.11[h]	5.0	3	-	-
Fairall 1116	300	9000	2.34[i]	2.2:	3	-	114000
NGC 1566	180[a]	5500	1.90[a]	4.5	2	1000	-
MCG -5-13-17	360	6500	2.10	4.7	1	600	36000
3A 0557-383	660	8500	2.86	10.0	2	-	-
Fairall 265	600	9000	0.87	3.5	3	-	-
NGC 2992	255[b]	4000	0.22[j]	20.0	1	400	19000
MCG -5-23-16	180	-	0.04[a]	10.1	1	1000	-
ESO 438-G9	500[c]	8000[c]	2.15[c]	2.9	4	900	26000
NGC 3783	270	7500	25.50[k]	3.2	2	800	34000
H 1143-182	410	7500	4.95[h]	3.6	1	200	31000
MCG -2-33-34	220	5500	10.24[l]	2.7	3	900	-
ESO 323-G77	720	8500	6.60	5.1	4	-	-
MCG -6-30-15	180	6000	1.80[l]	6.1	2	900	50000
IC 4329A	560	11000	7.02[m]	8.0	3	-	31000
I 1509-211	270	6000	3.16[l]	4.6	2	-	-
ESO 103-G35	840[d]	5000[d]	0.23[m]	9.6	1	-	-
Fairall 51	210[b]	7000	3.28[m]	4.0	3	-	-
ESO 141-G55	295[b]	10000	7.36[m]	3.6	3	-	26000
NGC 6814	125[b]	6000	2.85[m]	4.0	0	-	43000
NGC 6860	600[e]	9000[e]	-	-	-	-	-
H 2106-099	690	6500	5.91[h]	3.7	2	-	-
NGC 7213	1310	9500	2.88[n]	6.1	0	600	*
MCG -2-58-22	370[b]	11500	7.06[m]	5.8	1	-	31000

Notes:-
a- Dahari and De Robertis(1988).
b- Whittle (1985).
c- Kollatschny and Fricke (1983). FWZI estimated from their fig. 3a and b.
d- Phillips et al (1979). FWZI estimated from their fig. 2.

e- widths estimated from fig. 2 in Maia et al (1987).
f- Ward et al (1988).
g- Hawley and Phillips (1978).
h- Remillard et al (1986).
i- Maza and Ruiz (1989).
j- Shuder (1980).
k- Ward and Morris (1985).
l- Carter (1984).
m- Morris and Ward (1988).
n- Filippenko and Halpern (1984).
*- for the value of n_e given the equation used to derive T_e yields a negative temperature.
#- the Hβ flux is in units of 10^{-13} erg.cm^{-2}.s^{-1}.

7.2.1. Iron lines

A peculiarity about Seyfert galaxy spectra is the presence of strong, broad Fe II bands. Models devised to describe the emission line processes (e.g., Kwan and Krolik, 1981) have not been successful in reproducing their intensity. It is therefore useful to look more carefully at these lines, as they may hide important clues of the nature of the nucleus. The strength of the Fe II emission line bands at 4570, 5190 and 5320 Å, estimated on the scale from 1 to 4 introduced earlier, is listed in column 6 of table 7.7.

7.2.2. Emission line ratios

The electron density n_e, given in column 7 of table 7.7, was calculated from the intensity ratio of the sulphur 6725 Å doublet. The electron temperature T_e, which is listed in column 8 of the same table, was derived from the relative strengths of the [O III] lines. Both these parameters were calculated from the formulae given in chapter 2.2. If n_e was not known then T_e could still be derived by assuming that $n_e = 10^3$ cm^{-3}, as the density dependence on this quantity is small at the low densities that have been found for the other narrow line regions investigated here.

The ratio Hβ(narrow)/[O III] 5007 Å, which is listed in tables 6.2 and A4, is a potentially useful parameter that gives an indication of the relative emitting strengths of the broad and narrow line regions. It and other spectral parameters described here will be compared to the magnitude of the continuum flux changes in chapter 7.5.

The use of the Balmer and other line ratios to determine the reddening is documented in chapters 2.3.3 and 7.4.

7.2.3. Line widths

When talking about line widths in Seyfert galaxies it is necessary to distinguish between the widths of broad and narrow lines. In this work the full width at zero intensity ($FWZI_b$) of the broad lines and the full width at half intensity ($FWHI_n$) of the narrow lines have been measured. For the narrow lines the width was determined from the [O III] 4959, 5007 Å lines, as other lines were either blended or not strong enough. Where possible, this was measured from the high dispersion spectra listed in table 6.1. Otherwise the $FWHI_n$ was extracted from the literature. If no high dispersion data was available then low dispersion spectra taken with a slit width of less than 300 μm were used. In that case a correction for instrumental line broadening was made using the formula $w^2_{obs} = w^2_{true} + w^2_{inst}$ where w_{obs} is the observed width, w_{true} is the true width and w_{inst} is the instrumental broadening which was determined from the width of monochromatic arc lines (~7 Å). The results are shown in column 2 of table 7.7.

The broad line full widths at zero intensity ($FWZI_b$) measured are listed in column 3 of table 7.7. To determine these the Hα, Hβ and Hγ widths were measured on all available low dispersion spectra. Lines were not used if their strength at maximum was less than about 4 times the noise level. Line edges could be judged "by eye" to be the points where the line became indistinguishable from the continuum. As the broad lines may have faint wings, this measurement could have been subject to large errors. It was therefore decided to measure a $FWZI_b$ defined as the displacement between the two points where the line intensity is about 2% of the maximum line intensity. It is possible that widths are variable, or change from line to line. However, within the errors of measurement, no evidence of such differences could be found. Therefore all the determined widths were averaged, using a weighting of 2:1:1 to the Hα:β:γ lines respectively. Hβ received a lower weighting because of the possibility of Fe II blending, while Hγ was given a lower weighting because of its relative weakness.

7.2.4. Line profile and intensity variations

Changes in the strengths and profiles of emission lines can be used to determine the size and shape of the emission line region (review by Peterson, 1988). The following conclusions can be made about τ_{var}, the timescale of the variations, and τ_{LT}, the light travel time to the edge of the line emitting region, from the behaviour of spectral lines over a period of time:

- If no intensity or profile changes are seen then $\tau_{var} \ll \tau_{LT}$.
- If profile changes are detected then $\tau_{var} \sim \tau_{LT}$.
- If no profile changes are detected but the intensity of the lines changes then $\tau_{var} \gg \tau_{LT}$.

This argument in reverse justifies that the narrow line intensities remain constant over long timescales, as the narrow line region is believed to have a radius of well over a light year (Peterson, 1988).

Because of the limited amount of data available for some objects and the inability to detect variability in others, the profiles of only nine of the Seyfert nuclei from the sample were investigated. In Figure 7.4 the Hα and Hβ line profiles of these objects are plotted. The Hβ spectra were scaled so that the [O III] line strength for each galaxy remain constant while the Hα spectra were scaled so that the Hα peak height is the same for all spectra of that object. Spectra measured less than two months apart were combined. The vertical ordering of the spectra is chronological, with the earliest spectra being at the bottom.

Line intensity changes are visible in many spectra (e.g., MCG -2-58-22). Some of the spectra are too noisy to make conclusions about line profile changes, but on the whole profiles measured at different epochs look similar. As otherwise variations would have been detected on timescales shorter than a month, this shows that the broad line region is smaller than ~30 light days. This is in good agreement with current beliefs that the broad line region is a few light days in diameter (Peterson, 1988).

There are only a few cases for which a profile change is clearly visible, such as the strengthening of a red bump on the Balmer lines of IC 4329A. This might be a component making up the broad line profile that could be varying at a different rate compared to the other components. Such variations have been noted by some investigators (e.g., Menzies and Feast, 1983). It shows that some of the emitting material contributing to the broad lines lies further from the nucleus, probably in an intermediate zone between the broad and narrow line regions.

Figure 7.4(a). Hβ and Hα line profiles of Fairall 9, Fairall 1116 and MCG -2-58-22 (see text for description of vertical scale).

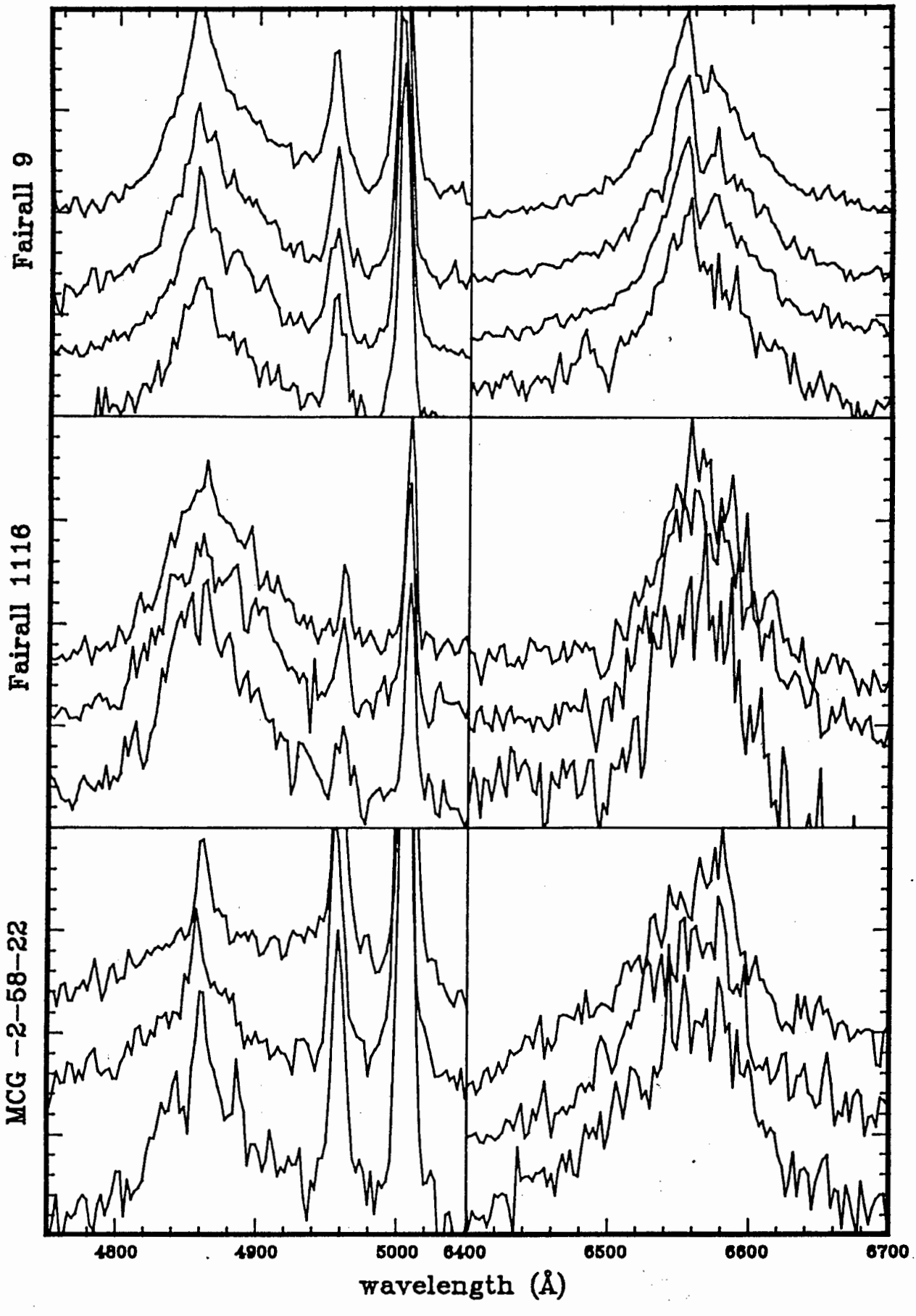

Figure 7.4(b). Hβ and Hα line profiles of ESO 323-G77, IC 4329A and 3A 0557-383 (see text for description of vertical scale).

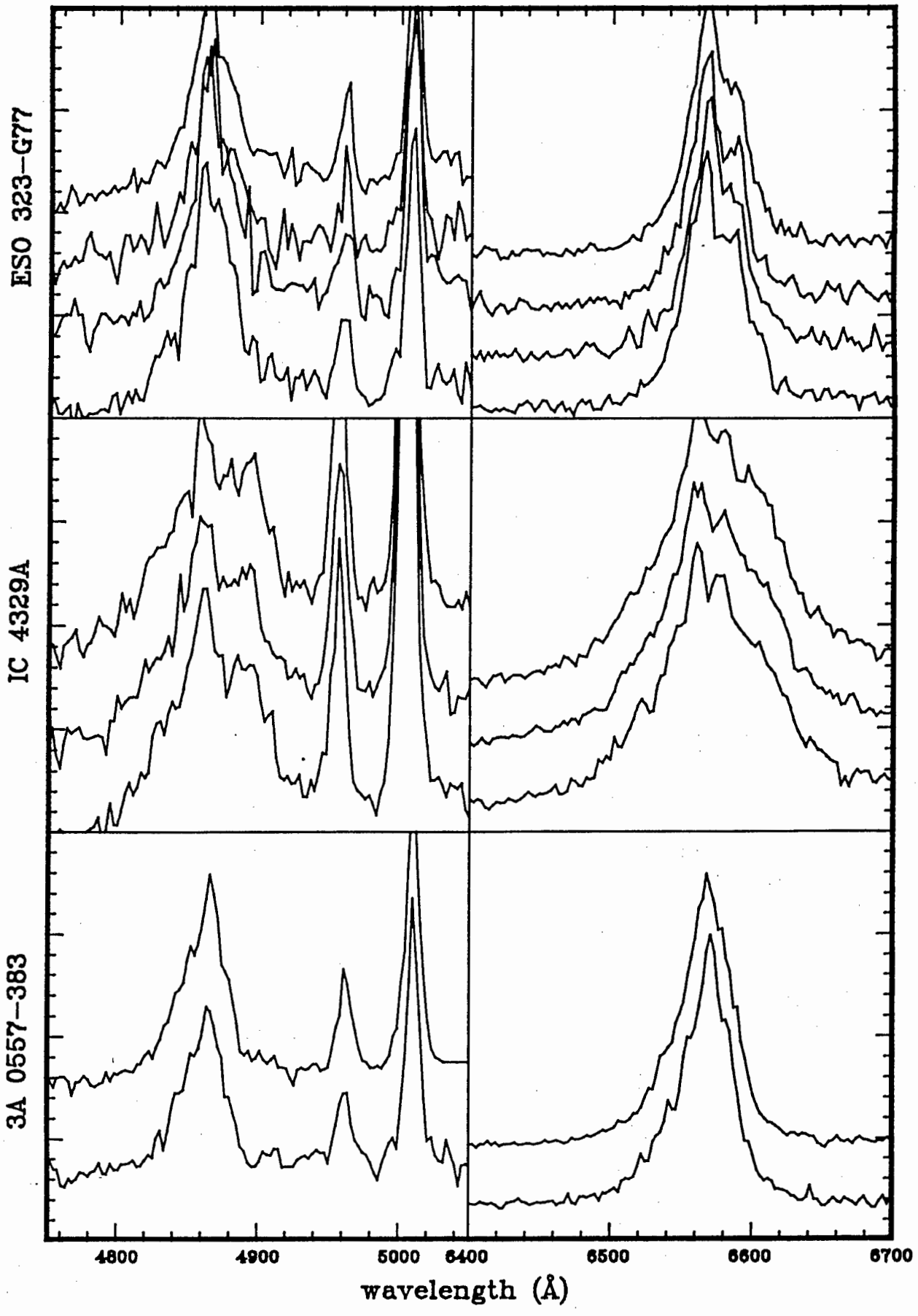

Figure 7.4(c). Hβ and Hα line profiles of NGC 3783, MCG -2-33-34 and MCG -5-13-17 (see text for description of vertical scale).

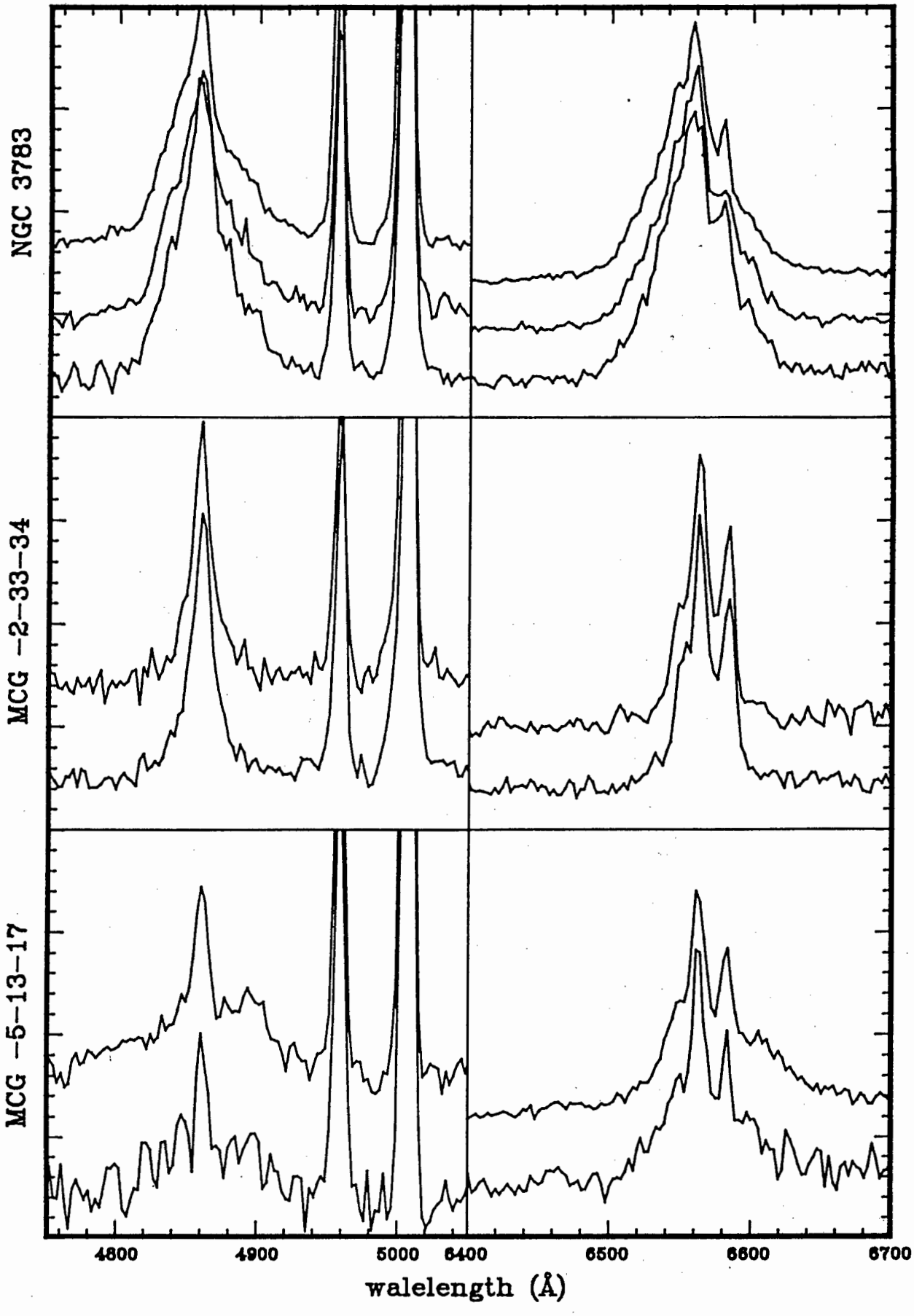

7.3. Morphology and Polarisation

Polarisation measurements for all objects are listed in table 7.8. With the exeption of Fairall 51 all highly polarised objects have a polarisation angle θ_p similar to the measured position angle of the galaxy's major axis, θ_o. This suggests that the polarisation is to a large extent caused by interstellar matter, as dust in a galaxy has a tendency to align itself with the galactic magnetic field. This view is supported by other polarimetric studies of Seyfert galaxies (e.g., Thompson and Martin, 1988). Spectropolarimetry of Seyfert galaxies (Martin et al, 1982, Brindle et al, 1990b) suggests that the polarisation is normally independent of spectral features, as would be expected for interstellar dust. The assumption that most of the polarisation is interstellar will later be used to estimate the reddening.

There does however seem to be some intrinsic polarisation in a few Seyfert nuclei. Spectropolarimetry of Fairall 51 by Brindle et al (1990b) shows that the broad lines are slightly more polarised than the continuum. A number of quasars have a significant amount of polarisation not explained by interstellar dust (Martin et al, 1983).

The spectropolarimetry of IC 4329A by Martin et al (1982) also showed that the amount of polarisation rises towards shorter wavelengths, a property also found in other objects (Brindle et al, 1990a). This, Martin et al (1982) argue, means that the interstellar dust grains in that galaxy are smaller than typical grains in our Galaxy. One important consequence of this is that a galactic reddening law with A_v = 3.1 E(B-V) would not be true under such circumstances. This possibility is discussed in chapter 8.

Two parameters related to the morphological properties of the underlying galaxy have been calculated for all objects and will be compared to their other properties. These are μ_o', the face-on central surface magnitude, and M_v, the absolute magnitude of the galactic disk component. They were derived from the values of μ_o and from the galaxy disk V-magnitudes given in table 4.3 using the relations given in chapter 2, and are listed in table 7.8. The method used to deduce these values has resulted in an underestimation of the central surface brightness of highly inclined spirals, as no corrections were made for the increased obscuration.

An inspection of the central surface magnitudes given in table 7.8 confirms the view that Seyfert galaxies are usually spirals. Spiral galaxies have

central surface magnitudes that are close to $\mu_o(V) = 20$ while for elliptical galaxies the central brightness is normally much higher (Binggeli et al, 1988). Most of the galaxies studied here have central surface magnitudes close to $\mu_o(V) = 20$. The values of M_v found are also typical of spirals.

For three galaxies, however, NGC 1566, MCG -6-30-15 and NGC 7213, the central surface brightness is much higher. NGC 1566 is a very nearby galaxy for which the bulge component could have extended into the 8"-40" diameter annulus used to measure the disk component surface magnitude. This effect is unlikely to explain the high surface brightness of the other two objects. It is therefore expected that these have strong, possibly dominating spheroidal components. NGC 7213 is in many other respects unlike the other galaxies of the sample. Many of its properties resemble those of radio galaxies, which are more likely to be elliptical systems than Seyfert galaxies (Lawrence, 1987). The properties of MCG -6-30-15, on the other hand, are mostly typical of those encountered in other Seyfert galaxies, exept that its nucleus and the host galaxy are rather faint. If this object was not relatively nearby, it is unlikely that it would have attracted much attention as its X-ray and infrared luminosities would have been below the HEAO-1 and IRAS detection limits. It is possibly a prototype for a whole sub-class of underluminous Seyfert 1 galaxies.

Table 7.8. The polarimetric and morphological characteristics.

Name	p(%)	θ_p	θ_o	$\Delta\theta_{p,o}$	μ_o'(V)	M_V
ESO 12-G21	0.75	106[a]	140	34	20.26	-20.98
TON S180	-	-	-	-	20.66	-21.21
NGC 526a	0.26	168[a]	100	68	20.16	-19.92
Fairall 9	0.40	2[a]	100	82	20.63	-21.64
IC 1816	-	-	-	-	20.09	-20.72
H 0307-730	-	-	-	-	20.20	-20.56
Fairall 1116	-	-	140	-	20.96	-21.77
NGC 1566	0.60	53[a]	-	-	19.15	-20.17
MCG -5-13-17	-	-	-	-	19.38	-20.25
3A 0557-383	4.63	117[a]	135	18	21.56	-20.51
Fairall 265	-	-	135	-	20.07	-20.88
NGC 2992	3.32	33[a]	15	18	20.63	-19.39
MCG -5-23-16	0.17	68[a]	55	13	20.79	-20.34
ESO 438-G9	0.47	-[b]	170	-	20.60	-20.90
NGC 3783	0.47	112[a]	165	53	19.93	-20.79
H 1143-182	-	-	-	-	20.07	-21.02
MCG -2-33-34	0.29	-[b]	-	-	-	-
ESO 323-G77	2.44	77[c]	-	-	19.64	-20.74
MCG -6-30-15	4.65	117[a]	115	2	19.01	-19.57
IC 4329A	5.74	44[a]	45	1	21.68	-20.75
I 1509-211	5.44	66[c]	-	-	20.85	-21.38
ESO 103-G35	0.43	20[a]	40	20	21.75	-19.68
Fairall 51	5.47	140[a]	0	40	21.11	-19.91
ESO 141-G55	1.42	0[a]	-	-	19.74	-21.54
NGC 6814	1.77	176[a]	-	-	19.96	-19.64
NGC 6860	1.06	173[c]	30	37	19.89	-21.13
H 2106-099	0.71	64[c]	-	-	20.95	-20.70
NGC 7213	0.39	137[a]	-	-	18.00	-21.03
MCG -2-58-22	0.49	80[a]	-	-	20.13	-22.14

Notes:- a) from Martin et al (1983) b) from Brindle et al (1990a) c) privately communicated by P. Barrett. All angles are given in degrees.

7.4. Calculation of the Nuclear Extinction

In chapter 2.3.3 several methods were proposed by which the obscuration of a Seyfert nucleus could be estimated. For this thesis the nuclear visual extinction A_V has been calculated using several of these methods, which are described in more detail below. Other procedures to estimate the reddening suggested in chapter 2 were not used because the spectral lines required could only be measured in a few objects. All derived A_V values are listed in table 7.9. From these an extinction value was adopted for other calculations in this thesis. It is given in the last column. The A_V values estimated by the various

methods are compared with each other in figure 7.5.

a) Balmer decrement. Assuming an intrinsic $H\alpha/H\beta$ ratio of 3.5 (see chapter 2), the extinction was calculated from the formula

$$A_V = 6.688 \log(F(H\alpha)/F(H\beta)) - 3.64$$

using the $H\alpha/H\beta$ ratios from table 7.7.

b) X-ray to $H\beta$ luminosity ratio. The extinction at $H\beta$ was derived by this method as described in chapter 2. A_V was found from this using the conversion equation

$$A_V = 0.863\ A\beta.$$

This and the previous formula were derived from a Whitford reddening law as given by Miller and Matthews (1972) with R = 3.1. The ratio of the X-ray to $H\beta$ luminosity can be calculated directly from the 2-10 keV X-ray fluxes (given in table 7.6) and the $H\beta$ fluxes (listed in table 7.7).

c) X-ray power law. Various authors have estimated the hydrogen column density N_H from the shape of X-ray spectra. This was converted to an extinction value by using the formula

$$A_V = 4.5\ 10^{-23}\ N_H(cm^{-2}) .$$

In doing this the hydrogen column densities given in the last column of table 7.6 were used.

d) Infrared power law. The displacements of the positions of the galaxies in a H-K vs. K-L diagram from the normal galaxy-AGN mixing line as given by Glass (1981) were converted to extinction values, as discussed in chapter 2.

e) Polarisation. Lower limits to the extinction were estimated from the empirical relationship $p < 9\ E(B-V)$ (Serkowski et al, 1975) and hence $A_V = 3.1\ E(B-V)$ was found using the values given in table 7.8. Serkowski et al (1975) found that E(B-V) is typically twice as large as the minimum value calculated with the above formula. If reddening in our galaxy is large the total extinction could be even higher as the angle of polarisation in the Galaxy could be different to the polarisation angle in the Seyfert galaxy observed, which means that the polarisation will decrease.

f) The flux variation gradient. The analysis of the variations of Seyfert nuclei carried out in this work suggests a new method of estimating the visual extinction of a Seyfert nucleus. Because of the variability one could measure the nuclear flux through each of the optical filters very accurately. It was noted in the discussion about the flux distribution that the shape of the flux continuum derived in this manner is similar for all galaxies observed if the effects of reddening are taken into account.

If one now assumes that there is one standard flux distribution that describes the spectra of all Seyferts then one may estimate the reddening of an object by comparing the shape of the continuum with the standard continuum spectrum. In other words, the reddening of a Seyfert nucleus can be estimated by comparing its FVG with the a standard unreddened FVG. This standard gradient is best determined empirically. In this thesis it was derived by averaging the gradients of three nuclei, Fairall 9, H 1143-182 and ESO 141-G55, for which all other methods used to determine the obscuration lead to the result that the extinction value $A_V \sim 0$. The adopted standard gradient was given in the last row of table 7.2.

Flux variation gradients measured for different filter combinations can be used to obtain independent estimates of the extinction. Four combinations were tried:

1) - U and B
2) - B and V
3) - V and R
4) - V and I

In order to derive the extinction from the measured and unreddened FVG's for filters 1 and 2, $\Gamma(1,2)$ and $\Gamma_o(1,2)$ the following formula was used

$$A_V = -2.5\ R\ (A_1/E(B-V)-A_2/E(B-V))^{-1}\ \log(\Gamma(1,2)/\Gamma_o(1,2))$$

with an R value of 3.1 and the $A_m/E(B-V)$ values from table 7.1. This formula can be derived from the relation between flux and magnitude given earlier in the chapter. The advantages and problems of this procedure in comparison to the other extinction determination methods will be discussed in chapter 8.

Figure 7.5(a). A comparison of the A_V values derived with estabilished methods of calculating the extinction.

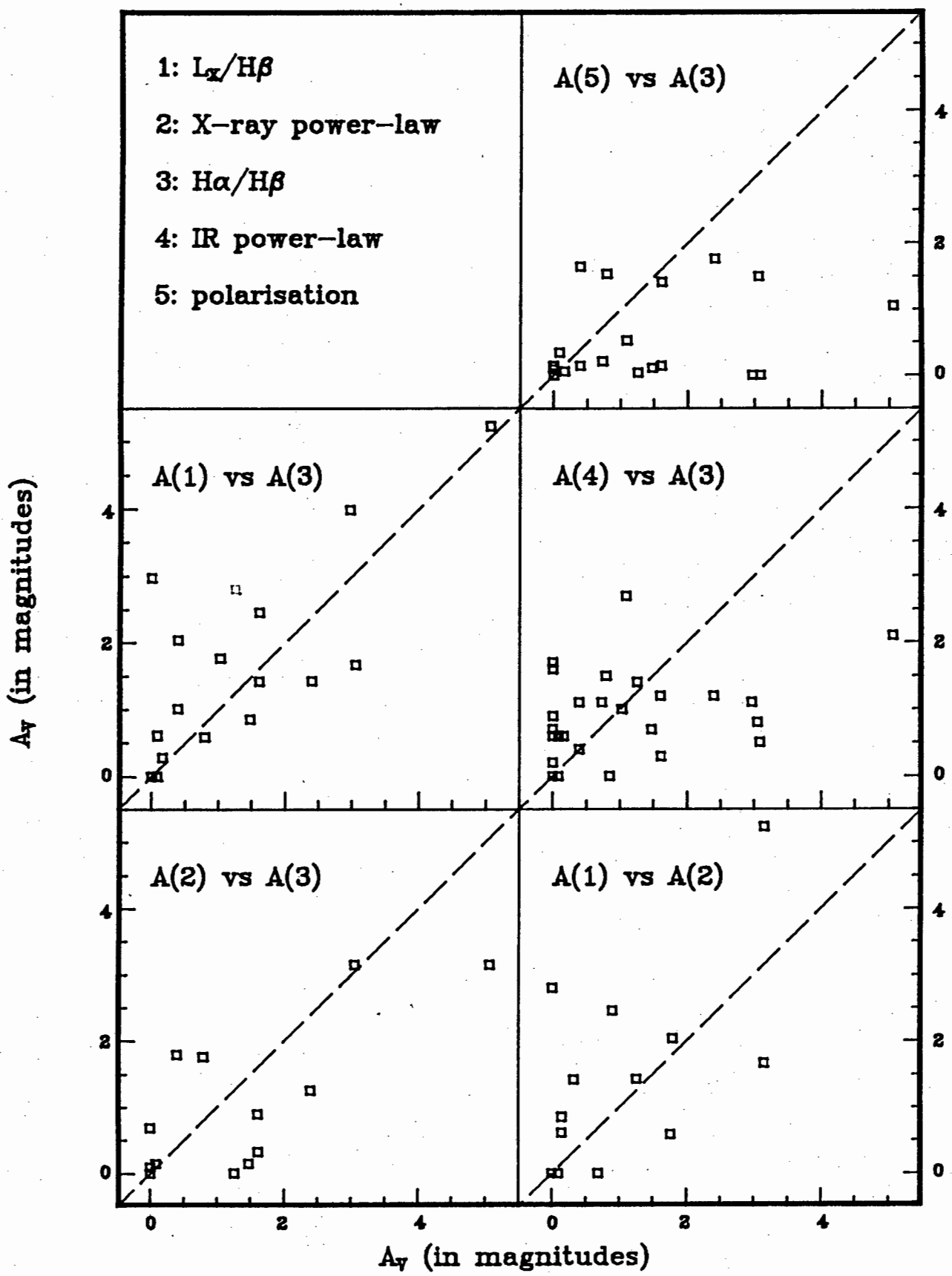

Figure 7.5(b). A comparison of the A_V values derived with the flux variation gradient method.

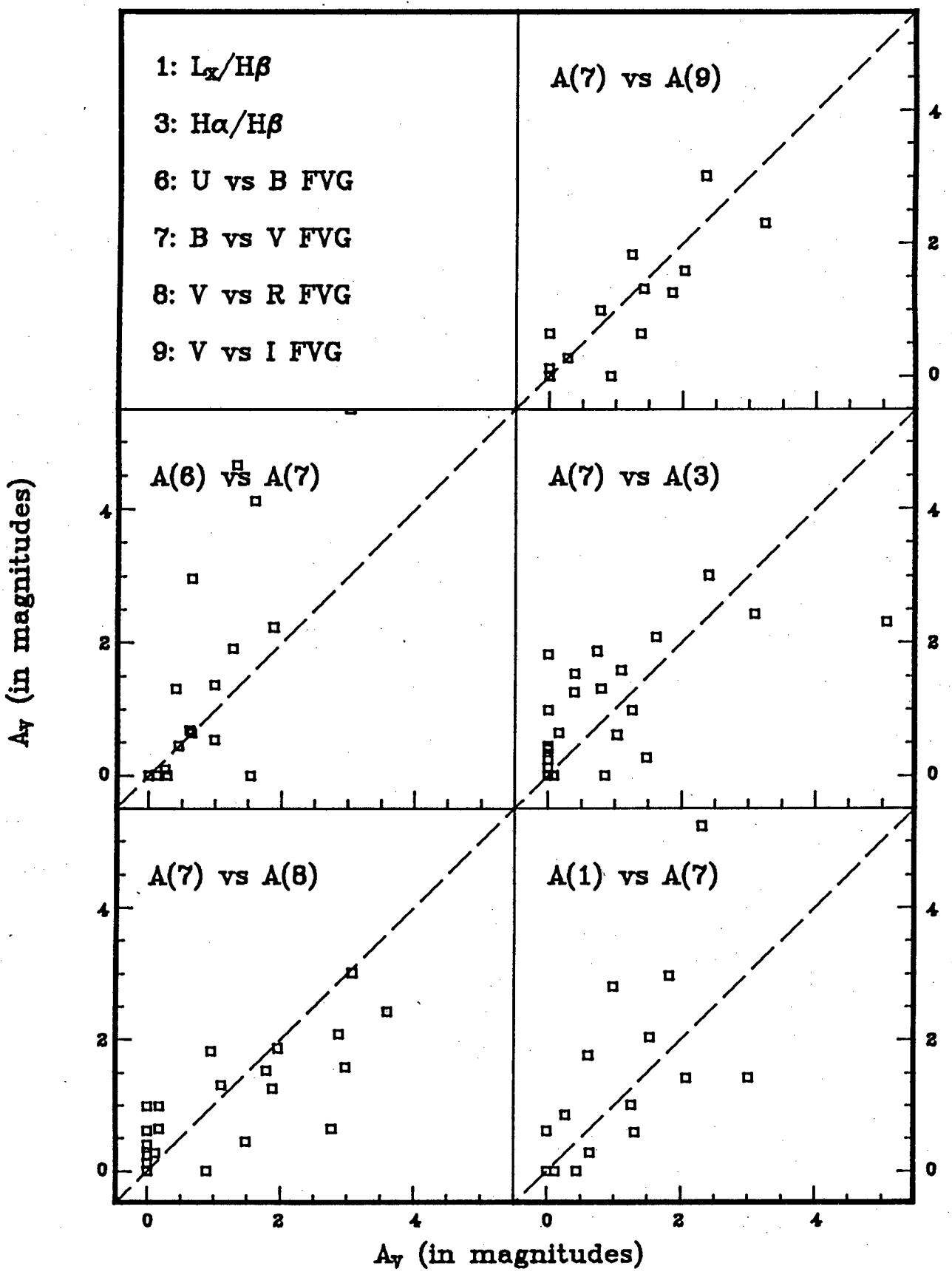

Table 7.9. Estimations of the extinction A_V. columns 2-10 give the extinction estimated using the methods labelled a to f above. f1 to f4 represent method f using U vs B, B vs V, V vs R and V vs I flux variation gradients. The adopted A_V value is given in the last column.

Name	a	b	c	d	e	f1	f2	f3	f4	av.
ESO 12-G21	1.26	2.80	0.00	1.4	>0.04	1.37	0.98	0.18	0.76	1.0
Ton S180	0.00	-	-	0.0	-	0.00	0.00	0.00	0.00	0.0
NGC 526a	0.00	2.97	7.65	0.9	>0.09	-	1.82	0.96	1.23	2.0
Fairall 9	0.00	0.00	0.09	1.7	>0.14	0.0*	0.0*	0.0*	0.0*	0.0
IC 1816	0.08	-	-	0.0	-	-	-	-	-	0.0
H 0307-730	1.03	1.76	-	1.0	-	0.68	0.61	0.00	-	1.0
Fairall 1116	0.00	-	-	1.6	-	0.09	0.24	0.00	-	0.1
NGC 1566	0.73	-	-	1.1	>0.21	2.23	1.87	1.96	-	1.2
MCG -5-13-17	0.85	-	-	0.0	-	0.00	0.00	0.89	0.92	0.6
3A 0557-383	3.05	1.67	3.15	0.8	>1.50	-	-	-	-	2.8
Fairall 265	0.00	-	-	0.7	-	1.31	0.40	0.00	-	0.2
NGC 2992	5.06	5.23	3.15	2.1	>1.05	-	2.30	-	3.23	4.5
MCG -5-23-16	3.08	7.04	5.85	0.5	>0.00	-	2.42	3.60	-	4.0
ESO 438-G9	0.00	-	-	0.6	>0.00	0.54	0.98	0.00	0.76	0.4
NGC 3783	0.00	0.00	0.68	0.9	>0.00	0.00	0.12	0.00	0.00	0.0
H 1143-182	0.08	0.00	-	0.6	-	0.0*	0.0*	0.0*	0.0*	0.0
MCG -2-33-34	0.00	0.00	0.00	0.2	>0.00	0.45	0.44	1.48	-	0.2
ESO 323-G77	1.09	-	-	2.7	>0.53	4.12	1.58	2.97	2.02	1.6
MCG -6-30-15	1.61	2.46	0.90	1.2	>1.41	3.82	-	2.87	2.34	2.2
IC 4329A	2.40	1.43	1.26	1.2	>1.76	5.50	3.01	3.07	2.34	2.4
I 1509-211	0.79	0.59	1.76	1.5	>1.53	4.65	1.31	1.11	1.41	1.0
ESO 103-G35	2.96	3.98	-	1.1	>0.00	-	-	-	-	3.5
Fairall 51	0.39	1.01	-	0.4	>1.64	1.91	1.26	1.88	1.84	1.2
ESO 141-G55	0.08	0.61	0.14	0.6	>0.34	0.0*	0.0*	0.0*	0.0*	0.1
NGC 6814	0.39	2.04	1.80	1.1	>0.14	0.00	1.53	1.79	-	1.6
NGC 6860	-	-	-	0.8	>0.30	2.96	0.64	2.77	1.37	1.8
H 2106-099	0.16	0.28	-	0.6	>0.06	0.64	0.64	0.18	0.00	0.3
NGC 7213	1.61	1.42	0.32	0.3	>0.14	-	2.08	2.87	-	1.6
MCG -2-58-22	1.47	0.85	0.14	0.7	>0.11	0.00	0.27	0.12	0.27	0.6

Notes:- The entries labelled with an asterisk were assumed to be 0.0

7.5. Variability

Finally, the nature and magnitude of the continuum flux variations and their relationship to other properties will be examined. The behaviour of the light curves is difficult to quantify. For example, the changes in some nuclei seem to be faster than in others, but large variations are not seen on timescales shorter than one month.

7.5.1. Comparison between variability and other properties

Before discussing the variability it is useful to calculate the luminosities of the nuclei from the sample. The luminosities per unit frequency at 5500 Å, derived from the distances from table 3.1 and the average V-band fluxes given in table 7.4 after these were dereddened using the adopted values of A_V, are given in the first column of table 7.11.

It is proposed to use the amplitude of the luminosity changes as a parameter to describe the variability. This amplitude could be given in absolute units, i.e., as $\Delta L/\nu$, or as a fraction of the average luminosity, i.e., $\Delta L/L$. A similar procedure was adopted by Chapman et al (1985) to describe the ultraviolet variability of Seyfert galaxies. These two quantities are also given in table 7.11. The first of these is sensitive to distance and extinction errors. The second quantity is unaffected by these errors but requires an accurate knowledge of the amount of contamination from extra-nuclear light.

An attempt was made to find any correlations between $L/\nu(V)$, $\Delta L/L(V)$ and other properties of the Seyferts derived in this work; the narrow and broad line widths, the Fe II band intensities (on a scale from 1 to 4), the Hβ to [O III] ratio, the central surface magnitude and the disk absolute magnitude. These parameters are compared graphically in figures 7.6. L/ν are plotted logarithmically in units of 10^{29} erg cm^{-2} s^{-1} Hz^{-1}.

There is a strong correlation (significant at the 0.1% level) between the nuclear luminosity and the absolute magnitude of the disk component of the host galaxy. It might be that this effect can be explained by some systematic error introduced during the analysis of the CCD images, as the furthest galaxies are fairly small on these images. It seems however more likely that this effect is real. Griersmith and Visvanathan (1979) derived an even higher galactic luminosity for Fairall 9 than was found in this study. A good correlation (significant at 1% level) also exists between the luminosity and the ratio of the emitting strength of the broad and narrow line region (parametrised by Hβ/[O III]). There are also indications that μ_o and the broad line width increase with increasing luminosity (correlations significant at 5% level).

It is clear that there is no relation between the relative nuclear luminosity variation amplitude and any of the parameters that this quantity is plotted

against in figure 7.6b.

7.5.2. Search for periodic variability

Several attempts have been made to determine the light curves of Seyfert galaxies (e.g., Penfold, 1979, De Ruyter and Lub, 1986). Some authors have suggested that the optical light variations in Seyfert galaxies are of a periodic nature (e.g., Bisch et al, 1987). Maybe the best evidence of such regular variations was the 130 day period proposed for NGC 4151 (Belokon et al, 1979). This period was however not seen in later data (Lyutyi and Oknyanskii, 1987). It seems therefore that variations are only regular over a limited time period, if they are indeed regular.

The observations made in this work, combined with the photometry of earlier investigators, form a large data set that will be examined for the purpose of identifying possible variations of a periodic nature. This was done through a Fourier analysis of the light curves of objects where nuclear flux changes were believed to have been detected without doubt. A method to Fourier analyse unevenly spaced data has been proposed by Deeming (1975). This technique, which has been used extensively to investigate the light curves of active nuclei (e.g., Lyutyi and Oknyanskii, 1987), has been employed in this analysis as well.

Some of the frequencies identified by this process are artifacts introduced by the spacing of the observations. For example, observations of astronomical objects can usually only be carried out for part of the year. Therefore it is expected that periods of one year would fit most data sets. Related to this is the fact that subsidiary peaks known as aliases will be found displaced from any real peaks by a frequency characterisic of the data spacing (e.g., 1 yr^{-1}) (Deeming, 1975).

A number of possible periods have been identified for most objects. They are listed in table 7.11. Frequencies that were believed to be artifacts of the nature described earlier were disregarded. The power spectrum of NGC 3783 is shown in figure 7.7. The highest peak corresponds to a period of 610 days.

Table 7.11. The luminosity (in the V-band), observed luminosity range and possible periods of the galaxies in the sample which are definitely variable.

Name	L/ν #	$\Delta L/\nu$ #	$\Delta L/L$	< P(days) 20-100d	100-1000d	> 1000d
ESO 12-G21	3.84	0.81	0.21	27.7	521	-
TON S180	4.31	0.99	0.23	24.1,39.0	403	-
Fairall 9	8.39	6.88	0.82	-	347	>5000
H 0307-730	1.19	0.46	0.39	not enough data		
Fairall 1116	3.83	1.15	0.30	36.4	-	1190
NGC 1566	0.30	0.09	0.30	32.9,39.5	617	1470
MCG -5-13-17	0.13	0.13	0.98	25.3,39.1	-	-
Fairall 265	1.40	0.21	0.15	25.1,27.1	134	-
ESO 438-G9	1.46	0.25	0.17	not enough data		
NGC 3783	0.45	0.29	0.65	24.4,72.9	610	1470
H 1143-182	1.59	0.64	0.40	21.8,27.0	446	-
MCG -2-33-34	0.20	0.05	0.25	not enough data		
ESO 323-G77	4.22	0.34	0.08	38.2,40.1	128	-
IC 4329A	4.63	2.41	0.52	26.9	305,575	1920
I 1509-211	4.20	0.88	0.21	-	410	-
Fairall 51	1.05	0.27	0.26	26.6	174,329	-
ESO 141-G55	3.26	2.41	0.74	22.1,26.1	333	-
NGC 6814	0.08	0.06	0.76	-	352	2780
NGC 6860	1.56	0.44	0.28	not enough data		
H 2106-099	2.20	0.66	0.30	not enough data		
MCG -2-58-22	7.76	5.98	0.77	27.7,29.3	-	4000?

Notes:-
#- in units of 10^{29} erg.cm^{-2}.s^{-1}.Hz^{-1}

A simple test was devised out in order to check the significance of the periods given above. The light curves of five of the galaxies investigated were modified in such a way that the times of the observations were retained but new magnitudes were generated so that the invented light curve had behaviour trends typical of the true light curve. The period finding procedure was repeated on these curves. The following cases were constructed:
A: A light curve with large, slow magnitude changes (for Fairall 9).
B&C: Two light curves with fairly large and faster magnitude changes (for NGC 3783 and H 1143-182).
D&E: Two light curves with small magnitude changes (for NGC 6814 and Fairall 265).

Apart from preserving the general appearence of the light curves, the data points were generated in a random manner. Therefore none of the periods identified will be real. The results of the period finding procedure are given in table 7.12. This analysis found a number of frequencies that do not seem to

be caused by the nature of the data spacing. These are probably generated by the combination of the data spacing with the way that the curves were constructed in order to give them a 'typical' appearence.

This casts serious doubt on the reality of most of the periods listed above. Note however that no strong power spectrum peaks are present between 60 and 240 days for any of the five cases investigated. This suggests that there is a reasonable possibility of periods falling between these two values being real. All other possible periods, other than really strong peaks, should be rejected.

Table 7.12. The 20 most likely periods for the simulated light curves (in days).

Case A	Case B	Case C	Case D	Case E
21.3	22.2	25.0	21.6	20.9
21.4	27.6	25.1	27.0	28.8
23.9	28.1	25.3	27.5	29.7
27.2	28.5	26.8	29.1	29.9
28.3	28.7	44.1	29.3	30.0
28.7	29.8	54.1	29.4	31.8
28.9	30.2	59.0	29.6	32.8
29.0	30.4	60.7	29.7	32.9
29.4	34.3	61.3	29.9	33.1
29.6	237.0	61.7	30.1	33.3
29.8	287.0	62.2	30.2	36.9
33.2	325.0	625.0	316.0	37.1
298.0	431.0	676.0	352.0	248.0
321.0	581.0	735.0	400.0	258.0
347.0	667.0	1140.0	446.0	269.0
382.0	847.0	1320.0	532.0	1090.0
417.0	1040.0	1560.0	1220.0	1320.0
1670.0	1390.0	1920.0	1430.0	1670.0
2630.0	1790.0	2500.0	2270.0	2270.0
4550.0	2940.0	3570.0	4550.0	3570.0

Figure 7.6(a). A comparison of the nuclear luminosity with other properties of the Seyfert galaxy. L/ν is in log form.

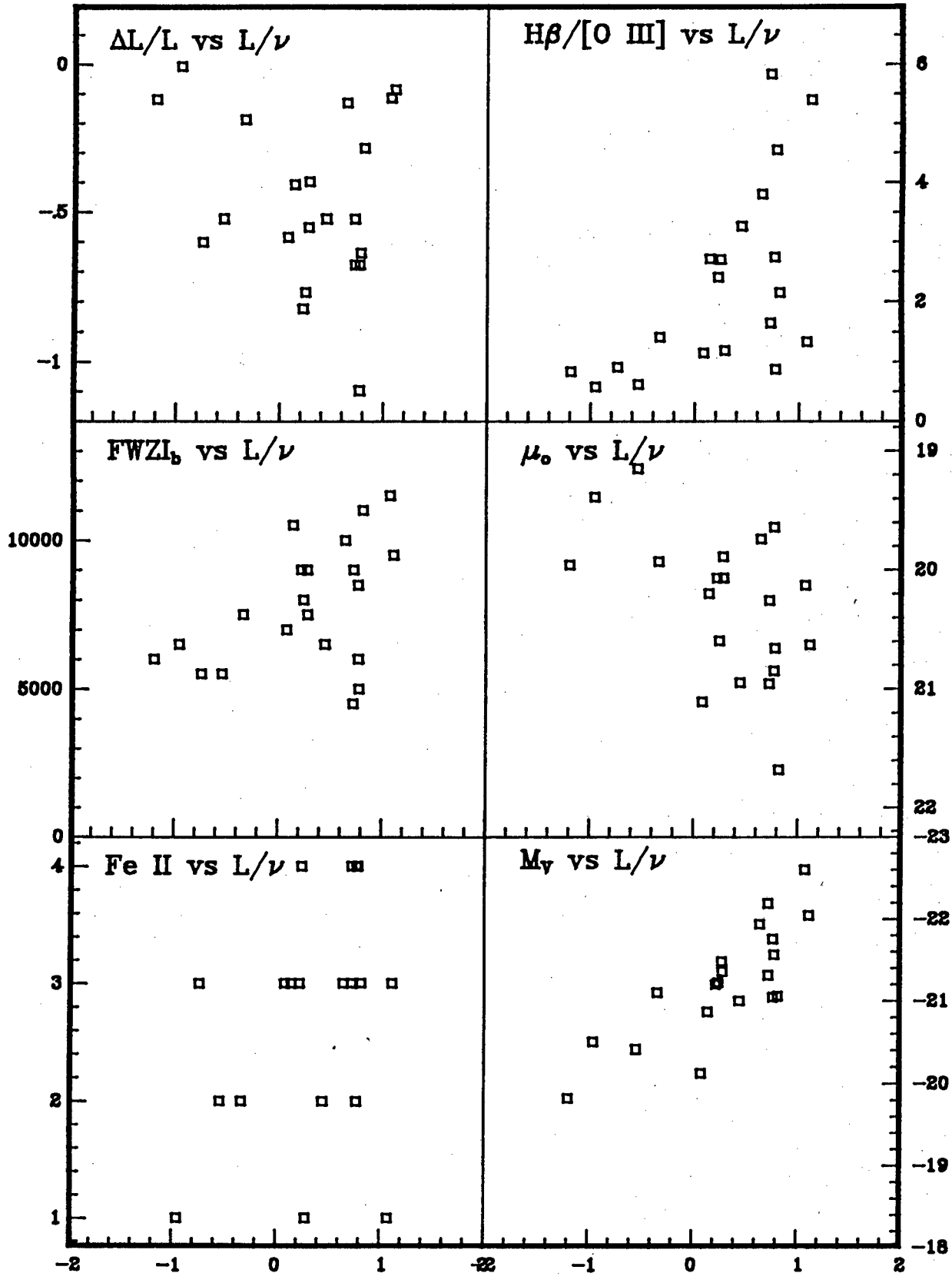

Figure 7.6(b). A comparison of the relative luminosity variation amplitude to other properties of the Seyfert galaxy.

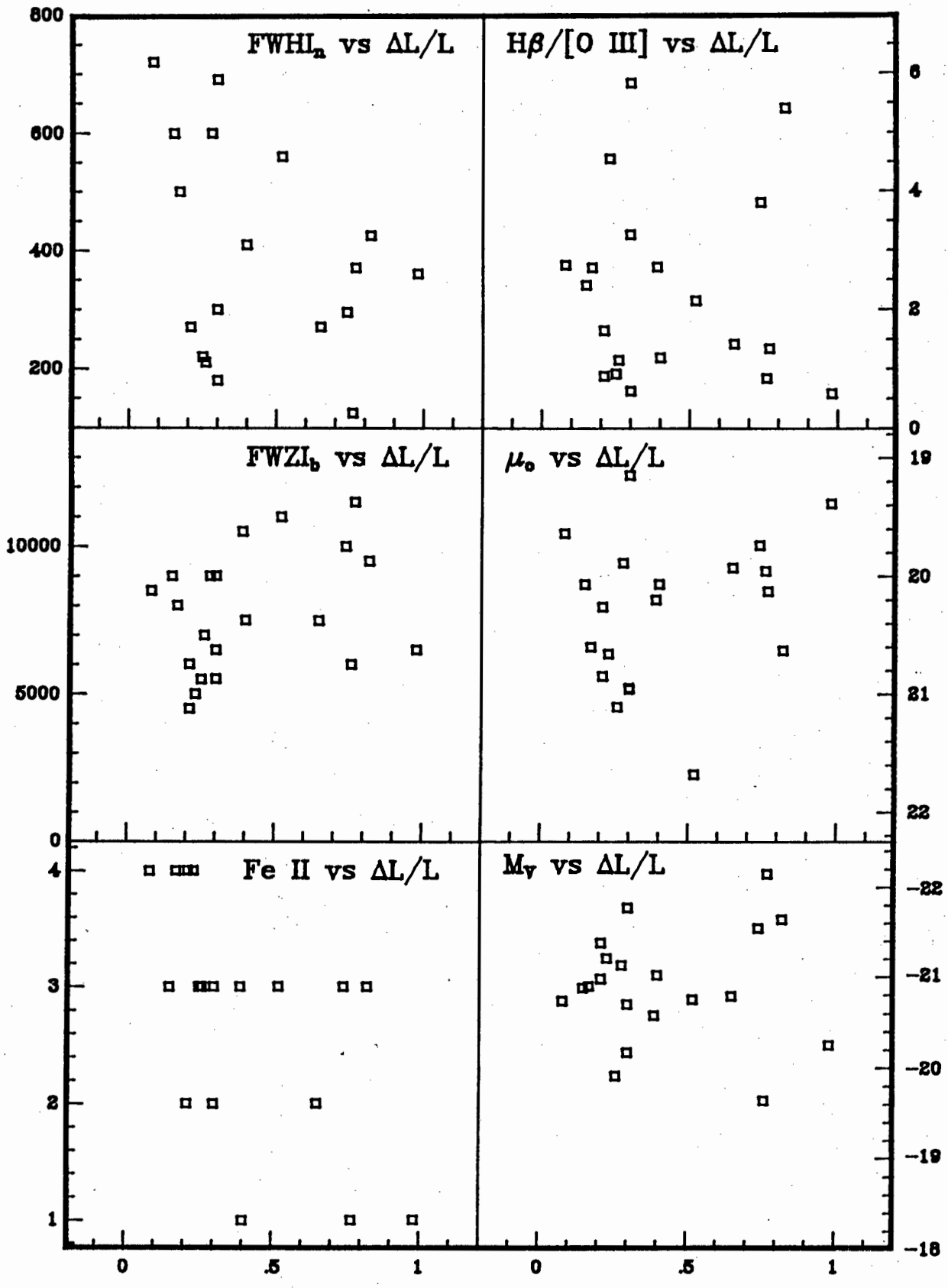

Figure 7.7. The Fourier transform of the light curve of NGC 3783. The highest peak corresponds to a frequency of 610 days.

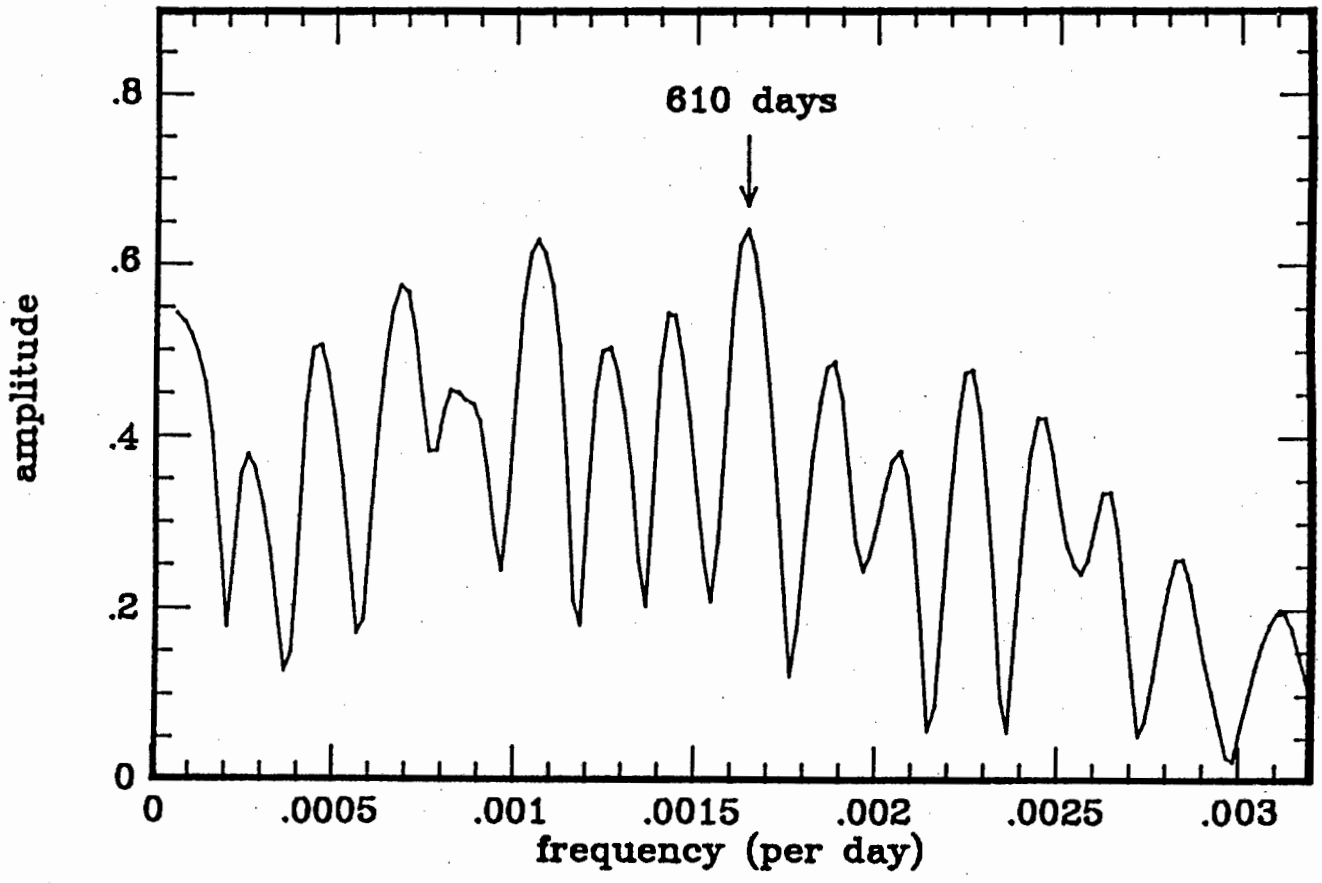

8. Discussion

In this chapter three topics of special interest, around which much of this thesis has been structured, will be discussed in more detail.

8.1. The Flux Distribution

The flux distributions of the galaxies investigated in this work, which were plotted in figure 7.2, all have characteristics typical of Seyfert galaxy spectra. The radiation of energy is relatively evenly distributed over the whole range of wavelengths displayed and, after the effect of reddening is taken into account, the flux is seen to strengthen towards the blue end of the spectrum. Some of the flux distributions were difficult to determine because of strong contamination of the nuclear flux by a galactic starlight component. Errors in the estimation of the extinction are expected to have affected the shorter wavelength fluxes in some of the distributions.

Flux variation gradients have been shown to be a useful tool for deriving the flux distribution of the variable component of Seyfert nuclei at optical wavelengths. This method however has a limitation in that it will not enable one to separate the broad emission line component from the nuclear continuum. Future work with FVG's should include use of the method in other wavelength regions as well as its application to more AGN's, particularly QSO's and BL Lac objects, which are generally highly variable and for which much photometric data are often available.

A visual inspection shows that about 2/3 of the flux distributions investigated look remarkably similar to each other. It is expected that the other 1/3 in fact also have the same shape but are affected by the two sources of error described above. It therefore seems reasonable to speculate that all Seyfert nuclei have an almost identical flux distribution, whose features are described below. Ultraviolet observations suggest that UV spectra are slightly flatter when the nucleus is bright (Masegosa et al, 1986), but the overall effect of this on the flux distribution is small.

An ultraviolet bump dominates the flux at optical wavelengths. Its shape suggests that it can be formed by a superposition of thermal blackbody radiation components from a hot body, possibly an accretion disk. The luminosity of the ultraviolet bump relative to the nuclear continuum is

roughly constant. It is difficult to tell with the limited IUE data available how far this bump extends into the UV. This information is needed if a determination of the temperature of this presumably thermal component is to be attempted. No conclusion can be made about whether any relationship exists between this temperature and any other property of the nucleus.

The near infrared flux can be crudely described by a power law with $\alpha = 1.2$. Its shape is however slightly convex. Near 1.5 μm the spectral index is much steeper than $\alpha = 1.2$. Dust may be influencing the flux distribution in the near infrared. Glass (1989) and Clavel et al (1989) found a delayed response of the 3.5 μm flux to continuum changes in other bands, and this was interpreted as a sign of dust. No 5 μm bump can be seen in any of the flux distributions. The spectra given by Glass et al (1982) also show no evidence of this feature. It is however true that the 1-5 μm flux is often strong when compared to the 10-100 μm flux. In order to explain this and the convex appearence of the near-infrared spectrum two possible mechanisms will be suggested. Firstly, there could be a 2000 K thermal component, which might be caused by gas from well outside the accretion disk, maybe from as far out as the narrow line region (Clavel et al, 1989). A second, more controversial possibility is that the power law has a frequency cut-off of $\sim 10^{14}$ Hz, much higher than is normally assumed.

It is proposed that the nature of the infrared radiation could be determined with the use of flux variation gradients. This method would enable one to identify the infrared radiation originating close to the nucleus since, as mentioned when describing the emission line variations, flux changes will only be detected if the flux is radiated from a small volume close to the nucleus. Other infrared components formed further from the nucleus, such as the flux from the narrow line region, could be subtracted.

The flux distributions shown in this thesis support the now commonly accepted view that thermal dust emission plays an important role in most Seyfert nuclei (see, e.g., Carleton et al, 1987). A power law with a low frequency cut-off cannot be made to resemble the 1-100 μm spectra of most Seyfert nuclei shown here, as the flux fall-off to longer wavelengths is too gradual to be explained by synchrotron self-absorption. If some day repeated flux measurements of Seyfert galaxies at wavelengths longer than 10 μm are made, it will be interesting to apply the flux variation gradient method to this region of the spectrum in order to try to identify the components responsible for this radiation. It is however possible that these components vary

independently of each other, in which case FVG's cannot be defined.

The similarity between the flux distributions investigated is not confined to the 0.1-100 μm range. The spectral index between the X-ray and infrared wavelength regimes was usually close to 1.2. It is probable that the range in $\alpha_{X,IR}$ determined would be narrowed if the X-ray and infrared fluxes could be measured simultaneously. It has also been seen that the power law does not extend to radio wavelengths (except in the case of NGC 7213, which, as has been mentioned, is peculiar to the sample).

On the whole the results of the analysis confirms previous knowledge of the nature of the flux distribution (e.g., Malkan and Filippenko, 1983, McAlary and Rieke, 1988). It has however also been possible to determine its shape much more accurately, a shape that requires more sophisticated models in order to be fitted.

8.2. Variations

The optical nuclear fluxes were shown to vary proportionally to each other. The shape of the flux distribution in that part of the spectrum therefore remains constant. It shows that, just as for the broad emission lines, the optical continuum flux originates from within a relatively small region. The timescales of the variations observed were of the order of about 30 days. This emitting region must therefore be much smaller than ~60 light-days, in agreement with current beliefs (e.g., Peterson, 1988).

The light curves studied in this thesis show a range of behaviour trends, three examples of which are: little change in flux; fairly rapid variations of a relatively small amplitude; slow but very substantial variations. It appears that these behaviour trends are associated with a Seyfert light curve for a long time and may therefore be a property of the galaxy. In this thesis it was attempted to quantify two characteristics of the light curves, the amplitude and timescale of the variations.

The relative amplitude of the luminosity variations was found to be independent of other nuclear and galactic parameters. This is significant because it shows that Seyfert galaxy central engines of different degrees of luminosity seem to be similar in other respects. The $\Delta L/L$ values given here are lower limits, as the sample has only been monitored for a relatively short

period. It is possible that $\Delta L/L$ is fairly large for all Seyferts.

No conclusive evidence of regular variations has been found. The 610 day period proposed for NGC 3783 cannot be confirmed without more observations. It was shown that periods close to 30 days or 1 year can be produced spuriously with the data sets available. Only the suggested periods between 60 and 240 days deserve a closer inspection. Interestingly, the period of 130 days found in NGC 4151 falls within this range. Fairall 265 and ESO 323-G77 have possible periods of a similar duration. The data sets from which these were derived are however small and the flux amplitude detected in these objects is minimal. This casts doubt on the reality of these periods. It would however be interesting to know if future observations would estabilish their reality, as it could imply that Seyfert nuclei have preferred periods of about 130 days.

8.3. The Extinction of the Nucleus

This sections aims to critically examine the methods tried to determine the nuclear extinction.

The Balmer decrement is shown to be a consistent tool for estimating the reddening with an accuracy expected to be better than 0.5 magnitudes. The main sources of error associated with this method are the fact that the intrinsic Balmer decrement is not known very well and may be different from object to object. Care also needs to be taken as the various components of the Balmer lines are believed to be formed in different regions (e.g., Alloin et al, 1985), each possibly having a different extinction value associated with it. This is best illustrated by the discrepancies in the A_v estimate of NGC 526a. The Balmer decrement for this galaxy was calculated from the narrow lines. The broad lines were not measured, but if they could be seen it is expected that their Balmer decrement would be large, as the X-ray spectra of this object's nucleus show evidence of extensive obscuration. This can be interpreted as the broad line being hidden behind as dense gas region. The Balmer line method may not yield an accurate estimate of the nuclear continuum extinction even when the broad line Balmer decrement can be measured because the ionising continuum source and the broad line region need not be equally obscured.

The method which is used to determine the extinction of the Hβ line emission from the X-ray to Hβ flux ratio proved to be fairly reliable. The ratio between these two quantities appears to be reasonably constant. Other than the errors introduced by this assumption the main source of uncertainty stems from the fact that the X-ray and optical observations were usually not made

simultaneously. It also needs to be remembered that the obscuration of the Balmer line emitting region may not be the same as the obscuration of the innermost parts of the nucleus.

Modelling the X-ray flux using a power law with gas extinction is shown in table 7.5 to give widely discrepant results, even though the method is able to distinguish between highly reddened and unreddened Seyfert nuclei. This is believed to be the result of the high sensitivity to the gas column density of the models used to fit the X-ray spectra. It is unlikely that much could be done to alleviate this problem. An additional source of uncertainty is the lack of knowledge about the gas-to-dust ratio in the obscuring regions. This ratio is critical for converting the gas extinction, which affects the infrared, to the dust extinction which affects the optical part of the spectrum.

The A_v values derived from the infrared power law extinction estimation method did not agree well with the A_v values obtained using other methods. This suggests that the slope of the flux distribution in the 1.2-2.2 μm range is not constant for all Seyferts. This could be the result of the effect on the infrared flux by dust components. The method is also fairly sensitive to small errors in the observed colours. Extracting A_v from A_K could also lead to errors if the reddening law is anomalous, a possibility discussed later. Finally, there is the possibility that the origin of much of the near-infrared radiation is not from synchrotron radiation (Clavel et al, 1989), which means that it may be subjected to less obscuration than the inner nucleus.

The polarisation method has also not proved to be very useful. Brindle et al (1990b) have found intrinsic polarisation in some nuclei. In some cases the foreground polarisation in our galaxy is very high (e.g. NGC 6814), which makes the determination of reddening inside these galaxies using this method virtually impossible. In order to apply this method more successfully the following steps would need to be taken. Firstly, spectropolarimetry is required to be able to confirm that the polarisation of the Seyfert is interstellar. Then polarisation measurements of field stars in that part of the sky should be made in order to derive the magnitude and position of the polarisation in our galaxy.

The derivation of the nuclear extinction using the flux variation gradients has been shown to be a reasonably accurate new method that determines the obscuration of the UV excess and power law flux, which are believed to

originate from some of the innermost regions of Seyfert nuclei. To realise its full potential this method still needs to be developed further. The standard unreddened FVG's cannot be determined accurately on the basis of this work only. Many more Seyfert nuclei with known negligible extinction need to be observed. It is also necessary to find out whether corrections for parameters such as the luminosity need to be applied when using this method. The technique cannot be used for objects showing little or no variation because of the resulting uncertainties in the gradients. In such cases 'variations' might also result from observational errors introduced by bad seeing or inaccurate centering.

All of the methods described above assume a reddening law as found in our galaxy with R, the ratio of selective-to-total extinction (= $A_v/E(B-V)$) equal to 3.1. It has however been strongly argued by The and Groot (1983) that this law is not universal. In regions of the Galaxy with star formation (e.g., the η Carina nebula) the value of R seems to be much higher. This is likely to be the result of the interstellar grains having a different size distribution, something that is probably linked to the unusual conditions inside H II regions.

It is therefore possible, one might say likely, that the nature of the extinction near Seyfert nuclei cannot be described by the galactic reddening law. This conclusion is reached by Martin et al (1982) on the basis of spectropolarimetric observations of IC 4329A. The flux variation gradient method offers an opportunity of deriving the reddening law in Seyfert galaxies, as the extinction is measured independently from the fluxes of each pair of filters examined. The fact that the extinctions derived from the Γ_{UB} values seem to be systematically higher than the A_v values derived from the other FVG's might be explained by such an anomalous reddening law. A study of the extinction law using flux variation gradients may be undertaken once the standard unreddened FVG's have been evaluated more accurately. Such an analysis could result in the discovery of intriguing new insights about the nature of Seyfert galaxies and interstellar matter in general.

9. Notes on Individual Objects

Listed below are some additional points of interest about the galaxies studied in this work. The spectral type assigned to each object by the author from the available spectra is added in brackets.

9.1. ESO 12-G21

Variations were recorded for this object. The flux distribution looks normal (the low J-band brightness is probably not real) and and ultraviolet bump can be seen. However Clavel and Joly (1984) found that the ultraviolet spectrum of this galaxy showed no sign of an accretion disk. This, these authors speculated, might be in some way related to the relatively small width of the broad lines. (type 1)

9.2. Ton S180

The spectrum of this galaxy shows Balmer lines that are strong but relatively narrow, as well as prominent Fe II bands. The forbidden lines are weak. The flux gradient through the U, B and V bands is very steep, which makes it difficult to explain it with a 26000 K blackbody. A much hotter blackbody would fit the flux curve better but would also result in an extremely large UV excess. It is possible that the large redshift results in a significant K-correction. Moderate flux variations were detected. (type 1)

9.3. NGC 526a

The nuclear extinction of this Seyfert determined by the various methods discussed before led to discrepant results. A likely reason for this is that the Balmer decrement was calculated from narrow lines only. This suggest that there is very little obscuration of the narrow line region. The large extinction derived using other methods probably arises from dense gas clouds inside the narrow line region. Inside these dense clouds the nucleus is expected to be not unlike a Seyfert 1 nucleus. This hypothesis is supported by the high infrared luminosity, found to be variable by Glass (private communication), and the strong X-ray flux. Because of the faintness of this nucleus and contamination by starlight in the optical, variations are difficult to detect and therefore uncertain. The flux distribution calculated looks similar to the distributions of less reddened objects. (type 1.9)

9.4. Fairall 9

At the time of discovery this object was one of the brightest Seyferts known. Then its luminosity decreased steadily over the next couple of years so that in 1984 its broad line component was almost non-existent. Since then, however, its brightness has been increasing, and the photometric data from this study cover part of the rise. The light curve shows that the rise has not been steady, and there is no clear indication of whether the luminosity of this object will rise to the 1977 level in the near future. The flux distribution looks typical of the distributions analysed in this work. The ultraviolet spectra have however been shown to be flatter when the nucleus is brighter (Masegosa et al, 1986). Clavel et al (1989) have shown that there is a delayed response of the infrared flux to continuum changes in the ultraviolet. They interpret this as evidence of a hot dust component with T ~ 1730 K. (type 1)

9.5. IC 1816

This galaxy has a very faint nucleus, and it was therefore not surprising that no evidence of variability was found. The low infrared luminosity and the non-detection of this galaxy by the X-ray satellites suggests that the non-thermal source is weak. The flux distribution derived in this work is believed to be heavily contaminated by starlight. (type 1.9)

9.6. H 0307-730

The nucleus is moderately obscured, but flux variations have been detected. The flux distribution rises very sharply towards the short wavelength end of the spectrum, indicating that the extinction may have been overestimated. (type 1)

9.7. Fairall 1116

This, the second most distant object in the sample, was not detected by the X-ray and IRAS satellites. This is expected to be a result of its apparent faintness because of its distance. The nucleus has a low extinction, a typical looking flux distribution and considerable variability. (type 1)

9.8. NGC 1566

Alloin et al (1985) showed that between December 1980 and January 1982 the spectrum changed from Seyfert 1.9 to Seyfert 1.2. During these variations the Balmer lines changed proportionally to the continuum, suggesting that the

broad line region is a single compact region smaller than 0.01 pc. The continuum near 3700 A may have risen faster than at 5000 A, which may indicate a second continuum component. Penfold (1979) also found signs of variability. The observations made by the author show virtually no variations. The high central surface brightness derived here is evidence of the bulge component dominating in the part of the galaxy where the measurement was made. The flux distribution shows signs of strong contamination by starlight. The extinction may also be underestimated. (type 1.5)

9.9. MCG -5-13-17

The galaxy's colours appear to be unusually blue. The central surface brightness is rather high. The nucleus is relatively faint but the relative variations of the nuclear flux have been very large. Dust plays an important part in the infrared part of the spectrum. (type 1.5)

9.10. 3A 0557-383

No variations could be detected, probably because of the observed faintness of the nucleus. Fairall et al (1982) report that X-ray observations of this galaxy showed a flare longer than a month. If one corrects for the large amount of obscuration by dust presumed for this object one finds that the nucleus of this galaxy is one of the most luminous in the sample. This conclusion is supported by the infrared observations, which show a strong, presumably non-thermal, component. (type 1)

9.11. Fairall 265

The broad Balmer lines show this galaxy is a type 1 Seyfert. The flux continuum also looks similar to other Seyfert 1s. Despite frequent observations the variability of this object is still not estabilished without doubt. This is not because of starlight contamination effects. The extinction of the nucleus is small. (type 1)

9.12. NGC 2992

Radio investigation of this object (Ward et al, 1980, Ulvestad and Wilson, 1984b) showed that only about 10% of the 6 cm radio flux comes from the nucleus. The rest originates from two radio lobes at a position angle of 160°, which differs by about 26° from the optical axis. Variations have been reported in the infra-red (Glass, private communication), but are difficult to

see in the optical, probably because of the large extinction and the contamination by extra-nuclear starlight, which also affects the flux distribution. (type 1.9)

9.13. MCG -5-23-16

The nuclear extinction of this object is large. Even the narrow line region seems highly obscured, as the hydrogen emission from this region has a large Balmer decrement. This is probably the result of interstellar dust extinction in that galaxy well outside the nucleus, as its inclination is close to 90°. No broad lines are visible, but the X-ray luminosity is large. It is therefore believed that there is a lot of gas inside the narrow line region obscuring the non-thermal source. No clear evidence of variations could be found. (type 2)

9.14. ESO 438-G9

The spectrum investigated by Kollatschny and Fricke (1983), displayed by them in their work, is clearly that of a type 1 Seyfert. The line flux ratio C IV 1550/Ly α in this object is 0.2, much lower than the typical value (Wu et al, 1983). There is a double absorption feature on the blue side of the Hα and Hβ lines, which may be evidence of mass ouflow from the broad line region. The flux distribution and variations of this galaxy are similar to those of the other Seyfert 1's studied here. Its nuclear extinction has been shown to be small. (type 1)

9.15. NGC 3783

Large variations have taken place in this galaxy during the last three years. Variability has been confirmed by other studies. Morris and Ward (1988) find evidence of line flux variations of the order of 30% over a 6 month period and by a factor of 2 over 8 years. Four components have been identified in the Balmer lines (Pelat et al, 1981). At least one of these have been found to be variable (Menzies and Feast, 1983). Stirpe et al (1988) showed that He II 4686 A had shown larger changes than other broad lines. Pelat et al (1981) interpret the redshifted component of the broad lines as possible evidence of an accretion disk with a radius of 1000 Schwarzschild radii and an inclination of 15 degrees. Wamsteker and Barr (1985) find evidence of matter outflow with a velocity of about 3100 km s^{-1}. Barr et al (1983) showed that the slope of the ultraviolet continuum is correlated to the UV luminosity. From the variability of the UV continuum they place an upper limit of 7 10^{15} cm on the

diameter of emitting region. This object is the best candidate in the sample for periodic variations. The Fourier analysis showed a strong likelyhood of a 610 day period. (type 1)

9.16. H 1143-182

The Fe II emission bands of this object are unusually weak. It exhibits a flux continuum and variations typical of objects with similar luminosity and low extinction. (type 1.5)

9.17. MCG -2-33-34

The flux distribution of this galaxy exhibits a "typical" Seyfert shape. At much shorter wavelengths it was found to have either a very steep X-ray spectrum with a photon index of 2.2 or a soft X-ray excess (Ward et al, 1988). Variations were detected in this galaxy. (type 1.5)

9.18. ESO 323-G77

The nuclear brightness given by Fairall (1986) appears to be overestimated. The aperture used for the measurement is quoted in that paper to be 10" in diameter. However the magnitude given agrees much better with a 30" aperture. The infrared brightness is exceptionally high. In contrast, the X-ray luminosity must be very low because the object has not been detected by any of the X-ray satellites. The variations in the nuclear flux have been difficult to detect, and they must therefore be of a small amplitude as, despite its relatively high obscuration, the nucleus is luminous at optical wavelengths. (type 1)

9.19. MCG -6-30-15

The high surface brightness indicates that the morphological type of this galaxy must be E or S0. This classification agrees with the low intensity of the galactic flux found. Seyfert nuclei are not normally suspected in such galaxies. Light variations in this galaxy are difficult to verify. A star close to the nucleus may cause spurious variations if the radius of the aperture chosen was close to the separation of the star and galaxy. (type 1)

9.20. IC 4329A

When Disney (1973) discovered the Seyfert nature of this object, he claimed that it was the nearest quasar. This conclusion was based on the extremely

high $H\alpha/H\beta$ ratio, which is indicative of a very high extinction of the nucleus. An unusually high extinction could be expected on the grounds that the galaxy's inclination is exactly 90°, and the nucleus is hidden by a dust lane. Infrared observations by Glass et al (1982), however, indicate that the infrared colours were typical of a Seyfert nucleus with an extinction of A_V = 1, which results in a nuclear luminosity comparable with typical Seyferts. This work suggests that the true extinction lies somewhere between these estimates. It has been suggested that the extinction law in this galaxy is anomalous (Martin et al, 1982). Variations are present and the flux distribution looks normal. The shape of the Balmer line profiles varied as well. (type 1)

9.21. IRAS 1509-211

The flux distribution of this galaxy looks normal. Despite, the object's faintness, variations are believed to have been observed. (type 1.5)

9.22. ESO 103-G35

There is no evidence for variability. This may be because there are only little data available. However the nucleus, which is very faint in relation to the rest of the galaxy, is highly obscured. The galaxy is a strong X-ray source, which may be indicative of a broad line region hidden behind a lot of gas. The narrow Balmer lines display a large decrement, indicating that the narrow line region is also obscured. Much of this obscuration could be due to interstellar dust, as the galaxy is highly inclined. (type 1.9)

9.23. Fairall 51

This is the only galaxy in the sample for which the polarisation is too high to be easily explained by interstellar scattering due to dust. It was therefore suspected to have intrinsic polarisation. This was confirmed by spectropolarimetry (Brindle et al, 1990b). Its variations and its flux distribution have been typical of the galaxies studies here. (type 1.5)

9.24. ESO 141-G55

This luminous Seyfert 1 galaxy has little or no nuclear obscuration. The luminosities recorded during the period of investigation have varied appreciably, but have on the whole been a bit lower than in the past (e.g., Hamuy and Maza, 1987). (type 1)

9.25. NGC 6814

Variation have been observed in this galaxy by numerous observers. Morris and Ward (1988) found that, while their [O III] fluxes agree well with those of Yee (1980) the Hβ flux was 4 times stronger. Ulvestad and Wilson (1984) find the radio source to be slightly elongated. The unusually steep nuclear flux gradient between the U and B bands is the result of a single point and therefore probably an artifact. The nucleus is faint and has moderately high extinction. Variations were detected. (type 1.5)

9.26. NGC 6860

Although no new spectroscopic observations of this object were made, the spectra displayed by Maia et al (1986) show that its Seyfert 1 classification is beyond doubt. Other characteristics of this galaxy, including the flux distribution, were also typical of the Seyfert 1s studied here. Although its nucleus is moderately obscured and starlight contamination appreciable, definite flux variations were detected. (type 1)

9.27. H 2106-099

Remillard et al (1986) suggest that this may be a variable X-ray source. Optical variations were detected in this work. The flux distribution looks typical of type 1 Seyferts. (type 1)

9.28. NGC 7213

This object exhibits a combination of characteristics of a Seyfert 1, a LINER and a radio galaxy. The flux distribution shows Seyfert-like characteristics. There is only very little evidence of variability. It has much broader narrow lines than any other galaxy in the sample. The electron density in the narrow line region is much higher than in the other object investigated in this work. The central surface magnitude of this galaxy is the largest found in the sample. This supports the proposed S0 classification of this galaxy by Phillips (1979). (LINER or type 1)

9.29. MCG -2-58-22

This galaxy has witnessed the most dramatic changes in brightness of the sample during the period of observation. These have also been noted spectroscopically. The radio maps of Ulvestad and Wilson (1984a) show a small radio lobe extending about 1" from the nucleus. The luminosity of both the nucleus and the host galaxy were amongst the highest measured. (type 1.5)

10. Conclusions

Flux distributions were derived for all Seyferts in the sample. These generally looked nearly identical to each other. They are in many cases believed to be more accurate representations of the flux distributions than had been achieved by earlier investigators. On the whole, flux components identified in Seyfert galaxies in previous studies were found in this work as well. These included the X-ray to infrared power law with a low frequency cut-off, the ultraviolet bump and infrared dust components. It is proposed that the intrinsic flux distributions of Seyfert nuclei resemble each other more closely than is normally supposed.

The optical flux distribution has been shown to be dominated by the ultraviolet bump. It is argued that this feature can be reproduced by a superposition of hot blackbody components, as one would expect to find in an accretion disk. The slightly convex looking near-infrared spectrum does not match the distribution with the 5 μm bump proposed by Edelson and Malkan (1986) very well. An excess, most likely of thermal origin, is found at a slightly shorter wavelength instead.

The parameter $\Delta L/L$ was used to describe the relative amplitude of the flux variations. This quantity was not found to be related to any other property of the Seyfert Galaxy. It therefore does not help to explain the origin of Seyfert properties such as the strength of the iron emission line bands. It is postulated that the nature of the variations is similar for Seyfert nuclei of all luminosities. Possible relationships have been suggested between the nuclear luminosity and the luminosity of the disk of the galaxy, the central surface magnitude and the ratio of the broad lines relative to the narrow lines.

After this investigation it must be concluded that the evidence for periodic flux variations in Seyfert nuclei is weak. Periods proposed by earlier workers (e.g., Bisch et al, 1987) have not been seen. The most likely candidate for regular variations from the sample of Seyfert galaxies studied here is NGC 3783, which may have a 610 day period.

A fairly accurate knowledge of the nuclear extinction is needed for any study of Seyfert luminosities. A new method for estimating this quantity has been proposed and this has been compared to existing methods. It is expected that this method can be used to narrow down the present uncertainty in the amount

of obscuration of Seyfert nuclei.

The results of this thesis encourage follow-up work in a number of areas.

The determination of flux variation gradients should be carried out for as many objects as possible, not only in the optical but also at ultraviolet and infrared wavelengths. Such a study would enable one to derive the shape of the flux distribution of Seyfert nuclei more accurately than has been possible to date. An investigation of well-defined flux distributions would go a long way towards answering some important questions raised by this thesis.

- Is the shape of the continuum identical in all Seyfert galaxies?
- If there are differences in the continuum shapes, are these in any way systematic (e.g., is the ultraviolet bump stronger in more luminous nuclei)?
- What does the flux distribution of Seyfert nuclei tell us about the reddening law in these galaxies and what does this imply about the environment of these nuclei?

The flux variation gradients have also been shown to be powerful tools for estimating the nuclear obscuration. The finer details of this method of measuring the extinction can still be improved. The extinction values calculated in this work were derived by comparing the gradients with standard unreddened flux variation gradients derived empirically from three objects only, all of which were fairly luminous. The standard gradients should be derived from a much larger sample of Seyfert nuclei with negligible reddening. Such a study might show that the standard gradients are dependent on properties such as the luminosity. As mentioned above, the reddening law may have to be modified as well.

A more thorough investigation of the morphological properties of Seyfert galaxies is needed in order to check whether brighter nuclei are really associated with brighter galaxies, and this examination should be extended to nearby quasars.

More photometric observations are required in order to check whether the possible periods that have been suggested for some objects still fit the data. It is however recommended that such studies are restricted to a few well studied Seyfert nuclei. The observational effort spent on such an investigation can be enormous and no period has been identified in Seyfert galaxies to date whose existence has been universally accepted. Nuclei that vary regularly over many cycles, like NGC 4151, can suddenly change their behaviour. This branch of research could however yield some important results

if periods of similar magnitude were to be discovered in many objects. For example, are the 130 day oscillations witnessed for a long time in NGC 4151 also present in other galaxies?

Finally, as this thesis was being completed, the author became aware of the claims made by a group of Soviet astronomers who believe to have discovered 160 minute variability in a large number of Seyfert galaxies (Kotov and Lyutyi, 1989). In the present form the photometric data described in this thesis cannot be used to find such short periods; observations spaced up to four days apart were usually combined and the exact times of the measurements were not recorded (although these can be extracted from the raw data).

The claim made by Lyutyi and collaborators has highly important consequences, not only for our understanding of AGN's, but also for cosmology (Kotov and Lyutyi, 1989). In order to test this claim it is desirable to analyse Seyfert light curves obtained at sites outside the Soviet Union, ideally using an independent reduction procedure, as this would rule out instrumental and methodological causes for the 160 min period.

The analysis of the data in this thesis is therefore not complete and maybe it never will be. Some of the follow-up work will be undertaken by the author, and the results will later be published in scientific journals. It is however also hoped that the observations and results presented in this thesis will still be used by other astronomers, of this and future generations, and that these will still lead to discoveries undreamed of when this thesis was conceived.

Appendix: Photometry and Spectroscopy by other Observers

In this appendix results are given from other studies of the galaxies investigated here. Table A1 is a list of UBVRI measurements that have been extracted from the literature. Table A2 lists UBVRI observations made at SAAO by D. Kilkenny that have not been published previously. Table A3 gives the results of JHKL photometry obtained by Ian Glass. Ultraviolet spectroscopic data are given in table A4. Line intensity ratios derived from other spectroscopic studies are listed in table A5.

Table A1. Photometric data of the program objects published in the literature. ϕ is the diameter (in arcseconds) of the aperture used. The code letter for the reference is in the second column.

HJD 244+	Rf	log ϕ "	V	σ_V	B-V	σ_{BV}	U-B	σ_{UB}	V-R	σ_{VR}	V-I	σ_{VI}
ESO 12-G21												
	a	1.26	14.73		0.57		-.25					
Ton S180												
4146	b	1.19	14.41	04	0.19	04	-.94	05				
6350	c	1.23	14.43	02	0.21	02	-.95	03	0.23	02	0.25	02
6350	c	1.38	14.43	02	0.20	02	-.94	03	0.28	02	0.25	02
6434	c	1.23	14.38	02	0.17	02	-.97	03	0.22	02	0.28	:
6434	c	1.38	14.36	02	0.17	02	-.95	03	0.21	02	0.23	:
6435	c	1.23	14.36	02	0.19	02	-.98	03	0.19	02	0.19	:
6435	c	1.38	14.35	02	0.23	02	-.99	03	0.26	02	0.37	:
6436	c	1.23	14.39	02	0.19	02	-.97	03	0.22	02	0.27	:
6436	c	1.38	14.39	02	0.16	02	-.94	03	0.22	02	0.09	:
NGC 526a												
4146	b	1.19	14.60	04	0.97	04	0.09	05				
6315	c	1.23	14.54	02	1.04	02	0.17	03	0.52	02	1.12	02
6319	c	1.23	14.56	02	1.00	02	0.19	03	0.55	02	1.16	02
Fairall 9												
3049	d	1.15	13.43	03	0.27	02	-.88	02				
3078	d	1.15	13.39	03	0.28	02	-.90	02				
3102	d	1.15	13.35	01	0.25	01	-.94	01				
3103	d	1.15	13.36	01	0.25	01	-.94	01				
3104	d	1.15	13.35	01	0.25	01	-.93	01				
3108	d	1.15	13.34	01	0.25	01	-.92	01				
3134	d	1.15	13.30	03	0.25	02	-.89	02				
3135	d	1.15	13.30	03	0.26	02	-.92	02				
3136	d	1.15	13.31	03	0.26	02	-.93	02				
3368	d	1.15	13.26	01	0.23	01	-.94	01				
3433	e	1.34	13.23	01	0.20	01	-.95	01				
3454	f	1.30	13.34	05	0.21	02	-.90	02				
3455	f	1.30	13.33	05	0.24	02	-.92	02				
3456	f	1.30	13.35	01	0.23	02	-.92	02				
3457	f	1.30	13.23	01	0.25	02	-.90	02				
3458	f	1.30	13.33	01	0.25	02	-.90	02				
3459	f	1.30	13.31	01	0.24	02	-.94	02				
3460	f	1.30	13.35	01	0.24	02	-.93	02				
3460	d	1.15	13.26	01	0.33	01	-.90	01				
3462	f	1.30	13.36	01	0.23	02	-.92	02				
3462	d	1.15	13.30	01	0.30	01	-.92	01				
3463	f	1.30	13.35	01	0.24	02	-.92	02				
3464	f	1.30	13.34	01	0.24	02	-.92	02				
3465	f	1.30	13.37	01	0.25	02	-.93	02				
3472	f	1.30	13.42	01	0.25	02	-.90	02				
3483	d	1.15	13.43	01	0.32	01	-.92	01				

Table A1. (continued)

HJD 244+	Rf	log ϕ "	V	σ_V	B-V	σ_{BV}	U-B	σ_{UB}	V-R	σ_{VR}	V-I	σ_{VI}
Fairall 9 (continued)												
3515	f	1.30	13.42	01	0.26	02	-.88	02				
3730	g	1.19	13.10	01	0.19	01	-.87	02				
3731	g	0.98	13.15	01	0.16	01	-1.01	02				
3731	g	1.19	13.10	01	0.19	01	-.99	02				
3731	g	1.37	13.03	01	0.22	01	-.97	02				
3731	g	1.52	12.98	01	0.25	01	-.95	02				
4171	h	1.16	13.51		0.26		-.94					
4171	h	1.49	13.29		0.33		-.90					
4172	h	1.16	13.45		0.25		-.98					
4172	h	1.49	13.33		0.32		-.93					
4174	h	1.16	13.51		0.26		-.94					
4175	h	1.16	13.49		0.24		-.94					
4175	h	1.49	13.28		0.35		-.89					
4176	h	1.16	13.44		0.25		-.93					
4176	h	1.49	13.28		0.32		-.90					
4466	i	1.20	13.43	01	0.27	01	-1.01	02				
4901	j	1.04	13.54	03	0.28	03	-1.02	04				
5619	h	1.20	14.23		0.64		-.72					
5619	h	1.04	14.39		0.65		-.70					
5620	h	1.20	14.26		0.61				0.51		0.91	
5620	h	1.04	14.42		0.55				0.49		0.87	
5649	h	1.20	14.29		0.65						0.91	
6252	c	1.23	14.11	02	0.54	02	-.81	03	0.47	02	0.93	02
6252	c	1.38	13.99	02	0.62	02	-.75	03	0.47	02	0.85	02
6298	c	1.23	14.02	02	0.51	02	-.82	03	0.43	02	0.85	02
6298	c	1.38	13.88	02	0.56	02	-.76	03	0.42	02	0.87	02
6299	c	1.23	13.99	02	0.52	02	-.83	03	0.41	02	0.82	02
6299	c	1.38	13.92	02	0.50	02	-.78	03	0.45	02	0.87	02
6313	h	1.20	14.13		0.41		-.64				0.80	
6315	c	1.23	14.00	02	0.47	02	-.87	03	0.45	02	0.83	02
6315	c	1.38	13.87	02	0.52	02	-.82	03	0.44	02	0.87	02
6316	c	1.23	13.99	02	0.50	02	-.88	03	0.42	02	0.88	:
6316	c	1.38	13.87	02	0.55	02	-.87	03	0.44	02	0.86	02
6319	c	1.23	13.99	02	0.50	02	-.90	03	0.44	02	0.84	02
6319	c	1.38	13.88	02	0.51	02	-.84	03	0.43	02	0.87	02
6437	c	1.23	14.15	02	0.55	02	-.85	03	0.50	02	0.90	:
6437	c	1.38	14.01	02	0.61	02	-.78	03	0.51	02	0.90	:
6443	c	1.23	14.12	02	0.60	02	-.89	03	0.45	02	0.88	:
6443	c	1.38	14.02	02	0.60	02	-.74	03	0.50	02	0.94	:
6444	c	1.23	14.10	02	0.57	02	-.85	03	0.46	02	0.88	:
6444	c	1.38	14.01	02	0.60	02	-.79	03	0.49	02	0.95	:
H 0307-730												
	k	1.30	14.90	04	0.58	05	-.28	05				

Table A1. (continued)

HJD 244+	Rf	log ϕ "	V	σ_V	B-V	σ_{BV}	U-B	σ_{UB}	V-R	σ_{VR}	V-I	σ_{VI}
Fairall 1116												
6299	c	1.23	14.67		0.43		-.80		0.39		0.84	
6299	c	1.38	14.58		0.46		-.75		0.39		0.93	
6316	c	1.23	14.70		0.45		-.84		0.38		0.47	
6316	c	1.38	14.60		0.46		-.78		0.37		0.81	
NGC 1566												
1695	l	1.23	12.51		0.90		0.21					
2310	m	1.49	11.84	04	0.95	05	0.31	05				
2334	m	1.16	12.58	04	0.92	05	0.27	06				
2334	m	1.49	11.80	06	0.93	07	0.34	08				
2394	m	1.16	12.61	02	0.92	02	0.29	04				
2394	m	1.49	11.76	02	0.91	02	0.36	02				
2422	m	1.16	12.59	02	0.93	03	0.26	03				
2422	m	1.49	11.80	01	0.94	01	0.29	05				
2451	m	1.16	12.60	01	0.93	01	0.24	03				
2451	m	1.49	11.81	01	0.92	01	0.34	02				
2457	m	1.16	12.63	03	0.93	04	0.19	05				
2457	m	1.49	11.82	04	0.91	05	0.35	05				
2484	m	1.16	12.61	02	0.93	02	0.24	04				
2484	m	1.49	11.83	03	0.91	03	0.34	04				
2727	m	1.16	12.71	04	0.87	05	0.28	06				
2748	m	1.16	12.63	02	0.93	03	0.25	03				
2748	n	1.49	11.83	05	0.95	05	0.28	07				
2756	n	1.19	12.68	05	0.95	05	0.37	07				
2756	n	1.53	11.79	05	0.90	05	0.31	07				
2779	m	1.16	12.61	01	0.92	02	0.29	01				
2807	m	1.16	12.60	01	0.93	01	0.27	02				
3049	m	1.16	12.60	02	0.93	02	0.29	04				
4280	i	1.18	12.64	01	0.88	01	0.09	02				
4281	i	1.48	11.89	01	0.89	01	0.21	02				
4282	i	1.48	11.89	01	0.90	01	0.18	02				
4283	i	1.48	11.91	01	0.92	01	0.20	02				
4284	b	1.19	12.58	04	0.87	04	0.08	05				
4286	b	1.19	12.59	04	0.92	04	0.08	05				
4289	i	1.19	12.56	01	0.88	01	0.05	02				
4316	i	0.90	13.42	01	0.85	01	-.04	02				
4316	i	1.18	12.70	01	0.89	01	0.10	02				
6115	c	1.23	12.57	:	0.96	02	0.35	03	0.61	02	1.20	:
6115	c	1.53	11.79	:	0.95	02	0.31	03	0.58	02	1.22	02
6117	c	1.23	12.55	:	0.95	02	0.37	03	0.61	02	1.28	02
6117	c	1.53	11.78	:	0.92	02	0.37	03	0.59	02	1.23	02
6315	c	1.23	12.56	02	0.95	02	0.33	03	0.60	02	1.23	02
6315	c	1.38	12.18	02	0.94	02	0.35	03	0.63	02	1.23	02
6315	c	1.53	11.78	02	1.04	02	0.46	03	0.58	02	1.19	02
6348	c	1.23	12.55	02	0.92	02	0.32	03	0.61	02	1.24	02
6348	c	1.38	12.21	02	0.92	02	0.33	03	0.60	02	1.22	02
6348	c	1.53	11.79	02	0.90	02	0.35	03	0.60	02	1.22	02

Table A1. (continued)

HJD 244+	Rf	log ϕ "	V	σ_V	B-V	σ_{BV}	U-B	σ_{UB}	V-R	σ_{VR}	V-I	σ_{VI}
NGC 2992												
4283	o	1.19	13.78	04	1.06	03	0.40	04				
6116	c	1.23	13.63	:	1.11	02	0.34	03	0.71	02	1.46	02
6116	c	1.38	13.19	:	1.08	02	0.31	03	0.67	02	1.41	02
6117	c	1.23	13.62	:	1.12	02	0.30	03	0.69	02	1.44	02
6117	c	1.38	13.23	:	1.07	02	0.30	03	0.67	02	1.37	02
6121	c	1.23	13.64	:	1.12	02	0.47	:	0.70	02	1.44	02
6121	c	1.38	13.25	:	1.10	02	0.31	03	0.67	02	1.37	02
6145	c	1.23	13.64	02	1.12	02	0.34	03	0.73	02	1.44	02
6145	c	1.38	13.24	02	1.10	02	0.26	03	0.66	02	1.41	02
6180	c	1.23	13.58	02	1.12	02	0.05	:	0.71	02	1.44	02
6180	c	1.23	13.60	02	1.08	02	0.38	03	0.74	02	1.46	02
6180	c	1.38	13.22	02	1.09	02	0.31	03	0.68	02	1.42	02
6439	c	1.23	13.67	02	1.15	02	0.28	03	0.71	02	1.43	:
6439	c	1.38	13.29	02	1.05	02	0.27	03	0.69	02	1.39	:
6444	c	1.23	13.68	02	1.11	02	0.35	03	0.73	02	1.46	:
6444	c	1.38	13.25	02	1.04	02	0.28	03	0.68	02	1.50	:
6444	c	1.38	13.22	02	1.03	02	0.32	03	0.65	02	1.37	:
MCG -5-23-16												
4284	b	1.19	13.69	04	1.05	04	0.45	05				
6116	c	1.38	13.45	:	1.04	02	0.49	03	0.63	02	1.34	02
6118	c	1.23	13.65	:	1.02	02	0.44	03	0.66	02	1.34	02
6118	c	1.38	13.44	:	1.03	02	0.52	03	0.62	02	1.34	02
6121	c	1.23	13.67	:	1.02	02	0.44	03	0.67	02	1.35	02
6121	c	1.38	13.41	:	1.04	02	0.49	03	0.64	02	1.31	02
6144	c	1.23	13.64	02	1.03	02	0.48	03	0.64	02	1.31	02
6144	c	1.38	13.42	02	1.03	02	0.49	03	0.61	02	1.30	02
6180	c	1.23	13.63	02	1.09	02	0.41	03	0.62	02	1.30	02
6180	c	1.38	13.44	02	1.02	02	0.46	03	0.62	02	1.30	02
6180	c	1.38	13.41	02	1.03	02	0.50	03	0.63	02	1.32	02
6434	c	1.23	13.68	02	0.99	02	0.48	03	0.64	02	1.31	02
6434	c	1.38	13.50	02	1.04	02	0.42	03	0.61	02	1.30	:
6435	c	1.23	13.69	02	1.04	02	0.50	03	0.59	02	1.26	:
6435	c	1.38	13.50	02	1.05	02	0.44	03	0.65	02	1.32	:
6436	c	1.38	13.50	02	1.01	02	0.46	03	0.67	02	1.35	:
6437	c	1.38	13.49	02	1.03	02	0.51	03	0.65	02	1.35	:
6440	c	1.23	13.67	02	1.05	02	0.46	03	0.61	02	1.30	:
6441	c	1.38	13.44	02	1.03	02	0.43	03	0.65	02	1.47	:

Table A1. (continued)

HJD 244+	Rf	log ϕ "	V	σ_V	B-V	σ_{BV}	U-B	σ_{UB}	V-R	σ_{VR}	V-I	σ_{VI}
NGC 3783												
1695	1	1.08	13.49		0.56		-.70					
2190	m	1.16	13.32	03	0.60	01	-.69	02				
2190	m	1.49	12.68	02	0.71	02	-.42	03				
2218	m	1.16	13.27	01	0.55	02	-.65	03				
2218	m	1.49	12.67	03	0.69	03	-.44	04				
2422	m	1.16	13.31	03	0.62	03	-.67	04				
2422	m	1.49	12.73	02	0.73	03	-.40	05				
2430	m	1.16	13.41	03	0.52	02	-.58	03				
2430	m	1.49	12.75	03	0.68	03	-.37	08				
2450	m	1.16	13.40	02	0.65	02	-.60	04				
2450	m	1.49	12.76	02	0.75	03	-.32	03				
2458	m	1.16	13.33	01	0.59	02	-.63	02				
2458	m	1.49	12.68	01	0.73	01	-.44	08				
2485	m	1.16	13.37	03	0.64	03	-.58	04				
2485	m	1.49	12.76	01	0.75	02	-.32	03				
2517	m	1.16	13.23	03	0.55	03	-.70	04				
2517	m	1.49	12.66	02	0.68	03	-.45	05				
2520	m	1.16	13.25	03	0.55	02	-.68	03				
2520	m	1.49	12.65	01	0.68	01	-.44	01				
2543	m	1.16	13.44	03	0.67	02	-.60	03				
2565	m	1.16	13.26	01	0.64	01	-.67	02				
2565	m	1.49	12.70	03	0.73	02	-.40	02				
2569	m	1.16	13.31	02	0.64	03	-.64	04				
2569	m	1.49	12.71	02	0.74	03	-.38	05				
2599	m	1.16	13.29	03	0.59	02	-.59	03				
2606	m	1.16	13.26	01	0.60	03	-.69	04				
2606	m	1.49	12.70	01	0.70	01	-.43	01				
2621	m	1.16	13.46	03	0.43	02	-.52	03				
2621	m	1.49	12.67	03	0.75	03	-.51	08				
2780	m	1.16	13.19	01	0.54	01	-.69	01				
2808	m	1.16	13.12	02	0.50	02	-.74	01				
2890	m	1.16	13.25	01	0.60	01	-.66	02				
2893	m	1.16	13.27	01	0.57	01	-.65	01				
2919	m	1.16	13.22	04	0.55	04	-.72	03				
2921	m	1.16	13.18	03	0.53	02	-.73	03				
2958	m	1.16	13.24	02	0.58	02	-.68	02				
2981	m	1.16	13.25	02	0.60	02	-.63	04				
2987	m	1.16	13.31	01	0.66	01	-.58	04				
2989	m	1.16	13.34	01	0.67	01	-.53	01				
4283	b	1.19	13.43	04	0.61	04	-.58	05				
4285	b	1.19	13.45	04	0.63	04	-.56	05				
4289	i	1.19			0.69	01	-.63	02				
4290	i	1.37	13.04	01	0.73	01	-.50	02				
5057	b	1.19	13.16	04	0.41	04	-.73	05				
6115	c	1.23	13.12	:	0.61	02	-.75	03	0.56	02	1.03	02
6115	c	1.38	12.92	:	0.67	02	-.65	03	0.58	02	1.10	02
6116	c	1.23	13.03	:	0.62	02	-.72	03	0.59	02		
6116	c	1.38	12.88	:	0.67	02	-.60	03	0.58	02	1.11	02

Table A1. (continued)

HJD 244+	Rf	log ϕ "	V	σ_V	B-V	σ_{BV}	U-B	σ_{UB}	V-R	σ_{VR}	V-I	σ_{VI}
NGC 3783 (continued)												
6118	c	1.23	13.11	:	0.62	02	-.73	03	0.57	02	1.05	02
6118	c	1.38	12.86	:	0.70	02	-.62	03	0.57	02	1.07	02
6143	c	1.23	13.10	02	0.62	02	-.77	03	0.55	02	1.04	02
6143	c	1.38	12.89	02	0.66	02	-.68	03	0.58	02	1.07	02
6145	c	1.23	13.10	02	0.56	02	-.77	03	0.57	02	1.05	02
6145	c	1.38	12.87	02	0.64	02	-.66	03	0.59	02	1.13	02
6180	c	1.23	13.11	02	0.60	02	-.78	03	0.61	02	1.09	02
6180	c	1.38	12.89	02	0.62	02	-.69	03	0.57	02	1.12	02
6202	c	1.23	13.20	02	0.62	02	-.73	03	0.59	02	1.09	02
6204	c	1.23	13.17	02	0.64	02	-.77	03	0.57	02	1.05	02
6252	c	1.23	13.14	02	0.52	02	-.80	03	0.61	02	1.06	02
6252	c	1.38	12.85	02	0.59	02	-.65	03	0.57	02	1.05	02
6437	c	1.23	13.08	02	0.49	02	-.81	03	0.63	02	1.07	:
6437	c	1.38	12.84	02	0.58	02	-.71	03	0.59	02	1.09	:
6439	c	1.23	13.05	02	0.49	02	-.82	03	0.60	02	1.03	:
6439	c	1.38	12.88	02	0.55	02	-.74	03	0.61	02	1.09	:
6440	c	1.23	13.09	02	0.50	02	-.89	03	0.60	02	1.05	:
6444	c	1.23	13.09	02	0.50	02	-.90	03	0.62	02	1.07	:
6444	c	1.38	12.84	02	0.57	02	-.77	03	0.61	02	1.12	:
H 1143-182												
6181	c	1.23	14.56		0.62		-.96		0.32		0.65	
6444	c	1.23	14.67	01	0.73	01	-.98	02	0.33	01	0.63	:
	k	1.18	14.58	04	0.45	05	-.56	05				
MCG -6-30-15												
4285	b	1.19	13.58	04	0.95	04	0.34	05				
4292	b	1.19	13.65	04	0.97	04	0.35	05				
6145	c	1.23	13.47	02	0.95	02	0.30	03	0.63	02	1.25	02
6145	c	1.38	13.29	02	0.95	02	0.31	03	0.60	02	1.23	02
6180	c	1.23	13.46	02	0.96	02	0.36	03	0.64	02	1.24	02
6180	c	1.38	13.29	02	0.94	02	0.32	03	0.65	02	1.24	02

Table A1. (continued)

HJD 244+	Rf	log ϕ "	V	σ_V	B-V	σ_{BV}	U-B	σ_{UB}	V-R	σ_{VR}	V-I	σ_{VI}
IC 4329A												
1121	p	1.00	14.44		0.96		0.51					
1121	p	1.57	13.33		0.97		0.25					
2191	m	1.16	13.66	02	1.10	01	0.34	02				
2191	m	1.49	13.29	03	1.07	01	0.43	02				
2218	m	1.16	13.64	05	1.12	04	0.32	04				
2218	m	1.49	13.23	03	1.11	02	0.47	04				
2250	m	1.16	13.71	01	1.15	04	0.37	01				
2250	m	1.49	13.33	01	1.09	01	0.35	04				
2451	m	1.16	13.72	01	1.14	02	0.33	05				
2451	m	1.49	13.38	04	1.12	03	0.27	01				
2457	m	1.16	13.65	05	1.16	04	0.37	04				
2457	m	1.49	13.29	03	1.12	02	0.41	04				
2485	m	1.16	13.65	01	1.12	03	0.33	01				
2485	m	1.49	13.29	04	1.09	03	0.39	04				
2516	m	1.16	13.61	03	1.12	03	0.39	05				
2516	m	1.49	13.26	04	1.11	03	0.37	04				
2519	m	1.16	13.64	02	1.09	01	0.34	04				
2519	m	1.49	13.27	01	1.07	01	0.37	01				
2544	m	1.16	13.64	05	1.12	01	0.35	04				
2544	m	1.49	13.32	01	1.10	02	0.37	04				
2569	m	1.16	13.67	03	1.13	01	0.32	01				
2569	m	1.49	13.32	01	1.10	02	0.38	02				
2606	m	1.16	13.69	02	1.14	02	0.34	03				
2606	m	1.49	13.33	01	1.10	01	0.33	04				
2808	m	1.16	13.93	02	1.13	01	0.42	03				
2892	m	1.16	13.93	04	1.15	02	0.45	08				
2960	m	1.16	13.89	04	1.18	05	0.39	02				
2982	m	1.16	13.86	01	1.15	02	0.42	02				
4292	b	1.19	13.74	04	1.10	04	0.31	05				
4675	b	1.19	13.75	04	1.09	04	0.30	05				
4676	b	1.19	13.76	04	1.10	04	0.29	05				
6115	c	1.23	13.66	:	1.15	02	0.28	03	0.85	02	1.51	02
6115	c	1.38	13.47	:	1.14	02	0.34	03	0.82	02	1.51	02
6118	c	1.23	13.65	:	1.13	02	0.37	03	0.86	02	1.53	02
6118	c	1.38	13.45	:	1.14	02	0.29	03	0.81	02	1.53	02
6119	c	1.23	13.64	:	1.14	02	0.32	03	0.81	02	1.50	02
6119	c	1.38	13.47	:	1.12	02	0.36	03	0.82	02	1.48	02
6120	c	1.23	13.60	:	1.15	02	0.35	03	0.81	02	1.50	02
6120	c	1.38	13.46	:	1.10	02	0.29	03	0.81	02	1.51	02
6121	c	1.23	13.63	:	1.14	02	0.31	03	0.83	02	1.51	02
6121	c	1.38	13.46	:	1.10	02	0.32	03	0.82	02	1.48	02
6143	c	1.23	13.61	02	1.09	02	0.34	03	0.87	02	1.53	02
6143	c	1.38	13.43	02	1.10	02	0.33	03	0.83	02	1.51	02
6145	c	1.23	13.62	02	1.15	02	0.35	03	0.83	02	1.50	02
6145	c	1.38	13.44	02	1.13	02	0.34	03	0.82	02	1.48	02
6180	c	1.23	13.62	02	1.17	02	0.31	03	0.85	02	1.53	02
6180	c	1.38	13.46	02	1.13	02	0.42	03	0.84	02	1.53	02
6180	c	1.38	13.46	02	1.12	02	0.37	03	0.84	02	1.51	02
6204	c	1.23	13.62	02	1.12	02	0.29	03	0.82	02	1.49	02
6252	c	1.23	13.63	02	1.17	02	0.44	03	0.86	02	1.53	02
6252	c	1.38	13.48	02	1.15	02	0.47	03	0.87	02	1.53	02

Table A1. (continued)

HJD 244+	Rf	log ϕ "	V	σ_V	B-V	σ_{BV}	U-B	σ_{UB}	V-R	σ_{VR}	V-I	σ_{VI}
ESO 103-G35												
4872	b	1.19	14.53	04	0.98	04	0.44	05				
6181	c	1.23	14.42	02	1.08	02	0.43	03	0.59	02	1.24	02
6181	c	1.38	14.22	02	1.03	02	0.43	03	0.60	02	1.35	02
6315	c	1.23	14.46	02	1.05	02	0.36	03	0.63	02	1.32	02
6315	c	1.38	14.22	02	1.03	02	0.39	03	0.62	02	1.22	02
6318	c	1.23	14.45	02	1.06	02	0.40	03	0.62	02	1.24	02
6318	c	1.38	14.22	02	1.02	02	0.35	03	0.61	02	1.26	02
Fairall 51												
3032	d	1.02	14.39	03	0.75	03	-.24	03				
3368	d	1.02	14.46	01	0.71	01	-.27	01				
6115	c	1.23	14.20	:	0.78	02	-.17	03	0.64	02	1.19	02
6115	c	1.38	14.02	:	0.79	02	-.13	03	0.67	02	1.23	02
6180	c	1.23	14.24	02	0.84	02	-.19	03	0.64	02	1.20	02
6180	c	1.38	14.05	02	0.82	02	-.10	03	0.64	02	1.27	02
6201	c	1.23	14.31	02	0.83	02	-.11	03	0.64	02	1.22	02
6252	c	1.23	14.33	02	0.80	02	-.16	03	0.63	02	1.21	02
6252	c	1.38	14.10	02	0.85	02	-.05	03	0.65	02	1.22	02
6300	c	1.23	14.16	02	0.78	02	-.22	03	0.67	02	0.57	02
6300	c	1.38	13.97	02	0.79	02	-.15	03	0.67	02	1.26	02
6315	c	1.23	14.16	02	0.77	02	-.25	03	0.66	02	1.19	02
6315	c	1.38	13.99	02	0.74	02	-.16	03	0.69	02	1.26	02
6316	c	1.23	14.18	02	0.75	02	-.22	03	0.68	02	1.22	02
6316	c	1.38	13.97	02	0.77	02	-.13	03	0.66	02	1.22	02
6319	c	1.23	14.18	02	0.76	02	-.23	03	0.67	02	1.24	02
6319	c	1.38	13.96	02	0.79	02	-.18	03	0.65	02	1.25	02

Table A1. (continued)

HJD 244+	Rf	log ϕ "	V	σ_V	B-V	σ_{BV}	U-B	σ_{UB}	V-R	σ_{VR}	V-I	σ_{VI}
ESO 141-G55												
4433	j	1.04	13.70	03	0.26	03	-.99	04				
4872	b	1.19	13.67	04	0.17	04	-.94	05				
4873	b	1.19	13.70	04	0.21	04	-.93	05				
4896	j	1.04	13.65	03	0.30	03		04				
6116	c	1.23	13.77	:	0.28	02	-1.02	03	0.39	02	0.75	02
6116	c	1.38	13.64	:	0.35	02	-.97	03	0.41	02	0.79	02
6180	c	1.23	13.69	02	0.25	02	-.99	03	0.42	02	0.75	02
6180	c	1.38	13.62	02	0.30	02	-1.00	03	0.41	02	0.76	02
6202	c	1.23	13.76	02	0.38	02	-1.03	03	0.43	02	0.76	02
6204	c	1.23	13.75	02	0.32	02	-.96	03	0.40	02	0.74	02
6252	c	1.23	13.88	02	0.31	02	-.93	03	0.47	02	0.83	02
6252	c	1.38	13.76	02	0.33	02	-.89	03	0.44	02	0.82	02
6299	c	1.23	13.97	02	0.38	02	-.88	03	0.46	02	0.86	02
6299	c	1.38	13.87	02	0.38	02	-.82	03	0.48	02	0.83	02
6315	c	1.23	14.03	02	0.43	02	-.91	03	0.46	02	0.87	02
6315	c	1.38	13.92	02	0.45	02	-.86	03	0.48	02	0.90	02
6318	c	1.23	14.10	:	0.39	02	-.88	03	0.51	02	0.90	02
6318	c	1.23	14.04	02	0.40	02	-.88	03	0.49	02	0.86	02
6318	c	1.38	13.93	02	0.43	02	-.84	03	0.48	02	0.86	02
6319	c	1.23	14.02	02	0.40	02	-.92	03	0.46	02	0.86	02
6319	c	1.38	13.92	02	0.45	02	-.86	03	0.48	02	0.87	02
6349	c	1.23	14.03	02	0.32	02	-.93	03	0.51	02	0.89	02
6349	c	1.38	13.86	02	0.41	02	-.90	03	0.47	02	0.78	02
6350	c	1.23	13.98	02	0.35	02	-.87	03	0.47	02	0.81	02
6350	c	1.38	14.05	:	0.28	:	-.86	:	0.36	:	0.90	:

Table A1. (continued)

HJD 244+	Rf	log ϕ "	V	σ_V	B-V	σ_{BV}	U-B	σ_{UB}	V-R	σ_{VR}	V-I	σ_{VI}
NGC 6814												
1068	q	1.18	13.71	07	1.07	06	0.20	08				
2160	r	1.00	14.21		1.12		0.37					
2218	m	1.16	13.73	11	1.15	01						
2218	m	1.49	12.97	01	1.08	01	0.37	07				
2250	m	1.16	13.70	04	1.17	05	0.37	09				
2250	m	1.49	12.98	03	1.07	02	0.42	07				
2278	m	1.16	13.80	11	1.07	05	0.26	12				
2278	m	1.49	13.00	06	1.08	05	0.40	07				
2310	m	1.16	13.83	11	1.06	05	0.18	12				
2310	m	1.49	13.03	06	1.07	05	0.31	07				
2517	m	1.16	13.73	03	1.07	02	0.15	07				
2517	m	1.49	13.00	06	1.08	06	0.50	07				
2520	m	1.16	13.77	02	1.07	03	0.26	05				
2520	m	1.49	13.02	01	1.07	05	0.34	06				
2523	m	1.16	13.74	02	1.06	04	0.24	04				
2523	m	1.49	12.99	01	1.08	02	0.38	07				
2543	m	1.16	13.79	11	1.09	05	0.31	12				
2543	m	1.49	13.03	06	1.09	05	0.44	07				
2569	m	1.16	13.72	03	1.08	02	0.36	05				
2569	m	1.49	13.02	01	1.08	01	0.37	05				
2604	m	1.16	13.69	01	1.09	01	0.34	05				
2604	m	1.49	13.05	06	1.08	06	0.30	05				
2607	m	1.16	13.72	01	1.08	02	0.32	07				
2607	m	1.49	13.01	02	1.09	02	0.37	05				
2631	m	1.16	13.72	02	1.10	01	0.26	06				
2631	m	1.49	13.01	02	1.12	02	0.37	02				
2635	m	1.16	13.76	02	1.12	04	0.19	12				
2635	m	1.49	13.01	06	1.14	05	0.29	07				
2654	m	1.16	13.68	02	0.96	04	-.05	08				
2654	m	1.49	12.97	02	1.02	01	0.11	01				
2689	m	1.16	13.79	11	0.98	05	0.09	11				
2689	m	1.49	13.01	02	1.06	02	0.23	01				
2723	m	1.16	13.74	03	1.02	02	0.04	06				
2892	m	1.16	13.58	01	0.89	03	-.22	07				
2961	m	1.16	13.56	01	0.91	03	-.17	01				
2982	m	1.16	13.63	02	0.99	02	0.04	04				
2988	m	1.16	13.62	01	1.00	02	0.05	08				
3009	m	1.16	13.76	03	1.08	03	0.32	07				
3049	m	1.16	13.65	01	0.96	02	-.02	04				
3078	m	1.16	13.71	11	1.02	05	0.19	12				
4406	o	1.34	13.28	04	1.10	03	0.51	04				
4432	s	1.18	13.80	04	1.19	09	-.20	26				
4433	s	1.40	13.51	01	1.15	06						
4870	o	1.04	13.97	04	0.83	03	-.19	04				
4871	b	1.19	13.64	04	0.94	04	-.06	05				
5079	t	1.15	13.52		0.89		-.24					
5207	t	1.15	13.65		0.87		-.10					
5531	u	1.44	13.11	03	1.00	06						
5554	t	1.15	13.61		0.89		-.27					
5578	u	1.44	13.21	02	0.93	03	-.04	07				
5579	u	1.44	13.17	02	1.05	03	-.17	06				
5584	b	1.19	13.63	04	0.98	04	-.01	05				

Table A1. (continued)

HJD 244+	Rf	log ϕ "	V	σ_V	B-V	σ_{BV}	U-B	σ_{UB}	V-R	σ_{VR}	V-I	σ_{VI}
NGC 6814 (continued)												
5591	t	1.15	13.65		0.95		-.29					
5606	u	1.15	13.78	03	0.84	04	-.08	09				
5606	u	1.44	13.10	03	0.98	05	-.22	09				
5608	u	1.15	13.87	04	1.00	05	-.12	11				
5608	u	1.44	13.16	03	1.05	04	-.29	07				
5614	u	1.37	13.23	01	1.00	02	0.06	08				
5616	u	1.44	13.15	02	0.98	04	-.05	10				
5616	u	1.15	13.82	02	0.91	04	-.21	10				
5617	u	1.15	13.67	02	0.90	04	-.16	10				
5617	u	1.44	13.13	03	1.02	04	-.17	13				
5636	u	1.15	13.70	02	1.12	04	-.16	08				
5914	u	1.44	13.31	02	1.03	03						
5938	u	1.37	13.30	01	1.17	03						
5941	u	1.15	13.92	03	1.08	08	-.08	11				
5941	u	1.44	13.26	03	1.05	06						
5942	u	1.44	13.23	02	1.08	03	0.20	09				
5942	u	1.15	13.80	02	1.17	04	0.15	11				
5944	u	1.15	13.93	03	1.17	08						
5944	u	1.44	13.26	03	1.10	05	0.20	08				
5946	u	1.44	13.30	03	0.96	05						
6180	c	1.23	13.58	02	1.04	02	0.17	03	0.73	02	1.47	02
6180	c	1.38	13.26	02	1.09	02	0.20	03	0.72	02	1.47	02
6204	c	1.23	13.64	02	1.01	02	-.09	03	0.70	02	1.42	02
6291	u	1.44	13.27	03	1.14	05						
6293	u	1.44	13.28	03	1.02	06						
6294	u	1.44	13.30	02	1.04	06	0.18	14				
6296	u	1.44	13.23	02	1.19	05						
6297	u	1.44	13.23	02	1.10	03						
6318	c	1.23	13.68	02	1.08	02	0.31	03	0.73	02	1.47	02
6318	c	1.38	13.33	02	1.08	02	0.34	03	0.73	02	1.46	02
6319	c	1.23	13.65	02	1.07	02	0.32	03	0.71	02	1.45	02
6319	c	1.38	13.29	02	1.10	02	0.32	03	0.73	02	1.42	02
6345	u	1.44	13.22	02	1.13	04						
6345	u	1.15	13.83	03	1.17	06						
6346	u	1.44	13.34	03	1.03	05	0.18	12				
6622	u	1.44	13.26	02	1.12	05						
6623	u	1.44	13.18	02	1.19	04	0.30	11				
6626	u	1.44	13.31	02	1.12	03						
6644	u	1.18	13.81	01	1.10	01	0.52	04				
6644	u	1.65	12.30	01	1.06	01	0.30	02				
6645	u	1.18	13.80	01	1.14	01	0.54	06				
6651	u	1.18	13.81	01	1.09	01	0.42	02				
6652	u	1.18	13.79	01	1.12	01	0.45	03				
6653	u	1.18	13.79	01	1.12	01	0.48	02				
6654	u	1.18	13.82	01	1.13	01	0.46	02				
6655	u	1.18	13.81	01	1.12	01	0.48	03				
6656	u	1.18	13.81	01	1.13	01	0.54	03				
6657	u	1.18	13.77	01	1.15	01	0.51	03				
6671	u	1.15	13.95	02	0.98	05						
6673	u	1.44	13.25	02	1.07	04	0.39	13				
6674	u	1.44	13.35	02	1.19	06						
6680	u	1.44	13.22	02	1.14	03	0.56	12				

Table A1. (continued)

HJD 244+	Rf	log ϕ "	V	σ_V	B-V	σ_{BV}	U-B	σ_{UB}	V-R	σ_{VR}	V-I	σ_{VI}
H 2106-099												
	k	1.18	14.32	04	0.48	05	-.63	05				
NGC 7213												
3371	g	1.57	11.18	01	0.97	01	0.45	02				
3373	g	1.57	11.18	01	0.96	01	0.45	02				
4145	o	1.35	11.64	05	0.97	04	0.43	04				
4146	b	1.19	12.09	04	1.02	04	0.47	05				
4433	j	1.20	12.04	03	0.97	03	0.39	04				
4896	j	1.20	12.00	03	0.93	03	0.45	04				
5584	b	1.19	12.07	04	1.00	04	0.43	05				
6204	c	1.23	12.01	02	1.00	02	0.40	03	0.60	02	1.23	02
6252	c	1.23	11.99	02	0.96	02	0.39	03	0.62	02	1.24	02
6252	c	1.38	11.61	02	0.94	02	0.43	03	0.61	02	1.23	02
6299	c	1.23	12.02	02	0.95	02	0.38	03	0.62	02	1.25	02
6299	c	1.38	11.59	02	0.96	02	0.42	03	0.59	02	1.22	02
6316	c	1.23	12.00	02	0.98	02	0.39	03	0.61	02	1.23	02
6316	c	1.38	11.58	02	0.96	02	0.40	03	0.60	02	1.22	02
6319	c	1.23	11.97	02	0.96	02	0.46	03	0.60	02	1.22	02
6319	c	1.38	11.56	02	0.98	02	0.40	03	0.59	02	1.21	02
6349	c	1.23	11.98	02	0.97	02	0.41	03	0.62	02	1.26	02
6349	c	1.38	11.63	02	1.00	02	0.48	03	0.61	02	1.24	02
6351	c	1.23	11.97	02	0.96	02	0.37	03	0.62	02	1.26	02
6351	c	1.38	11.61	02	0.94	02	0.38	03	0.60	02	1.23	02
MCG -2-58-22												
4107	v	1.40	14.21	03	0.68	03	-.59	06				
4901	j	1.04	14.30	03	0.51	03	-.84	04				
5261	j	1.04	14.10	03	0.38	03	-.94	04				
6316	c	1.23	13.76	02	0.36	02	-.98	03	0.42	02	0.77	02
6316	c	1.38	13.62	02	0.43	02	-.94	03	0.41	02	0.80	02
6318	c	1.23	13.79	02	0.36	02	-1.00	03	0.41	02	0.77	02
6318	c	1.38	13.65	02	0.42	02	-.90	03	0.42	02	0.81	02
6319	c	1.23	13.77	02	0.35	02	-.99	03	0.43	02	0.78	02
6319	c	1.38	13.65	02	0.40	02	-.91	03	0.45	02	0.82	02

References:- (a) Veron-Cetty and Veron, 1989, (b) Veron-Cetty, 1984, (c) Hamuy and Maza, 1987, (d) Martin et al, 1978, (e) West et al, 1978, (f) Danks, 1979, (g) Griersmith, 1980, (h) Glass, 1986, (i) Griersmith et al, 1982, (j) Mallama, 1983, (k) Remillard et al, 1986, (l) Osmer et al, 1974, (m) Penfold, 1979, (n) Wegner, 1979, (o) Veron-Cetty et al, 1982, (p) Disney, 1973, (q) De Vaucouleurs et al, 1978, (r) Khachikian and Weedman, 1974, (s) Dibai et al, 1981, (t) Bisch et al, 1987, (u) Doroshenko, 1988, (v) Doroshenko and Terebizh, 1981.

Table A2. Unpublished UBVRI aperture photometry by D. Kilkenny.

HJD 244+	log ϕ "	V	B-V	U-B	V-R	V-I
NGC 1566						
5346	1.32	12.22	0.85		0.60	1.20
5346	1.18	12.54	0.82		0.59	1.19
5346	1.04	12.87	0.77		0.58	1.17
5348	1.32	12.24	0.87	0.02	0.62	1.17
5348	1.18	12.60	0.82	-.08	0.60	1.19
5348	1.04	12.90	0.80	-.07	0.59	1.19
5348	0.95	13.11	0.76	-.11	0.58	1.15
5350	1.32	12.22	0.87	0.03	0.60	1.19
5350	1.18	12.53	0.82	-.06	0.63	
5350	1.04	12.85	0.80	-.17	0.58	1.17
5350	0.95	13.01	0.77	-.21	0.57	1.14
5374	1.32	12.26	0.91	0.10	0.57	1.17
5374	0.95	13.10	0.80	-.06	0.56	1.14
5375	1.32	12.25	0.88	0.11	0.63	1.26
5375	0.95	13.03	0.82	-.11	0.58	1.13
5380	1.32	12.21	0.88	0.04	0.60	1.20
5380	0.95	12.96	0.78	-.22	0.56	1.10
5710	1.32	12.26	0.88	0.16	0.59	1.18
5715	1.32	12.32	0.94	0.32	0.61	1.23
5715	0.95	13.19	0.89	0.15	0.65	1.27
6465	0.95	13.24	0.92	0.27	0.62	1.24
NGC 2992						
5349	1.32	13.45	1.05	0.36	0.73	1.41
5349	1.18	13.82	1.12	0.40	0.75	1.44
5349	1.04	14.16	1.22	0.39	0.76	1.46
5351	1.32	13.45	1.04	0.42	0.71	1.40
5351	1.18	13.83	1.12	0.39	0.75	1.46
5374	1.32	13.46	1.08	0.36	0.70	1.41
5374	0.95	14.36	1.14	0.48	0.77	1.49
5375	1.32	13.41	1.05	0.39	0.72	1.42
5375	0.95	14.33	1.18	0.48	0.87	1.61
5380	1.32	13.44	1.10	0.39	0.72	1.41
5466	1.32	13.46	1.03	0.36	0.67	1.36
5466	0.95	14.23	1.24	0.45	0.78	1.45
6465	1.32	13.43	1.04	0.39	0.70	1.37

Table A2. (continued)

HJD 244+	log ϕ "	V	B-V	U-B	V-R	V-I
NGC 3783						
5349	1.32	13.00	0.59	-.65	0.58	1.02
5349	1.18	13.21	0.52	-.73	0.57	1.00
5349	1.04	13.38	0.44	-.81	0.56	0.93
5349	0.95	13.42	0.45	-.85	0.55	0.91
5351	1.32	12.98	0.60	-.64	0.67	1.37
5351	1.18	13.18	0.53	-.72	0.57	0.97
5351	1.04	13.40	0.46	-.82	0.53	0.91
5375	1.32	13.07	0.60	-.59	0.59	1.09
5375	0.95	13.53	0.45	-.80	0.57	0.94
5380	1.32	13.02	0.64	-.59	0.59	1.07
5466	1.32	13.05	0.63	-.61	0.58	1.05
5466	0.95	13.52	0.45	-.81	0.55	0.93
6465	1.32	12.98	0.55	-.68	0.58	1.03
6465	0.95	13.41	0.39	-.84	0.53	0.87
ESO 141-G55						
5641	1.32	13.99	0.40	-.80	0.50	0.95
NGC 6814						
5490	1.32	13.39	1.02	0.05	0.72	1.41
5490	0.95	14.12	0.89	-.25	0.71	1.39
5641	1.32	13.44	1.07	0.20	0.72	1.44

Table A3. Infrared photometry performed by Ian Glass, corrected for interstellar reddening inside our Galaxy. f(K) is the fraction of extranuclear to total flux in the K band. The aperture diameter size ϕ is in arcseconds.

Name	J	H	K	L	ϕJHK	ϕL	f(K)	Ref
ESO 12-G21	12.44	11.41	10.81	9.90	12	9	0.5	a
Ton S180	13.40	12.57	11.60	10.05	12	12	0.2	a
NGC 526a	12.39	11.31	10.27	8.67	9	9	0.2	b
Fairall 9	11.82	10.72	9.78	8.42	12	9	0.2	b
IC 1816	12.21	11.47	11.18	10.85	12	9	0.9	a
H 0307-730	13.10	12.27	11.81	-	12	12	0.7	a
Fairall 1116	13.05	12.10	11.34	10.02	12	9	0.3	a
NGC 1566	11.24	10.36	9.85	9.01	6	6	0.6	b
MGC -5-13-17	11.67	10.96	10.61	9.89	12	9	0.8	a
3A 0557-383	12.33	11.25	10.07	8.15	9	9	0.1	b
Fairall 265	12.90	11.99	11.29	10.03	9	9	0.3	b
NGC 2992	11.91	10.90	10.27	9.28	6	6	0.5	b
MCG -5-23-16	11.50	10.65	10.06	8.89	9	9	0.5	b
ESO 438-G9	12.31	11.41	10.65	9.63	12	12	0.3	a
NGC 3783	11.52	10.58	9.75	8.33	9	9	0.2	b
H 1143-182	12.82	11.99	11.32	10.33	12	9	0.4	a
MCG -2-33-34	12.25	11.44	10.92	10.12	9	9	0.6	c
ESO 323-G77	10.72	9.60	8.72	7.49	12	12	0.2	a
MCG -6-30-15	11.73	10.77	10.04	8.67	9	9	0.4	c
IC 4329A	11.17	10.16	9.27	7.83	9	9	0.2	b
IRAS 1509-211	12.54	11.56	10.72	9.45	12	12	0.2	c
ESO 103-G35	12.37	11.53	11.18	9.74	9	9	0.8	b
Fairall 51	12.00	11.07	10.23	8.94	12	12	0.2	c
ESO 141-G55	12.15	11.16	10.14	8.57	9	9	0.2	b
NGC 6814	12.19	11.28	10.69	9.91	6	6	0.5	b
NGC 6860	11.64	10.73	10.03	8.87	12	12	0.4	a
H 2106-099	12.33	11.39	10.52	9.35	18	12	0.2	a
NGC 7213	10.85	10.03	9.47	8.36	6	6	0.5	b
MCG -2-58-22	12.48	11.43	10.32	8.88	9	9	0.1	b

References:- a) unpublished data, b) Glass and Moorwood (1985), c) Glass (1985).

Table A4. Ultraviolet line fluxes published in the literature. The units are 10^{-12} erg cm^{-2} s^{-1}.

Name	Lyα	CIV	CIII]	MgII	FeII	Ref
ESO 12-G21	0.22	0.12	0.06	0.13	0.90	a
Fairall 9	18.7	7.31	1.45	1.95	-	b
NGC 1566	gc	0.38	0.15	0.24	0.86	b
ESO 438-G9	0.44	<.09	-	0.19	0.72	c
NGC 3783	10.7	7.36	0.59	1.55	-	b
ESO 141-G55	10.4	5.36	1.12	1.53	-	b
NGC 7213	gc	1.29	0.68	-	-	b
MCG -2-58-22	6.68	5.10	-	1.30	-	b

"gc" indicates that Ly α could not be observed in these objects because of contamination from the strong geo-coronal Ly α emission line.

References:- a) Clavel and Joly (1984), corrected for extinction in the Galaxy, b) Wu et al (1983), observed fluxes, c) Kollatschny and Fricke (1983), corrected for extinction in the Galaxy.

Table A5. Optical spectral line intensities relative to [O III] 5007 Å, corrected for extinction in the Galaxy, from data published in the literature.

Galaxy Name	Ref	[NeV] 3427	[OII] 3727	[FeVII] 3757	[NeIII] 3868	H8 3889	Hε 3968	[SII] 4068	Hδ 4102
Fairall 9	a	-	0.08	-	0.25	2.08	0.67	-	1.00
H 0307-730	b	0.22	0.13	-	0.10	-	-	-	0.64
Fairall 1116	c	0.13	0.15	-	0.24	-	0.27	-	1.50
NGC 1566	d	0.11:	0.28	-	0.15	-	-	-	-
NGC 2992	e	-	0.20	-	0.05	0.01	0.02	0.01	0.01
ESO 438-G9	f	-	0.43	-	-	-	-	-	0.59
NGC 3783	g	0.33	0.15	0.10	0.22	0.52	0.53	0.04	0.65
H 1143-182	b	-	0.14	-	0.07	-	-	-	0.18
MCG-2-33-34	h	-	0.11	-	0.05	0.04	0.13	-	0.16
MCG-6-30-15	i	0.10	0.23	-	0.10	-	-	-	-
IC 4329A	i	-	0.06	-	-	-	-	-	-
IRAS 1509-21	h	0.04	0.13	-	0.04	-	0.02	-	0.03
ESO 103-G35	i	-	0.39	-	0.07	-	-	0.04	-
Fairall 51	i	0.24	0.21	-	0.12	-	-	-	-
ESO 141-G55	i	-	0.10	-	0.12	0.08	0.50	-	0.77
NGC 6814	i	0.14	0.13	-	0.09	-	-	-	0.60
H 2106-099	b	-	0.15	-	0.34:	-	-	-	1.13
NGC 7213	j	0.14	0.43	-	0.34	0.09	0.14	0.22	0.17
MCG-2-58-22	i	-	0.37	-	-	0.89	-	-	-

Table A5. (continued)

Galaxy Name	Hγ 4340	[OIII] 4363	HeII 4686	Hβ 4861	[OIII] 4959	[OIII] 5007	[FeVII] 5721	HeI 5876
Fairall 9	2.58	0.08	-	8.33	0.33	1.00	-	1.42
H 0307-730	1.40	-	-	4.18	-	1.00	-	-
Fairall 1116	2.51	<--	0.27	5.04	0.38	1.00	-	1.01
NGC 1566	0.22:	-	-	0.53	0.37	1.00	-	-
NGC 2992	0.02	0.01	0.02	0.13	0.32	1.00	0.01	0.03
ESO 438-G9	1.24	0.05:	0.05:	2.70	0.35	1.00	-	0.35
NGC 3783	0.88	0.05	0.53	1.68	0.32	1.00	0.04	0.21
H 1143-182	0.39	-	0.25	0.83	-	1.00	-	0.08
MCG-2-33-34	0.38	-	0.06	1.17	0.31	1.00	-	0.08
MCG-6-30-15	0.49	0.09	0.09	1.58	0.34	1.00	0.07	-
IC 4329A	0.71	-	-	2.53	0.39	1.00	-	1.00
IRAS 1509-21	0.18	-	0.02	0.74	0.27	1.00	-	0.08
ESO 103-G35	-	-	-	0.15	0.32	1.00	-	-
Fairall 51	0.57	<--	0.10	1.13	0.35	1.00	0.03	0.24
ESO 141-G55	1.14	<--	-	3.36	0.25	1.00	0.03	0.79
NGC 6814	0.49	0.08	-	1.31	0.33	1.00	-	-
H 2106-099	1.47	-	-	3.47	-	1.00	-	1.40
NGC 7213	0.52	0.20	0.06	1.44	0.35	1.00	0.04	<.09
MCG-2-58-22	0.72	0.07	-	2.07	0.30	1.00	-	0.69

Table A5. (continued)

Galaxy Name	[FeVII] 6087	[OI] 6300	[FeX] 6364	[NII] 6548	Hα 6563	[NII] 6584	[SII] 6716	[SII] 6731	FeII
Fairall 9	0.17	0.08	-	-	21.6	-	-	-	4
H 0307-730	-	-	-	-	12.0	-	-	-	3
Fairall 1116	-	-	-	-	-	-	-	-	0
NGC 1566	-	-	-	0.16	2.47	0.47	0.13	-	0
NGC 2992	0.01	0.15	0.04	0.32	4.86	0.97	0.45	0.40	0
ESO 438-G9	-	0.08:	-	0.49	7.92	1.00	0.22	0.24	4
NGC 3783	0.09	0.05	0.06	0.10	4.41	0.29	0.05	0.06	0
H 1143-182	-	-	-	-	3.05	-	-	-	1
MGC-2-33-34	-	0.02	0.02	-->	1.98	<--	0.11	-	4
MCG-6-30-15	0.20	0.04	0.07	-->	8.20	<--	0.21	<--	2[h]
IC 4329A	0.09	0.10	-	-	19.1	<--	0.27	<--	0
IRAS 1509-21	-	0.03	0.03	-->	3.32	<--	0.13	<--	2
ESO 103-G35	-	0.20	0.06	-->	1.44	<--	0.58	<--	1[h]
Fairall 51	0.07	0.03	0.04	-->	5.63	<--	0.15	<--	3[h]
ESO 141-G55	0.06	-	-	-	10.9	<--	-	-	0
NGC 6814	-	-	-	-	3.94	<--	0.18	<--	0
H 2106-099	-	-	-	-	15.3	-	-	-	2
NGC 7213	-	0.83	0.28	0.16	9.04	0.48	0.27	0.27	0
MCG-2-58-22	-	-	-	-	9.35	<--	0.36	<--	0

Table A5. (continued, listing only those galaxies for which line intensities have been measured in the wavelength range 7000-10000 Å)

Galaxy Name	HeI 7065	[ArIII] 7136	[OII] 7319	[FeXI] 7889	OI 8447	[SIII] 9069	[SIII] 9532	P8 9546
NGC 2992	0.01	-	-	-	-	-	-	-
NGC 3783	0.17	0.02	0.04	0.03	0.14	0.04	0.10	0.28
MCG -2-33-34	0.04	0.01	-	0.03	0.08	0.05	0.15	-
MCG -6-30-15	0.40	-	-	0.14	0.47	0.15	0.31	0.48
IC 4329A	0.45	0.06	0.04	-	1.29	0.29	0.62	1.04
I 1509-211	0.06	-	-	-	0.28	0.09	0.20	-
ESO 103-G35	-	0.09	0.16	-	-	0.31	0.68	-
Fairall 51	0.14	0.02	-	-	0.25	0.09	0.26	0.15
ESO 141-G55	0.23	0.02	-	-	0.51	0.05	0.12	0.18
NGC 6814	-	-	-	-	-	0.13	0.28	0.19
MCG -2-58-22	-	-	0.07	-	0.35	0.07	0.12	-

References:- a) Hawley and Phillips (1978), b) Remillard et al (1986), c) Maza and Ruiz (1989), d) Martin (1974), e) Shuder (1980), f) Kollatschny and Fricke (1983), g) Ward and Morris (1985), h) Carter (1984), i) Morris and Ward (1988), j) Filippenko and Halpern (1984).

References

Allen, D.A., 1979. *Mon. Not. R. astr. Soc.* **186**, 1P.

Alloin, D., Pelat, D., Phillips, M., Whittle, M., 1985. *Astrophys. J.* **288**, 205.

Appenzeller, I., Ostreicher, R., 1988. *Astron J.* **95**, 45.

Baker, J.G., Menzel, D.H., 1938. *Astrophys. J.* **88**, 53.

Baldwin, J.A., Phillips, M.M., Terlevich, R., 1981. *Publ. astr. Soc. Pac.* **93**, 5.

Baldwin, J.A., Stone, R.P.S., 1984. *Mon. Not. R. astr. Soc.* **206**, 241.

Balzano, V.A., 1983. *Astrophys. J.* **268**, 602.

Barr, P., Willis, A.J., Wilson, R., 1983. *Mon. Not. R. astr. Soc.* **202**, 453.

Belokon, E.T., Babadzanjanz, M.K., Lyutyi, V.M., 1979. *Astron. Astrophys. Suppl. Ser.* **31**, 383.

Bessell, M.S., 1979. *Publ. astr. Soc. Pac.* **91**, 589.

Binggeli, B., Sandage, A., Tammann, G.A., 1988. *Ann. Rev. Astron. Astrophys.* **26**, 509.

Bisch, S.M., Pastoriza, M.G., Dottori, H., Busko, I., 1987. *IAU Symp. 121*, 185.

Brindle, C., Hough, J.H., Bailey, J.A., Axon, D.J., Ward, M.J., Sparks, W.B., McLean, I.S., 1990a. *Mon. Not. R. astr. Soc.* **244**, 577.

Brindle, C., Hough, J.H., Bailey, J.A., Axon, D.J., Ward, M.J., Sparks, W.B., McLean, I.S., 1990b. *Mon. Not. R. astr. Soc.* **244**, 604.

Brocklehurst, M., 1972. *Mon. Not. R. astr. Soc.* **157**, 211.

Burbidge, M.E., Strittmatter, P.A., Smith, H.E., Spinrad, H., 1972. *Astrophys. J. Lett.* **178**, L43.

Burstein, D., Heiles, C., 1982. *Astron. J.* **87**, 1165.

Carleton, N.P., Elvis, M., Fabbiano, G., Lawrence, A., Ward, M.J., Willner, S.P., 1987. *Astrophys. J.* **318**, 595.

Carter, D., 1984. *Astr. Express* **1**, 61.

Chapman, G.N.F., Geller, M.J., Huchra, J.P., 1985. *Astrophys. J.* **297**, 151.

Chavira, E., 1958. *Bol. Tonántzintla y Tacubaya* **17**, 15.

Chini, R., Kreysa, E., Biermann, P.L., 1989. *Astron. Astrophys.* **219**, 87.

Choloniewski, J., 1981. *Acta Astron.* **31**, 293.

Clavel, J., Joly, M., 1984. *Astron. Astrophys.* **131**, 87.

Clavel, J., Wamsteker, W. ,Glass, I.S., 1989. *Astrophys. J.* **337**, 236.

Collin-Souffrin, S., Joly, M., Dumont, S., Pequignot, D., 1986. *Astron. Astrophys.* **166**, 27.

Dahari, O., De Robertis, M.M., 1988. *Astrophys. J. Suppl.* **67**, 249.

Danks, A.C., Wamsteker, W., Vogt, N., Salinari, P., Tarenghi, M., Duerbeck, H.W., 1979. *Astrophys. J. Lett.* **227**, L59.

Deeming, T.J., 1975. *Astrophys. Space Sci.* **36**, 137.

De Grijp, M.H.K., Miley, G.K., Lub, J., 1987. *Astron. Astrophys. Suppl. Ser.* **70**, 95.

De Grijp, M.H.K., Miley, G.K., Lub, J., De Jong, T., 1985. *Nature* **314**, 240.

De Ruiter, H.R., Lub, J., 1986. *Astron. Astrophys. Suppl. Ser.* **63**, 59.

De Vaucouleurs, G., Buta, R., 1983. *Astron J.* **88**, 939.

De Vaucouleurs, G., De Vaucouleurs, A., 1961. *Mem. R. astr. Soc.* **68**, 69.

De Vaucouleurs, G., De Vaucouleurs, A., 1964. *Reference Catalog of Bright Galaxies*, University of Texas.

De Vaucouleurs, G., De Vaucouleurs, A., Corwin, H.G., 1978. *Astron. J.* **83**, 1331.

Dibai, E.A., Doroshenko, V.T., Postnov,K.A., 1981. *Pisma Astron. Zh.* **7**, 295.

Disney, M.J., 1973. *Astrophys. J. Lett.* **181**, L55.

Doroshenko, V.T., Terebizh, V.Y., 1981. *Astrofizika* **17**, 667.

Doroshenko, V.T., 1988. *Astrofizika* **28**, 233.

Edelson, R.A., 1987. *Astrophys. J.* **313**, 651.

Edelson, R.A., Malkan, M.A., 1986. *Astrophys. J.* **308**, 59.

Fairall, A.P., 1977. *Mon. Not. R. astr. Soc.* **180**, 391.

Fairall, A.P., 1980. *Mon. Not. R. astr. Soc.* **192**, 389.

Fairall, A.P., 1986. *Mon. Not. R. astr. Soc.* **218**, 453.

Fairall, A.P., 1988. *Mon. Not. R. astr. Soc.* **233**, 691.

Fairall, A.P., Jones, A., 1988. Southern Redshifts Catalogue and Plots, *Publication of the University of Cape Town Astronomy Department* no. **10**.

Fairall, A.P., Mc Hardy, I.M., Pye, J.P., 1982. *Mon. Not. R. astr. Soc.* **198**, 13P.

Filippenko, A.V., Halpern, J.P., 1984. *Astrophys. J.* **285**, 458.

Fitch, W.S., Pacholczyk, A.G., Weymann, R.J., 1967. *Astrophys. J.* **150**, L67.

Freeman, K.C., 1970. *Astrophys. J.* **160**, 811.

Glass, I.S., 1981. *Mon. Not. R. astr. Soc.* **197**, 1067.

Glass, I.S., 1985. *Mon. Not. astr. Soc. South Africa* **44**, 60.

Glass, I.S., 1986. *Mon. Not. R. astr. Soc.* **219**, 5P.

Glass, I.S., 1989. *IAU Symp. 134*, 382.

Glass, I.S., Moorwood, A.F.M., 1985. *Mon. Not. R. astr. Soc.* **214**, 429.

Glass, I.S., Moorwood, A.F.M., Eichendorf, W., 1982. *Astron. Astrophys.* **107**, 276.

Grandi, S.A., 1983. *Astrophys. J.* **268**, 591.

Griersmith, D., Visvanathan, N., 1979. *Astron. Astrophys.* **79**, 329.

Griersmith, D., 1980. *Astron. J.* **85**, 789.

Griersmith, D., Hyland, A.R., Jones, T.J., 1982. *Astron. J.* **87**, 1106.

Griffiths, R.E., Doxsey, R.E., Johnston, M.D., Schwartz, D.A., Schwarz, J., Blades, J.C., 1979. *Astrophys. J. Lett.* **230**, L21.

Halpern, J.P., Filippenko, A.V., 1984. *Astrophys. J.* **285**, 475.

Hamuy, M., Maza, J., 1987. *Astron. Astrophys. Suppl. Ser.* **68**, 383.

Harnett, J.I, 1987. *Mon. Not. R. astr. Soc.* **227**, 887.

Hawley, S.A., Phillips, M.M., 1978, *Astrophys. J.* **225**, 780.

Hayes, M.J.C., Culhane, J.L., Bell Burnett, S.J., 1980. *Mon. Not. R. astr. Soc.* **192**, 1P.

Heckman, T.M., 1980. *Astron. Astrophys.* **87**, 152.

Hummer, D.G., Storey, P.J., 1987. *Mon. Not. R. astr. Soc.* **224**, 801.

Kalinkov, M., Kuneva, I., Tsvetsanov, Z., Filipov, L., 1989. *IAU Symposium 134*, 565.

Khachikian,E.Y., Weedman, D.W., 1974. *Astrophys. J.* **192**, 581.

Kollatschny, W., Fricke, K.J., 1983. *Astron. Astrophys.* **125**, 276.

Kotov, V.A., Lyutyi, V.M., 1989. *Bull. Crim. Astrophys. Obs.* **79**, 130.

Kwan, J., Krolik, J.H., 1981. *Astrophys. J.* **250**, 478.

Lang, K.R., 1974. 'Astrophysical Formulae', 2nd Ed., Springer.

Lauberts, A., 1982. *The ESO/Uppsala Survey of the ESO B Atlas.*

Lawrence, A., 1987. *Publ. astr. Soc. Pac.* **99**, 308.

Lyutyi, V.M., Oknyanskii, V.L., 1987. *Sov. Astron.* **31**, 245.

Maia, M.A.G., Da Costa, L.N., Willmer, C., Pellegrini, P.S., Rite, C., 1987. *Astron. J.* **93**, 546.

Malkan, M.A., Filippenko, A.V., 1983. *Astrophys. J.* **275**, 477.

Mallama, A.D., 1983. *Jour. AAVSO* **12**, 69.

Marshall, F.E., Boldt, E.A., Holt, S.S., Mushotzky, R.F., Pravdo, S.H., Rothschild, R.E., Serlemitsos, P.J., 1979. *Astrophys. J. Suppl.* **40**, 657.

Martin, P.G., Stochman, H.S., Angel, J.P.R., Maza, J., Beaver, E.A., 1982. *Astrophys. J.* **255**, 65.

Martin, P.G., Thompson, I.B., Maza, J., Angel, J.R.P., 1983, *Astrophys. J.* **266**, 470.

Martin, W.L., 1974. *Mon. Not. R. astr. Soc.* **168**, 109.

Martin, W.L., Penfold, J.E., Glass, I.S., 1978. *Mon. Not. R. astr. Soc.* **184**, 15p.

Masegosa, J., Moles, M., Penston, M.V., 1986. *Mon. Not. R. astr. Soc.* **218**, 541.

Maza, J., Ruiz, M.T., 1989. *Astrophys. J. Suppl.* **69**, 353.

Maza, J., Ruiz, M.T., Gonzalez, L.E., Wischnjewsky, M., 1989. *Astrophys. J. Suppl.* **69**, 349.

Mc Alary, C.W., Mc Laren, R.A., Mc Gonegal, R.J., Maza, J., 1983, *Astrophys. J. Suppl.* **52**, 341.

Mc Alary, C.W., Rieke, G.H., 1988. *Astrophys. J.* **333**, 1.

Mendoza, C., 1983. *IAU Symp. 103*, 143.

Menzies, J.W., Cousins, A.W.J., Banfield, R.M., Laing, J.D., 1989. *S.A.A.O. Circ.* **13**, 1.

Menzies, J.W., Feast, M., 1983. *Mon. Not. R. astr. Soc.* **203**, 1P.

Miley, G.K., Neugebauer, G., Soifer, B.T., 1985. *Astrophys. J. Lett.* **293**, L11.

Miller, J.S., Mathews, W.G., 1972. *Astrophys. J.* **172**, 606.

Morris, S.L., Ward, M.J., 1988. *Mon. Not. R. astr. Soc.* **230**, 639.

Mushotzky, R.F., 1982. *Astrophys. J.* **256**, 92.

Mushotzky, R.F, Marshall, F.E., Boldt, E.A., Holt, S.S., Serlemitos, P.J., 1980. *Astrophys. J.* **235**, 377.

Oke, J.B., Sargent, W.L.W., 1968. *Astrophys. J.* **151**, 807.

Osmer, P.S., Smith, M.G., Weedman, D.W., 1974. *Astrophys. J.* **189**, 187.

Osterbrock, D.E., 1981. *Astrophys. J.* **249**, 462.

Osterbrock, D.E., 1984. *Quart. Jour. R. Soc.* **25**, 1.

Osterbrock, D.E., 1988. *Publ. astr. Soc. Pac.* **100**, 412.

Osterbrock, D.E., 1989. 'Astrophysics of Gaseous Nebulae and Active Galactic Nuclei', University Science Books, Mill Valley, California.

Osterbrock, D.E., de Robertis, M.M., 1985, *Publ. astr. Soc. Pac.* **97**, 598, 1129.

Page, T., 1967. *Astron. J.* **72**, 821.

Pelat, D., Alloin, D., Fosbury, R.A.E., 1981. *Mon. Not. R. astr. Soc.* **195**, 787.

Penfold, J.E., 1979. *Mon. Not. R. astr. Soc.* **186**, 297.

Peterson, B.M., 1988. *Publ. astr. Soc. Pac.* **100**, 18.

Petre, R., Mushotzky, R.F., Krolik, J.H., Holt, S.S., 1984. *Astrophys. J.* **280**, 499.

Phillips, M.M., 1979. *Astrophys. J.* **227**, L121.

Phillips, M.M., Feldman, F.R., Marshall, F.E., Wamsteker, W., 1979. *Astron. Astrophys.* **76**, L14.

Piccinotti, G., Mushotzky, R.F., Boldt, E.A., Holt, S.S., Marshall, F.E., Serlemitsos, P.J., Shafer, R.A., *Astrophys. J.* **253**, 485.

Pineda, F.J., Devaille, J.P., Grindlay, J.E., Schnopper, H.W., 1980. *Astrophys. J.* **237**, 414.

Reichert, G.A., Mushotzky, R.F., Petre, R., Holt, S.S., 1985. *Astrophys. J.* **296**, 69.

Remillard, R.A., Bradt, H.V., Buckley, D.A.H., Roberts, W., Schwartz, D.A., Tuohy, I.R., Wood, K., 1986. *Astrophys. J.* **301**, 742.

Sadler, E.M., 1984. *Astron. J.* **89**, 53.

Savage, B.D., Mathis, J.S., 1979. *Ann. Rev. Astron. Astrophys.* 17, 73.

Schnopper, H.W., Davis, M., Delvaille, J.P., Geller, M.J., Huchra, J.P., 1978. *Nature* **275**, 719.

Serkowski, K., Mathewson, D.S., Ford, V.L., 1975. *Astrophys. J.* **196**, 261.

Seyfert, C.K., 1943. *Astrophys. J.* **97**, 28.

Shuder, J.M., 1980. *Astrophys. J.* **240**, 32.

Stirpe, G.M., De Bruyn, A.G., Van Groningen, E., 1988. *Astron. Astrophys.* **200**, 9.

Stone, R.P.S., Baldwin, J.A., 1983. *Mon. Not. R. astr. Soc.* **204**, 347.

Sun, W.-H., Malkan, M.A., 1989. *Astrophys. J.* **346**, 68.

Terlevich, R., 1989. *RGO preprint*.

The, P.S., Groot, M., 1983. *Astron. Astrophys.* **125**, 75.

Thompson, I.B., Martin, P.G., 1988. *Astrophys. J.* **330**, 121.

Turner, T.J., Pounds, K.A., 1989. *Mon Not. R. astr. Soc.* **240**, 833.

Ulrich, M.-H., 1971. *Astrophys. J. Lett.* **165**, L61.

Ulvestad, J.S., Wilson, A.S., 1984a. *Astrophys. J.* **278**, 544.

Ulvestad, J.S., Wilson, A.S., 1984b. *Astrophys. J.* **285**, 439.

Unger, S.W., Lawrence, A., Wilson, A.S., Elvis, M., Wright, A.E., 1987. *Mon. Not. R. astr. Soc.* **228**, 521.

Veron-Cetty, M.-P., 1984. *Astron. Astrophys. Suppl. Ser.* **58**, 665.

Veron-Cetty, M.-P., Veron, P., 1986. *Astron. Astrophys. Suppl. Ser.* **65**, 241.

Veron-Cetty, M.-P., Veron, P., 1989. 'A Catalogue, of Quasars and Active Galactic Nuclei', *ESO Scientific Report* no.7.

Veron-Cetty, M.-P., Veron, P., Tarenghi, M., 1982. *Astron. Astrophys.* **113**, 46.

Walker, A.R., 1984. S.A.A.O. Users Manual: 'CCD Photometry using ASPIC Programs'.

Wamsteker, W., Barr, P., 1985. *Astrophys. J. Lett.* 292, L45.

Wandel, A., Mushotzky, R.F., 1986. *Astrophys. J. Lett.* **306**, L61.

Ward, M.J., 1989. *IAU Symp. 134* , 308.

Ward, M.J., Done, C., Fabian, A.C., Tennant, A.F., Shafer, R.A., 1988. *Astrophys. J.* **324**, 767.

Ward, M., Elvis, M., Fabbiano, G., Carleton, N.P., Willner, S.P., Lawrence, A., 1987. *Astrophys. J.* **315**, 74.

Ward, M.J., Morris, S., 1985. *Mon. Not. R. astr. Soc.* **207**, 867.

Ward, M.J., Penston, M.V., Blades, J.C., Turtle, A.J., 1980. *Mon. Not. R. astr. Soc.* **193**, 563.

Ward, M.J., Wilson, A.S., Penston, M.V., Elvis, M., Maccacaro, T., Tritton, K.P., 1978. *Astrophys. J.* **223**, 788.

Weedman, D.W., 1970. *Astrophys. J.* **159**, 405.

Weedman, D.W., 1977. *Ann. Rev. Astron. Astrophys* **15**, 69.

Wegner, G., 1979. *Astrophys. Space Sci.* **60**, 15.

West, R.M., Danks, A.C., Alcaino, G., 1978. *Astron. Astrophys.* **62**, L13.

Whittle, M., 1985. *Mon. Not. R. astr. Soc.* **213**, 1.

Wills, B.J., Netzer, H., Wills, D., 1985. *Astrophys. J.* **288**, 94.

Wilson, A.S., Penston, M.V., 1979. *Astrophys. J.* **232**, 389.

Wilson, W.J., Schwartz, P.R., Neugebauer, G., Harvey, P.M., Becklin, E.E., 1972. *Astrophys. J.* **177**, 523.

Winkler, H., 1989. *S.A.A.O. Circ.* **13**, 63.

Winkler, H., Van Wyk, F., Glass, I.S., 1990. to be published in *S.A.A.O. Circ.*.

Wood, K.S., Meekins, J.F., Yentis, D.J., Smathers, H.W., McNutt, D.P., Bleach, R.D., Byram, E.T., Chubb, T.A., Friedman, H., Meidav, M., 1984. *Astrophys. J. Suppl.* **56**, 507.

Wu, C.-C., Boggess, A., Gull, T.R., 1983. *Astrophys. J.* **266**, 28.

Yee, H., 1980. *Astrophys. J.* **241**, 894.